8
Hyperspectral Remote Sensing

Eyal Ben Dor, Tim Malthus, Antonio Plaza, and Daniel Schläpfer

8.1
Introduction

Hyperspectral Remote Sensing (HRS) and Imaging Spectroscopy (IS), are two technologies that can provide detailed spectral information from every pixel in an image. Whereas HRS refers mostly to remote sensing (from a distance), the emerging IS technology covers all spatial–spectral domains, from microscopic to macroscopic. IS capability is an innovative development of the charge–coupled device (CCD), which was invented by the two 2009 Nobel prize in Physics winners Willard Boyle and George Smith from Bell Laboratories in 1969. They provided the first assembly capable of generating digital images. In 1972 A. Goetz realized that it was possible to use the CCD for spectral applications and after developing the first portable spectrometer together with significant improvements in the area array assembly, a combined spatial and spectral capability was designed and successfully operated from orbit (LANDSAT program). In general, HRS / IS is a technology that provides spatial and spectral information simultaneously, improving our understanding of the remote environment. It enables accurate identification of both targets and phenomena as the spectral information is presented on a spatial rather than point (pixel) basis. HRS / IS technology is well accepted in remote sensing as a tool for many applications, such as in geology, ecology, geomorphology, limnology, pedology, atmospheric and forensic sciences, especially for cases in which other remote sensing means have failed or are incapable of obtaining additional information. Although innovative approaches have been developed over the past 10 years, the power of HRS / IS technology remains unknown to many potential end-users, such as decision makers, farmers, environmental watchers in both the private and governmental sectors, city planners, stock holders and others. This is mainly because the use of HRS / IS sensors still relies on the relatively high cost of its final products and on the need for professional manpower to operate the instrument and process the data.

Airborne Measurements for Environmental Research. Manfred Wendisch & Jean–Louis Brenguier
Copyright © 2012 copyright holder, location
ISBN: 3-527-XXXXX-X

In February 2010 the company ASD celebrated its 20th anniversary with key people in the HRS field (Goetz, 2010). The consensus there was that HRS/IS technology is still far from reaching its potential, with significant growth still ahead. Nonetheless, today, in addition to the growing number of scientific papers and conferences focusing on this technology, the HRS/IS discipline is very active: commercial sensors are being built and sold, orbital sensors are in advanced planning stages, people are becoming more educated on the topic, national and international funds are being directed toward studying and using this technology, and interest from the private sector is on the rise. The aim of this chapter is to provide the reader with a comprehensive overview of this promising technology from historical to operational perspectives by the recognized experts in the field.

8.2 Definition

HRS is an advanced tool that provides high spatial/spectral resolution data from a distance, with the aim of providing near-laboratory-quality radiance (and subsequent related information) for each picture element (pixel) from a distance. This information enables the identification of targets based on the spectral behavior of the material in question (mainly absorption features of chromophores–see further on). This approach has been found to be very useful in many terrestrial, atmospheric and marine applications (Clark and Roush, 1984; Goetz and Wellman, 1984; Gao and Goetz, 1990; Dekker et al., 2001; Asner and Vitousek, 2005). The classical definition for HRS given by Goetz and his colleagues in 1985 Goetz et al. (1985) remains valid today: *"The acquisition of images in hundreds of contiguous registered spectral bands such that for each pixel a radiant spectrum can be derived."* This definition covers all spectral regions [i.e. VIS (visible), NIR (near infrared), SWIR (shortwave infrared), MWIR (midwave infrared) and LWIR (longwave infrared)], all spatial domains and platforms (microscopic to macroscopic; ground, air and space platforms) and all targets (solid, liquid and gas). Although not mentioned in Goetz's definition, not only are a "high number of bands" needed for this technology, but also high spectral resolution, i.e., a narrow bandwidth (FWHM), and an appropriately large sampling interval across the spectrum. The accepted bandwidth for HRS technology was set to approx. 10 nm 25 years ago (Goetz, 1987). However, today, narrower bandwidths are available and desirable in order to broaden HRS's capability. The former spectral resolution of 10 nm was proposed mainly for the first HRS application (geology); new issues, such as assessing vegetation fluorescence, are now, requiring bandwidths of less than 1 nm (Guanter et al., 2006; Grace et al., 2007).. The idea is to collect near-laboratory-quality radiation from a far distance and apply spectral-based analytical tools to interpret the data. Using this approach, HRS provides information in addition to the traditional cognitive remote sensing mapping and increases our ability to sense Earth remotely. HRS can thus be defined as *"spatial spectrometry from afar"* which adopts spectral routines, models and methodology and merges them with spatial information. Whereas in the laboratory, conditions are constant, optimal and well-controlled, in the acquisition of high-quality spectral data in airborne / spaceborne cases, significant interference is encountered, such as the short dwell time of data acquisition over a given pixel, and hence a lower SNR, atmospheric attenuation of gases and aerosols and the uncontrolled illumination conditions of the source and objects. This makes HRS a very challenging technology that involves many disciplines, including: atmospheric science, electro-optical engineering, aviation, computer science, statistics and applied mathematics and more. The major aim of HRS is to extract physical information from raw HRS data across the spectrum (radiance) which can be easily converted to describe inherent properties of the targets in question, such as reflectance and emissivity. Under laboratory conditions, the spectral information across the VIS–NIR–SWIR–MWIR–LWIR spectral regions can be quantitatively analyzed for all Earth materials, natural and artificial, such as vegetation, water, gases, artificial material, soils and rocks, with many already available in spectral libraries. It was shown that if a HRS sensor with high SNR is used, an analytical spectral approach can be incorporated to yield new products never before sensed by other remote sensing means (Clark et al., 1990; Krüger et al., 1998). The high spectral resolution of HRS technology combined with temporal coverage enables better recognition of targets, a quantitative analysis of phenomena and extracting information.

Allocating spectral information temporally in a spatial domain provides a new dimension that neither the traditional point spectroscopy nor air photography can provide separately. HRS can thus be described as an "expert" Geographic Information System (GIS) in which surface layers are built on a pixel-by-pixel basis rather than a selected group of points with direct and indirect chemical and physical information. Spatial recognition of the phenomenon in question is better performed in the HRS domain than by traditional GIS technique. HRS consists of many points (actually the number of pixels in the image) that are used to generate thematic layers, whereas in GIS, only a few points are used for this purpose. Figure 8.1 shows the concept of the HRS technology, where every pixel is characterized by a complete spectrum of ground targets (and their mixtures) that can be quantitatively analyzed within the spatial view. The capability of acquiring quantitative information from many points on the ground at almost the same time provides another innovative aspect of HRS technology: it freezes time for all spatial pixels at almost the same point, subsequently permitting adequate temporal analysis. HRS technology is thus a promising tool that adds many new aspects to the existing mapping technology and improves our capability to remote-sense materials from far distances.

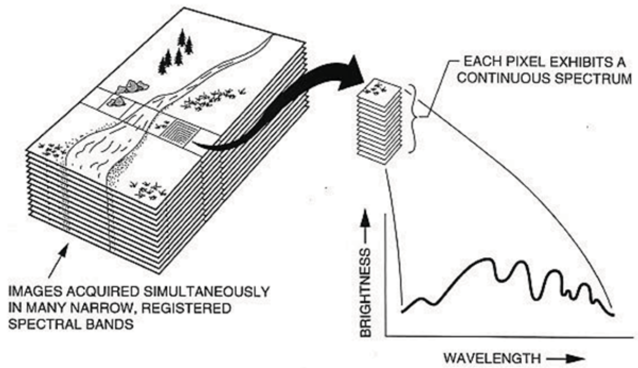

Fig. 8.1 The concept of HRS/IS: Each pixel element has a continuous spectrum that is used to analyze the surface and atmosphere

8.3 Development and History

A. Goetz, initially working at NASA–JPL is considered a mentor and pioneer scientist in HRS technology together with his colleague Gregg Van from NASA JPL. In 2009, Goetz published a paper in a special issue of Remote Sensing of Environment (Goetz, 2009) that was dedicated, upon his retirement, to honoring his activity in this field (MacDonald et al., 2009). The paper reviewed the history of HRS's development since 1970 from Goetz's personal viewpoint entitled: *Three decades of hyperspectroscopy remote sensing of the Earth: a personal view*. It was the first paper to summarize the efforts and difficulties involved in establishing this technology in the US. Generally speaking, HRS technology was driven by geologists and geophysicists who realized that the Earth's surface mineralogy consists of significant and unique spectral fingerprints across the SWIR and MWR, LWIR spectral regions (later, the VIS–NIR spectral region was also explored). This knowledge was gained from comprehensive work with laboratory spectrometers and was followed by a physical explanation of the reflectance spectral response of minerals in rocks and soil. Workers such as Hunt and Salisbury (1970, 1971); Hunt et al. (1971a,b); Clark (1999) and others, who created the first collations of available soil and rock spectral libraries, provided the justification to continue developing HRS technology. Not only was Earth material studied spectrally using this new-found knowledge, but also the outer reaches of the planet showed remarkable information based on these libraries (e.g., Clark et al. (2005)).

HRS capability leans heavily on the invention of the CCD assembly in 1969 (Smith, 2001) which provided the first step toward digital imaging. These and further achievements acted as a precursor to establishing a real image spectrometer that would rely on the commercial hybrid focal plane array that was available at that time (in 1979): the first sensor of this kind was used in the shuttle mission SMIRR (shuttle multispectral IR radiometer) in 1981, providing promising results. Based on this success, Goetz and Vane (in 1983) submitted a proposal to NASA to build an airborne HRS sensor (airborne imaging spectrometer-AIS) which was sensitive to capturing mineral information across the SWIR region (Goetz, 2009). The 2D detector arrays consisting of HgCdTe detectors (32 x 32 elements) which enabled, for the first time, generating images at wavelength greater than 1.1 μm. The array detector did not need a scan and provided sufficient improvement in the SNR to suit airborne applications. The AIS was a rather large instrument, and was flown onboard a C–130 aircraft. It had two versions, with two modes being used in each: the "tree mode" from 0.9-2.1 mm and the "rock mode" from 1.2-2.4 mm. The Instantaneous Field of View (IFOV) of the AIS-1 was 1.91 mrad and of the AIS–2, 2.05 mrad; the ground IFOV (GIFOV) (from 6 km) was 11.4 m and 12.3 m, respectively, and the FOV was 3.7° and 7.3°, respectively. The image swath was 365 m for AIS–1 and 787 m for AIS-2, with a spectral sampling interval of 9.3 nm and 10.6 nm, respectively. The AIS–1 was flown from 1982 to 1985 and the AIS–2, a later version with spectral coverage of 0.8 to 2.4 mm and 64–pixel width (Vane and Goetz, 1988) was flown shortly thereafter, in 1986. In those days, methods to account for atmospheric attenuation were not available; nonetheless, by simple approximation, the sensor and the HRS concept were able to show that minerals can be identified and spatially mapped over an arid-environment terrain. The proceedings of a conference that summarized the activity and first results of the AIS missions were published by NASA in 1985 and 1986 (Van 1986). There, Goetz tells the following story: while processing the AIS data of an overpass over cuprite in Nevada, an unknown spectrum was encountered. At that time, spectral libraries of mineral and rock material had not yet been developed, and the unknown spectrum could not be recognized. In addition to this difficulty, misinterpretation of the rock in question by X-ray analysis led to a dead end. It was only when Dr. Rowan reran the X-ray analysis of the unknown rock that the material was discovered to be boundogtonite. This finding was then confirmed by a laboratory spectral measurement, which scientifically closed the case and proved that the HRS technology was able to detect the mineral boundogtonite from afar. Aside from this first and significant proof of the sensor's capability, the boundogtonite story had another important impact on the future development of HRS/IS technology: boundogtonite may be s associated with gold, and the media at the time (mostly the TV stations) went on the air with the breaking news that "a new methodology to trace gold from the air domain has been discovered by NASA scientists." (In retrospect, this incident proved to be highly detrimental to HRS in the long run.) Soon after, in 1984, Dr. Vane submitted another proposal to NASA to build AVIRIS (Airborne Visible and Infrared Imaging Spectrometer). Approval of this proposal was based mainly on the success of AIS and more likely than not on the boundogtonite story. The first developed AVIRIS lasted three years (1984-1987), with its first flight taking place in 1987. Although being a relatively low–quality SNR instrument (compared to today's HRS/IS sensors and especially to the current upgraded AVIRIS sensor), the first AVIRIS demonstrated excellent performance relative to the AIS. The sensor covered the entire VIS–NIR–SWIR region with 224 bands (around 10-nm width), with 20 m GIFOV and around 10 x 10 km swath. It was a whiskbroom sensor with a SNR of around 100 carried onboard an ER-2 aircraft from 20 km altitude. Since then, the AVIRIS sensor has undergone upgrades and today, the instrument is significantly different from the one first operated in 1987. The major differences are its SNR (100 in 1987 relative to $>$ 1000 today), spectral coverage (400-2500 nm vs 350-2500 nm today) and spatial resolution (20 m vs. 2 m today). The instrument can fly on different platforms at lower altitudes and has opened up new capabilities for potential users in many applications. Even today, with many new HRS sensors having become available worldwide, both commercially and nationally, the AVIRIS sensor is still considered to be the best HSR sensor ever manufactured (Goetz, 2009). This is due in large part to careful maintenance and upgrade of the sensor over the years by NASA JPL personnel, led by Dr. R. Green, and to the growing interest of the US HRS community in using the data and in continuing to show remarkable results and to develop new applications. The AVIRIS program has established an active HRS community in the US that has rapidly matured. Based on this capability and success, other sensors have been developed and built over the past two decades worldwide. The next section details this evolution. To sum up this section, it can be concluded that the AVIRIS program was a significant precursor and driving force for HRS technology as a whole and one must appreciate the efforts made by NASA to that end.

8.4 HRS Sensors

8.4.1 General

The growing number of researchers in the HRS community can be seen by their attendance at the yearly proceedings of the AVIRIS Workshop Series, organized by JPL since 1985 (starting with AIS, and today with HySPRI–see later) and other workshops organized by international groups such as: WHISPers and EARSel SIG IS. In 1993, a special issue of Remote Sensing of Environment was published, dedicated to HRS technology in general and to AVIRIS in particular (Vane, 1993). This broadened the horizon for many potential users who still had not heard about HRS technology, ensuring that the activity would continue. Today, new HRS programs are up and running at NASA, such as the M^3 project in collaboration with the Indian Space Agency to study the moon's surface, along with preparations to place a combined optical and thermal hyperspectral sensor in orbit (the HyspIRI project, Knox et al. (2010)). In addition to the AIS and AVIRIS missions, NASA also successfully operated a thermal hyperspectral mission known as TIMS (Thermal Infrared Multispectral Scanner) in ca. 1980-1983 (Kahle and Goetz, 1983), and also collaborated on other HRS initiatives in North America. The TIMS and then later, the ASTER spacecraft sensors showed the thermal region's promising capability for obtaining mineral-based information. Apparently, the TIR HRS capability due to it costs and performance was set aside, and it has only recently begun to garner new attention, in new space initiatives (HyspIRI) and in new airborne sensors (e.g., TASI–600 and MASI600 from ITRES, Hyper–Com from TELOPS, SEBASS from Aerospace Corporation, and Owl from SpecIm). In parallel to the US's national HRS activity, a commercial HRS sensor was developed in ca. 1980. The Geophysical & Environmental Research Corporation (GER) of Millbrook, NY developed the first commercial HRS system which acquired 576 channels across 0.4 to 2.5 μm in 1981, first described by Chiu and Collins (1978). After the GER HRS came a 63–channel sensor (GERIS-63) that was operated from around 1986 to 1990: this was a whiskbroom sensor that consisted of 63 bands (15–45 nm bandwidth) across the VIS–NIR–SWIR region with a 90° FOV (Ben–Dor et al., 1994). The sensor was flown over several areas worldwide and demonstrated the significant potential of the HRS concept. Although premature at that time, GER then began to offer commercial HRS services. However, it appears that the market was not yet educated enough and the very few scientists that were exposed to this technology at the time could not support the GER activity. Thus, the GER initiative was ahead of its time by about two decades, and it reestablished its commercial activity in 2000.

The GER sensor was brought to Europe in May and June 1989 for demonstration purposes and a campaign organized by several European users (known as EISAC-89) was conducted. The results of this mission were impressive and pushed the European community to learn more about this technology (Itten, 2007). At around the time of the first AIS mission (1981), the Canadians had also developed an imaging device known as FLI (fluorescence line imager). In the mid 1980s, Canada Monitec Ltd. developed and used a limited pushbroom scanner, the FLI / PMI, with 228 channels across 430 to 805 nm (Borstad et al., 1985; Gower and Borstad, 1989). This sensor was also brought to the EISAC–89 campaign and in 1991, the first EARSeL Advances in Remote Sensing issue (Volume 1, Number 1, February 1991), which was dedicated to HRS, provided the outcomes of this campaign, demonstrating that atmospheric attenuation, calibration and validation were the major issues that needed to be tackled. It is interesting to note that most of the authors were satisfied with the results but their demand for more data was blocked by an inability to access data and sensors until DLR entered the scene. DLR's interest in HRS began in around 1986 when they announced plans for ROSIS (a pushbroom instrument offering 115 bands between 430 and 850 nm) which only became operational in 1992 and was continuously upgraded until 2003 (Holzwarth et al., 2003; Doerffer et al., 1989; Kunkel et al., 1991). In 1996, DLR owned and operated the DAIS 7915 (GER) sensor (see further on) and then operated the HyMAP (hyperspectral mapping) in several campaigns in Europe and Africa. They recently own the HySpeX sensor, together with GFZ in Germany (2012) that will enable freedom and comfort to operate HSR sensor with out leaning on a third party. Both bodies (DLR and GFZ) together with other German groups initiated, in 2007, a new and ambiguous initiative to place high–quality HRS sensor in orbit, termed EnMap (see further on).

Based on the growing interest of the EU scientific community in HRS technology, especially after the successful EISAC–89 campaign, it was obvious that AVIRIS, the most advanced sensor at that time, would be brought to Europe for a large campaign. AVIRIS was deployed in the Mac–Europe campaign in 1991 (Clever, 1999) onboard the NASA ER-2 aircraft, and covered test sites in Germany, The Netherlands, France, Iceland, Italy, England, Spain, Austria, see Itten et al. (1992). The success of the campaigns on the one hand, and the complexity and cost involved in bringing AVIRIS (or any other HRS sensor) on the other, were the driving forces for a new initiative in Europe to be independent in term of sensors, data availability, research capacity and experience. This led to the purchase of HRS sensors by several bodies in Europe: in Germany (CASI, by the Free University of Berlin and DAIS 7915 by DLR) and in Italy (MIVIS by CNR). In addition, plans were made for the development of more general sensors for the benefit of all EC members and were established via the ESA PRODEX project APEX (Itten et al., 2008), and by some limited commercial activities. The DAIS–7915 was a GER whiskbroom instrument characterized by 72 channels across the VIS–NIR–SWIR region and 7 bands in the TIR region (3.0–12.6 μm). It had a 26° FOV and GIFOV between 5 and 20 m. This instrument was offered in 1996 as a large-scale facility instrument to European researchers, and served as a test-bed in a large number of international flight campaigns. Although it was not the ideal sensor in terms of SNR and operational capabilities, the DAIS 7915 was operated by DLR until 2002 when it could no longer satisfy the higher SNRs being requested by the community. The experience gained from the DAIS 7915 campaigns was very valuable in terms of opening up the HRS field to more users, developing independent operational and maintenance capabilities, educating the younger generation and opening fruitful discussions among emerging HRS community members in Europe. Italy's activity in HRS technology began in 1994 with the purchase and operation of the MIVIS system, a Daedalus whiskbroom sensor, by the CNR. The MIVIS is a passive scanning and imaging instrument that is composed of four spectrometers which simultaneously record reflected and emitted radiation. It has 102 spectral bands from the VNIR to the TIR spectral range and the wavelength ranges between 0.43 and 12.7 μm, with an IFOV of 2 mrad and a digitized FOV of 71.1°. The band position was selected to meet research needs that were already known at that time for environmental remote sensing, such as agronomy, archeology, botany, geology, hydrology, oceanography, pedology, urban planning, atmospheric sciences, and more. The CNR under the LARA project has flown the instrument very intensively since 1994 onboard a CASA 212 aircraft, acquiring data mostly over Italy but also in cooperation with other nations, such as Germany, France and the US (Bianci et al., 1996).

In Canada, a new airborne VIS–NIR sensor was developed in 1989 by ITRES (Alberta, Canada), known as CASI (compact airborne spectrographic imager). The sensor was a pushbroom programmed sensor aimed at monitoring vegetation and water bodies. ITRES provided data-acquisition as well as processing services and also sold a few instruments to individuals who operated the system and then developed measurement protocols for a limited market (the Free University of Berlin in 1996). In 1996, ITRES developed a research instrument for Canadian Center for Remote Sensing (CCRS) known as SFSI (shortwave infrared full spectrum imager), and recently (2010), they developed an instrument for the TIR region (8-11.5 mm) named TASI-600 and an instrument for the MIR region (3-5 mm) named MASI-600 with 64 channels (55 nm bandwidth). The CASI offers several modes, between 512 bands (spectral modes) and 20 preselected bands (spatial modes), with intermediate numbers of spectral bands and pixels being programmable. The spectral range is between 400 and 1000 nm with a FOV of 29.6° and a GFOV of 2.1 mrad. The SFSI provides 120 bands (115 used in practice) across the 1219 to 2445 nm spectral region.

The FOV is 9.4° and across-track pixels' IFOV is 0.33 mrad. The TASI-600 is a pushbroom thermal imager with 64 / 32 spectral channels ranging from 8 to 11.5 nm with 600 pixels across track. The FOV is 38° and the IFOV is 0.49 mrad. The MASI-600 has 64 bands across 3 to 5 mm with 32 nm bandwidth and a FOV of 40° and IFOV of 1.2 mrad. ITRES provides to the community also the SASI sensor operates across the SWIR region (950-2450nm) with 100 spectral bands at 15nm sampling interval and 40o FOV. The National research Council of Canada modify the SASI sensor to have 160 spectral channels covering the 850 nm to 2500 nm spectral range and 38o FOV.

8.4.2 Current HRS Sensors in Europe

Another HRS company, the Finnish Specim-Spectral Imaging Ltd., has gone quite a long way and can be considered an important benchmark in the HRS arena. From 1995, when the company was founded, they were able to significantly reduce the cost of HRS sensors, making them available to many more users. Two airborne sensors, AISA-Eagle and AISA-Hawk for the VIS–NIR and SWIR regions, respectively, were developed, using the PGP (prism-grating-prism) concept invented by Specim in the 1990s. The PGP design enables the construction of a small low–cost spectrometer that is suitable for industrial and research purposes in the wavelength range of 320 to 2700 nm. Its small size and ease of maintenance and operation, along with the ability to mount the sensor onboard small platform, have made the Specim sensor accessible to many users who could not otherwise afford to enter the expensive HRS field. According to Specim, in 2010 more than 70 instruments had been sold worldwide, reflecting the growing interest in this technology in general and in low–cost capability in particular. This revolution has enabled user independence in terms of data acquisition and operation while providing a breakthrough in HRS strategy in Europe: no longer does one need to count on joint campaigns; the user can plan the mission and the flight, and process the data for his / her particular needs at a relatively low cost. Although the SNR and data performance of the new IS was not at the level of AVIRIS or HyMAP, the Specim products enabled enlarging HRS capabilities in mission planning, simulation, flight operation, data acquisition, archiving, corrections, calibration and education. Riding on their success, Specim announced, in 2009, that 'contracts for a total value of €1.4 M' had been signed with governmental institutions and private remote sensing companies in Germany, Malaysia, Brazil and China.

Recent achievements in HRS technology are due, to a certain extent, on the fact that more companies are building and manufacturing small-size HRS sensors for ground and air applications (e.g., HeadWall Photonics: http://www.headwallphotonics.com/). Whereas the VIS–NIR sensor is much easier to build, as it is based on available and reliable detectors, the SWIR region is still more problematic.

Two more activities in Europe can be considered milestones in HRS technology: the first is INTA Spain's activity in HRS and the second is the Norwegian company Norsk Elektro Optikk (NEO), which manufactured a new HRS sensor. In 2001, INTA (Instituto Nacional de Tecnica Aeroespacil) Spain entered the HRS era by first exploring the field and then running a joint venture with Argon ST (a company resulting from a merger between Daedalus Enterprises and S.T. Research Corporation) in 1998, conducting their first campaign in ca. 2003 in Southern Spain. The follow-up campaigns demonstrated the HRS concept's promise and in 2005, the AHS was purchased by INTA: it was first operated in Spain and then in other European countries as well. The AHS consisted of 63 bands across the VIS–NIR–SWIR region and 7 bands in the TIR region with a FOV of 90° and IFOV of 2.5 mrad, corresponding to a ground-sampling distance (GSD) of 2 to 7 m. This sensor was flown onboard a CASA 212 aircraft and operated by personal from INTA. The sensor has been operational in Spain and Europe (via ESA (European Space Agency) and VITO (Vlaams Instituut Voor Technologisch Onderzoek)

) since 2005 and remains in good condition. The system is well maintained and undergoes a yearly check-up at Argon ST laboratories. Experience gained over the years, along with mechanical upgrading (both electronic and optical), ensure that the sensor will stay operational for a long time.

In ca. 1995, NEO developed a small IS satellite sensor (HISS - Hyperspectral Imager for Small Satellites) for ESA, covering the spectral range from 400 nm to 2500 nm. As ESA did not have any immediate plans for launching such an instrument at the time, the experience gained from the HISS was used to develop a hyperspectral camera for airborne applications-the ASI. The first prototype was built in 1998-99. In 2001, a collaboration with the Norwegian Defense Research Establishment (FFI) was initiated which is still continue today. In the framework of this cooperation, the ASI (Applied Spectral Imaging) camera participated in a multinational military measurement campaign in France in 2002. An upgraded version of the instrument was flown in 2003 and 2004 in different multinational military field trials. In 2004, airborne HRS data were also acquired for several local civilian research institutions. The cooperation with these institutions was continued in 2005 when a further upgraded version of the instrument was flown successfully, including a HRS camera module covering the SWIR region (900-1700 nm), in addition to the VIS and NIR region (400-1000 nm). All of these research activities led to the development of a line of hyperspectral cameras (HySpex) which are well suited for a wide variety of applications in both the civilian and military domains. Main characteristics of the sensor are coverage of the entire range (400-2500 nm) with more than 400 bands with 3.7 and 6.25 nm band width two different sensors (the VNIR 640 and SWIR 320). The sensor underwent several experiments in Europe with proven success but has not yet aggressively entered the commercial remote sensing arena.

Beside the AVIRIS sensor, today the HyMAP sensor has become available: this is a commercially designed and operated system that was based on the Probe-1 sensor (operated in ca. 1998 by Applied Signal and Image Technology (ASIT) USA). Several campaigns in the US demonstrated the promising commercial capability of HRS technology (Kruse et al., 2000). Integrated Spectronics Australia designed and operated the HyMAP sensor for rapid and efficient wide-area imaging for mineral mapping and environmental monitoring. The sensor can be defined as a high SNR instrument with high spectral resolution, ease of use, a modular design concept, calibrated spectroradiometry, proven in-field operation and heavy load capacity. It is a whiskbroom sensor with 100 to 200 bands (usually 126) across the 450 to 2450 nm spectral region with bandwidths ranging from 10 to 20 nm. The SNR is in the range of 500:1 with 2 to 10 m spatial resolution. It is characterized by a 60° to 70° swath width and furnished with an onboard radiometric and spectral calibration assembly. In 1999, a group shoot using the HyMAP sensor was conducted in the US. A report by Kruse et al. (2000) declared the sensor to be the best available at the time. Since then, the HyMAP sensor has been operated worldwide, providing high-quality HRS data to its end-users and opening up a new era in HRS data quality. It has been operated in Europe, Australia, the US and Africa in specific campaigns and through Hy Vista activity, which provides end-to-end solutions for the potential customer. HyMAP can thus also be considered a benchmark in HRS technology, which was reached in ca. 1999 by Probe-1 and then afterwards by HyMAP sensors. The problem with HyMAP is that the sensor is limited and is operated only byHyVista, and hence its use is strongly dependent on their schedule and availability. Moreover, the cost of the data is still prohibitive for the daily-use capability that is desired from HRS technology. It can be concluded that there is still a significant gap between high SNR and low cost / easy operation in sensors: ideally, this gap might be bridged by fusing the AISA and HyMAP characteristics that are based on two different technologies: push broom and whisk broom respectively. As more and more companies undertake moving HRS technology forward, we believe that in the near future such a fusion will be possible and we will see more low–cost, high-quality data and more applications emerging from this capability.

The above provides only the milestone stages in HRS technology over the years. Several of the sensors and activities may not have been mentioned. The reader is therefore directed to a comprehensive description of all HRS sensors until 2008 made by Prof. Gomez from George Mason University in the US, and to a summary of all remote sensing organizations worldwide and all institutes, private sectors and abbreviations commonly used with this technology at:www.tau.ac.il/ rslweb/pdf/HyperspectralImagingSystems.pdf . A historical list of HRS sensors compiled by Michael Schaepman is available from http://www.geo.unizh.ch/~schaep/research/apex/is_list.html

8.4.3 Satellite HRS Sensors

Among the airborne HRS benchmarks mentioned earlier, orbital HRS activity has contributed greatly to the blossoming HRS activity. The first initiative to place an HRS sensor in orbit took place in the early 1990s when a group of scientists chaired by Goetz started work on the NASA HRS mission HIRIS. This was part of NASA's High Resolution Imaging Spectrometer Earth Observation System program. The idea was to place an AVIRIS-like sensor in orbit with a full range between 0.4 and 2.5 μm and a spatial resolution of 30 m. A report that provides the capacity of this sensor, including its technical and application characteristics, was issued in several copies Goetz (1987). This report was the first document that showed the intention to go into space with HRS. The HIRIS mission was terminated, apparently due to the Challenger space shuttle disaster which significantly changed the space programs at NASA.

The scientists, however, agreed that using HRS in orbit is an important task that needs to be addressed Nieke et al. (1997). A report by Hlao and Wong (2000) submitted to the US Air Force in 2000 assessed the technology as still premature and still lagging behind other remote sensing technologies such as air photography. The next benchmark in orbital HRS was Hyperion, part of the NASA New Millennium Program (NMP). The Hyperion instrument was built by TRW Inc. (Northrop Grumman Space Technology) using focal planes and associated electronics remaining from the Lewis spacecraft, a product of the NASA Small Satellite Technology Initiative (SSTI) mission that fell in 1997. The integration of Hyperion took less than 12 months from Lewis's spare parts and was sent into orbit onboard the EO-1 spacecraft. The mission, planned for 3 years, is still operational today with a healthy sensor and data, although the SNR is poor. The instrument covers the VIS–NIR–SWIR region from 422$,nm to 2395 nm with two detectors and 244 bands of 10 nm bandwidth. The ground coverage FOV provided a 7.5 km swath and 30 m GSD. The first datasets cost around 2500 USD and had a lower SNR than originally planned. Nonetheless, over the years, and despite its low quality, the instrument has brought new capability to sensing the globe by temporal HRS coverage, justifying the effort to place a better HRS sensor in space. As of the summer of 2009, Hyperion data are free of charge, which has opened up a new era for potential users. In ca. 2001, the CHRIS (compact high-resolution imaging spectrometer) sensor was launched into orbit onboard the PROBA bus. It was developed by the Sira Electro Optic group and supported by the European Space Agency (ESA).

The CHRIS sensor is a high spatial resolution hyperspectral spectrometer (18 m at nadir) with a FOV resulting in 14 km swath. One of its most important characteristics is the possibility of observing every ground pixel at the same time, in five different viewing geometry sets (nadir, $+/-55°$ and $+/-36°$). It is sensitive to the VIS–NIR region (410-1059 nm) and the number of bands is programmable, with up to 63 spectral bands. Although limited in its spectral region, the instrument provides a first view of the Bi Directional Reflectance Distribution Function (BRDF) effects for vegetation and water applications, and it is robust as it is still operating today. The "early" spaceborne planning missions in both the US and Europe comprised, among others, the following projects: IRIS, HIRIS (NASA), GEROS (GER, US), HERO (CSA), PRISM, Spectra (all ESA), SIMSA and SAND. Although most of these initiatives were not further funded and are not active today, they demonstrated governmental agencies' interest in investing in this technology, albeit with a fearful and cautious attitude. Other orbital sensors, such as MODIS, MERIS and ASTER, can also be considered part of the HRS activities in space, but in terms of both spatial (MODIS and MERIS) and spectral (ASTER) resolution, these sensors and projects still lag behind the ideal HRS sensor that we would like to see in orbit with high spectral (more than 100 narrow bands) and spatial (less than 30 m) resolutions. It is important to mention, however, that a new initiative to study the moon and Mars using HRS technology is currently active under a collaboration between NASA and ISA (India), within which the M3 mission to the moon has recently provided remarkable results by mapping a thin layer of water on the moon's surface (Pieters et al., 2009b,a). In addition, missions to Mars, such as CRISM (Compact Reconnaissance Imaging Spectrometer for Mars) show that it is now understood that HRS technology can provide remarkable information about materials and objects remotely.

EnMAP (Environmental Mapping and Analysis Program) is a German hyperspectral satellite mission providing high-quality hyperspectral image data on a timely and frequent basis. Its main objective is to investigate a wide range of ecosystem parameters encompassing agriculture, forestry, soil and geological environments, coastal zones and inland waters. This will significantly increase our understanding of coupled biospheric and exospheric processes, thereby enabling the management and guaranteed sustainability of our vital resources. Launch of the EnMAP satellite is envisaged for 2015 (updates in 2012). The basic working principle is that of a pushbroom sensor, which covers a swath (across-track) width of 30 km, with a GSD of 30 x 30 m. The second dimension is given by the along-track movement and corresponds to about 4.4 ms exposure time. This leads to a detector frame rate of 230 Hz, which is a performance-driving parameter for the detectors, as well as for the instrument control unit and the mass memory. HySPIRI is a new NASA initiative to place a HRS sensor in orbit and is aimed at complementing EnMAP, as its data acquisition covering the globe periodically.

It is important to mention that other national agencies are aiming to place HRS sensor in orbit as well. A good example is PRISMA of the Italy's space agency. PRISMA is a pushbroom sensor with swath of 30–60 km, GSD of 20–30 m (2.5–5 m PAN) with a spectral range of 0.4–2.5 μm. The satellite launch was foreseen by the end of 2013, but it seems that some delay is encountered and the new lunch date is unknown.

To keep everyone up to date and oriented on the efforts being made in HRS pace activities, a volunteer group was founded in November of 2007 by Dr. A. Held and Dr. K. Staenz named ISIS (International Satellite Imaging Spectrometry, http://www.isiswg.org). The ISIS group provides a forum for technical and programming discussions and consultation among national space agencies, research institutions and other spaceborne HRS/IS data providers. The main goals of the group are to share information on current and future spaceborne IS ("hyperspectral") missions, and to seek opportunities for new international partnerships to the benefit of the global user community. The initial "ISIS Working Group" was established following the realization that there were a large number of countries planning IS ('hyperspectral') satellite missions with little mutual understanding or coordination. Meetings of the working group have been held in Hawaii (IGARSS 2007), Boston (IGARSS 2008), Tel Aviv (EARSeL 2009), Hawaii (IGARSS 2010), and Ottawa (IGARSS 2011). The technical presentations by the ISIS group have garnered interest from space agencies and governmental and industrial sectors in this promising technology. An excellent review on current and planned civilian space hyperspectral sensor for Earth observation is given by Buckingham and Staenz (2008).

8.5 Potential and Applications

Merging of spectral and spatial information, as is done within HRS technology, provides an innovative way of studying many spatial phenomena at various resolutions. If the data are of high quality, they allow near-laboratory level spectral sensing of targets from afar. Thus, the information and knowledge gathered in the laboratory domain can be used to process the HRS data on a pixel-by-pixel basis. The "spheres" that can feasibly be assessed by HRS technology are: atmosphere, pedosphere, lithosphere, biosphere, hydrosphere and cryosphere. Different methods of analyzing the spectral information in the HRS data are known, the basic one consisting of comparing the pixel spectrum with a set of spectra taken from a well-known spectral library. This allows the user to identify specific substances, such as minerals, chlorophyll, dissolved organics, atmospheric constituents, and specific environmental contaminants, before moving ahead with other more sophisticated approaches. The emergence of hyperspectral imaging moved general remote sensing applications from the area of basic landscape classification into the realm of full spectral quantification and analysis. The same type of spectroscopy applications which have been utilized for decades by chemists and astronomers are now accessible through both NADIR and oblique viewing applications. The spectral information enables the detection of indirect processes, such as contaminant release, based on changes in spectral reflectance of the vegetation or leaves. The potential thus lies in the spectral recognition of targets using their spectral signature as a footprint and on the spectral analysis of specific absorption features that enable a quantitative assessment of the matter in question. Although many applications remain to be developed, within the last decade, significant advances have been made in the development of applications using hyperspectral data, mainly due to the extensive availability of today's airborne sensors. Whereas a decade ago, only a few sensors were available and used in the occasional campaign, today, many small and user-friendly HRS sensors that can operate on any light aircraft are available. Hydrology, disaster management, urban mapping, atmospheric study, geology, forestry, snow and ice, soil, environment, ecology, agriculture, fisheries and oceans and national security are only a few of the applications for HRS technology today. In 2001, van der Meer and De Jong published a book with several innovative applications for that time (van der Meer and Jong, 2001). Since then, new applications have emerged and the potential of HRS has been discussed and analyzed by many authors at conferences, in proceedings papers and full-length publications. In a recent paper, Staenz (2009) provides his present and future notes on HRS, which very accurately summarize the technology up to today. In the following, we paraphrase and sharpen Staenz's points. It is clear from the numerous studies which have been carried out that HRS technology has significantly advanced the use of remote sensing in different applications (e.g., AVIRIS 2007). In particular, the ability to extract quantitative information has made HRS a unique remote sensing tool. For example, this technology has been used by the mining industry for exploration of natural resources, such as the identification and mapping of the abundance of specific minerals. HRS is also recognized as a tool to successfully carry out ecosystem monitoring, especially the mapping of changes due to human activity and climate variability. This technology also plays an important role in the monitoring of coastal and inland waters. Other capabilities include the forecasting of natural hazards, such as mapping the variability of soil properties which can be linked to landslide events and monitoring environmental disturbances, such as resource exploitation, forest fires, insect damage and slope instability in combination with heavy rainfall. As already mentioned, HRS can be used to assess quantitative information about the atmosphere such as water vapor content, aerosol load, methane, carbon dioxide and oxygen content. HRS can also be used to map snow parameters, which are important in characterizing a snow pack and its effect on water runoff. Moreover, the technology has shown potential for use in national security, e.g., in surveillance and target identification, verification of treaty compliance (e.g., Kyoto Accord on Greenhouse Gas Emission), and disaster preparedness and monitoring (Staenz, 2009). Some recent examples show both the quantitative and exclusive power of HRS technology in: detection of soil contamination (e.g.Kempter and Sommer (2003)), soil salinity (e.g., Ben–Dor et al. (2002)), species of vegetation (e.g., Ustin et al. (2008)), atmospheric EM imissions of methane (Noomem et al., 2005), Detection of ammonium (Gersman et al., 2008), asphalt condition (Herold. et al., 2008), water quality (Dekker et al., 2001) and urban mapping (Ben–Dor, 2001). Many other applications can be found in the literature and still others are in the R&D phase in the emerging HRS community. Nonetheless, although promising, one should remember that HRS technology still suffers from some difficulties and limitations. For example, the large amount of data produced by the HRS sensors hinders this technology's usefulness for geometry analysis or for visual cognition (e.g., building structures and roads) and one has to weight the added value promised by the technology for one's applications. There are other remote sensing tools and the user should consult with an expert before using HRS technology. Since the emergence of HRS, many technical difficulties have been overcome in areas such as sensor development, data handling, aviation and positioning, and data processing and mining. However, there are several main issues today which require solutions to move this technology toward more frequent operational use. These include: a lack of reliable data sources with a high SNR are required to retrieve the desired information and temporal coverage of the region of interest; although analytical tools are now readily available, there is a lack of robust automated procedures to process data quickly with a minimum of user intervention; the lack of operational products is obviously due to the fact that most efforts to date have been devoted to the scientific development of HRS; interactions with other HRS communities have not yet developed-there are many applications, methods and know–how in the laboratory–based HRS disciplines, but no valid connection between the communities; systems that can archive and handle large amounts of data and openly share the information with the public are still lacking; only a thin layer of the surface can be sensed; there is no standardization for data quality or quality indicators; not much valid experience exists in merging HRS data with that of other sensors (e.g., LIDAR, SAR); many sensors have emerged in the market but their exact operational mechanism is unknown, biasing an accurate assessment; thermal HRS sensors are just starting to emerge (whereas point thermal spectrometers are existing ; Christensen et al. (2000)); oblique view and ground–based HRS measurements have not yet been developed: the cost of deriving the information product is too high, since the analysis of HRS data is currently too labor-intensive (not yet automated); it is not yet recognized by potential users as a routine vehicle such as, for example, air photography; not too many experts in this technology are available. Several authors have summarized this technology's potential to learn from history, such as Itten (2007); Schaepman et al. (2009) and Staenz (2009).

It is anticipated that HRS technology will catch up when new high-quality sensors are placed in orbit and the data become available to all (preferably in reflectance values), when the air photography industry uses the HRS data commercially, and when new sensors that are inexpensive and easy to use are developed along with inexpensive aviation (such as UnmAnned Vehicled UAV).

8.6 Sensor Principles

Imaging spectrometers typically use a 2D matrix array (e.g., a Charge Couple Device (CCD) or Focal Plane Array (FPA))that produces a 3D data cube (spatial dimensions and a third spectral axis). These data cubes are built in a progressive manner by (1) sequentially recording one full spatial image after another, each at a different wavelength, or (2) sequentially recording one narrow image (1 pixel wide, multiple pixels long) swath after another with the corresponding spectral signature for each pixel in the swath. Some common techniques used in airborne or spaceborne applications are depicted in Figure 8.2. The first two approaches shown are basic ones, used to generate images such as those used in LANDSAT (Figure 8.2a) and SPOT (Figure 8.2b). They show the concept of measuring reflected radiation in a discrete detector or in a line array.

Multichannel sensors such as LANDSAT TM are optical mechanical system un which discrete, fixed detector elements are scanned across the target perpendicular to the flight path by a mirror and these detector convert the reflected solar photons from each pixel in the scene into an electronic signal . The detector elements are placed behind filters that pass broad portion of the spectrum. One approaches to increase the residence time of a detector in the UFOV is to use line arrays of detector elements (Figure 8.5b. This type of sensor is presented by the French satellite sensor SPOT.

There are limitations and trade-offs associated with the use of multiple line arrays, each with its own spectral band-pass filter. If all of the arrays are placed in the focal plane of the telescope, then the same ground locations are not imaged simultaneously in each spectral band. If a beam-splitter is used to facilitate simultaneous data acquisition, the signal is reduced by 50 % or more for each additional spectral band acquired in a given spectral region. Furthermore, instrument complexity increases substantially if more than 6 to 10 spectral bands are desired. Two other approaches to IS are shown in Figure 8.2c, 8.2d. The line array approach (also known as whiskbroom configuration) and the area array approach (also known as pushbroom configuration). The line array approach is analogous to the scanner approach (Figure 8.2b), except that the light from a pixel is passed into a spectrometer where it is dispersed and focused onto a line array. Thus, each pixel is simultaneously sensed in as many spectral bands as there are detector elements in the line array. For high spatial resolution imaging of ground IFOVs of 10m to 30 m, this concept is suitable only for an airborne sensor that flies slowly enough so that the integration time of the detector array is a small fraction of the integration time. Because of the high velocities of spacecraft, an imaging spectrometer designed for the Earth's orbit requires the use of two distinguished area arrays of the detector in the focal plane of the spectrometer (Figure 8.2d), thereby obviating the need for an optical scanning mechanism (pushbroom configuration).

Area arrays of up to 800x800 elements of silicon were developed for wide-field and planetary camera. However the stat of infrared array development for wavelength beyond 1.1mm is not so advance. Line array are available in several materials up to few hindered detector elements in length. Two of the most attractive materials are mercury-cadmium-telluride (HgCdTe) and indium antimonite (InSb). InSb array of 512 elements having very high quantum efficiency and detector with similar element-to-element responsibility have developed. The InSb arrays respond to wavelengths from 0.7–5.2 mm. A comprehensive description of both push broom and whisk broom technologies with advantageous and disadvantageous can be found in Sellar and Boreman (2005).

The key to HRS/IS is the detector array. Line arrays of silicon, sensitive to radiation at wavelengths of 035 to 1.1 μm, are available commercially in dimensions of up to 5,000 elements in length. The state of IR array development for wavelengths beyond 1.1 μm is not yet advanced. Two of the most attractive materials are mercury cadmium telluride (HgCdTe) and indium antimonite (InSb).

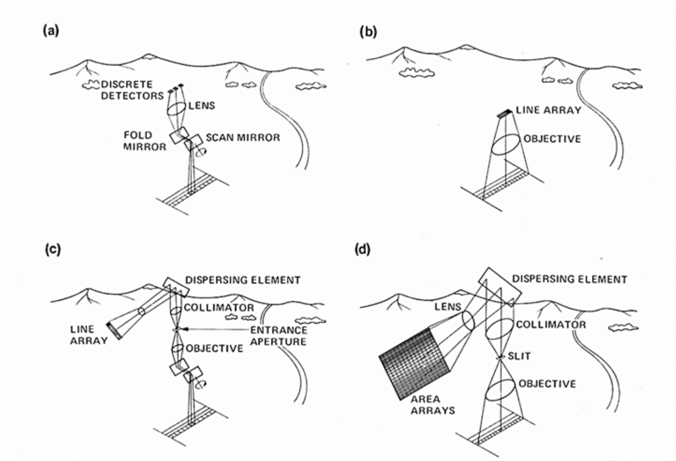

Fig. 8.2 Four approaches to sensors for multispectral imaging: (a) multispectral imaging with discrete detectors (LANDSAT type); (b) multispectral imaging with line arrays (SPOT type); (c) imaging spectroscopy with line arrays (AVIRIS type, whiskbroom); (d) imaging spectroscopy with area array (AISA type, pushbroom).

8.7 Planning of an HRS Mission

In this section, we describe the planning of a mission for an airborne campaign: we do not cover the possible activities involved for a spaceborne mission. Planning a mission is a task that requires significant preparation and knowledge of the advantages and disadvantages of the technology. The idea behind using HRS is to get an advanced thematic map as the final product which no other technology can provide. In the planner's mind, the major step toward achieving the main perquisite of a thematic map is to generate a reflectance or emission image from the raw data. First, a scientific (or applicable) question has to be asked, such as: Where can saline soil spots be found over a large area? For such a mission, the user has to determine whether there exists spectral information on the topic which is being covered by the current HRS sensor. This investigation might consist of self-examination or a literature search of both the area in question and the advantageous of using HRS (many times HRS is an overkill technology for answering simple thematic questions) . Once this investigation is done, the question is: What are the exact spectral regions that are important for the phenomenon in question and what pixel size is needed? In addition, the question of what SNR values will enable such detection should be raised. Having this information in hand, the next step is to search for the instrument. Sometimes a particular instrument is available and there is no other choice. In this case, the first spectral investigation stage should focus on the available HRS sensor and its spectral performances (configuration, resolution, SNR ect.) infrastructure. It is recommended that the spectral information on the thematic question be checked at the sensor-configuration stage. In some sensors, especially pushbroom ones, it is possible to program the spectral configuration using a new arrangement of the CCD assembly. In this respect, it is important that the flight altitude be taken into consideration (for both pixel size and integration time) along with aircraft speed. Most sensors have tables listing these components and the user can use them to plan the mission frame. As within this issue the user can configure the bands with different Full Width Half Max (FWHM) and positions, it should be remembered that combined with spatial resolution, this might affect the SNR. When selecting the sensor, it is important to obtain (if this is the first use) a sample cube to learn about the sensor's performance. It is also good to consult with other people who have used this equipment. Getting information on when and where the last radiometric calibration was performed as well as obtaining information about the sensor stability and uncertainties is very important. It is better if the calibration file of the sensor is provided but if not, the HRS owner should be asked for the last calibration date and its temporal performances. Quality Assurance (QA) of the sensor's radiance must be done in order to assure a smooth step to the next stage namely atmospheric correction. Methods and tools to inspect these parameters were developed under EUFAR JRA2 initiative and recently also by Brook and Ben Dor 2011. The area in question is generally covered by 30 % overlap between the lines. This has to be carefully planned in advance taking into consideration the swath of the sensor and other aircraft information (e.g. stability, length on the air, speed and altitude preferences, navigation systems). A preference for flying toward or against the direction of the Sun's azimuth needs to be decided upon, and it is recommended that the Google Earth interface be used to allocate the flight lines and to provide a table for each line with starting and ending points for all flight lines. One also needs to check if the GPS (Ground Positioning System) INS (Inertial Navigation System) system is available and configure the system to be able to ultimately allocate this information in a readable and synchronized form.

A list of go / no go items should be established. For instance, a forecast for the weather should be on hand 24 h in advance, with updates every 3 h. If possible, a representative should be sent to the area in question to report on cloud coverage close to acquisition time. In our experience, one should be aware of the fact that a 1 / 2 cover over the area in question will turn into almost 100 % coverage of the flight lines that appeared to be free of clouds. Moreover, problems that may emerge at the airport need to be taken into consideration, such as: the GPS system is not functioning or the altitude obtained from air control is different from that which was planned. The go / no go checklist should be used for these issues as needed. Each go / no go list is individual, and one should be established for every mission.

The aircrew members (operators, navigator and pilot) must be briefed before and debriefed after the mission. A logbook document should be prepared for the aircrew members (pilot and operator) with every flight line reported by them. It is important to plan a dark current acquisition before and after each line acquisition. Acquisition of a vicarious calibration site (in the area of interest or on the way to this area) in question should also be planned for, that is well prepared and documented in advance. Radio contact with the aircrew should be obtained at a working frequency before, during and after the overpass. A ground team should be prepared and sent to the area in question for the following issues: (1) calibrating the sensor's radiance and examining its performance (Brook and Ben-Dor, 2011), (2) validating the atmospheric correction procedure and (3) collecting information that will be useful further on for thematic mapping (e.g., chlorophyll concentration in the leaves). The ground team should be prepared according to a standard protocol and it should be assured that they are furnished with the necessary equipment (such as video and still cameras, field spectrometer, maps, Sun photometer and GPS). After data acquisition, the data should be immediately backed up and quality-control checks run to determine data reliability. Afterwards, the pilot logbook, ground documentation and any other material that evolved during the mission should be collected.

In general and to sum up the above: A mission has to be leaded by a senior person who is responsible to coagulate the end user needs, the ground team work, the airborne crew activity and the processing stages done by experts. He is responsible to interview the end user and understand the question at hand, he responsible to allocate a sensor for the mission and meet with the sensor owner and operator ahead of the mission and arrange a field campaign by a ground team. Other responsibilities such as arranging logistics and briefing of all teams as well as backing up the information just after the mission end i.e. at the airport are also part of his duties and are very important. A checklist and documents on every stage are available in many bodies (e.g. DLR, TAU) but in general it can be developed by any group by gathering information from main HSR leading bodies (DLR, NASA, INTA).

8.7.1 Spectrally–Based Information

A A sensed matter interact with electromagnetic (EM) radiation where photons are absorbed or emitted via several processes. On the Earth's surface (solid and liquid) and in its atmosphere (gasses and aerosols), the interaction across the VIS–NIR–SWIR-TIR regions is sensed by HRS means to give addi-

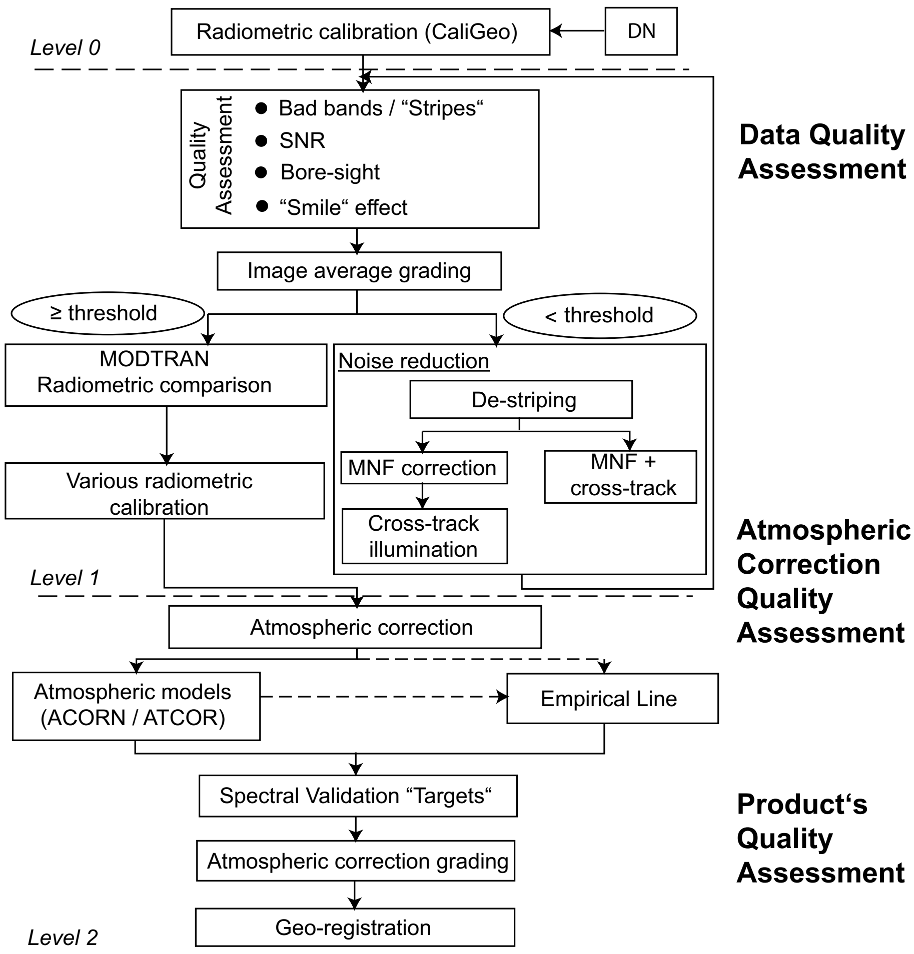

Fig. 8.3 A data processing chain, as used at RSL-TAU (Remote Sensing Laboratory at Tel Aviv University) with the AISA–Dual sensor. Note that at three stages, quality assurance is crucial: the raw data (including radiance), the atmospheric correction stage (reflectance and emittance) and the thematic mapping stage.

tional spectral information relative to the common multiband sensors . The spectral response of the EM interaction with matter can be displayed as radiance, reflectance, transmittance or emittance, depending on the measurement technique and on the illumination source used. Where interactions occur, a spectrum shape can be used as a footprint to assess and identify the matter in question. Variations in the position of local minima (or maxima, termed "peaks") and baseline slope and shape are the main indicators used to derive quantitative information on the sensed material. The substance (chemical or physical) that significantly affects the shape and nature of the target's spectrum is termed "chromophore". A chromophore that is active in energy absorbance (e.g., chlorophyll molecule in vegetation) or emission (e.g., fluorescence) at a discrete wavelength is termed a "chemical chromophore". A chromophore that governs the spectrum's shape [such as the slope and albedo (e.g., particle size, refraction index)] is termed "physical chromophore". Often, the spectral signals related to a given chromophore overlap with the signals of other chromophores, thereby hindering the assessment of a specific chromophore. The spectrum of a given sample, which is the result of all chromophores' interactions, can be used to analyze and identify the matter if a spectral-based method for that end spectrum is used. Fourier , and other spectral tools (e.g., Wavelet Transforms, Principle Component Analysis) that are usually applied to laboratory spectra can be excellent tools for application to HRS data provided the data are of good quality. A comprehensive review of chemical and physical chromophores in soils and rocks, as an example, can be found in Irons et al. (1989); Ben–Dor et al. (1999); Clark (1999); Malley et al. (2004); McBratney and Rossel (2006). A compilation table that provides the chromophores of known Earth targets in all spheres is given in Table 8.1. The table, which covers all spectral regions (VIS, NIR, SWIR and TIR), may be of interest for HRS technology from field, air and space levels.

The chemical chromophores in the VIS–NIR–SWIR regions refer to two basic chemical mechanisms: (1) overtones and combination modes in the NIR–SWIR region that emerge from the fundamental vibrations in the TIR regions and (2) electron processes in the VIS region which are in most cases crystal-field and charge–transfer effects. The physical chromophores in this region refer mostly to particle size distribution and to refraction indices of the matter in question. The electronic processes are typically affected by the presence of transition metals, such as iron, and although smeared, they can be used as a diagnostic feature for iron minerals (around 0.80–0.90 μm, crystal field and around 0.60–0.70 μm, charge transfer). Accordingly, all features in the VIS–NIR–SWIR–TIR spectral regions have a clearly identifiable physical basis. In solid–fluid Earth materials, three major chemical chromophores can be roughly categorized as follows: (1) minerals (mostly clay, iron oxide, primary minerals-feldspar, Si, insoluble salt, and hard–to–dissolve substances such as carbonates, phosphates, etc.), (2) organic matter (living and decomposing), and (3) water (solid, liquid, and gas phases). In gaseous Earth materials, the two main chemical chromophores are: (1) gas molecules and (2) aerosols of minerals, organic matter and ice.

Figure 8.2 presents a summary of possible chromophores in soils and rocks (from Ben–Dor et al. (1999)). Basically the (passive) EM sources for HRS are the Sun and Earth's radiation (Sun: VIS–NIR–SWIR, Sun and Earth: TIR). Assuming that in a photon pack emitted from a given source (E; E_S for Sun, E_E

Tab. 8.1 A summary of possible chromophores in all spheres of interest for our planet by remote sensing using the spectral.

350–1000 VIS–NIR nm

Sphere	Pedo-sphere	Litho-sphere	Bio-sphere	Hydro-sphere	Cryo-sphere	Atmo-sphere
Abs-Electronic	Fe, Ni+	Chloro-phyll+	+			
Scattering-Particles	Particle size,	Particle size,	Leaf Structure	Particle size,	Particle size,	Mie, Raleigh
Emission -			Fluorescence			
Abs-Overtones		OH- 3d	H_2O	H_2O		O_2, H_2O, O_3

100–2500 nm SWIR

Sphere	Pedo-sphere	Litho-sphere	Bio-sphere	Hydro-sphere	Cryo-sphere	Atmo-sphere
Abs-Electronic						
Scattering-Particles	Albedo-Particle size	Albedo-particle size	Leaf structure		Particle	Mie
Emission-Electronic						
Abs-Overtones Combi-nation modes	OH, C-H, N-H^+	+	+	H_2O	H_2O	H_2O, CO_2, O_2, CH_3

3000–12500 nm MIR–TIR

Sphere	Pedo-sphere	Litho-sphere	Bio-sphere	Hydro-sphere	Cryo-sphere	Atmo-sphere
Abs-Electronic						
Scattering-Particles						
Emission-Electronics	Temp	Temp	Temp	Temp	Temp	
ABS Funda-mentals	Emissivity, SI-O, Al-O, Fe-O	Emissivity, SI-O, Al-O, Fe-O	Emissivity C=O	Emissivity H_2, OM	Emissivity	SO_4

+: some other causes for the spectral mechanism visualization

for Earth), some may be absorbed (E_a), reflected (E_r) or transmitted (E_t)(at a given wavelength and incident angle). The energy balance (in term of fluxes) on a given sense target for every sphere (atmosphere, geosphere and hydro-

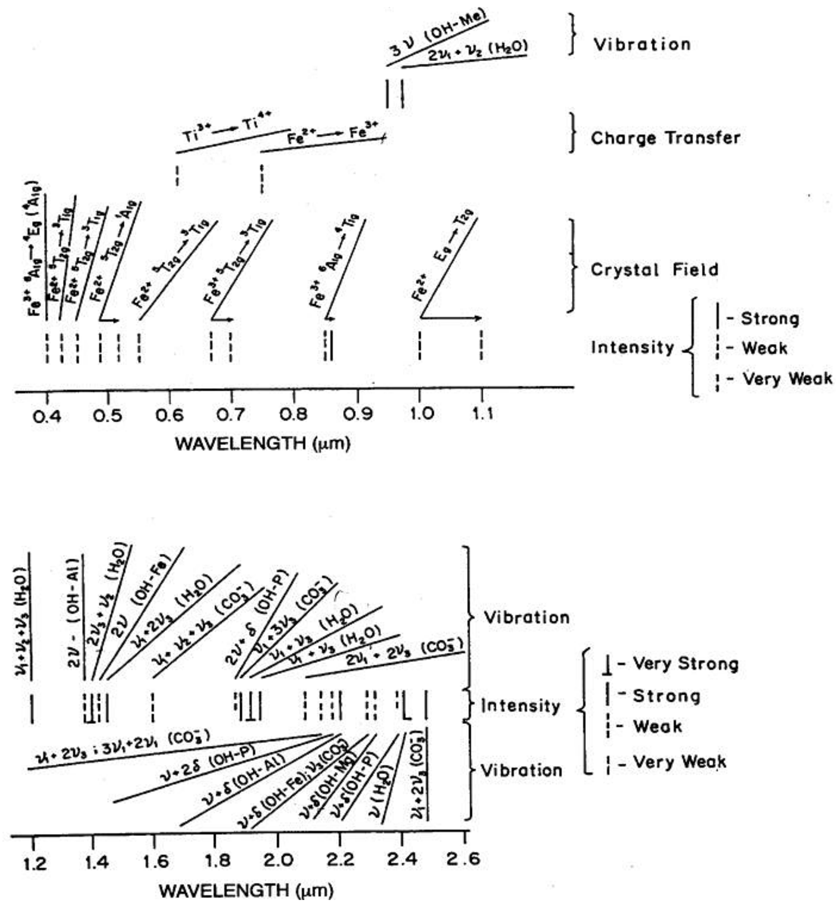

Fig. 8.4 Compilation of chromophores in soil and rocks: VIS–NIR electronic processes and overtones, SWIR overtones and combination modes, taken from Ben–Dor et al. (1999).

sphere) can be written (for every wavelength) as follows:

$$E = E_t + E_a + E_r \,, \tag{8.1}$$

where $E = E_S + E_E$ If we assume that we know the source energy (E_S), dividing Eq. (8.1) by E gives:

$$1 = \tau + \alpha + \rho \,, \tag{8.2}$$

where τ (transmittance), α (absorptance), ρ (reflectance) are coefficients of E_T, E_A, E_R, respectively describing each process's magnitude, and each can range from 0 to 1. In some cases, the Sun emits photons (Es) that pass through the atmosphere and hit the ground. Across the spectral range where the atmosphere is (semi) transparent to the photons (known as atmospheric window, or the atmosphere attenuation are modeled),$0 < \tau < 1$. Atmospheric correction techniques estimate this coefficient τ_a in order to obtain the correct fluxes hitting the ground surface. The Earth's solid surface is considered opaque, so $\tau = 0$. In this condition Eq. (8.2) becomes:

$$1 = \alpha + \rho\,. \tag{8.3}$$

Figure 8.5 provides a schematic view of two mediums for remote sensing, the atmosphere and the geosphere, as related to the above coefficients.

This schematic illustration shows an ideal condition where a Lambertian reflectance is dominant with no adjacency effects. This is to illustrate the basic parameters that are sensed by the remote sensing sensor. It should be pointed out that if surface water is being sensed addition interactions of the water with the sun photons is taking place as shown in Figure 8.5.

As seen , the irradiance flux on the water surface can be reflected back to the sensor, penetrate in to the water body, absorbed by the water body, heat the sea surface and reflected back to the water, atmosphere and then to the sensor. The energy balance is as follow:

$$E = E_{\mathrm{tw}} + E_{\mathrm{aw}} + (E_{\mathrm{rw}} + E_{\mathrm{rss}})\,. \tag{8.4}$$

E_{tw} is the energy transferred in the water body, E_{aw} is the energy absorbed in the water body, E_{rw} is the energy reflected back from the water surface and E_{rss} is the energy reflected back from the sea surface. Dividing Eq. (8.4) by the total energy provides the above coefficients:

$$1 = \tau_{\mathrm{w}} + \alpha_{\mathrm{w}} + \rho_{\mathrm{w}} + \rho_{\mathrm{ss}}\,. \tag{8.5}$$

In case the water are clean and τ_{w} is known (depending on the water depth, wd) $1 > \rho_{\mathrm{ss}} > 0$. If the water are dirt, $\rho_{\mathrm{ss}} = 0$ and $\tau_{\mathrm{w}} \to 0$ then we get similar expression as in Eq. (8.1):

$$1 = \alpha_{\mathrm{w}} + \rho_{\mathrm{w}}\,. \tag{8.6}$$

There is also an intermediate condition where all coefficients are greater then 0 that tends to be rather complicated for solving the sensor radiance for each coefficient.

Again, these description and illustration are schematic and does not take into account BRDF effects, specular reflectance and adjacency effects.

Generally, for solid surface we are trying to recover ρ, termed spectral albedo or simply "reflectance", to account for α (absorbtance) which has a meaningful physical explanation. The same applies to the atmosphere but then we use τ (transmittance) to assess α. For water surface more coefficients are encountered that as discussed previously makes the sensing more complicated depending on the water conditions (τ_w). Doing so spectrally can discriminate between the chemical compound being in the atmosphere, geosphere and hydrosphere. Assessing the atmospheric interaction in region τ is the main procedure used to generate ρ and analyze it for thematic mapping in the atmospheric correction technique procedure-see further on). The E can be calculated (or measured) according to Planck's displacement law of a black body entity (depending on its temperature). This calculation shows that the radiant frequencies are different using the Sun (VIS–NIR–SWIR) or Earth (TIR) and thus demonstrates separate HRS approaches using the Sun (mostly done) and the Earth (just emerging) as radiation sources. When the Sun serves as the radiant source, the reflectance ρ of the surface is used as a diagnostic parameter to map the environment. When the Earth serves as the radiant source, the emissivity (ϵ) and the temperature (T) are used as diagnostic parameters. These parameters can be derived from the acquired radiances using several methods to remove atmospheric attenuation [mostly τ, and then after separating between T and ϵ (in the TIR region) or extracting ρ (in the VIS–NIR–SWIR region)]. The reflectance and emissivity are inherent properties of the sensed matter that do not change with external conditions (e.g., illumination or environmental conditions) and hence are used as diagnostic parameters. They both provide, if high spectral resolution is used, spectral information about the chromophores within the matter being studied.

According to Kirchhoff's law, the absorptivity of a perfect black body material is equal to its emissivity (in equilibrium) and thus reflectance has a strong relation to emissivity across the spectral region studied, i.e., $\epsilon = 1 - \rho$. In atmospheric windows where $\tau \neq 0$ across the VIS–NIR–SWIR–MWIR and LWIR region, HRS can be performed even not across a classical atmospheric window using atmospheric correction techniques (see later) as shown in Figure 8.6. Whereas the LWIR (8–12 μm) is sufficient for remote sensing of the Earth (if the temperature is known), as is the VIS–NIR–SWIR region, the MWIR (3–5 μm) region is more problematic for HRS remote sensing of the Earth, as both Sun and Earth Planck functions provide low radiation in their natural position (Sun $6000^\circ K$, Earth $300^\circ K$) and overlap across this region. Hence the MWIR region across 3 to 5 μm is usuable for hot (Earth) targets that enable the dominant photons to be above the Sun's background across this region. It should be noted that ρ and α are important parameters for assessing the Earth's surface composition, but if they are known in advance (e.g., ground targets with known ρ), τ can be extracted at specific wavelengths and hence can provide information about the atmospheric constituents (gases and aerosols). In other words. HRS can be also a tool to quantitatively study the atmosphere.

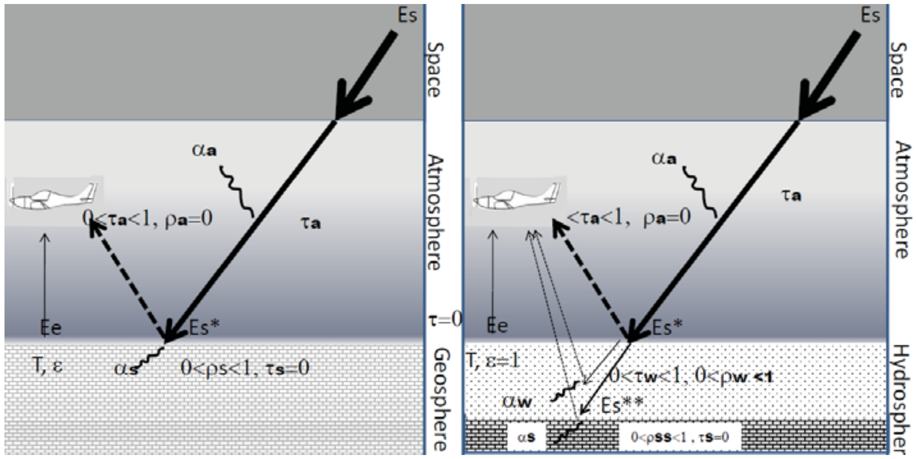

Fig. 8.5 Schematic views of two and three mediums (atmosphere and geosphere (left panel) and atmosphere, hydrosphere, geosphere (sea surface) (right panel) respectively).where Eq. (8.3) holds in each mediums. In Figure 8.3a the absorbance of sun radiation (Es) was indirectly observed by transmittance and reflectance. In the atmosphere, the reflectance (ρ) is 0 and absorbance (α) is obtained via transmittance (τ). In the geosphere, transmittance (τ) is 0 and absorption(α) is obtained via reflectance (ρ). In Figure 8B the interaction in the atmosphere is identical to Figure 8.3a. In the water body medium, transmittance of the water (w) determine the contribution of the sea surface reflectance (ss) well as the water surface reflectance (w) and all are responsible for water absorbance (w). See text for more explanation.

Whereas in the VIS region, only limited information on terrestrial systems is available, important information about many of the Earth's materials can be extracted from the NIR-SWIR region. This is because in the VIS region, the electronic processes responsible for broad spectral features are dominant, whereas in the NIR-SWIR region, overtone and combination modes of fundamental vibrations responsible for noticeable spectral features are dominant. Many of the Earth's materials show significant spectral absorption in the NIR-SWIR region, which serves as a unique fingerprint for mineral identification (Hunt and Salisbury, 1970, 1971; Hunt et al., 1971a,b). In addition, atmospheric gases, such as oxygen, water vapor, carbon dioxide and methane, produce specific absorption features in the VIS–NIR–SWIR regions (Goetz 1991). Lying in the narrow band's width (usually <10 nm) that HRS is capable of generating, are spatial qualitative and quantitative indicators for ecologists, land managers, pedologists, geologists, limnologists, atmospheric scientists and engineers, for which the selection of appropriate methods is dependent on the particular management objectives and the characteristics of the indicators.

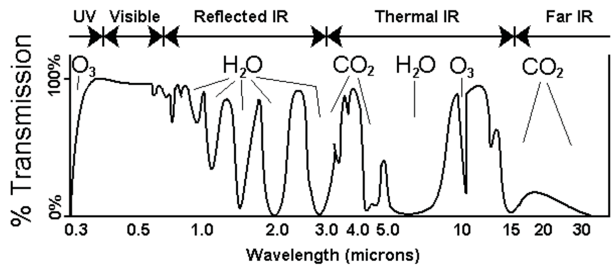

Fig. 8.6 The atmospheric transmittance windows for HRS activity. When the atmosphere is not completely opaque, photons still reach the ground. Also defined are the regions for HRS.

In general the above mentioned spectral information is part of the radiance at sensor, amongst other factors (such as sun angle, viewing angle, terrain relief, atmosphere attenuation ect). To extract the spectral information that are considered inherent properties of the sensed matter a special data analyses stages must be applied such as: data quality inspection, atmospheric correction and data mining. These issues are discussed in the following section.

8.8 Data Analysis

8.8.1 General

Data-processing is performed following a chain procedure (an example of such a procedure, used at the Remote Sensing Laboratory at Tel Aviv University, is given in Figure 8.3). The procedure starts with quality assessment (and assurance, QA) of the raw data and data preprocessing to obtain reliable radiance information and later, a final product (thematic maps). For each stage, quality indicators (QI) are used for the QA. These two quality steps were developed through the EUFAR FP7 project (EU project # 227159) and can be adapted to the user's needs. Then the data should undergo atmospheric correction to yield reliable reflectance (or emittance) data (using QI for this stage). The cube is then transferred to the "thematic processing" stage in which background knowledge (supervised classification) or absence of information (unsupervised classification) are used.

8.8.2 Atmospheric Correction

As already stated in previous sections, the goal of HRS techniques is to provide accurate measurements of surface inherent properties from at–sensor radiance acquired with HRS instruments. As most of the HRS sensors are operating today across the VIS–NIR–SWIR region, the reflectance value (i.e., the spectral albedo) is the most useful parameter. The current section is thus dealing with atmosphere correction of the VIS NIR SWIR region only. The results are either directional surface reflectance quantities or the spectral albedo values (Nicodemus et al., 1977) (note: we use the term "reflectance" hereafter as a generic term of a relation between reflected and incoming radiative flux, see Eq.8.2). This radiometric conversion of the measured radiance to reflectance is referred to as *"atmospheric correction"* already in early remote sensing literature (Dozier and Frew, 1981). Note that the term "correction" is appropriate as long as data are adjusted to match a given ground reference by empirical methods. However, it may be misleading for methods relying on physical radiative transfer models. The term *"atmospheric compensation"* would be a more appropriate description in this case, as the atmospheric effects are compensated in from correctly calibrated imagery, however it has not yet been widely established. In a first section, empirical normalization methods are summarized which allow for fast and efficient atmospheric correction, whereas model based methods are given in the subsequent sections.

Empirical Reflectance Normalization

All empirical atmospheric correction methods have in common that a-priori knowledge about the surface spectral albedo is put in relation to the imagery in order to find factors for a normalization of the atmospheric effect (Smith et al., 1987). Hereafter, a collection of methods is compiled which is suited for systems of unsecured calibration state and / or if fast results are required. These methods may be applied on uncalibrated image data, i.e., directly on the digital numbers DN_s. The flat field approach uses a spectrally flat spectrum from within the image for normalization to calculate a flat field (quasi-) reflectance ρ_{ff} such that:

$$\rho_{\mathrm{ff}} = \frac{DN_{\mathrm{s}}}{DN_{\mathrm{ff}}}\,, \tag{8.7}$$

where DN_{s} is the (uncalibrated) digital number signal at the sensor and DN_{ff} is the signal of a selected spectrum. This normalization may result in reflectance values above 100 % as the selected flat field reflectance is usually below 100 %. The *known/bright target approach* uses the known (or assumed) reflectance ρ_b of one typically bright target in the image such that the whole (calibrated) image data may be normalized by the at–sensor measurement DN_b at the target by the transformation:

$$\rho = \frac{DN_s}{DN_b} \cdot \rho_b \,. \tag{8.8}$$

A variation of the bright target approach is the *"Quick Atmospheric Correction"*-method (QUAC), see Bernstein et al. (2008): instead of taking one pixel as a reference, the relation of a generic expected average reflectance to the average signal in the image is taken as reference for correction of the full image.

The *empirical line correction* uses a combination between dark and bright targets in a scene. If two or more objects are known, a linear function is derived for each spectral band between measured signal and reflectance. The linear fit is done between the known reflectances ρ_i and the respective measurements DN_i, such that a slope $\Delta\rho/\Delta DN$ of the function $\rho(DN)$ with a typical offset for dark objects DN_{dark} can be found. This function is then used for normalization of all spectra of the image using the equation:

$$\rho = (DN_s - DN_{\mathrm{dark}}) \cdot \frac{\Delta\rho}{\Delta DN} \,. \tag{8.9}$$

The empirical line works satisfactorily well for flat terrain and small FOV imagery, but is at its limit in mountainous areas and if repeatable corrections are required for an image series.

At–Sensor Radiance Description

Other than the empirical correction methods, the physical atmospheric correction of imaging spectroscopy data relies on an appropriate description of the at-sensor radiance from known parameters. In imaging spectroscopy, the at-sensor radiance is composed of three major components comprising the direct reflected and the backscattered radiance from the surface and the atmosphere. The thermal emission may be neglected for the wavelength range up to 2500 nm as long as the temperature of the surface is below 350 K. Thus, the at-sensor radiance L_s may be in a good approximation described as a sum of the direct ground reflected radiance $L_{\mathrm{g,dir}}$, the so-called adjacency radiance $L_{\mathrm{g,adj}}$, and the atmospheric radiance L_{atm}:

$$L_{\mathrm{s}} = L_{\mathrm{g,dir}} + L_{\mathrm{g,adj}} + L_{\mathrm{atm}} \,. \tag{8.10}$$

We now use ρ as the in-field hemispherical-directional reflectance factor (also denoted as $HDRF_{\mathrm{meas}}$), ρ_{adj} as the large–scale spectral albedo of the surface, and s as the spherical albedo of the atmosphere. The terms in equation

8.10 may then be written in a good approximation for the direct component $L_{g,dir} = \frac{1}{\pi} \cdot E_g \cdot \rho \cdot \tau_u$, the adjacency radiance $L_{g,adj} = \frac{1}{\pi} \cdot E_g \cdot \rho_{adj} \cdot \tau_{u,adj}$, and the atmospheric radiance $L_{atm} = \frac{1}{\pi} E_0 \cdot s$. The term E_0 is the top of atmosphere irradiance and E_g is the total irradiance (solar flux) on a ground surface element, which may be written as $E_g = E_0 \tau_d \cos\varphi + E_{dif} \cdot V_{sky} + E_{ter}$. The latter depends on the local solar incidence angle φ and includes the total diffuse irradiance E_{dif}, scaled by the fraction of the visible sky (skyview factor V_{sky}) and the terrain irradiance E_{ter}. The parameter τ_d is the downward atmospheric transmittance; τ_u and $\tau_{u,adj}$ are the upward transmittances of the atmosphere for the direct and the adjacency radiative paths, respectively.

A different formulation of the at-sensor radiance is derived, if the adjacency term is written using the back-reflected radiance from the ground coupled by the single scattering albedo s of the atmosphere (compare (Tanré et al., 1979)). Here, all ground reflected radiance is summarized in the term $L_{g,tot}$. This results in the relation:

$$L_s = L_{g,tot} + L_{atm} = t_u \cdot E_g \cdot \rho \cdot \frac{1}{\pi \cdot (1 - \rho_{adj} \cdot s)} + L_{atm} \,, \tag{8.11}$$

where the parameters are as described for Eq. 8.10. Such formulations of the at-sensor radiance are the basis for the atmospheric correction task.

Radiative Transfer–Based Atmospheric Correction

Radiative transfer codes (RTCs) such as MODTRAN®-5 (Berk et al., 2002) or 6S-V (Vermote et al., 2006) are well suited for forward simulation of the at–sensor signal from given boundary conditions. However, they are not built for the task of inversion for surface reflectance properties from radiometric images. For this purpose, atmospheric correction software is required. Examples of such software are ATCOR (Richter and Schläpfer, 2002), HAATCH (Qu et al., 2001) FLAASH (Cooley et al., 2002), TAFKAA (Gao et al., 2000), or ACORN (Green, 2001). Such software allows an efficient inversion of the calibrated imagery on the basis of set of equations bellow. By inversion and reformulation of Eq. (8.10), the surface reflectance may be retrieved by the equation:

$$\rho = \frac{\pi \cdot d^2 \cdot \left(L_s - L_{g,adj} - L_{atm}\right)}{t_u \cdot \left(t_d \cdot E_0 \cos\varphi + E_{dif} \cdot V_{sky} + E_{ter}\right)} \,. \tag{8.12}$$

The components of this equation are to be derived from:

- physical model of a radiative transfer code: $L_{atm}, E_{dif}, \cdot\tau_d, \tau_u$
- boundary conditions of terrain: incidence angle φ, sky view factor V_{sky},

- astronomical data: the average extraterrestrial solar constant E_0 and the dependency on the relative Earth-Sun distance described by parameter d, and
- iteration of atmospheric correction: $L_{\mathrm{g,adj}}$ and terrain irradiance E_{ter}.

As all of the parameters except E_0 and d vary per pixel, it is not efficiently feasible to calculate the radiative transfer directly for each pixel. Precalculated look-up tables (LUTs) are normally employed. These LUTs are interpolated with the pixel properties to find the applicable parameters for the correction.

A different approach is to perform the atmospheric compensation in the "apparent reflectance" domain after dividing the at-sensor radiance by the ground solar irradiance, propagated to the at-sensor level $E_{0,s}$:

$$\rho_s = \frac{\pi \cdot d^2 \cdot L_s}{E_{0,s}}, \rho_{\mathrm{atm}} = \frac{\pi \cdot d^2 \cdot L_{\mathrm{atm}}}{E_{0,s}}, \text{ and } \rho_{\mathrm{adj}} = \frac{\pi \cdot d^2 \cdot L_{\mathrm{adj}}}{E_{0,s}} \tag{8.13}$$

These terms are typically used over flat ground, introducing a total transmittance term $\tau_{tot} = \tau_d \dot{\tau}_u$, which relates the at-sensor reflectance to the ground reflectance. The inversion of Eq. (8.11) for reflectance results in:

$$\rho = \frac{(\rho_{\mathrm{s}} - \rho_{\mathrm{atm}})\left(1 - \rho_{\mathrm{adj}} \cdot s\right)}{\tau_{\mathrm{tot}}}. \tag{8.14}$$

If the adjacency reflectance is further assumed to be the same as the pixel reflectance (i.e., $\rho_{\mathrm{adj}} = \rho$), the equation is reduced to:

$$\rho = \frac{(\rho_{\mathrm{s}} - \rho_{\mathrm{atm}})}{\tau_{\mathrm{tot}} + (\rho_{\mathrm{s}} - \rho_{\mathrm{atm}}) \cdot s}. \tag{8.15}$$

This is a basic atmospheric correction equation which may be used in simple atmospheric correction programs or for fast inversion of a radiative transfer code. Note that working in the reflectance domain is critical for airborne instruments as this approximation relies on accurate knowledge of the radiance at sensor level. An additional modeling step is required to infer the at-sensor radiance level $E_{0,s}$ from the data.

Process of Complete Atmospheric Correction

A complete atmospheric correction as implemented in atmospheric correction routines follows these steps:

- create a LUT, containing the parameters of the above equations in relation to the parameters at a fixed number of data points (covering the expected range),

- calculate skyview factor, height, and incidence angle from DEM (Digital Elevation Model), using the solar zenith and azimuth angles,
- derive atmospheric parameters from imagery (i.e., water vapor and aerosol load of the atmosphere),
- make fixed preselections (e.g., flight altitude and aerosol model),
- invert the LUT, i.e., derive the parameters by multilinear interpolation for each pixel,
- use Eq. 7 or Eq. 10 to perform the atmospheric correction, and
- perform an iteration of the above steps for adjacency correction and for the calculation of the terrain irradiance.

Some variations of this procedure exist, as the parameterization of the problem may differ and the LUT may be pre-calculated or calculated for each scene directly while correcting the data. An ideal high level standard procedure combines geometric and atmospheric processing (Schläpfer and Richter, 2002). Linked parameters are the viewing angle per pixel, the absolute distance from the aircraft to each pixel location, or the relative airmass between sensor and pixel. Furthermore, other DEM related parameters, such as height, slope or aspect are required for radiometric correction algorithms and can only be used if the image is brought to the same geometry as the DEM. The dependencies within the atmospheric correction part lead to iterative reflectance retrieval steps, specifically for adjacency correction purposes. The final step of the processing should be a correction of the reflectance anisotropy (i.e., a BRDF correction). Some details regarding crucial correction steps are given hereafter.

Atmospheric parameter retrieval

Imaging spectrometers offer the inherent capability for automatic retrieval of the radiometrically critical parameters atmospheric water vapor content and aerosol load (optical thickness). For the atmospheric water vapor, the 940 / 1130 nm water vapor absorption bands are typically used for the retrieval of columnar water vapor over land on a per-pixel basis (Schläpfer et al., 1998). The aerosol optical thickness is normally calculated using the dark dense vegetation approach (DDV, Kaufman and Tanré (1996)), interpolating the aerosol load to areas not covered by vegetation. These two methods allow for a mostly autonomous atmospheric correction of imaging spectrometry data.

Adjacency correction

The correction of the atmospheric adjacency effect is of high relevance, especially for limnological applications (Tanré et al., 1987) . The effect is significant in a horizontal range from 100 m up to 1.5 km starting at flight altitudes of 1000 m above ground and higher. Thus, each pixel has to be corrected with respect to the average reflectance of the adjacent areas. This can be done in an efficient way by the definition of a spatial convolution function which takes a distance-weighted average of the adjacent area in the image to calculate an adjacency weighting factor. The corresponding radiance has to be simulated in the radiative transfer code as indirect ground reflected radiance according to the aforementioned parameterization.

Shadow correction

Cast shadows, cloud shadows and shadows from building are often present in imaging spectroscopy data. They receive mostly diffuse irradiance which is sufficient to provide enough signal for data analysis with state of the art sensor systems. Correction approaches try to classify the shadowed areas first and then apply a separate correction model to these parts of the image such that shadows are removed in optimal situations (Adler-Golden et al., 2002; Richter and Muller, 2005). The correction model takes into account the diffuse nature of the irradiance in the cast shadow areas and needs to consider the skyview factors correctly for an accurate correction.

BRDF correction

The derivation of spectral albedo (i.e. the bi-hemispherical reflectance BHR) from directional reflectance values is the task of BRDF correction. The operational correction of BRDF effects in images is not yet solved satisfactorily progress has been made on this issue (Feingersh et al., 2010) . The correction of the BRDF-effects may be performed if the BRDF properties of the observed target(s) and the (diffuse) irradiance distribution is known. For operational use, an anisotropy factor needs to be calculated for each pixel, which accounts for the relation between measured hemispherical-directional reflectance ($HDRF_{meas}$ and the spectral albedo (bi–hemispherical reflectance, BHR; also known as *'white sky albedo'*). The anisotropy factor has to be inferred from an appropriate BRDF–model or from measurements. The finally calculated spectral albedo product is a quantity which may be easily compared in multitemporal analysis and which may be used for unbiased object classification.

8.8.3 Atmosphere Information Retrieval from HRS Data

Based on the relatively high spectral resolution obtain by the HRS sensors, one can use the specific absorption features of atmospheric gases (natural or contaminated) and evaluate their column content on a pixel-by-pixel basis. This may provide an innovative way of mapping the gases' spatial distribution and of spotting new quantitative information on the atmospheric conditions at very high spatial resolution. The gases that are active across the VIS–NIR–SWIR–MWIR spectra are divided into two sectors: 1) a major sector in which the spectral response of the gases is well detected (high fraction and strong absorption) and 2) a minor sector in which the spectral response is low and difficult to assess due to the low fraction of the gases and relatively weak absorption features. The major gas group is composed of O_2, H_2O and CO_2, whereas the minor gas group consists of O_3, N_2O, CO, CH_3 (in the VIS–NIR–SWIR) and SO_2 and NO_2 (in the TIR). Table 8.7 provides the absorption features of the above gas components across the VNIR–SWIR–TIR spectral region along with the atmospheric windows. The advantage of assessing the above gases on a pixel-by-pixel basis is significant. It can help accurately extract surface reflectance by estimating the gases' absorption (and hence their atmospheric transmission) on a pixel-by-pixel column basis. Consequently, calculating water vapor directly from the image (first demonstrated by Gao and Goetz (1995)) is now a very common way of achieving high performance of atmospheric correction methods. Whereas H_2O is considered to be a non–uniformly spatially distributed gas, other major gases, i.e., CO_2 and O_2, are known to be well mixed-hence their use as indicators to assess atmospheric phenomena that might affect the spatial distribution of the gas in question. For example, over rough terrain, if spatial changes are encountered using a well-mixed gas, this might indicate different elevations as the column pixel volume over high terrain consists of less molecules than that over low terrains for a particular gas. Based on this, Ben–Dor and Kruse (1996) and later,Green (2001) showed that it is possible to construct a DEM structure of the studied area solely from the HRS radiance information and the CO_2 peak. Furthermore, as O_2 is also a well-mixed gas, it can be used to estimate, on a pixel-by-pixel basis, the Mie scattering effect across the VIS–NIR region and hence can be used to better extract the surface reflectance, assuming that the scattering is not a spatially homogeneous phenomenon. Using one absorption peak of the H_2O at 1.38 μm, Gao et al. (1993) showed that a non–visible cirrus cloud can be detected and mapped based on the high scattering properties of the ice particles within the cloud volume. Ben Dor (1994) suggested taking precautions in using these absorption peaks over high terrain and bright targets and in another paper (Ben–Dor et al., 1994), suggested that the O_2 peak be used to map the cirrus cloud distribution in the VNIR region (0.760 μm). Based on this idea, Schläpfer et al. (2006) was able to quantitatively assess a smoke plume over a fire area using the scattering effect on the O_2 absorption peak. Alakian et al. (2008) developed a method to retrieve the microphysical and optical properties in aerosol plumes (L–APOM) in the VIS region as well. Recently, Chudnovsky et al. (2009) mapped a dust plume over the Bodele Depression in northern Chad using Hyperion data and the SWIR region. Another innovative study that shows the applicability of HRS in the atmosphere was performed by Roberts et al. (2010). They showed that if high SNR data are available, it is also possible to detect the distribution of minor gases. Using AVIRIS 2006 data over a marine (dark) environment, they were able to detect, on a pixel–by–pixel basis, the emission of methane over the Coal Oil Point (COP) marine seep fields, offshore of Santa Barbara, California, and the La Brea Tar Pits in Los Angeles, California. In the TIR region, there are several examples of the detection of plumes of toxic gases based on the fundamental vibration peak across the atmospheric windows between 2.5 and 16 μm. Using SO_2 emission in the TIR region at 8.58 and 8.82 μm, Shimoni et al. (2007) were able to spot shade on a plume emitted over an industry refinery zone with additional information extracted from the VIS region. Figure 8.7 provides a summary for the absorption positions of all the above mentioned gases across the VIS–NIR–SWIR–TIR spectral region. In summary, it can be concluded that HRS technology is not only capable of deriving surface information, it also has the proven capability to extract quantitative information on atmosphere constituents in an innovative way that none of the current remote sensing means can provide.

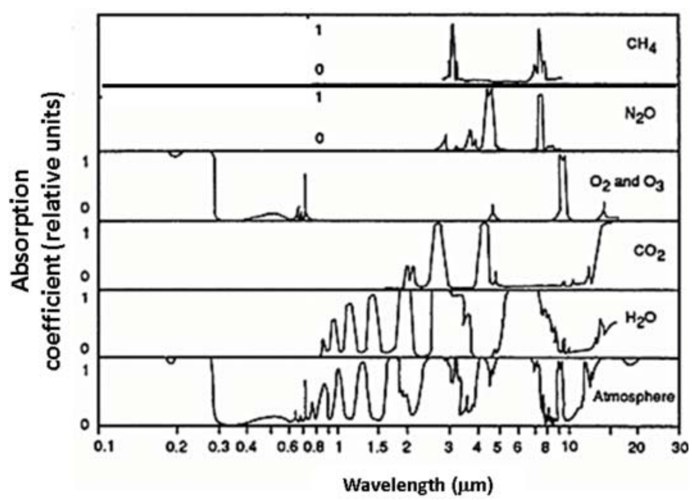

Fig. 8.7 The absorption position of all gases across the VIS–NIR–SWIR–TIR region .

8.8.4 Mapping Methods and Approaches

Over the last few years, many techniques for mapping and processing of HRS data have been developed (Schaepman et al., 2009). The special characteristics of hyperspectral datasets pose different processing problems, which must be tackled under specific mathematical formulations, such as classification (Landgrebe, 2003; Richards and Jia, 2006) or spectral unmixing (Adams et al., 1986). These problems also require specific dedicated processing software and hardware platforms(Plaza and Chang, 2007).

In previous studies (Plaza et al., 2009), available techniques were divided into full-pixel and mixed-pixel techniques, where each pixel vector defines a spectral signature or fingerprint that uniquely characterizes the underlying materials at each site in a scene. Mostly based on previous efforts in multispectral imaging, full-pixel techniques assume that each pixel vector measures the response of one single underlying material (Schaepman et al., 2009). Often, however, this is not a realistic assumption. If the spatial resolution of the sensor is not good enough to separate different pure signature classes at the macroscopic level, these can jointly occupy a single pixel, and the resulting spectral signature will be a composite of the individual pure spectra, often called endmembers in hyperspectral terminology (Boardman et al., 1995). Mixed pixels can also result when distinct materials are combined into a homogeneous or intimate mixture, which occurs independently of the spatial resolution of the sensor. To address these issues, many spectral unmixing approaches have been developed under the assumption that each pixel vector measures the response of multiple underlying materials (Kruse, 1988; Keshava and Mustard, 2002).

Spectral unmixing has been an alluring goal for exploitation, from the earliest days of hyperspectral imaging (Goetz et al., 1985) until today. Regardless of the spatial resolution, the spectral signatures collected in natural environments are invariably a mixture of the signatures of the various materials found within the spatial extent of the ground instantaneous field view of the imaging instrument (Adams et al., 1986). In this case, the measured spectrum may be decomposed into a combination of pure spectral signatures of soil and vegetation, weighted by areal coefficients that indicate the proportion of each macroscopically pure signature in the mixed pixel (Keshava and Mustard, 2002). The availability of hyperspectral imagers with a number of spectral bands exceeding the number of spectral mixture components (Green et al., 1998) has allowed casting the unmixing problem in terms of an over determined system of equations in which, given a set of pure spectral signatures (called endmembers), the actual unmixing to determine apparent pixel abundance fractions can be defined in terms of a numerical inversion process (Harsanyi and Chang, 1994; Bateson and Curtiss, 1996; Plaza et al., 2004; Berman et al., 2004; Chang et al., 2006; Rogge et al., 2006; Wang and Chang, 2006; Zaer and Gader, 2008).

A standard technique for spectral mixture analysis is *linear* spectral unmixing (Heinz and Chang, 2001; Plaza et al., 2004), which assumes that the spectra collected by the spectrometer can be expressed in the form of a linear combination of end members weighted by their corresponding abundances. It should be noted that the linear mixture model assumes minimal secondary reflections and / or multiple scattering effects in the data-collection procedure, and hence the measured spectra can be expressed as a linear combination of the spec-

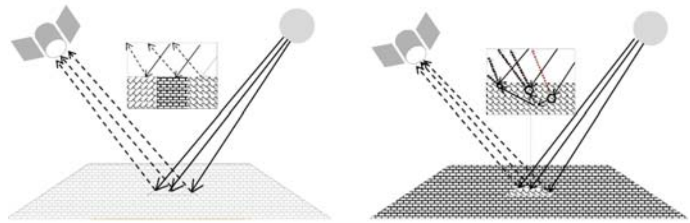

Fig. 8.8 Linear (left panel) versus nonlinear (right panel) mixture models: single versus multiple scattering. .

tral signatures of materials present in the mixed pixel (see Figure 8.8a). Although the linear model has practical advantages, such as ease of implementation and flexibility in different applications (Chang, 2003), *nonlinear* spectral unmixing may best characterize the resultant mixed spectra for certain end member distributions, such as those in which the endmember components are randomly distributed throughout the instrument's FOV (Guilfoyle et al., 2001). In those cases, the mixed spectra collected by the imaging instrument are better described by assuming that part of the source radiation is multiply scattered before being collected at the sensor (see Figure 8.8b). In addition, several machine-learning techniques have been applied to extract relevant information from hyperspectral data during the last decade. Taxonomies of remote sensing data processing algorithms (including hyperspectral analysis methods) have been developed in the literature (Richards and Jia, 2006; Schowengerdt, 1997). It should be noted, however, that most available hyperspectral data–processing techniques focus on analyzing the data without incorporating information on the spatially adjacent data, i.e., hyperspectral data are usually not treated as images, but as unordered listings of spectral measurements with no particular spatial arrangement (Rogge et al., 2006). The importance of analyzing spatial and spectral patterns simultaneously has been identified as a desired goal by many scientists devoted to multidimensional data analysis.

In certain applications, however, the integration of high spatial and spectral resolution is mandatory to achieve sufficiently accurate mapping and / or detection results. For instance, urban area mapping requires sufficient spatial resolution to distinguish small spectral classes, such as trees in a park, or cars on a street (Bruzzone and Marconcini, 2006). Due to the small number of training samples and the high number of features available in remote sensing applications, reliable estimation of statistical class parameters is another challenging goal (Foody, 1999). As a result, with a limited training set, classification accuracy tends to decrease as the number of features increases. This is known as the Hughes effect (Landgrebe, 2003). High–dimensional spaces have been demonstrated to be mostly empty, thus making density estimation even more difficult. One possible approach to handling the high–dimensional nature of hyperspectral data sets is to consider the geometrical properties rather than the statistical properties of the classes. The good classification performance demonstrated by support vector machines (SVMs) using spectral signatures as input features (Camps-Valls and Bruzzone, 2005) can be further increased by taking advantage of semi-supervised learning and contextual information. The latter is performed through a combination of kernels dedicated to spectral and contextual information, while in the former the learning is provided with some supervised information in addition to the wealth of unlabeled data. Among the great many methods proposed in the literature for such approaches, we focus on the transductive SVM for semi-supervised learning (Bruzzone L and Marconcini, 2006), or a composite kernel–based methodology for contextual information integration at the kernel level (Camps–Valls et al., 2006) have shown great success in practice.

As most of the methods reviewed here deal with endmember extraction and data mining from the reflectance or emittance cubes (an unsupervised approach), there are methods in which the endmembers are known in advance or the spectral model to map the pixels has already been developed (supervised approach). One of the first and most usable endmember-based approaches in HRS is the SAM (Spectral Angle Mapper, Kruse et al. (1993)) which is based on the angle calculated between two spectral vectors: the pixel and the selected endmember. Since then, many other spectral-based techniques have been developed, where most recently, spectral-based models that are generated in a spectral domain (e.g., PLS or neural network) are implemented on a pixel-by-pixel basis to the image cube in question. This method enables quantitative mapping of selected properties on the Earth's surface such as infiltration rate (Ben-Dor et al., 2004) organic matter content (Stevens et al., 2008), salinity (Ben–Dor et al., 2002) and more.

Finally, although the mapping and classification techniques described above hold great promise for hyperspectral data processing, they also introduce new computational challenges. With the recent explosion in the amount and complexity of hyperspectral data, parallel processing and high-performance computing (HPC) practices have necessarily become requirements in many remote sensing missions, especially with the advent of low–cost systems such as commodity clusters (Plaza and Chang, 2007). On the other hand, although hyperspectral analysis algorithms map nicely to clusters and networks of workstations, these systems are generally expensive and difficult to adapt to on–board data processing requirements introduced by several applications, such as wild land fire tracking, biological threat detection, monitoring of oil spills and other types of chemical contamination. In those cases, low-weight and low-power integrated components are essential to reducing the mission's payload and obtaining analyzed results quickly enough for practical use. In this regard, the emergence of specialized hardware devices such as field-programmable gate arrays (FPGAs) has helped in bridging the gap toward real–time analysis of remotely sensed hyperspectral data.

8.9 Sensor Calibration

8.9.1 General

In combination, calibration and validation can be regarded as a single process that encompasses the entire remote sensing system, from sensor to data product. The objective of both is to develop a quantitative understanding and characterization of the measurement system and its biases in both space and time (National Research Council, 2007). Calibration of hyperspectral sensor data is a critical activity for a number of reasons. First, we need to have confidence in the reliability of data delivered by such sensors. Second, as many of the products that we are deriving from hyperspectral data are quantitative, we need to know that the data from which they are derived are accurate (this holds for qualitative data as well). We often test the accuracy of remote sensing data products by performing *validation* of the subsequent datasets; thus the raw data delivered by sensors must be well calibrated and the products derived from them also well validated. Calibration and validation (cal/val) are therefore activities that form an integral component of the efficient use of any form of Earth Observation (EO) data and in the maintenance of the scientific value of EO data archives. As HRS data are acquired in Digital Number (DN) values, but for most applications we need radiometric information as an input to extract reflectance or emissivity values, accurate transfer from one stage to another is crucial. In this respect, radiometric and spectroscopic assurance is required. Radiometric calibration refers to the process of extracting physical units from the original raw spectroscopic data and of assigning the channels in the sensors to a meaningful wavelength.

Cal/val is therefore a fundamentally important scientific activity and should be a continuous component in any remote sensing program, providing an independent check on the performance of both space–based, airborne and ground–based hyperspectral sensors and processing algorithms.

In general, one can say that the *calibration* of EO data is critical if we are to reliably attribute detected changes observed in data to real environmental changes occurring at ground level. Without calibration, we are unable to rule out the influence of other factors, such as instrument error or influences of the atmosphere. This problem is exacerbated by the myriad of sensors operated by multiple countries and organizations. Calibration allows the traceability of sensor data to the same physical standards and is routinely required as sensors decay throughout their lifetime. Calibration is thus critical if we want to reliably extract information from measured radiance, compare information acquired from different regions and different times, compare and analyze HRS observations with measurements provided by other instruments and extract information from spectral image measurements using physically based computer models.

Validation refers to the independent verification of the physical measurements made by a sensor as well as of the derived geophysical variables. Validation allows for the verification and improvement of the algorithms used (e.g., for atmospheric correction and vegetation state). To achieve this, conventional, ground–based observations are required using calibrated and traceable field instrumentation and associated methods. To this end, several indicators are valid and developed to check the accuracy of the calibration stage and to provide the user with a reliable feeling about his data set.

The definition of all the common terms used here for cal / val are taken from the Committee of Earth Observation Satellites (CEOS) as follows:

- *Calibration* - The process of quantitatively defining the responses of a system to known, controlled signal inputs
- *Validation* - The process of assessing, by independent means, the quality of the data products derived from the system outputs
- *Traceability* - Property of a measurement result relating the result to a stated metrological reference (*free definition and not necessarily SI*) through an unbroken chain of calibrations of a measuring system or comparisons, each contributing to the stated measurement uncertainty
- *Uncertainty* - Parameter that characterizes the dispersion of the quantity values that are being attributed to a measured mean, based on the information used
- *Vicarious calibration* - Vicarious calibration refers to techniques that make use of natural or artificial sites on the surface of the Earth for post calibration of air borne or space borne sensors

8.9.2 Calibration for HSR Sensor

Calibration translates electrical output DN values (voltages or counts) to reliable physical-based units (radiometric information) by determining the transfer functions and coefficients necessary to convert a sensor reading. The coefficients are extracted throughout a careful measurement stage in the laboratory using well-calibrated facilities and traceable standards. There are a number of components ensuring a thorough calibration approach. Radiometric and spectral responses need to be accurately monitored through the lifetime of a sensor to monitor changes in response as it ages over time. In the case of spaceborne hyperspectral sensors, both pre-launch and post (on-orbit) launch calibration is undertaken, either directly or using vicarious targets-on-orbit and vicarious calibration enable taking into account changes in calibration over time (using the moon's surface for example Kieffera et al. (2003)). Airborne hyperspectral sensors have the advantage over spaceborne sensors that they can be removed from the aircraft and re-subjected to rigorous laboratory calibration tests similar to those performed for pre-launch calibration of spaceborne sensors. This is often performed prior to and after a flying 'season'. The calibration coefficients from each season can also be used to track the sensor's deterioration over its years of operation.

Pre-flight calibration

The three key components to pre-launch calibration are radiometric, spectral and spatial. To achieve radiometric calibration involves the use of a calibrated integrating sphere whose ideal output is homogeneous and large enough to illuminate all elements in a sensor array with the same radiance. An absolute radiometric calibration determines the relationship between sensor signals and radiance for all spectral channels. Varying the output of the integrating sphere also allows for the study of the linearity between sensor response and radiance and the assessment of the SNR at radiance levels similar to those encountered when sensing the Earth's surface (Gege et al., 2009).

Spectral calibration typically uses a monochromatic to produce a collimated narrow beam of light that is blocked by transmission filters and is thus tuneable to different wavelengths. Measurements performed here allow for determination of: spectral response function, center wavelength, spectral smile, spectral sampling distance, the spectral range of pixels, and spectral resolution, and to perform a wavelength calibration (Oppelt and Mauser, 2007).

Spatial calibration (geometric) can most accurately be achieved with the movement of a point light source across the sensor array whose beam is controlled by a slit (Gege et al., 2009). This allows for along–track and across–track calibration of the sensor array. Measurements performed here allow for the derivation of: line spread function across track; center coordinates for each CCD in the array; across–track sampling distance; pixel instantaneous FOV; total sensor FOV and the modulation transfer function (the reparability of adjacent targets as a function of distance and contrast, Oppelt and Mauser (2007).

In-flight / In-orbit calibration

This involves the use of in–built calibration sources and / or vicarious calibration or cross calibration to other satellite sensors. The critical issue at this stage is to be able to monitor changes in sensor performance over time (Pearlman et al., 2003). For example, Hyperion, the first fully spaceborne hyperspectral sensor, relied on the diffuse reflectance of an in–built Spectralon ™reflectance surface illuminated by the Sun or a lamp, in calibrations performed once every two weeks. The moon and other opportunistic Earth surface targets were also used to monitor sensor performance over time (Jarecke and Yokoyama, 2000; Pearlman et al., 2003; Ungar et al., 2009). Cross-calibration to data from the LANDSAT 7 ETM+ sensor was also frequently performed.

EnMAP, the new German–built hyperspectral sensor scheduled for launch in 2015, will carry for calibration a full aperture diffuser, coupled with an integrating sphere with various calibration lamps. A shutter mechanism also allows for dark measurements to be performed. APEX, a joint Belgian-Swiss airborne sensor development, carries an in–flight characterization facility using a stabilized lamp coupled with vicarious and cross calibration (Nieke et al., 2008; Itten et al., 2008).

Vicarious calibration

Vicarious calibration is also used as an in–flight check on sensor performance (e.g., Green and Shimada (1997); Green and Pavri (2000); Secker et al. (2001)). The approach can use homogeneous targets on the land surface (e.g., dry lake beds, desert sands, ice sheets, water bodies etc.) or artificial targets of varying brightness if the sensor has sufficient spatial resolution (Brook and Ben-Dor, 2011). The sites or targets must be well-characterized and ideally, reflectance should be measured at the ground surface using calibrated spectroradiometers simultaneous with sensor overflight. Increasingly sophisticated ground–based instrumentation is being used to provide autonomous and near-continuous measurement of the characteristics at many of these sites (e.g., Brando et al. (2010)). Correction involves either top-down (correction of 'top-of-atmosphere' sensor data to ground-leaving reflectance using an atmospheric correction model) or bottom-up (correction of ground target reflectance to top of atmosphere radiance using a radiative transfer model taking into account atmospheric transmission and absorption e.g., MODTRAN). Increasingly, a combination of measurements obtained at varying scales and resolutions (e.g., in situ, airborne and satellite) are being used to provide the basis for assessment of the on-orbit radiometric and spectral calibration characteristics of spaceborne optical sensors (e.g., Green et al. (2003a)).

The smaller pixel sizes of airborne imagery compared to typical image satellite resolutions, along with targeted deployment, means that artificial vicarious calibration targets can be rapidly deployed in advance of specific airborne campaigns. Such targets can also help overcome the difficulties of finding sufficient natural homogeneous targets of varying brightness. Smart Vicarious Calibration (SVC), see Brook and Ben-Dor (2011), uses artificial agricultural black polyethylene nets of various densities as calibration targets, set up along the aircraft's trajectory. The different-density nets, when combined with other natural bright targets, can provide full coverage of a sensor's dynamic range. The key to the use of any form of vicarious calibration target is the use of simultaneous field-based measurement of their reflectance properties and positions; uncertainties are reduced if a number of calibration targets are used, a large number of reflectance measurements are made of each target, and their positions are accurately located (Secker et al., 2001).

Vicarious calibration therefore provides an indirect means of quality assurance of remotely sensed data and sensor performance that is independent of direct calibration methods (use of on–board radiance sources or panels). This is important as on–board illumination sources may themselves degrade over time.

In all calibration efforts, *traceability*, the process of ensuring measurements, is related through an unbroken chain of comparisons to standards held by National Metrology Institutes (e.g., NIST, PTB and NPL), is the key to allowing true inter-comparability between different sensors' raw and product datasets (Fox, 2004). The chain is implemented via the use of 'transfer standards' that allow traceability back to official 'primary' radiometric standards using internationally agreed-upon systems of units (SI) and rigorous measurement and test protocols. Integral to the establishment of traceability is the quantification and documentation of associated uncertainties throughout the measurement chain; the fewer the number of steps in the chain the lower the uncertainty. The advantages of maintaining traceability include a common reference base and quantitative measures of assessing the agreement of results for different sensors or measurements at different times. However, current traceability guidelines lack guidance on temporal overlap or interval length for the measurements in the unbroken chain of comparisons (Johnson et al., 2004).

The successful implementation of cal / val activity needs careful planning of issues such as coordination of activities, selection and establishment of networks of sites, the development and deployment of instrumentation to support measurement campaigns, the adoption of common measurement and data distribution / availability protocols.

8.10 Summary and Conclusion

This chapter provides a snapshot of the emerging HRS technology. Although many aspects of this promising technique are not covered herein, we hope to have provided the reader with a sense of its potential for the future, as evidenced by past accomplishments. Aside from being a technology that can provide added value to the remote sensing arena, it is an expansion of the spectroscopy discipline that has been significantly developing worldwide for many years. Very soon, when sensors in air and orbit domains begin to provide SNR values that are similar to those acquired in the laboratory, all spectral techniques available today will be able to implement the HRS data and forward the applications in a generation or two. HRS technology is emerging and the general scientific community use is growing. The number of sensors is also on the rise and new companies are entering into commercial activities. The most important step in the processing of HRS data is to obtain accurate reflectance or emittance information on every pixel in the image; at that point, a sophisticated analytical approach can be used. This means that aside from the atmospheric correction method, the data has to be physically reliable and stable at the sensor level. Mixed pixel analysis and spectral models to account for specific questions are only a few examples of what this technology can achieve. The forthcoming HRS sensors in orbit are expected to drive this technology forward by providing temporal coverage of the globe at low cost and by showing decision-makers that the technology can add much to other space missions. The growing sensor-development activity in the market will also permit a "sensor for all" which will also push the technology forward. As many limitations still exist, such as the TIR region not being fully covered, the information only being obtainable from a very thin layer, the time investment, high cost of data processing and great effort needed to obtain a final product, investment in this technology is worthwhile. If the above limitations can be overcome, and other sensors' capabilities merged with it, then HRS technology can be the vehicle to real success, moving from a scientific demonstration technology to a practical commercial tool for remote sensing of the Earth.

1 List of Acronyms and Abbreviations

1D	One–Dimensional
2D	Two–Dimensional
3D	Three–Dimensional
2D–C	2D Cloud Probe
2D–P	2D Precipitation Probe
2D–S	2D Stereo Probe
AATS	NASA Ames Airborne Tracking Sunphotometer
AC	Alternating Current
ADC	Analogue Digital Converter
AIDA	Aerosol Interaction And Dynamics In The Atmosphere
AIS	Airborne Imaging Spectrometer
AISA	Airborne Imaging Spectrometer for different Applications
AMS	Aerosol Mass Spectrometer
AMSU	Advanced Microwave Sounding Unit
2 AOS	Acousto Optical Spectrometer
APEX	Airborne Prism Experiment
APM	Aerodynamic Particle Mass Analyzer
APS	Aerodynamic Particle Sizer
ARM	Atmospheric Radiation Measurements
ASD	Analytical Spectral Device
ASI	Airborne Spectral Imager
ASSP	Axially Scattering Spectrometer Probe
ATCOR	Atmospheric and Topographic Correction
AVIRIS	Airborne Visible and Infrared Imaging Spectrometer
BC	Black Carbon
BCP	Backscatter Cloud Probe
BHR	Bi–Hemisphere Reflection
BRDF	Bidirectional Reflectance Distribution Function
BSRN	Baseline Surface Radiation Network

3

	CASI	Compact Airborne Spectrographic Imager
	CAS	Cloud and Aerosol Spectrometer
	CAS–DPOL	Cloud and Aerosol Spectrometer With Depolarization
	CCD	Charge–Coupled Device
	CCN	Cloud Condensation Nuclei
	CCNC	cloud Condensation Nuclei Counter
	CCRS	Canadian Center for Remote Sensing
	CDP	Cloud Droplet Probe
	CEOS	Committee of Earth Observation Satellites
	CEP	Cloud Extinction Probe
	CFD	Computational Fluid Dynamics
	CFDC	Continuous Flow Diffusion Chamber
	CFMC	Continuous Flow Mixing Chamber
	CHRIS	Compact High–Resolution Imaging spectrometer
1	CIN	Cloud Integrating Nephelometer
	CIMS	Chemical Ionization Mass Spectrometer
	CIP	Cloud Imaging Probe
	CIRA	Centro Italiano Ricerche Aerospaziali
	CLH	Closed Path TDL Hygrometer
	CMOS	Complementary Metal Oxide Semiconductors
	CNR	Council of National Research
	COSSIR	Conical Scanning Millimeter–Wave Imaging Radiometer
	CPC	Condensation Particle Counter
	CPI	Cloud Particle Imager
	CPSD	Cloud Particle Spectrometer With Depolarization
	CRISM	Compact Reconnaissance Imaging Spectrometer
	CSI	Cloud Spectrometer and Impactor
2	CVI	Counterflow Virtual Impactor

	DAIS	Digital Airborne Imaging Spectrometer
	DDV	Dense Vegetation Approach
	DEM	Digital Elevation Model
	DFG	Deutsche Forschungsgemeinschaft
	DGPS	Differential Global Positioning System
	DLR	Deutsches Zentrum für Luft– und Raumfahrt
	DMA	Differential Mobility Analyzer (R: Radial; C: Cylindrical)
	DMS	Differential Mobility Spectrometer
	DMT	Droplet Measurement Technologies (Boulder, USA)
	DN	Digital Number
1	DOF	Depth Of Field
	DRI	Desert Research Institute
	DOF	Depth Of Field
	DSD	Drop Size Distribution
	EARSeL	European Remote Sensing Laboratories
	EAS	Electrical Aerosol Spectrometer
	EnMAP	Environmental Mapping and Analysis Program
	EO	Earth Observation EO–1 Earth Orbiter 1
	ESA	European Space Agency
	EUFAR	European Facility for Airborne Research
	EWG	Expert Working Group
2		

	FHP	Five–Hole Probe
	FIMS	Fast Integrated Mobility Spectrometer
	FINCH	Fast Ice Nucleus Chamber
	FISH	Fast In Situ Stratospheric Hygrometer
	FLAASH	Fast Line–of–sight Atmospheric Analysis of Spectral Hypercubes
	FLI	Fluorescence Line Imager
	FOG	Fiber Optic Gyro
	FOV	Field–Of–View
	FPGA	Field Programmable Gate Array
	FPA	Focal Plane Array
	FSSP	Forward Scattering Spectrometer Probe
	FTS	Fourier Transform Spectrometer
	FWHM	Full Width at Half Maximum
1	GC–MS	Gas Chromatography–Mass Spectrometry
	GER	Geophysical and Environmental Research Corporation
	GIFOV	Ground IFOV
	GIS	Geographic Information System
	GPS	Global Positioning System
	GSD	Ground–Sampling Distance
	HALO	High Altitude and Long Range Research Aircraft
	HDRF	Hemisphere Diffuse Reflectance Function
	HISS	Hyper Image Space Spectrometer
	HIAPER	High–performance Instrumented Airborne Platform for Environmental Research
	HOLODEC	Holographic Detector For Clouds
	HPC	High Performance Computing
	HPD	Hybrid Photodetector
	HRS	Hyperspectral Remote Sensing
2		

	HTW	Harvard Total Water Hygrometer
	HVPS	High Volume Precipitation Spectrometer
	HyMAP	Hyperspectral Mapper
	IAGOS	In–Service Aircraft for a Global Observing System
	IC	Ion Chromatography
	ICAO	International Civil Aviation Organization
	IDI	Isokinetic Diffuser–Type Inlet
	IF	Intermediate Frequency
	IfT	Leibniz Institute for Tropospheric Research
	IFOV	Instantaneous FOV
	ILIDS	Interferometric Laser Imaging for Droplet Sizing
	ILS	Instrument Line Shape
	IMU	Inertial Measurement Unit
1	IN	Ice Nuclei
	INAA	Instrumental Neutron Activation Analysis
	INS	Inertial Navigation System
	INSPECTRO	INfluence of clouds on the SPectral actinic flux in the lower TROposphere
	INTA	Instituto Nacional de Técnica Aeroespacial Ąă
	IR	Infrared
	IS	Imaging Spectroscopy
	ISA	International Standard Atmosphere
	ISIS	International Spaceborne Imaging Spectroscopy
	ITRES	Integral Technology for Remote Sensing
	IWC	Ice Water Content
	IWV	Integrated Water Vapor
2	IWP	Ice Water Path

	LaMP	Laboratoire de Météorologie Physique
	LANDSAT	Land Satellite
	LED	Light–Emitting Diode
	LIDAR	Light Detection and Ranging
	LIM	Leipzig Institute for Meteorology
	LNA	Low Noise Amplifiers
	LO	Local Oscillator
	LTI	Low Turbulence Inlet
	LUT	Look Up Table
	LWC	Liquid Water Content
	MAAP	Multi–Angle Absorption Photometer
	MASI	Midwave Airborne Spectral Imager
	MARSS	Microwave Airborne Radiometer Scanning System
	MAS	MODIS Airborne Simulator
	MASP	Multiangle Aerosol Spectrometer
1	MIR	Mid IR
	MIVIS	Multispectral Environment Imaging Sensor
	MLS	Microwave Limb Sounder
	MODTRAN	Moderate Resolution Transmission Code
	MPI	Max–Planck–Institute
	MSL	Mean Sea Level
	MSU	Microwave Sounding Unit
	MVD	Median Volume Diameter
	MW	Microwave
	NA	Numerical Aperture
	NASA	National Aeronautics and Space Administration
	NCAR	National Center for Atmospheric Research
	NERC	Natural Environment Research Council
	NEO	Norsk Elektro Optikk
	NDI	Nested Diffuser–Type Inlet
	NIR	Near IR
2		

	NIST	National Institute of Standards and Technology
	NMP	New Millennium Program
	NOAA	National Oceanic and Atmospheric Administration
	NPOESS	National Polar–Orbiting Operational Environmental Satellite System
	NSF	National Science Foundation
	Nu	Nusselt Number
	OAP	Optical Array Probe
	OPC	Optical Particle Counter
	PALMS	Particle Analysis by Laser Mass Spectrometer
	PCA	Principle Component Analysis
	PCASP	Passive Cavity Aerosol Spectrometer Probe
	PDA	Phase Doppler Analyzer
	PDA	Photodiode Array
	PDI	Phase Doppler Interferometer
	PDPA	Phase Doppler Particle Analyzer
	PGP	Prism–Grating–Prism
1	PILS	Particle Into Liquid Sampler
	PIP	Precipitation Imaging Probe
	PIXE	Particle–Induce X–Ray Emission
	PM1	Particulate Matter with Particle Diameter $< 1.0\,\mu$m
	PM2.5	Particulate Matter with Particle Diameter $< 2.5\,\mu$m
	PMS	Particle Measuring Systems Inc.
	PMT	Photomultiplier Tube
	PRISM	Processes Research for Imaging Spectrometer Mission
	PROBA	Project for On–Board Autonomy
	PSA	Particle Surface Area
	PSAP	Particle Soot Absorption Photometer
	PSD	Particle Size Distribution
	PSL	Polystyrene Latex Beads
	PSM	Particle Size Magnifier
	PSR	Polarimetric Scanning Radiometer
2	PVM	Particle Volume Monitor

	QA	Quality Assurance
	QI	Quality Indicators
	QUAC	Quick Atmospheric Correction
	Re	Reynold's Number
	REO	Research Electro–Optics Inc.
	RF	Radio Frequency
	RH	Relative Humidity
	RICO	Rain in Cumulus Over the Ocean
	ROSIS	Reflective Optics System Imaging Spectrometer
1	RSL	Remote Sensing Laboratory
	RSR	Relative Spectral Response
	RT	Receiver Transmitter
	SAR	Synthetic Aperture RADAR
	SDI	Solid Diffuser–Type Inlet
	SEMS	Scanning Electrical Mobility Spectrometer
	SFSI	Short–Wave IR Full Spectrum Imager
	SID	Small Ice Detector
	SMART	Spectral Modular Airborne Radiation sysTem
	SMPS	Scanning Mobility Spectrometer
2		

SMIRR	Shuttle Multispectral Infrared Radiometer
SNR	Signal–to–Noise Ratio
SP–2	Single Particle Soot Photometer
SPECIM	Spectral Imagers
SSFR	Solar Spectral Flux Radiometer
SSMI / S	Special Sensor Microwave Imager / Sounder
SST	Sea Surface Temperature
SSTI	Small Satellite Technology Initiative
SPOT	System Probatoire d’Observation de la Terre
STP	Standard Temperature and Pressure
STRAP	Stabilized Radiometer Platform
SVM	Support Vector Machine
SWE	Snow Water Equivalent
SWIR	Short–Wave Infrared
TAS	True Air Speed
TASI	Thermal Airborne Spectral Imager
TAU	Tel Aviv University
TDL	Tunable Diode Laser Absorption Spectrometer
1 TOA	Top of Atmosphere
TOR	Thermal–Optical Reflectance
TIMS	Thermal Infrared Multispectral Scanner
TM	Thematic Mapper
TIR	Thermal IR
TWC	Total Water Content
UK	United Kingdom
UV	Ultraviolet
UHSAS	Ultrahigh Sensitivity Aerosol Spectrometer
UNAM	Univ. Nac. Autonoma de Mexico
UTC	Universal Time Coordinated
VIS	Visible
VIPS	Video Ice Particle Sampler
VITO	Flemish Institute for Technological Research
VNIR	Visible and Near IR
VOC	volatile Organic Compounds
WICC	Wide Stream Impaction Cloud Water Collector
WMO	World Meteorological Organization
XRF	X–Ray Fluorescence

1

References

Abel, S. J., Haywood, J. M., Highwood, E. J., Li, J., and Buseck, P. R.: Evolution of biomass burning aerosol properties from an agricultural fire in southern Africa, Geophys. Res. Lett., 30, 1783, 2003.

Ackerman, S. and Cox, S.: Aircraft observations of the shortwave fractional absorptance of non-homogeneous clouds, J. Appl. Meteor., 20, 1510–1515, 1981.

Adams, J., Smith, M., and Johnson, P.: Spectral mixture modeling: a new analysis of rock and soil types as the Viking Lander 1 site, J. Geophys. Res., 91, 8098–8112, 1986.

Adler-Golden, S., Matthew, M., Anderson, G., Felde, G., and Gardner, J.: An algorithm for de-shadowing spectral imagery, in Proc. 11th Airborne Earth Science Workshop, edited by R. Green, 2002.

Adrian, R. J.: Laser Velocimetry, in Fluid Mechanics Measurements, edited by E. Richard J. Goldstein, chap. 4, pp. 175–299, Taylor & Francis, Washington, DC, 1996.

Aiken, A. C., Decarlo, P., Kroll, J., Worsnop, D., Huffman, J., Docherty, K., Ulbrich, I., Mohr, C., Kimmel, J., Sueper, D., Sun, Y., Zhang, Q., Trimborn, A., Northway, M., Ziemann, P., Canagaratna, M., Onasch, T., Alfarra, M., Prevot, A., Dommen, J., Duplissy, J., Metzger, A., Baltensperger, U., and Jimenez, J.: O / C and OM / OC ratios of primary, secondary, and ambient organic aerosols with high–resolution time–of–flight aerosol mass spectrometry, Environ. Science Tech., 42, 4478–4485, 2008.

Alakian, A., Marion, R., and Briottet, X.: Retrieval of microphysical and optical properties in aerosol plumes with hyperspectral imagery: L-APOM method, Remote Sens. Environ., 113, 781–793, 2008.

Albrecht, H.-E., Borys, M., Damaschke, N., and Tropea, C.: Laser Doppler and Phase Doppler Measurement Techniques, Springer-Verlag, 2003.

Allan, J. D., Jimenez, J., Williams, P., Alfarra, M., Bower, K., Jayne, J., Coe, H., and Worsnop, D.: Quantitative sampling using an Aerodyne aerosol mass spectrometer: 1. Techniques of data interpretation and error analysis, J. Geophys. Res., 108, 2003.

Allan, J. D., Deliab, A., Coea, H., Bower, K., Alfarraa, M., Jimenezc, J., Middlebrookd, A., Drewnicke, F., Onaschf, T., Canagaratnaf, M., and Worsnopf, J. J. D.: A generalised method for the extraction of chemically resolved mass spectra from aerodyne aerosol mass spectrometer data, J. Aerosol Sci., 35, 909–922, 2004.

Allen, M. D. and Raabe, O. G.: Slip correction measurements for aerosol particles of doublet and triangular triplet aggregates of spheres, J. Aerosol Sci., 16, 57–67, 1985.

Alonso, M.: Reducing the diffusional spreading rate of a Brownian particle by an appropriate non–uniform external force field, J. Aerosol Sci., 33, 439–450, 2002.

Amediek, A., Ehret, G., Fix, A., Wirth, M., Quatrevalet, M., Büdenbender, C., and Kiemle, C.: CHARM–F: Airborne Demonstrator for Spaceborne CO_2 and CH_4 Lidars, 4^{th} International Workshop on CO_2/CH_4 DIAL Remote Sensing, 3–5 November 2010, Oberpfaffenhofen, Deutschland, 2010.

An, W. J., Pathak, R. K., Lee, B. H., and Pandis, S. N.: Aerosol volatility measurement using an improved thermodenuder: Application to secondary organic aerosol, J. Aerosol Sci., 38, 305–314, 2007.

Ancellet, G.: Compact Airborne Lidar for Tropospheric Ozone: Description and Field Measurements, Appl. Opt., 37, 24, 5509–5521, 1998.

Ancellet, G. and Ravetta, F.: Analysis and validation of ozone variability observed by lidar during the ESCOMPTE–2001 campaign, Atmos. Res., 74, 435–460, 2005.

Anderson, J. G.: Absolute Concentration of O(p–3) In Earths Stratosphere, Geophys. Res. Lett., 2, 231–234, 1975.

Anderson, J. G.: Absolute Concentration of OH($x^2\pi$) In Earths Stratosphere, Geophys. Res. Lett., pp. 165–168, 1976.

Anderson, J. G., Toohey, D., and Brune, W.: Free–Radicals Within The Antarctic Vortex–The Role Of CFCs In Antarctic Ozone Loss, Science, 251, 39–46, 1991.

Anderson, T., Charlson, R., and Covert, D.: Calibration of a counterflow virtual impactor at aerodynamic diameters from 1 to 15 μm, Aerosol Sci. Technol., 19, 317–329, 1993.

Anderson, T., Covert, D. S., Marshall, S. F., Laucks, M. L., Charlson, R. J., Waggoner, A. P., Ogren, J. A., Caldow, R., Holm, R. L., Quant, F. R., Sem, G. J., Wiedensohler, A., Ahlquist, N. A., and Bates, T. S.: Performance characteristics of a high–sensitivity, three–wavelength, total scatter / backscatter nephelometer, J. Atmos. Oceanic Technol., 13, 967–986, 1996.

Anderson, T. L. and Ogren, J. A.: Determining aerosol radiative properties using the TSI 3563 integrating nephelometer, Aerosol Sci. Technol., 29, 57–69, 1998.

Andrés–Hernández, M., Kartal, D., Reichert, L., Burrows, J., Meyer Arnek, J., Lichtenstern, M., Stock, P., and Schlager, H.: Peroxy radical observations over West Africa AMMA 2006: Photochemical activity in the outflow of convective systems, Atmos. Chem. Phys., 9, 3681–3695, 2009.

Andrés–Hernández, M. D., Stone, D., Brookes, D. M., Commane, R., Reeves, C. E., Huntrieser, H., Heard, D. E., Monks, P. S., Burrows, J. P., Schlager, H., Kartal, D., Evans, M. J., Floquet, C. F. A., Ingham, T., Methven, J., and Parker, A. E.: Peroxy radical partitioning during the AMMA radical intercomparison exercise, Atmos. Chem. Phys., 10, 10 621–10 638, 2010.

Ankilov, A., Baklanov, A., Colhoun, M., Enderle, K., Gras, J., Julanov, Y., Kaller, D., Lindner, A., Lushnikov, A., Mavliev, R., McGovern, F., O'Connor, T., Podzimek, J., Preining, O., Reischl, G., Rudolf, R., Sem, G., Szymanski, W., Vrtala, A., Wagner, P., Winklmayr, W., and Zagaynov, V.: Particle size dependent response of aerosol counters, Atmos. Res., 62, 209–237, 2002a.

Ankilov, A., Baklanov, A., Colhoun, M., Enderle, K., Gras, J., Julanov, Y., Kaller, D., Lindner, A., Lushnikov, A., Mavliev, R., McGovern, F., O'Connor, T., Podzimek, J., Preining, O., Reischl, G., Rudolf, R., Sem, G., Szymanski, W., Vrtala, A., Wagner, P., Winklmayr, W., and Zagaynov, V.: Intercomparison of number concentration measurements by various aerosol particle counters, Atmos. Res., 62, 177–207, 2002b.

Annegarn, H. J., Flanz, M., Kenntner, T., Kneen, M. A., Helas, G., and Piketh, S. J.: Airborne streaker sampling for PIXE analysis, Nuclear Instruments & Methods in Physics Research Section B–Beam Interactions with Materials and Atoms, 109, 548–550, 1996.

ANSI: Recommended Practice for Atmospheric and Space Flight Vehicle Coordinate Systems, American National Standards Institute. American National Standard, ANSI / AIAA R–004–1992, 1992.

Apel, E., Hills, A., Lueb, R., Zindel, S., Eisele, S., and Riemer, D.: A fast–GC / MS system to measure C–2 to C–4 carbonyls and methanol aboard aircraft, J. Geophys. Res., 108, 2003.

Ardon–Dreyer, K., Levin, Z., and Lawson, R. P.: Characteristics of immersion freezing nuclei at the south pole station in Antarctica, Atmos. Chem. Phys. Discuss., 11, 1–30, 2011.

Arijs, E., Nevejans, D., and Ingels, J.: Positive ion composition measurements and acetonitrile in the upper stratosphere, Nature, 303, 314–316, 1983.

Arnold, F. and Henschen, G.: First mass analysis of stratospheric negative ions, Nature, 257, 521–522, 1978.

Arnold, F., Krankowsky, D., and Marien, K.: First mass spectrometric measurements of positive ions in the stratosphere, Nature, 267, 1977.

Arnold, F., Fabian, R., Henschen, G., and Joos, W.: Stratospheric trace gas analysis from ions: H_2O and HNO_3, Planet. Space Sci., 28, 681–685, 1980.

Arnold, S., Methven, J., Evans, M., Chipperfield, M., Lewis, A., Hopkins, J., McQuaid, J., Watson, N., Purvis, R., Lee, J., Atlas, E., Blake, D., and Rappengluck, B.: Statistical inference of OH concentrations and air mass dilution rates from successive observations of nonmethane hydrocarbons in single air masses, J. Geophys. Res., 112, 2007.

Arnott, W. P., Dong, Y., Purcell, R., and Hallett, J.: Direct airborne sampling of small ice crystals and the concentration and phase of haze particles, in Paper presented at the 9th Symposium on Meteorological Observations and Instrumentation, Am. Meteorol. Soc., Charlotte, N. C., 1995.

Arnott, W. P., Hamasha, K., Moosmüller, H., Sheridan, P. J., and Ogren, J. A.: Towards aerosol light–absorption measurements with a 7–wavelength aethalometer: Evaluation with a photoacoustic instrument and 3–wavelength nephelometer, Aerosol Sci. Technol., 39, 17–29, 2005.

Arnott, W. P., Walker, J. W., Moosmüller, H., Elleman, R. A., Jonsson, H. H., Buzorius, G., Conant, W. C., Flagan, R. C., and Seinfeld, J. H.: Photoacoustic insight for aerosol light absorption aloft from meteorological aircraft and comparison with particle soot absorption photometer measurements: DOE Southern Great Plains climate research facility and the coastal stratocumulus imposed perturbation experiments, J. Geophys. Res., 111, 2006.

Ashbourn, S., Jenkin, M., and Clemitshaw, K.: Laboratory and modelling studies of the response of a peroxy radical chemical amplifier to HO_2 and a series of organic peroxy radicals, J. Climate, 29, 233, 1998.

Asner, G. and Vitousek, P.: Remote analysis of biological invasion and biogeochemical change, in Proceedings of the National Academy of Sciences of the United States of America, vol. 102 (12), pp. 4383–4386, 2005.

ASTM: Standard test method for calibration of a pyranometer using a pyrheliometer, ASTM, pp. G167–05, 2005.

Atkinson, D. B.: Solving chemical problems of environmental importance using cavity ring–down spectroscopy, Analyst, 128, 117–125, london, 2003.

Atkinson, R.: Gas phase tropospheric chemistry of organic compounds: A review, Atmos. Environm., 24A, 1990.

Atkinson, R.: Atmospheric chemistry of VOCs and NO_x, Atmos. Environm., 34, 2063, 2000.

Atkinson, R., Winer, A., and Pitts, J. J.: Estimation of night–time N_2O_5 concentrations from ambient NO_2 and NO_3 radical concentrations and the role of N_2O_5 in night–time chemistry, Atmos. Environ., 20, 331–339, 1986.

Atkinson, R., Baulch, D., Cox, R., Crowley, J., Hampson, R., Hynes, R., Jenkin, M., Rossi, M., and Troe, J.: Evaluated kinetic and photochemical data for atmospheric chemistry: Volume II–gas phase reactions of organic species, Atmos. Chem. Phys., 6, 3625–4055, doi:10.5194/acp–6–3625–2006, 2006.

Auriol, F., Gayet, J.-F., Febvre, G., Jourdan, O., Labonnote, L., and Brogniez, G.: In situ observations of cirrus cloud scattering phase function with 22° and 46° halos : Cloud field study on 19 February 1998, J. Atmos. Sci., 58, 3376–3390, 2001.

Austen, I.: For the spy in the sky, new eyes, New York Times, june 20, 2002.

Austin, R. J., Heymsfield, A. J., and Stephens, G. L.: Retrievals of ice cloud microphysical parameters using CloudSat millimeter wave radar and temperature, J. Geoph. Res., 2008.

Avissar, R., Holder, H. E., Abehserra, N., Bolch, M. A., Novick, K., Canning, P., Prince, K., Magalhaes, J., Matayoshi, N., Katul, G., Walko, R. L., and Johnson, K. M.: The Duke university helicopter observation platform., Bull. Am. Meteor. Soc., 90, 939 – 954, 2009.

Axford, D.: On the accuracy of wind measurements using an inertial platform in an aircraft, and an example of a measurement of the vertical mesostructure of the atmosphere, J. Appl. Meteor., 7, 645–666, 1968.

Aydin, K. and Tang, C.: Millimeter wave radar scattering from model ice crystal distributions, IEEE Transactions on Geoscience and Remote Sensing, 35, 140–146, 1997.

Azzopardi, B.: Measurement of drop sizes, Int. J. Heat Mass Transfer, 22, 1245–1279, 1979.

Bachalo, W.: A Method for Measuring the Size and Velocity of Spheres by Dual Beam Light Scatter Interferometry, Applied Optics, 19, 1980.

Bachalo, W.: Droplet Analysis Techniques: Their Selection and Applications, Liquid Particle Size Measurement Techniques, in Liquid Particle Size Measurement Techniques, edited by R. I. Tishkoff, J.M. and J. Kennedy, STP 848, p. 191, ASTM, doi: 10.1520/STP32613S, 1983.

Bachalo, W.: Experimental Methods in Multiphase Flows, International Journal on Multiphase Flow, 20, Suppl., 261–295, 1994.

Bachalo, W. and Houser, M.: Phase Doppler Spray Analyzer for Simultaneous Measurements of Drop Size and Velocity Distributions, Optical Engineering, 23, 1984.

Bachalo, W. and Houser, M.: Spray Drop Size and Velocity Measurements Using the Phase/Doppler Particle Analyzer, proceedings of the International Conference on Liquid Atomization and Spray Systems (Third International), 1985.

Bader, M. J., Clough, S. A., and Cox, G. P.: Aircraft and Dual Polarization Radar Observations of Hydrometeors in Light Stratiform Precipitation, Q. J. R. Meteorolog. Soc., 113, 491–515, 1987.

Bahreini, R., Jimenez, J. L., Wang, J., Flagan, R. C., Seinfeld, J. H., Jayne, J. T., and Worsnop, D. R.: Aircraft–based aerosol size and composition measurements during ACE–Asia using an Aerodyne aerosol mass spectrometer, J. Geophys. Res., 108, 2003.

Bahreini, R., Dunlea, E. J., Matthew, B. M., Simons, C., Docherty, K., DeCarlo, P., Jimenez, J., Brock, C. A., and Middlebrook, A. M.: Design and operation of a pressure–controlled inlet for airborne sampling with an aerodynamic aerosol lens, Aerosol Sci. Technol., 42, 465–471, 2008.

Baker, A., Rauthe–Schoch, A., Schuck, T., Brenninkmeijer, C., van Velthoven, P., Wisher, A., and Oram, D.: Investigation of chlorine radical chemistry in the Eyjafjallajokull volcanic plume using observed depletions in non–methane hydrocarbons, Geophys. Res. Lett., 38, doi: 10.1029/2011GL047571, 2011.

Baker, B. and Copson, E.: The Mathematical Theory of *Huygens*' Principle, Chelsea Publ. Company, New York, 1950.

Baker, B., Mo, Q., Lawson, R., O'Connor, D., and Korolev, A.: Drop Size Distributions and the Lack of Small Drops in RICO Rain Shafts, J. of Appl. Meteor. and Climatol., 48, 616–623, 2009a.

Baker, B., Mo, Q., Lawson, R., O'Connor, D., and Korolev, A.: The Effects of Precipitation on Cloud Droplet Measurement Devices, Journal of Atmospheric and Oceanic Technology, 26, 1404–1409, 2009b.

Bakwin, P. S., Tans, P. P., Stephens, B. B., Wofsy, S. C., Gerbig, C., and Grainger, A.: Strategies for measurement of atmospheric column means of carbon dioxide from aircraft using discrete sampling, J. Geophys. Res., 108, 4514, doi:4510.1029 / 2002JD003306, 2003.

Ball, S. M. and Jones, R.: Broad–band cavity ring–down spectroscopy, Chem. Rev., 103, 5239–5262, 2003.

Ball, S. M. and Jones, R.: Cavity ring–down spectroscopy: techniques and applications, chap. Broad–band cavity ring–down spectroscopy, pp. 57–88, Blackwell Publishing Limited, ISBN: 978–1–4051–7688–0, 2009.

Ball, S. M., Langridge, J., and Jones, R.: Broadband cavity enhanced absorption using light emitting diodes, Chem. Phys. Lett., 398, 68–74, 2004.

Bange, J.: Airborne Measurement of Turbulent Energy Exchange Between the Earth Surface and the Atmosphere, Sierke Verlag, 174 pp, ISBN 978-3-86844-221-2, 2009.

Bange, J. and Roth, R.: Helicopter–Borne Flux Measurements in the Nocturnal Boundary Layer Over Land–a Case Study, Boundary Layer Meteorol., 92, 295–325, 1999.

Bange, J., Beyrich, F., and Engelbart, D. A. M.: Airborne Measurements of Turbulent Fluxes during LITFASS–98: A Case Study about Method and Significance, Theor. Appl. Climatology, 73, 35–51, 2002.

Bange, J., Spieß, T., Herold, M., Beyrich, F., and Hennemuth, B.: Turbulent Fluxes from Helipod Flights above Quasi–Homogeneous Patches within the LITFASS Area, Boundary Layer Meteorol., 121, 127–151, 2006a.

Bange, J., Zittel, P., Spieß, T., Uhlenbrock, J., and Beyrich, F.: A New Method for the Determination of Area–Averaged Turbulent Surface Fluxes from Low–Level Flights Using Inverse Models, Boundary Layer Meteorol., 119, 527–561, 2006b.

Bannehr, L. and Glover, V.: Preprocessing of airborne pyranometer data, NCAR Tech. Note NCAR / TN–364+STR, p. 35, 1991.

Bannehr, L. and Schwiesow, R.: A technique to account for the misalignment of pyranometers installed on aircraft, J. Atmos. Oceanic Technol., 10, 774–777, 1993.

Barbour, N. M.: Inertial navigation sensors. Lecture Series, Paper 2. Low–Cost Navigation Sensors and Integration Technology, NATO Research and Technology Organisation, Rto Educational Notes, RTO–EN–SET–116(2010) AC / 323(SET–116)TP / 311, ISBN 978–92–837–0109–5., ftp: / / ftp.rta.nato.int / / PubFullText / RTO / EN / RTO–EN–SET–116(2010) / / / EN–SET–116(2010)–02.pdf, 2010.

Barkey, B. and Liou, K.: Polar nephelometer for light–scattering measurements of ice crystals, Optics Letters, pp. 232–234, 2001.

Baron, P. and Willeke, K.: Aerosol Measurement, Principles, Techniques and Applications, 2nd Edition, John Wiley and Sons, New York, 1160 pp., 2005.

Baron, P. A. and Willeke, K.: Aerosol measurement: Principles, techniques and applications, John Wiley and Sons, 24nd edn., 2001.

Barrick, J. D. W., Ritter, J. A., Watson, C. E., Wynkoop, M. W., Quinn, J. K., and Norfolk, D. R.: Calibration of NASA Turbulent Air Motion Measurement System, Technical Paper 3610, NASA, 1996.

Bartenbach, S., Williams, J., Plass–Dulmer, C., Berresheim, H., and Lelieveld, J.: In–situ measurement of reactive hydrocarbons at Hohenpeissenberg with comprehensive two–dimensional gas chromatography (GC x GC–FID): use in estimating HO and NO_3, Atmos. Chem. Phys., 7, 1–14, 2007.

Bateson, C. and Curtiss, B.: A method for manual end member selection and spectral unmixing, Remote Sens. Environ., 55, 229–243, 1996.

Battaglia, A., Sturniolo, O., and Prodi, F.: Analysis of polarization radar returns from ice clouds, Atmos. Res., 59–60, 231–250, 2001.

Battaglia, A., Tanelli, S., Kobayashi, S., Zrnic, D., Hogan, R., and Simmer, C.: Multiple–scattering in radar systems: A review, J. Quant. Spectrosc. Radiat. Transfer, 111, 917–947, 2010.

Battan, L. J.: Radar observation of the atmosphere, The University of Chicago Press, 325 pp., 1973.

Baumgardner, D., Jonsson, H., Dawson, W., O'Connor, D., and Newton, R.: The cloud, aerosol and precipitation spectrometer (CAPS): A new instrument for cloud investigations, Atmos. Res., 59–60, 251–264, 2001.

Baumgardner, D., Kok, G., and Raga, G.: Warming of the Arctic lower stratosphere by light absorbing particles, Geophys. Res. Lett., 31, 2004.

Baumgardner, D., Chepfer, H., Raga, G., and Kok, G.: The Shapes of Very Small Cirrus Particles Derived from In Situ Measurements, Geophys. Res. Lett., 32, doi:10.1029/2004GL021300, 2005.

Baumgardner, M., Silva, L., Biehl, L., and Stoner, E.: Reflectance properties of soils, Advances in Agronomy, 38, 1–44, 1985.

Beard, K. V. and Chuang, C.: A New Model for the Equilibrium Shape of Raindrops, J. Atmos. Sci., 44, 1509, 1987.

Beaton, S.: The ophir air temperature radiometer, NCAR Technical Note, NCAR/TN–471+EDD, 2006.

Belyaev, S. P. and Levin, L. M.: Techniques for collection of representative aerosol samples, J. Aerosol Sci., 5, 325–338, 1974.

Ben–Dor, E.: Imaging Spectroscopy, chap. 9: Imaging Spectroscopy for Urban Applications, pp. 243–281, Kluwer Academic Press, edited by F. van der Meer, 2001.

Ben–Dor, E. and Kruse, F.: Detection of atmospheric gases using GER 63 channel scanner data acquired over Makhtesh Ramon, Negev Israel, International Journal of Remote Sensing, 17, 1215–1232, 1996.

Ben–Dor, E., Goetz, A., and Shapiro, A.: Estimation of cirrus cloud and aerosol scattering in hyperspectral image data, in Proceedings of the International Symposium on Spectral Sensing Research, pp. 582–593, San Diego, California, USA, 1994.

Ben–Dor, E., Irons, J., and Epema, A.: Manual of Remote Sensing, chap. Soil Spectroscopy, pp. 111–188, J. Wiley & Sons Inc., New–York, Chichester, Weinheim, Brisbane, Singapore, Toronto, 3. edn., edited by A. Rencz, 1999.

Ben–Dor, E., Patkin, K., Banin, A., and Karnieli, A.: Mapping of several soil properties using DAIS–7915 hyperspectral scanner data, International Journal of Remote Sensing, 23, 1043–1062, 2002.

Ben-Dor, E., Goldshalager, N., Braun, O., Kindel, B., A.F.H.Goetz, Bonfil, D., Agassi, M., Margalit, N., Binayminy, Y., and Karnieli, A.: Monitoring of infiltration rate in semiarid soils using airborne hyperspectral technology, International Journal of Remote Sensing, 25, 1–18, 2004.

Benedict, L. H., Nobach, H., and Tropea, C.: Estimation of turbulent velocity spectra from laser Doppler data, Meas. Sci. Technol., 11, 1089–1104, 2000.

Berden, G. and Engeln, R.: Cavity Ring–Down Spectroscopy: Techniques and Applications, John Wiley and Sons, New York, 322 pp., 2009.

Berden, G., Peeters, R., and Meijer, G.: Cavity ring–down spectroscopy: experimental schemes and applications, Int. Rev. Phys. Chem., 19, 565–607, 2000.

Bergstrom, R., Pilewskie, P., Russell, P., Redemann, J., Bond, T., Quinn, P., and Sierau, B.: Spectral absorption properties of atmospheric aerosols, Atmos. Chem. Phys., 7, 5937–5943, 2007.

Berhendt, A., Wulfmeyer, V., Kiemle, C., Ehret, G., Flamant, C., Schaberl, T., Bauer, H.-S., Kooi, S., Ismail, S., Ferrare, R., and Browell, E.: Intercomparison of water vapor data measured with lidar during IHOP_2002, Part 2: Airborne to airborne systems, J. Atmos. Oceanic Technol., 24, 22–39, 2007.

Berk, G., Anderson, P., Bernstein, L., Fox, M., Alder-Golden, S., Chetwynd, J., Hoke, M., and Lewis, P.: Modtran5: A reformulated atmospheric band model with auxiliary species and practical mutliple scattering options, p. 8, Proc. NASA / AVIRIS Workshop 2002, 2002.

Berman, M., Kiiveri, H., Lagerstorm, R., Ernst, A., Dumme, R., and Huntington, J.: ICE: a statistical approach to identifying endmembers in hyperspectral images, IEEE Transaction on Geoscience and Remote Sensing, 42, 2085–2095, 2004.

Bernstein, L., Adler-Golden, S. M., Sundberg, R. L., and Ratkowski, A. J.: In–scene–based atmospheric correction of uncalibrated VISible–SWIR (VIS–SWIR) hyper– and multi–spectral imagery, in Proc. SPIE 7107, doi:10.1117 / 12.808193, 2008.

Bertaux, J.-L. and Delan, A.: Vertical distribution of H_2O in the stratosphere as determined by UV fluorescence in situ measurements, Geophys. Res. Lett., 5, 1017–1020, 1978.

Bertram, T., Perring, A., Wooldridge, P., Crounse, J., Kwan, A., Wennberg, P., Scheuer, E., Dibb, J., Avery, M., Sachse, G., Vay, S., Crawford, J., McNaughton, C., Clarke, A., Pickering, K., Fuelberg, H., Huey, G., Blake, D., Singh, H., Hall, S., Shetter, R., Fried, A., Heikes, B., and Cohen, R.: Direct Measurements of the Convective Recycling of the Upper Troposphere, Science, 315, 816–820, 2007.

Beuttell, R. G. and Brewer, A. W.: Instruments for the measurement of the visual range, J. Sci. Instrum., 26, 357–359, 1949.

Bevly, D. M. and Cobb, S.: GNSS for vehicle control, Artech House, Boston, MA, 2010.

Bhawar, P. D. G., Summa, D., Flamant, C., Althausen, D., Behrendt, A., Kiemle, C., Bosser, P., Cacciani, M., Champollion, C., Iorio, T. D., Engelmann, R., Herold, C., Pal, S., Wirth, M., and Wulfmeyer, V.: 2011: The water vapour intercomparison effort in the framework of the Convective and Orographically–Induced Precipitation Study: airborne–to–ground–based and airborne–to–airborne lidar systems, Q. J. R. Meteorolog. Soc., 137, 325–348, 2011.

Bianci, R., Cavalli, R., Fiumi, L., Marino, C., and Pignatti, S.: CNR LARA project: Evaluation of two years of Airborne spectrometry, in 2nd International Airborne Remote Sensing Conference and Exhibition, San Fransico, California USA, pp. 534–543, 1996.

Bickel, W. and Bailey, W. M.: Stokes vectors, Mueller matrices, and polarized light scattering, Am. J. Phys., 53, 468–478, 1985.

Bierwirth, E., Wendisch, M., Jäkel, E., Ehrlich, A., Schmidt, K., Stark, H., Pilewskie, P., Esselborn, M., Gobbi, G., Ferrare, R., Müller, T., and Clarke, A.: New method to retrieve aerosol layer absorption coefficient from airborne flux density and actinic radiation measurements, J. Geophys. Res., Accepted, 2010.

Bigg, E. K.: Discrepancy between observation and prediction of concentrations of cloud condensation nuclei, Atmos. Res., 20, 82–86, 1986.

Bilbro, J., Fichtl, G., Fitzjarrald, D., Krause, M., and Lee, R.: Airborne Doppler lidar wind field measurements, Bull. Amer. Meteorol. Soc., 65, 384–359, 1984a.

Bilbro, J., DiMarzio, C., Fitzjarrald, D., Johnson, S., and Jones, W.: Airborne Doppler lidar measurements, Appl. Opt., 25, 3952–3960, 1986.

Bilbro, J. W., Fichtl, G., Fitzjarrald, D., and Krause, M.: Airborne Doppler lidar wind field measurements, Bull. Am. Meteorol. Soc., 65, 348–359., 1984b.

Bin Abas, M. R., Rahman, N. A., Omar, N., Maah, M. J., Samah, A. A., Orosc, D., Ottoc, A., and Simoneit, B.: Organic composition of aerosol particulate matter during a haze episode in Kuala Lumpur, Malaysia, Atmos. Environ., 38, 4223–4241, 2004.

Biskos, G., Reavell, K., and Collings, N.: Description and theoretical analysis of a differential mobility spectrometer, Aerosol Sci. Technol., 39, 527–541, 2005.

Biter, C., Dye, J., Huffman, D., and King, W. D.: The drop response of the CSIRO liquid water content, J. Atmos. Ocean Technol., 4, 359–367, 1987.

Black, M., Burpee, R., and Marks, F.: Vertical motion characteristics of tropical cyclones determined with airborne Doppler radial velocities, J. Atmos. Sci., 53, 1887–1909, 1996.

Blackwell, W., Barrett, J., Chen, F., Leslie, R., Rosenkranz, P., Schwartz, M., and Staelin, D.: NPOESS Aircraft Sounder Testbed–Microwave (NAST–M): Instrument description and initial flight results, IEEE Trans. Geosci. Remote Sensing, 39, 2444–2453, 2001.

Blake, N., Blake, D., Chen, T., Collins, J., Sachse, G., Anderson, B., and Rowland, F.: Distribution and seasonality of selected hydrocarbons and halocarbons over the western Pacific basin during PEM–West A and PEM–West B, J. Geophys. Res., 102, 28 315–28 331, 1997.

Blanchard, R.: A new algorithm for computing inertial altitude and vertical velocity, IEEE Trans. Aerosp. Elecron. Syst., AES–7, 1143–1146, 1971.

Blomquist, B., Huebert, B., Howell, S., Litchy, M., Twohy, C., Schanot, A., Baumgardner, D., Lafleur, B., Seebaugh, R., and Laucks, M.: An evaluation of the community aerosol inlet for the NCAR C–130 research aircraft, J. Atmos. Oceanic Technol., 18, 1387–1397, 2001.

Blyth, A., Lasher-Trapp, S., Cooper, W., Knight, C., and Latham, J.: The role of giant and ultragiant nuclei in the formation of early radar echoes in warm cumulus clouds, J. Atmos. Sci., 60, 2557–2572, 2003.

Boardman, J., Kruse, F., and Green, R.: Mapping target signatures via partial unmixing of AVIRIS data, pp. 23–26, Proceedings of JPL Airborne Erath Science Workshop, 1995.

Boegel, W. and Baumann, R.: Test and Calibration of the DLR–Falcon Wind Measuring System by Maneuvers, J. Atmos. Oceanic Technol., 8, 5–18, 1991.

Boers, R., Melfi, S., and Palm, S. P.: Cold–air outbreak during GALE: lidar observations and modeling of boundary layer dynamics, Mon. Wea. Rev., 119, 1132–1147, 1991.

Boers, R., Mitchell, R., and Krummel, P.: Correction of aircraft pyranometer measurements for diffuse radiance and alignment errors, J. Geophys. Res., 103, 16 753–16 758, 1998.

Bognar, J. and Birks, J.: Miniaturized Ultraviolet Ozonesonde for Atmospheric Measurements, Anal. Chem., 68, 3059–3062, 1996.

Bohl, W.: Technische Strömungslehre, Vogel Verlag, Würzbug, Germany, p. 137, 1998.

Bohn, B., Kraus, A., Müller, M., and Hofzumahaus, A.: Measurement of atmospheric $O_3 \rightarrow O(^1D)$ photolysis frequencies using filterradiometry, J. Geophys. Res., 109, 2004.

Bohn, B., Corlett, G. K., Gillmann, M., Sanghavi, S., Stange, G., Tensing, E., Vrekoussis, M., Bloss, W., Clapp, L., Kortner, M., Dorn, H.-P., Monks, P. S., Platt, U., Plass-Dulmer, C., Mihalopoulos, N., Heard, D. E., Clemitshaw, K. C., Meixner, F., Prevot, A. S. H., and Schmitt, R.: Photolysis frequency measurement techniques: results of a comparison within the ACCENT project, Atmos. Chem. Phys., 8, 5373–5391, 2008.

Bohn, D. and Simon, H.: Mehrparametrige Approximation der Eichräume und Eichflächen von Unterschall- bzw. Überschall-5-Loch-Sonden, Archiv für Technisches Messen und Messtechnische Praxis, 3, 31–37, 1975.

Bohren, C. and Huffman, D.: Absorption and Scattering of Light by Small Particles, John Wiley and Sons, New York, 1983a.

Bohren, C. F. and Battan, L. J.: Radar Backscattering by Inhomogeneous Precipitation Particles, J. Atmos. Sci., 37, 1821–1827, 1980.

Bohren, C. F. and Huffman, D. R.: Absorption and Scattering of Light by Small Particles, John Wiley & Sons, Inc, 544 pp., 1983b.

Boiffier, J.-L.: The Dynamics of Flight – the Equations, Wiley, Chichester, UK, 1998.

Bollinger, M., Sievers, R., Fahey, D., and Fehsenfeld, F.: Conversion of nitrogen dioxide, nitric acid to nitric oxide by gold–catalysed reduction with carbon monoxide, Anal. Chem., 55, 1981–1986, 1983.

Bond, T. C. and Bergstrom, R. W.: Light Absorption by Carbonaceous Particles: An Investigative Review, Aerosol Sci. Technol., 40, 27–67, 2006.

Bond, T. C., Anderson, T. L., and Campbell, D.: Calibration and Intercomparison of Filter-Based Measurements of Visible Light Absorption by Aerosol, Aerosol Sci. Technol., 30, 582–600, 1999.

Bonsang, B., Kanakidou, M., and Lambert, G.: NMHC in the Marine Atmosphere–Preliminary–Results of Monitoring at Amsterdam Island, J. Atmos. Chem., 11, 169–178, 1990.

Born, M. and Wolf, E.: Principles of Optics, Pergamon, Oxford, 1965.

Born, M. and Wolf, E.: Principles of Optics, Cambridge University Press, 7 edn., 2003.

Borrmann, S. and Jaenicke, R.: Application of microholography for ground–based in situ measurements in stratus cloud layers: A case study, J. Atmos. Oceanic Tech., 10, 277–293, 1993.

Borrmann, S., Luot, B., and Mishchenko, M.: Application of the T-matrix method to the measurement of aspherical (ellipsoidal) particles with forward scattering optical particle counters, J. Aerosol Sci., 31, 789–799, 2000.

Borstad, G. A., Edel, H. R., Gower, J. F. R., and Hollinger, A. B.: Analysis of test and flight data from the Fluorescence Line Imager, Canadian Special Publication of Fisheries and Aquatic Sciences, Ottawa Department of Fisheries and Oceans, 83, 1985.

Bosart, B., Lee, W.-C., and Wakimoto, R. M.: Procedures to improve the accuracy of airborne Doppler radar data, J. Atmos. Oceanic Technol., 19, 322–339, 2002.

Bösenberg, J.: Ground–Based Differential Absorption Lidar for Water–Vapor and Temperature Profiling: Methodology, Appl. Opt., 37, 3845–3860., 1998.

Bou Karam, D., Flamant, C., Knippertz, P., Reitebuch, O., Pelon, J., Chong, M., and Dabas, A.: Dust emissions over Sahel associated with the West African Monsoon inter–tropical discontinuity region: A representative case study, Q. J. Roy. Meteorol. Soc., 134, 621–634, 2008.

Boulter, J. E., Cziczo, D., Middlebrook, A., Thomson, D., and Murphy, D.: Design and performance of a pumped counterflow virtual impactor, Aerosol Sci. Technol., 40, 969–976, 2006.

Bozoki, Z., Pogány, A., and Szabó, G.: Photoacoustic instruments for practical applications: present, potentials and future challenges, Appl. Spectrosc. Rev., in press, 2011.

Bradshaw, J. D., Rodgers, M., Sandholm, S., Kesheng, S., and Davis, D.: A 2–photon laser–induced fluorescence field instrument for ground–based and airborne measurements of atmospheric NO, J. Geophys. Res. D: Atmos., 90, 2861–2873, 1985.

Brando, V., Keen, R., Daniel, P., Baumeister, A., Nethery, M., Baumeister, H., Hawdon, A., Swan, G., Mitchell, R., Campbell, S., Schroeder, T., Park, Y.-J., Edwards, R., Steven, A., Allen, S., Clementson, L., and Dekker, A.: The Lucinda Jetty Coastal Observatory's role in satellite ocean colour calibration and validation for Great Barrier Reef coastal waters, Proceedings IEEE Oceans 2010, Sydney, Australia, 2010.

Brands, M., Kamphus, M., Böttger, T., Schneider, J., Drewnick, F., Roth, A., Curtius, J., Voigt, C., Borbon, A., Beekmann, M., Bourdon, A., Perrin, T., and Borrmann, S.: Characterization of a newly developed aircraft–based laser ablation aerosol mass spectrometer (ALABAMA) and first field deployment in urban pollution plumes over Paris during MEGAPOLI 2009, Aerosol Sci. Technol., 2010.

Brandtjen, R., Klüpfel, T., Perner, D., and Knudsen, B. M.: Airborne measurements during the European Arctic Stratospheric Ozone Experiment: Observation of OClO, Geophys. Res. Lett., 21, 1363–1366, 1994.

Brass, M. and Röckmann, T.: Continuous–flow isotope ratio mass spectrometry method for carbon and hydrogen isotope measurements on atmospheric methane, Atmos. Meas. Tech. Discuss., 3, 2433–2476, 2010.

Braun, W. and Carrington, T.: Line measurements for concentration measurements and photochemistry, J. Quant. Spectrosc. Radiat. Transfer, 9, 1133–1143, 1969.

Brenguier, J. and Amodei, L.: Coincidence and dead–time corrections for particle counters. Part I: A general mathematical formalism, J. Atmos. Ocean. Tech., 6, 575–584, 1989.

Brenguier, J., Baumgardner, D., and Baker, B.: A review and discussion of processing algorithms for FSSP concentration measurements, J. Atmos. Ocean. Tech., 11, 1409–1414, 1994.

Brenguier, J., Bourrianne, T., Coelho, A., Isbert, J., Peytavi, R., Trevarin, D., and Wechsler, P.: Improvements of droplet size distribution measurements with the Fast-FSSP (Forward Scattering Spectrometer Probe, J. Atmos. Ocean. Tech., 15, 1077–1090, 1998.

Brenninkmeijer, C. A. M., Crutzen, P., Boumard, F., Dauer, T., Dix, B., R. Ebinghau and, D. F., Fischer, H., Franke, H., Friess, U., Heintzenberg, J., Helleis, F., Hermann, M., Kock, H. H., Koeppel, C., Lelieveld, J., Leuenberger, M., Martinsson, B. G., Miemczyk, S., Moret, H., Nguyen, H. N., Nyfeler, P., Oram, D., Sullivan, D. O., Penkett, S., Platt, U., Pupek, M., Ramonet, M., Randa, B., Reichelt, M., Rhee, T., Rohwer, J., Rosenfeld, K., Scharffe, D., Schlager, H., Schumann, U., Slemr, F., Sprung, D., Stock, P., Thaler, R., Valentino, F., van Velthoven, P., Waibel, A., Wandel, A., Waschitschek, K., Wiedensohler, A., Xueref-Remy, I., Zahn, A., Zech, U., and Ziereis, H.: Civil Aircraft for the regular investigation of the atmosphere based on an instrumented container: The new CARIBIC system, Atmos. Chem. Phys., 7, 4953–4976, 2007.

Bringi, V. N. and Chandrasekar, V.: Polarimetric Doppler Weather Radar: Principles and Applications, Cambridge University Press, 636 pp., 2001.

Brinkmann, J., Hackenthal, E.-M., Krämer, M., Schüle, M., Schütz, L., and Sprengart-Eichel, C.: Particle distribution, composition and processing during cloud, fog and rain cycles. In: Dynamics and Chemistry of Hydrometeors; Final report of the Collaborative Research Centre 233: 'Chemie und Dynamik der Hydrometeore', J. Wiley & Sons, ISBN 3–527–27727–7, 2001.

Brock, C. A., Schroder, F., Karcher, B., Petzold, A., Busen, R., and Fiebig, M.: Ultrafine particle size distributions measured in aircraft exhaust plumes, J. Geophys. Res., 105, 26 555–26 567, 2000.

Brock, C. A., Cozic, J., Bahreini, R., Froyd, K. D., Middlebrook, A. M., McComiskey, A., Brioude, J., Cooper, O. R., Stohl, A., Aikin, K. C., de Gouw, J. A., Fahey, D. W., Ferrare, R. A., Gao, R. S., Gore, W., Holloway, J. S., Hübler, G., Jefferson, A., Lack, D. A., Lance, S., Moore, R. H., Murphy, D. M., Nenes, A., Novelli, P. C., Nowak, J. B., Ogren, J. A., Peischl, J., Pierce, R. B., Pilewskie, P., Quinn, P. K., Ryerson, T. B., Schmidt, K. S., Schwarz, J. P., Sodemann, H., Spackman, J. R., Stark, H., Thomson, D. S., Thornberry, T., Veres, P., Watts, L. A., Warneke, C., and Wollny, A. G.: Characteristics, sources, and transport of aerosols measured in spring 2008 during the aerosol, radiation, and cloud processes affecting Arctic Climate (ARCPAC) Project, Atmos. Chem. Phys., 11, 2423–2453, 2011.

Brook, A. and Ben-Dor, E.: Supervised Vicarious Calibration (SVC) of hyperspectral remote sensing data, submitted to Remote Sensing of Environment, 2011.

Brookes, D.: Characterisation of a PERCA instrument and measurements of peroxy radicals during the West African Monsoon 2006, Ph.D. thesis, University of Leicester, 2009.

Brooks, B. J., Smith, M. H., Hill, M. K., and O'Dowd, C. D.: Size–differenciated volatility analysis of internally mixed laboratory-generated aerosol, J. Aerosol Sci., 33, 555–579, 2002.

Brooks, B. J., McQuaid, J. B., Smith, M. H., Crosier, J., Williams, P. I., Coe, H., and Osborne, S.: Intercomparison of VACC– and AMS–derived nitrate, sulphate and ammonium aerosol loadings during ADRIEX, Q. J. R. Meterol. Soc., 133, 77–84, 2007.

Brough, N., Reeves, C. E., Penkett, S. A., Dewey, K., Kent, J., Barjat, H., Monks, P., Ziereis, H., Stock, P., Huntrieser, H., and Schlager, H.: Intercomparison of aircraft instruments on board the C–130 and Falcon 20 over southern Germany during Export 2000, Atmos. Chem. Phys., 3, 2127–2138, 2003.

Browell, E., Carter, A., Shipley, S., Allen, R., Butler, C., Mayo, M., Siviter(Jr.), J., and Hall, W.: NASA multipurpose airborne DIAL system and measurements of ozone and aerosol profiles, Appl. Opt., 22, 522–534, 1983.

Browell, E., Ismail, S., and Grant, W.: Differential absorption lidar (DIAL) measurements from air and space, Appl. Phys. B, 67, 399–410, 1998.

Brown, E. N., Friehe, C. A., and Lenschow, D. H.: The use of pressure fluctuations on the nose of aircraft for measuring air motion, J. Clim. and Appl. Meteorol., 22, 171–180, 1983.

Brown, P.: Use of Holography for Airborne Cloud Physics Measurements, J. Atmos. Ocean. Technol., 6, 293–306, 1989.

Brown, P. R. A. and Francis, P. N.: Improved Measurements of the Ice Water Content in Cirrus Using a Total–Water Probe, J. Atmos. Oceanic Technol., 12, 410–414, 1995.

Brown, R. G. and Hwang, P.: Introduction to random signals and applied Kalman filtering: With MATLAB exercises and solutions, Wiley, New York, 1997.

Brown, S. S.: Absorption spectroscopy in high–finesses cavities for atmospheric studies, Chem. Rev., 103, 5219–5238, 2003.

Brown, S. S., Dubé, W., Osthoff, H., Stutz, J., Ryerson, T., Wollny, A., Brock, C., Warneke, C., de Gouw, J., Atlas, E., Neuman, J., Holloway, J., Lerner, B., Williams, E., Kuster, W., Goldan, P., Angevine, W., Trainer, M., Fehsenfeld, F., and Ravishankara, A.: Vertical profiles in NO_3 and N_2O_5 measured from an aircraft: Results from the NOAA P–3 and surface platforms during NEAQS 2004, J. Geophys. Res., 112, doi: 10.1029/2007JD008883, 2007.

Broxmeyer, C.: Inertial navigation systems. McGraw–Hill Electronic Sciences Series, McGraw-Hill, New York, 1964.

Bruegge, C., Conel, J., Green, R., Margolis, J., Holm, R., and Toon, G.: Water vapor column abundance retrievals during FIFE, J. Geophys. Res., 97, 18 759–18 768, 1992.

Brune, W. H., Anderson, J., and Chan, K.: In–situ Observations of ClO In the Antarctic–ER–2 Aircraft Results From 54°S To 72°S Latitude, J. Geophys. Res. D: Atmos., 94, 16 649–16 663, 1989a.

Brune, W. H., Anderson, J., and Chan, K.: In–situ Observations of BrO Over Antarctica–ER–2 Aircraft Results From 54°S To 72°S Latitude, J. Geophys. Res. D: Atmos., 94, 16 639–16 647, 1989b.

Brune, W. H., Faloona, I., Tan, D., Weinheimer, A., Campos, T., Ridley, B., Collins, S. V. J., Sachse, G., and Jacob, L. J. D.: Airborne in–situ OH and HO_2 observations in the cloud–ree troposphere and lower stratosphere during SUCCESS, Geophys. Res. Lett., 25, 1701–1704, 1998.

Bruneau, D.: Fringe–imaging Mach–Zehnder interferometer as a spectral analyzer for molecular Doppler wind lidar, Appl. Opt., 41, 503–510, 2002.

Bruneau, D. and Pelon, J.: Simultaneous measurements of particle backscattering and extinction coefficients and wind velocity by lidar with a Mach–Zehnder interferometer: principle of operation and performance assessment, Appl. Opt., 42, 1101–1114, 2003.

Bruneau, D., Quaglia, P., Flamant, C., Meisonnier, M., and Pelon, J.: Airborne lidar LEANDRE II for water–vapor profiling in the troposphere. II. First results, Appl. Opt., 40, 3462–3475, 2001a.

Bruneau, D., Quaglia, P., Flamant, C., and Pelon, J.: Airborne lidar LEANDRE II for water–vapor profiling in the troposphere. I. System description, Appl. Opt., 40, 3450–3461, 2001b.

Brunelli, N. A., Flagan, R. C., and Giapis, K. P.: Radial Differential Mobility Analyzer for One Nanometer Particle Classification, Aerosol Sci. Technol., 43, 53–59, 2009.

Bruns, M., Bühler, S., Burrows, J. P., Heue, K.-P., Platt, U., Pundt, I., Richter, A., Rozanov, A., Wagner, T., and Wang, P.: Retrieval of Profile Information from Airborne Multi Axis UV / visible Skylight Absorption Measurements, Appl. Opt., 43, 4415–4426, 2004.

Bruun, H. H.: Hot–Wire Anemometry, Oxford University Press, Oxford, U.K., 507 p., 1995.

Bruzzone, L., M. C. and Marconcini, M.: Classification of remote sensing images from urban areas using fuzzy probabilistic models, IEEE Transactions and Remote Sensing Letter, 3, 40–44, 2006.

Bruzzone L, M. C. and Marconcini, M.: A novel transductive SVM for semisupervised classification of remote sensing, IEEE Transactions on Geoscience and Remote Sensing, 2006.

Buchhave, P., George Jr., W. K., and Lumley, J. L.: The measurement of turbulence with the laser–Doppler anemometer, Annu. Rev. Fluid Mech., 11, 443–503, 1979.

Bucholtz, A.: Rayleigh–scattering calculations for the terrestrial atmosphere, Appl. Opt., 34, 2765–2773, 1995.

Bucholtz, A. and Jonsson, H.: Modified Kipp & Zonen pyranometers and pyrgeometers for use on atmospheric research aircraft, J. Atmos. Oceanic Technol., in preparation, 2010.

Bucholtz, A., Bluth, R., Kelly, B., Taylor, S., Batson, K., Sarto, A., Tooman, T., and McCoy Jr., R.: The Stabilized Radiometer Platform (STRAP)–An actively stabilized horizontally level platform for improved aircraft irradiance measurements, J. Atmos. Oceanic Technol., 25, 2161–2175, doi: 10.1175/2008JTECHA1085.1, 2008.

Buck, A.: The Lyman–alpha absorption hygrometer, in Moisture and Humidity Symposium, Washington, D.C., pp. 411–436, Instrument Society of America, Research Triangle Park, NC, 1985.

Buck, A. L.: The variable–path Lyman–alpha hygrometer and its operating characteristics, Bull. Amer. Meteor. Soc., 57, 1113–1118, 1976.

Buck, A. R. C.: Development of a cryogenic dew frost point hygrometer, in Proceedings Seventh Symposium Meteorological Observation Instrumentation, pp. 322–326, American Meteor Society, 1991.

Buckingham, R. and Staenz, K.: Review of current and planned civilian space hyperpsectral sensors for EO, Canadian Journal of Remote Sensing, 34 Suppl.1, S187–S197, 2008.

Buehler, S., Jimenez, C., Evans, K., Eriksson, P., Rydberg, B., Heymsfield, A., Stubenrauch, C., Lohmann, U., Emde, C., John, V., Sreerekha, T., and Davis, C.: A concept for a satellite mission to measure cloud ice water path, ice particle size, and cloud altitude, Quart. J. Roy. Meteor. Soc., 133, 109–128, 2007.

Bufton, J. L., Itabe, T., Strow, L. L., Korb, C. L., Gentry, B. M., and Weng, C. Y.: Frequency–doubled CO_2 lidar measurement and diode laser spectroscopy of atmospheric CO_2, Appl. Opt., 22, 2592–2602, 1983.

Bundke, U., Nillius, B., Jaenicke, R., Wetter, T., Klein, H., and Bingemer, H.: The Fast Ice Nucleus Chamber FINCH, Atmos. Res., 90, 180–186, 2008.

Bundke, U., Reimann, B., Nillius, B., Jaenicke, R., and Bingemer, H.: Development of a Bioaerosol single particle detector (BIO IN) for the Fast Ice Nucleus Chamber FINCH, Atmos. Meas. Tech., 3, 1–9, 2010.

Bunker, A. F.: Turbulence and shearing stresses measured over the north Atlantic Ocean by an airplane–acceleration technique, J. Atmos. Sci., 12, 445–455, 1955.

Burnet, F. and Brenguier, J.-L.: Validation of droplet spectra and water content measurements, Phys. Chem. Earth (B), 24, 249–254, 1999.

Burnet, F. and Brenguier, J.-L.: Comparison between standard and modified forward scattering spectrometer probes during the small Cumulus microphysics studies, J. Atmospheric and Oceanic Technology, 19, 1516–1531, 2002.

Burton, S. P., Ferrare, R. A., Hostetler, C. A., Hair, J. W., Kittaka, C., Vaughan, M. A., Obland, M. D., Rogers, R. R., Cooks, A. L., Harper, D. B., and Remer, L. A.: Using airborne high spectral resolution lidar data to evaluate combined active plus passive retrievals of aerosol extinction profiles, J. Geophys. Res., 115, 2010.

Butler, T. J. A., Mellon, D., J. Kim, J. L., and Orr-Ewing, A. J.: Optical–Feedback Cavity Ring–Down Spectroscopy Measurements of Extinction by Aerosol Particles, J. Phys. Chem. A, 113, 3963–3972, 2009.

Cahen, C. and Mégie, G.: A spectral limitation of the range resolved differential absorption lidar technique, J. Quant. Spectrosc. Radiat. Transfer, 25, 151–157, 1981.

Cahen, C., Mégie, G., and Flamant, P.: Lidar monitoring of the water vapor cycle in the troposphere, J. Appl. Meteorol., 21, 1506–1515, 1982.

Cain, S., Ram, M., and Woodward, S.: Qualitative and quantitative wind tunnel measurements of the airflow through a shrouded airborne aerosol sampling probe, J. Aerosol Sci., 29, 1157–1169, 1998.

Cain, S. A. and Ram, M.: Numerical simulation studies of the turbulent airflow through a shrouded airborne aerosol sampling probe and estimation of the minimum sampler transmission efficiency, J. Aerosol Sci., 29, 1145–1156, 1998.

Cairo, F., Pommereau, J. P., Law, K. S., Schlager, H., Garnier, A., Fierli, F., Ern, M., Streibel, M., Arabas, S., Borrmann, S., Berthelier, J. J., Blom, C., Christensen, T., D'Amato, F., Di Donfrancesco, G., Deshler, T., Diedhiou, A., Durry, G., Engelsen, O., Goutail, F., Harris, N. R. P., Kerstel, E. R. T., Khaykin, S., Konopka, P., Kylling, A., Larsen, N., Lebel, T., Liu, X., MacKenzie, A. R., Nielsen, J., Oulanowski, A., Parker, D. J., Pelon, J., Polcher, J., Pyle, J. A., Ravegnani, F., Riviere, E. D., Robinson, A. D., Rockmann, T., Schiller, C., Simoes, F., Stefanutti, L., Stroh, F., Some, L., Siegmund, P., Sitnikov, N., Vernier, J. P., Volk, C. M., Voigt, C., von Hobe, M., Viciani, S., and Yushkov, V.: An introduction to the SCOUT–AMMA stratospheric aircraft, balloons and sondes campaign in West Africa, August 2006: rationale and roadmap, Atmos. Chem. Phys., 10, 2237–2256, 2010.

Camps–Valls, G., Gomez–Chova, L., Munoz–Mari, J., Vila–Frances, J., and Calpe–Maravilla, J.: Composite kernels for hyperspectral image classification, IEEE Geosciences and Remote Sensing Letters, 3, 93–97, doi: 10.1109/LGRS.2005.857031, 2006.

Camps-Valls, G. and Bruzzone, L.: CAREFUL: Authors and title DO NOT MATCH according to IEEE explore: Prasad, S. and L.M. Bruce Overcoming the small sample size problem in hyperspectral classification and detection tasks, IEEE Transactions on Geoscience and Remote Sensing, 43, 1352–1362, 2005.

Canagaratna, M., Jayne, J., Jimenez, J., Allan, J., Alfarra, M., and Zhang, Q.: Chemical and microphysical characterization of ambient aerosols with the aerodyne aerosol mass spectrometer, Mass spectrometry reviews, 26, 185–222, 2007.

Cantrell, C. and Stedman, D.: A possible technique for the measurement of atmospheric peroxy radicals, Geophys. Res. Lett., 9, 846, 1982.

Cantrell, C., Stedman, D., and Wendel, G.: Measurements of atmospheric peroxy radicals by chemical amplification, Anal. Chem., 56, 1496, 1984.

Cantrell, C., Shetter, R., Lind, J., McDaniel, A., Calvert, J., Parrish, D., Fehsenfeld, F., Buhr, M., and Trainer, M.: An improved chemical amplifier technique for peroxy radical measurements, J. Geophys. Res., 98, 2897, 1993.

Cantrell, C., Edwards, G., Stephens, S., Mauldin, L., Kosciuch, E., Zondlo, M., and Eisele, F.: Peroxy radical observations using chemical ionization mass spectrometry during TOPSE, J. Geophys. Res., 108, 8371, 2003a.

Cantrell, C., Edwards, G., Stephens, S., Mauldin, R.L. Zondlo, M., Kosciuch, E., Eisele, F., Shetter, R., Lefer, B., Hall, S., Flocke, F., Weinheimer, A., Fried, A., Apel, E., Kondo, Y., Blake, D., Blake, N., Simpson, I., Bandy, A., Thornton, D., Heikes, B., Singh, H., Brune, W., Harder, H., Martinez, M., Jacob, D., Avery, M., Barrick, J., Sachse, G., Olson, J., Crawford, J., and Clarke, A.: Peroxy radical behaviour during the Transport and Chemical Evolution over the Pacific (TRACE–P) campaign as measured aboard the NASA P–3B aircraft, J. Geophys. Res., 108, 8787, doi: 10.1029/2003JD003674, 2003b.

Cantrell, C. A., Shetter, R. E., Gilpin, T. M., Calvert, J. G., Eisele, F. L., and Tanner, D. J.: Peroxy radical concentrations measured and calculated from trace gas measurements in the Mauna Loa Photochemistry Experiment 2, J. Geophys. Res., 101, 14 653–14 664, 1996.

Caramori, P., Schuepp, P., Desjardins, R., and MacPherson, I.: Structural Analysis of Airborne Flux Estimates Over a Region, Journal of Climate, 7, 627–640, 1994.

Carrico, C. M., Kus, P., Rood, M. J., Quinn, P., and Bates, T. S.: Mixtures of pollution, dust, sea salt, and volcanic aerosol during ACE–Asia: Radiative properties as a function of relative humidity, J. Geophys. Res. D: Atmos., 108, 2003.

Castells, A., Carswell, J., and Chang, P.: A high–resolution Imaging Wind and Rain Airborne Profiler for tropical cyclones, in Geoscience and Remote Sensing Symposium(IGARSS), vol. 5, pp. 2013–2015, IEEE, 2001.

Cerni, T.: An infrared hygrometer for atmospheric research and routine monitoring, J. Atmos. Oceanic Technol., 11, 445–462, 1994.

Cess, R., Zhang, M., Minnis, P., Corsetti, L., Dutton, E., Forgan, B., Garber, D., Gates, W., Hack, J., Harrison, E., Jing, X., Kiehl, J., Long, C., Morcrette, J.-J., Potter, G., Ramanathan, V., Subasilar, B., Whitlock, C., Young, D., and Zhou, Y.: Absorption of Solar Radiation by Clouds: Observations Versus Models, Science, 267, 496–499, 1995.

Cézard, N., Dolfi–Bouteyre, A., Huignard, J.-P., and Flamant, P. H.: Performance evaluation of a dual fringe–imaging Michelson interferometer for air parameter measurements with a 355 nm Rayleigh–Mie lidar, Appl. Opt., 48, 2321–2332, 2009.

Chandra, S. and McFarland, A.: Shrouded probe performance: variable flow operation and effect of free stream turbulence, Aerosol Sci. Technol., 26, 111–126, 1997.

Chang, C.: Hyperspectral Imaging: Techniques for spectral detection and classification, Kluwer Academic Plenum Publishers, New York, 2003.

Chang, C., Wu, C., Liu, W., and Ouyang, Y.: A new growing method for simplex–based endmember extraction algorithms, IEEE Transactions on Geoscience and Remote Sensing, 44, 2804–2819, 2006.

Chang, E. J. and Kailasanatha, K.: Shock wave interactions with particles and liquid fuel droplets, Shock Waves, 12, 333–341, 2003.

Chapon, B., Delrieu, G., Gosset, M., and Boudevillain, B.: Variability of rain drop size distribution and its effect on the Z–R relationship: A case study for intense Mediterranean rainfall, Atmos. Res., 87, 52–65, 2008.

Chen, J., Conant, W., Rissman, T., Flagan, R., and Seinfeld, J.: Effect of angle of attack on the performance of an airborne counterflow virtual impactor, Aerosol Sci. Technol., 39, 485–491, 2005.

Chepfer, H., Brogniez, G., Sauvage, L., Flamant, P. H., Trouillet, V., and Pelon, J.: Remote sensing of cirrus radiative properties during EUCREX'94. Case study of 17 april 1994. Part 2: Microphysical modelling, Mon. Wea. Rev., 127, 486–503, 1999.

Chiu, H.-Y. and Collins, W.: Spectroradiometer for airborne remote sensing, Photogrammetric Engineering and Remote Sensing, 44, 507–517, 1978.

Chow, J.: Measurement methods to determine compliance with ambient air-quality standards for suspended particles, J. Air Waste Manage. Assoc., 45, 320–382, 1995.

Christensen, P., Bandfield, J., Hamilton, V., Howard, D., Lane, M., Piatek, J., Ruff, S., and Stefanov, W.: A thermal emission spectral library of rock-forming minerals, J. Geophys. Res., 105, 9735–9739, 2000.

Chuang, P., Saw, E., Small, J., Shaw, R., Sipperley, C., Payne, G., and Bachalo, W.: Airborne phase Doppler interferometry for cloud microphysical measurements, Aerosol Sci. Tech., 42, 685–703, 2008.

Chudnovsky, A., Ben-Dor, E., Kostinski, A., and Koren, I.: Mineral content analysis of atmospheric dust using hyperspectral information from space, Geophysical Research Letters, 36, 5811–5817, 2009.

Chylek, P.: Extinction and liquid water content of fogs and clouds, J. Atmos. Sci., pp. 296–300, 1978.

Chýlek, P. and Wong, J. G. D.: Erroneous Use of the Modified Kohler Equation in Cloud and Aerosol Physics Applications, J. Atmos. Sci., 55, 1473–1477, 1998.

Clague, L.: An Improved Device for Obtaining Cloud Droplet Samples, J. Applied Meteorology, pp. 549–551, 1965.

Clark, R.: Manual of Remote Sensing, Volume 3: Remote Sensing for the Earth Sciences, chap. Spectroscopy of rocks and minerals, and principles of spectrocopy, pp. 3–58, John Wiley & Sons, New York, third edn., edited by A.N. Rencz, 1999.

Clark, R. and Roush, T.: Reflectance spectroscopy: Quantitative analysis techniques for remote sensing applications, J. Geophys. Res., pp. 6329–6340, 1984.

Clark, R., Gallagher, A., and Swayze, G.: Material Absorption Band Depth Mapping of Imaging Spectrometer Data Using a Complete Band Shape Least–Squares Fit with Library, in Proceedings of the Second Airborne Visible / Infrared Imaging Spectrometer (AVIRIS), Workshop, Pasadena, California, 1990, pp. 176–186, JPL Publication 90-54, 1990.

Clark, R., Brown, R., Jaumann, R., Cruikshank, D., Nelson, R., Buratti, B., McCord, T., Lunine, J., Baines, K. H., Bellucci, G., Bibring, J.-P., Capaccioni, F., Cerroni, P., Coradini, A., Formisano, V., Langevin, Y., Matson, D. L., Mennella, V., Nicholson, P. D., Sicardy, B., Sotin, C., Hoefen, T. M., Curchin, J. M., Hansen, G., Hibbits, K., and Matz, K.-D.: Compositional maps of Saturn's moon Phoebe from imaging spectroscopy, Nature, 435, 66–69, 2005.

Clarke, A. D.: A thermo–optic technique for in situ analysis of size-resolved aerosol physicochemistry, Atmos. Environm., 25, 635–644, part A, General Topics, 1991.

Claussen, M.: Estimation of Areally–Averaged Surface Fluxes, Boundary Layer Meteorol., 54, 387–410, 1991.

Clemitshaw, K.: A Review of Instrumentation and Measurement Techniques for Ground–Based and Airborne Field Studies of Gas–Phase Tropospheric Chemistry, Crit. Rev. Env. Sci. Technol., 34, 1–108, doi: 10.1080/10643380490265117, 2004.

Clemitshaw, K., Carpenter, L., Penkett, S., and Jenkin, M.: A calibrated peroxy radical chemical amplifier (PERCA) instrument for ground–based measurements in the troposphere, JGR, 102, 405, 1997.

Clever, J.: The use of imaging spectrometry for agricultural applications, ISPRS Journal of Photogrammetry and Remote Sensing, 54, 299–304, 1999.

Clough, P. and Trush, B. A.: Mechanism of the Chemiluminescent Reaction between NO and O_3, Trans. Faraday Soc., 63, 915–925, 1967.

Clyne, M., Thrush, B. A., and Wayne, R. P.: Kinetics of the chemiluminescent reaction between nitric oxide and ozone, Trans. Faraday Soc., 60, 359–370, 1964.

Cober, S., Isaac, G., and Korolev, A.: Assessing the Rosemount icing detector with in situ measurements, J. Atmos. Ocean. Tech., 18, 515–528, 2001a.

Cober, S., Isaac, G., Korolev, A., and Strapp, J.: Assessing cloud-phase conditions, J. Appl. Meteor., 40, 1967–1983, 2001b.

Coddington, O., Pilewskie, P., Redemann, J., Platnick, S., Russell, P., Schmidt, K., Gore, W., Livingston, J., Wind, G., and Vukicevic, T.: Examining the impact of overlying aerosols on the retrieval of cloud optical properties from passive remote sensing, J. Geophys. Res., doi:10.1029/2009JD012829, 2010.

Coe, H.: Aerosol Mass Spectrometry. Atmospheric Techniques, Blackwell's Scientific Publishing, J. D. Allan and D. E. Heard, Ed., 2006.

Cohen, R.: Shattering of a liquid drop due to impact, Proc. Roy. Soc. Lond., A 435, 483–503, 1991.

Collaud Coen, M., Weingartner, E., Apituley, A., Ceburnis, D., Fierz–Schmidhauser, R., Flentje, H., Henzing, J. S., Jennings, S. G., Moerman, M., Petzold, A., Schmid, O., and Baltensperger, U.: Minimizing light absorption measurement artifacts of the Aethalometer: evaluation of five correction algorithms, Atmos. Meas. Tech, 3, 457–474, 2010.

Collins, D. R., Flagan, R. C., and Seinfeld, J. H.: Improved inversion of scanning DMA data, Aerosol Sci. Technol., 36, 1–9, 2002.

Colomb, A., Williams, J., Crowley, J., Gros, V., Hofmann, R., Salisbury, G., Klupfel, T., Kormann, R., Stickler, A., Forster, C., and Lelieveld, J.: Airborne measurements of trace organic species in the upper troposphere over Europe: the impact of deep convection, Environ. Chem., 3, 244–259, 2006.

Commane, R., Floquet, C. F. A., Ingham, T., Stone, D., Evans, M. J., and Heard, D. E.: Observations of OH and HO_2 radicals over West Africa, Atmos. Chem. Phys., 10, 8783–8801, 2010.

Comstock, J. M., Ackerman, T. P., and Mace, G. G.: Ground–based lidar and radar remote sensing of tropical cirrus clouds at Nauru Island: Cloud statistics and radiative impacts, J. Geophys. Res. Atmos., 107, 2002.

Comte–Bellot, G.: Hot–wire anemometry, Annual Review of Fluid Mechanics, 8, 209–231, 1976.

Conant, W. C., Seinfeld, J. H., Wang, J., Carmichael, G. R., Tang, Y. H., Uno, I., Flatau, P. J., Markowicz, K. M., and Quinn, P. K.: A model for the radiative forcing during ACE–Asia derived from CIRPAS Twin Otter and R/V Ronald H. Brown data and comparison with observations, J. Geophys. Res. D: Atmos., 108, 2003.

Cooley, T., Anderson, G., Felde, G., Hoke, M., Ratkowski, A., Chetwynd, J., Gardner, J., Adler-Golden, S., Matthew, M., Berk, A., Bernstein, L., Acharya, P., Miller, D., and Lewis, P.: FLAASH, a MODTRAN4-based atmospheric correction algorithm, its application and validation, in eoscience and Remote Sensing Symposium, 2002. IGARSS '02. 2002 IEEE International, pp. 1414–1418, 2002.

Cooper, W.: Cloud physics investigation by the University of Wyoming in HIPLEX 1977, vol. AS 119, Bureau of Reclamation Rep., 321 pp., 1977.

Cooper, W.: Effects of coincidence on measurements with A Forward Scattering Spectrometer Probe, J. Atmos. Oceanic Technol., 5, 823–832, 1988.

Cooper, W. and Rogers, D.: Effects of airflow trajectories around aircraft on measurements of scalar fluxes, J. Atmos. Ocean. Tech., 8, 66–77, 1991.

Cotton, R., Osborne, S., Ulanowski, Z., Hirst, E., Kaye, P., and Greenaway, R.: The ability of the small ice detector (SID–2) to characterize cloud particle and aerosol morphologies obtained during flights of the FAAM BAe–146 research aircraft, J. Atmos. Oceanic Tech., 27, 290–303, 2009.

Coulson, K.: Solar and Terrestrial Radiation–Methods and Measurements, Academic Press, New York, San Francisco, London, 1975.

Cox, C. and Monk, W.: Measurements of the roughness of the sea surface from photographs of the sun's glitter, J. Opt. Soc. Amer., 144, 838–850, 1954.

Cox, S. and Griffith, K.: Estimates of radiative divergence during phase III of the GARP Atlantic Tropical Experiment: Part I. Methodology, J. Atmos. Sci., 36, 576–585, 1979.

Craig, R. A.: Vertical eddy transfer of heat and water vapor in stable air, J. Atmos. Sci., 6, 123–133, 1949.

Craigie, J. H.: Epidemiology of stem rust in western Canada, Scientia Agricola, 25, 285–401, 1945.

Crawford, J., Davis, D., Chen, G., Shetter, R., Müller, M., Barrick, J., and Olson, J.: An assesment of cloud effects on photolysis rate coefficients: Comparison of experimental and theoretical values, J. Geophy. Res., 104, 5725–5734, 1999.

Crawford, T., Dobosy, R., and Dumas, E.: Aircraft wind measurement considering lift–induced upwash, Boundary Layer Meteorol., 1996.

Crawford, T. L. and Dobosy, R. J.: A Sensitive Fast-Response Probe to Measure Turbulence and Heat Flux from any Airplane, Boundary–Layer Meteorol., 59, 257–278, 1992.

Crawford, T. L., McMillen, R. T., Dobosy, R. J., and MacPherson, I.: Correcting Airborne Flux Measurements for Aircraft Speed Variation, Boundary Layer Meteorol., 66, 237–245, 1993.

Creasey, D., Heard, D., and Lee, J.: Absorption cross–section measurements of water vapour and oxygen at 185 nm. Implications for the calibration of field instruments to measure OH, HO_2 and RO_2 radicals, Geophys. Res. Lett., 27, 2000.

Cremer, M.: All integrated nose boom for wind and turbulence measurement, 30th Annual Symposium, Society of Flight Test Engineers, St. Louis, USA, 1999.

Crépel, O., Gayet, J.-F., Fournol, J.-F., and Oshchepkov, S.: A new airborne Polar Nephelometer for the measurements of optical and microphysical cloud properties. Part II: Preliminary tests, Annales Geophysicae, 15, 460–470, 1997.

Crewell, S., Fabian, R., Künzi, K., Nett, H., Wehr, T., Read, W., and Waters, J.: Comparison of ClO measurements by airborne and spaceborne microwave radiometers in the arctic winter stratosphere 1993, Geophys. Res. Lett., 22, 1489–1492, 1994.

Crosier, J., Allan, J. D., Coe, H., Bower, K. N., Formenti, P., and Williams, P. I.: Chemical composition of summertime aerosol in the Po Valley (Italy), northern Adriatic and Black Sea, Q. J. R. Meteorolog. Soc., 133, 61–75, 2007a.

Crosier, J., Jimenez, J. L., Allan, J. D., Bower, K. N., Williams, P. I., Alfarra, M. R., Canagaratna, M. R., Jayne, J. T., Worsnop, D. R., and Coe, H.: Description and use of the new jump mass spectrum mode of operation for the aerodyne quadrupole aerosol mass spectrometers (Q–AMS), Aerosol Sci. Technol., 41, 865–872, 2007b.

Crounse, J., Karena, A., McKinney, K., Kwan, A., and Wennberg, P.: Measurement of Gas–Phase Hydroperoxides by Chemical Ionization Mass Spectrometry, Anal. Chem., 78, 2006.

Crowther, B.: The design, construction, and calibration of a spectral diffuse / global irradiance meter, Ph.D. thesis, University of Arizona, 1997.

Cruette, D., Marillier, A., Dufresne, J. L., Grandpeix, J. Y., Nacass, P., and Bellec, H.: Fast temperature and true air speed measurements with the airborne ultrasonic anemometer–thermometer (AUSAT)., J. Atmos. Oceanic Technol., 17, 1020–1039, 2000.

Crutzen, P. J., Williams, J., Poschl, U., Hoor, P., Fischer, H., Warneke, C., Holzinger, R., Hansel, A., Lindinger, W., Scheeren, B., and Lelieveld, J.: High spatial and temporal resolution measurements of primary organics and their oxidation products over the tropical forests of Surinam, Atmos. Environ., 34, 1161–1165, 2000.

Cummins, H. Z., Knable, N., and Yeh, Y.: Observation of diffusion broadening of Rayleigh scattered light, Phys. Rev. Lett., 12, 150–153, 1964.

Curtius, J. and Arnold, F.: Measurements of aerosol sulfuric acid 1. Experimental setup, characterization, and calibration of a novel mass spectrometric system, J. Geophys. Res., 106, 31 965–31 974, 2001.

Curtius, J., Sierau, B., Arnold, F., de Reus, M., Strom, J., Scheeren, H., and Lelieveld, J.: Measurements of aerosol sulfuric acid 2. Pronounced layering in the free troposphere during ACE–2, J. Geophys. Res., 106, 31 975–31 990, 2001.

Curtius, J., Weigel, R., Vossing, H. J., Wernli, H., Werner, A., Volk, C. M., Konopka, P., Krebsbach, M., Schiller, C., Roiger, A., Schlager, H., Dreiling, V., and Borrmann, S.: Observations of meteoric material and implications for aerosol nucleation in the winter Arctic lower stratosphere derived from in situ particle measurements, Atmos. Chem. Phys., 5, 3053–3069, 2005.

Cziczo, D. J., Thomson, D. S., and Murphy, D. M.: Ablation, flux, and atmospheric implications of meteors inferred from stratospheric aerosol, Science, 291, 1772–1775, 1001.

Cziczo, D. J., DeMott, P. J., Brock, C., Hudson, P. K., Jesse, B., Kreidenweis, S. M., Prenni, A. J., Schreiner, J., Thomson, D. S., and Murphy, D. M.: A Method for Single Particle Mass Spectroscopy of Ice Nuclei, Aerosol Sci. Technol., 37, 460–470, 2003.

Dabas, A., Drobinski, P., Reitebuch, O., Richard, E., Delville, P., Flamant, P. H., and Werner, C.: Multi–scale analysis of a straight jet streak using numerical analyses and an airborne Doppler lidar, Geophys. Res. Lett., 30, 1049, 2003.

Dabberdt, W. R. S., Cole, H., Paukkunen, Hoerhammer, J., V. Antikainen, edited by Holton, J., Pyle, J., and Curry, J.: Encyclopedia of Atmospheric Sciences, chap. Radiosondes, pp. 1469–1476, Academic Press, London, 2002.

Damiani, R. and Haimov, S.: A High-Resolution Dual–Doppler Technique for Fixed Multiantenna Airborne Radar, IEEE Transactions on Geoscience and Remote Sensing, 44, 3475–3489, 2006.

Dari–Salisburgo, C., Carlo, P. D., Giammaria, F., Kajii, Y., and D'Altorio, A.: Laser Induced fluorescence instrument for NO_2 measurements: observations at a central Italy background site, Atmos. Environ., 43, 970–977, 2009.

Davis, A., Marshak, A., Gerber, H., and Wiscombe, W.: Horizontal structure of marine boundary–layer clouds from cm to km scales, J. Geophys. Res., 104, 6123–6144, 1999.

Davis, D., Heaps, W., and McGee, T.: Direct measurements of natural tropospheric levels of OH via an aircraft borne tunable dye–laser, Geophys. Res. Lett., 3, 331–333, 1976.

Davis, D. D., Bradshaw, J., Rodgers, M., Sandholm, S., and Kesheng, S.: Free tropospheric and boundary–layer measurements of NO over the central and eastern north pacific–ocean, J. Geophys. Res. D: Atmos., 92, 2049–2070, 1987.

Davis, E. J. and Schweiger, G.: The Airborne Microparticle, Springer, New York, 2002.

Davis, S., Avallone, L., Weinstock, E., Twohy, C., Smith, J., and Kok, G.: Comparisons of in situ measurements of cirrus cloud ice water content, J. Geophys. Res., 112, doi:10.1029/2006JD008214, 2007.

Davis, S., Avallone, L., Kahn, B., Meyer, K., and Baumgardner, D.: Comparison of airborne in situ measurements and MODIS retrievals of cirrus cloud optical and microphysical properties during the Midlatitude Cirrus Experiment (MidCiX), J. Geophys. Res., D02203, doi:10.1029/2008JD010284, 2009.

Davison, C. and MacLeod, J.: Naturally Aspirating Isokinetic Total Water Content Probe: Intake Deicing and Heat Transfer, in 1st AIAA Atmospheric and Space Environments, 22–25 June, 2009, San Antonio, Texas, AIAA–2009–3862, 2009.

Davison, C., MacLeod, J., and Strapp, J.: Naturally Aspirating Isokinetic Total Water Content Probe: Evaporator Design and Testing, in 1st AIAA Atmospheric and Space Environments, 22–25 June, 2009, San Antonio, Texas, AIAA–2009–3861, 2009.

de Gouw, J., Warneke, C., Karl, T., Eerdekens, G., van der Veen, C., and Fall, R.: Sensitivity and specificity of atmospheric trace gas detection by proton–transfer–reaction mass spectrometry, Int. J. Mass Spectrom., 223, 365–382, 2003.

de Gouw, J. A., Warneke, C., Stohl, A., Wollny, A. G., Brock, C. A., Cooper, O. R., Holloway, J. S., Trainer, M., Fehsenfeld, F. C., Atlas, E. L., Donnelly, S. G., Stroud, V., and Lueb, A.: Volatile organic compounds composition of merged and aged forest fire plumes from Alaska and western Canada, J. Geophys. Res. D: Atmos., 111, 2006.

De Leo, R. and Hagen, F.: Aerodynamic Perforemance of Rosemount Model 858 AJ Air data Sensor, Tech. Rep. 8767, Rosemount, 1976.

de Reus, M., Fischer, H., Arnold, F., de Gouw, J., Holzinger, R., Warneke, C., and Williams, J.: On the relationship between acetone and carbon monoxide in different air masses, Atmos. Chem. Phys., 3, 1709–1723, 2003.

DeCarlo, P. F., Kimmel, J. R., Trimborn, A., Northway, M. J., Jayne, J. T., Aiken, A. C., Gonin, M., Fuhrer, K., Horvath, T., Docherty, K. S., Worsnop, D. R., and Jimenez, J. L.: Field-deployable, high–resolution, time–of–flight aerosol mass spectrometer, Anal. Chem., 78, 8281–8289, 2006.

DeCarlo, P. F., Dunlea, E. J., Kimmel, J. R., Aiken, A. C., Sueper, D., Crounse, J., Wennberg, P. O., Emmons, L., Shinozuka, Y., Clarke, A., Zhou, J., Tomlinson, J., Collins, D. R., Knapp, D., Weinheimer, A. J., Montzka, D. D., Campos, T., and Jimenez, J. L.: Fast airborne aerosol size and chemistry measurements above Mexico City and Central Mexico during the MILAGRO campaign, Atmos. Chem. Phys., 8, 4027–4048, 2008.

Dekker, A., Brando, V., Anstee, J., Pinnel, N., Kutser, T., Hoogenboom, H., Pasterkamp, R., Peters, S., Vos, R., Olbert, C., and Malthus, T.: Imaging Spectrometry: Basic principles and prospective applications: Remote Sensing and Digital Image Processing, v. IV, chap. Imaging spectrometry of water, pp. 307–359, Kluwer Academic Publishers, Dordrecht, 2001.

Del Bianco, S., Carli, B., Cecchi-Pestellini, C., Dinelli, B., Gai, M., and Santurri, L.: Retrieval of minor constituents in a cloudy atmosphere with remote–sensing millimetre–wave measurements, Quart. J. Roy. Meteor. Soc., 133, 163–170, 2007.

Delanoë, J. and Hogan, R. J.: A variational scheme for retrieving ice cloud properties from combined radar, lidar, and infrared radiometer, J. Geophys. Res. Atmos., 113, 2008.

Delanoë, J., Protat, A., Testud, J., and Bouniol, D.: Statistical properties of the normalized ice particle size distribution, J. Geophys. Res. Atmos., 110, 2005.

Delanoë, J., Protat, A., Bouniol, D., Heymsfield, A., Bansemer, A., and Brown, P.: The characterization of ice cloud properties from Doppler radar measurements, J. Appl. Meteorol. Climatol., 46, 1682–1698, 2007.

Delene, J., D., Deshler, T., Wechsler, P., and Vali, G.: A balloon-borne cloud condensation nuclei counter, J. Geophys. Res., 103, 8927–8934, 1998.

DeMott, P., Möhler, O., Stetzer, O., Murakami, M., Leisner, T., Bundke, U., Klein, H., Kanji, Z., Cotton, R., Jones, H., Petters, M., Prenni, A., Benz, S., Brinkmann, M., Rzesanke, D., Saathoff, H., Nicolet, M., Gallavardin, S., Saito, A., Nillius, B., Bingemer, H., Abbatt, J., Ardon, K., Levin, Z., Ganor, E., Georgakopoulos, D., and Vali, G.: Resurgence in ice nucleation research, to be submitted to Bull. Amer. Meteor. Soc., 2010.

DeMott, P. J., Petters, M. D., Prenni, A. J., Carrico, C. M., Kreidenweis, S. M., Collett Jr., J. L., and Moosmüller, H.: Ice nucleation behavior of biomass combustion particles at cirrus temperatures, J. Geophys. Res., 114, doi:10.1029/2009JD012036, 2009.

Deng, M. and Mace, G. G.: Cirrus Microphysical Properties and Air Motion Statistics Using Cloud Radar Doppler Moments. Part I: Algorithm Description, J. Appl. Meteorol. Climatol., 45, 1690–1709, 2006.

Deng, M., Mace, G., Wang, Z., and et al.: TC4 Validation for Ice Cloud Profiling Retrieval Using CloudSat Radar and CALIPSO Lidar, J. Geophys. Res., 115, 2010.

Denning, R., Guidero, S., Parks, G., and Gary, B.: Instrument description of the airborne microwave temperature profiler, J. Geophys. Res., 94, 16 757–16 765, 1989.

Deshler, T. and Vali, G.: Atmospheric concentrations of submicron contact–freezing nuclei, J. Atmos. Sci., 49, 773–784, 1992.

Deshler, T., Johnson, B. J., and Rozier, W. R.: Balloonborne measurements of Pinatubo aerosol during 1991 and 1992 at 41°N–vertical profiles, size distributoin and volatility, Geophys. Res. Lett., 20, 1435–1438, 1993.

Dhaniyala, S., Flagan, R., McKinney, K., and Wennberg, P.: Novel aerosol / gas inlet for aircraft–based measurements, Aerosol Sci. Technol., 37, 828–840, 2003.

Dhaniyala, S., Wennberg, P., Flagan, R., Fahey, D. W., Northway, M., Gao, R., and Bui, T.: Stratospheric aerosol sampling: Effect of a blunt–body housing on inlet sampling characteristics, Aerosol Sci. Technol., 38(11), 1080–1090, 2004.

Di Carlo, P., Salisburgo, C. D., Aruffo, E., Biancofiore, F., Busilacchio, M., Giammaria, F., Reeves, C., Moller, S., and Lee, J.: Airborne Laser Induced Fluorescence system for simultaneous measurements of nitrogen dioxide and speciated NO_y, EGU meeting, 2011.

Dibb, J. E., Talbot, R. W., Seid, G., Jordan, C., Scheuer, E., Atlas, E., Blake, N. J., and Blake, D. R.: Airborne sampling of aerosol particles: Comparison between surface sampling at Christmas Island and P–3 sampling during PEM–Tropics B, J. Geophys. Res., 108, 2002.

Dibb, J. E., Talbot, R. W., Scheuer, E. M., Seid, G., Avery, M. A., and Singh, H. B.: Aerosol chemical composition in Asian continental outflow during the TRACE–P campaign: Comparison with PEM-West B, J. Geophys. Res., 108, 2003.

Dickerson, R. and Delany, A.: Modification of a commercial gas filter correlation CO detector for enhanced sensitivity, J. Atmos. Oceanic Technol., 5, 424–431, 1988.

DIN, .: Begriffe, Grössen und Formelzeichen der Flugmechanik, 1990.

Diskin, G., Podolske, J., Sachse, G., and Slate, T.: Open–path airborne tunable diode laser hygrometer, in Proceedings of SPIE, vol. 4817, pp. 196–204, 2002.

DLR: http://www.halo.dlr.de/instrumentation/inlets, 2009.

Doebelin, E.: Measurement systems: Application and design. 4th Ed., McGraw–Hill, New York, 1990.

Doerffer, R., Graßl, H., Kunkel, B., and van der Piepen, H.: ROSIS - an advanced imaging spectrometer for the monitoring of water color and chlorophyll fluorescence, Proc. Intern. Congress on Optical Sciences & Engineering. Conference 1129: Advanced Optical Instrumentation for Remote Sensing of the Earth's Surface from Space. Paris, April 24-28, 1989, 30, 117, 1989.

Dolson, D. A. and Klingshirn, M.: Laser–initiated Chemical Chain–reactions–Termination Kinetics of the Cl_2 / HBr / NO Chain System, J. Phys. Chem., 97, 6645–6649, 1993.

Donovan, D. P. and van Lammeren, A.: Cloud effective particle size and water content profile retrievals using combined lidar and radar observations–1. Theory and examples, J. Geophys. Res. Atmos., 106, 27 425–27 448, 2001.

Donovan, D. P., Quante, M., Schlimme, I., and Macke, A.: Use of equivalent spheres to model the relation between radar reflectivity and optical extinction of ice cloud particles, Appl. Opt., 43, 4929–4940, 2004.

Dorf, M., Bosch, H., Butz, A., Camy–Peyret, C., Chipperfield, M., Engel, A., Goutail, F., Grunow, K., Hendrick, F., Hrechanyy, S., Naujokat, B., Pommereau, J., Roozendael, M. V., Sioris, C., Stroh, F., Weidner, F., and Pfeilsticker, K.: Balloon–borne stratospheric BrO measurements: comparison with Envisat/SCIAMACHY BrO limb profiles, Atmos. Chem. Phys., 6, 2483–2501, 2006.

Dotan, I., Albritton, D. L., Lindinger, W., and Pahl, M.: Mobilities of Co^{2+}, N_2H^+, H_3O^+, $H_3O^+.H_2O$, and $H_3O^+.(H_2O)2$ Ions in N^{-2}, J. Chem. Phys., 65, 5028–5030, 1976.

Doviak, R. J. and Zrnic, D.: Doppler Radar and Weather Observations, Academic Press, San Diego, 2 edn., 1993.

Dowling, D. R. and Radke, L. F.: A summary of the physical properties of cirrus clouds., J. Appl. Meteor., 29, 970–978, 1990.

Dozier, J. and Frew, J.: Atmospheric corrections to satellite radiometric data over rugged terrain, Remote Sens. Environ., 11, 191–205, 1981.

Drummond, A. and MacPherson, J.: Aircraft flow effects on cloud drop images and concentrations measured by the NAE Twin Otter, J. Atmos. Oceanic Technol., 2, 633–643, 1985.

Drummond, J. W., Volz, A., and Ehhalt, D. H.: An optimized chemiluminescence detector for tropospheric NO measurements, J. Atmos. Chem., 2, 287–306, 1985.

Dubé, W. P., Brown, S., Osthoff, H., Nunley, M., Ciciora, S., Paris, M., McLaughlin, R., and Ravishankara, A.: Aircraft instrument for simultaneous, in–situ measurements of NO_3 and N_2O_5 via cavity ring–down spectroscopy, Rev. Sci. Instrum., 77, doi:10.1063 / 1061.2176058, 2006.

Dubovik, O.: Photopolarimetry in Remote Sensing, chap. Optimization of Numerical Inversion in Photopolarimetric Remote Sensing, pp. 65–106, Kluwer Academic Publishers, Dordrecht, Netherlands, edited by G. Videen, Y. Yatskiv and M. Mishchenko, 2004.

Dungey, C. E. and Bohren, C. F.: Backscattering by Nonspherical Hydrometeors as Calculated by the Coupled–Dipole Method–An Application in Radar Meteorology, J. Atmos. Oceanic Technol., 10, 526–532, 1993.

Dupont, P.: Contribution à l'étude du vol en atmosphère agitée. Rapport sur la campagne du POTEZ 540 à la Banne d'Ordanche du 19 au 30 Septembre 1936, Publications Scientifiques et Techniques du Ministère de l'Air, Gauthiers-Villard Eds., 1938.

Durden, S. L., Li, L., Im, E., , and Yueh, S.: A Surface Reference Technique for Airborne Doppler Radar Measurements in Hurricanes, J. Atmos. Oceanic Technol., 20, 269–275, 2003.

Durst, F., Melling, A., and Whitelaw, J.: Principle and Practice of Laser-Doppler Anemometry, Academic Press, London, 1981.

Dutton, E., DeLuisi, J., and Herbert, G.: Shortwave aerosol optical depth of Arctic haze measured on board the NOAA WP–3D during AGASP–II, April 1986, J. Atmos. Chem., 9, 71–79, 1989.

Dye, J.: A cautionary note on the use of de point–frost point hygrometers for frost point measurements, J. Appl. Meteorol., 12, 1230–1231, 1973.

Dyroff, C., Fuetterer, D., and Zahn, A.: Compact diode–laser spectrometer ISOWAT for highly sensitive airborne measurements of water–isotope ratios, Appl. Phys. B, 98, 537–548, 2010.

Eatough, D. J., Obeidi, F., Pang, Y., Ding, Y., Eatough, N. L., and Wilson, W. E.: Integrated and real–time diffusion denuder sampler for PM2.5, Atmos. Environ., 33, 835–2844, 1999.

Eddy, P., Natarajan, A., and Dhaniyala, S.: Subisokinetic sampling characteristics of high speed aircraft inlets: A new CFD–based correlation considering inlet geometries, J. Aerosol Sci., 37, 1853–1870, 2006.

Edwards, C. and Marx, K.: Analysis of the Ideal Phase–Doppler System: Limitations Imposed by the Single–Particle Constraint, Atomization and Sprays, 2, 319–366, 1992.

Edwards, G. D., Cantrell, C. A., Stephens, S., Hill, B., Goyea, O., Shetter, R., Mauldin, R., Kosciuch, E., Tanner, D., and Eisele, F.: Chemical ionization mass spectrometer instrument for the measurement of tropospheric HO_2 and RO_2, Anal. Chem., 75, 5217–5327, 2003.

Eerdekens, G., Ganzeveld, L., de Arellano, J. V. G., Klupfel, T., Sinha, V., Yassaa, N., Williams, J., Harder, H., Kubistin, D., Martinez, M., and Lelieveld, J.: Flux estimates of isoprene, methanol and acetone from airborne PTR–MS measurements over the tropical rainforest during the GABRIEL 2005 campaig, Atmos. Chem. Phys., 9, 4207–4227, 2009.

Ehret, G., Hoinka, K. P., Stein, J., Fix, A., Kiemle, C., and Poberaj, G.: Low–stratospheric water vapor measured by an airborne DIAL, J. Geophys. Res., 104, 351–359, 1999.

Ehret, G., Kiemle, C., Wirth, M., Amediek, A., Fix, A., and Houweling, S.: Space–borne remote sensing of CO_2, CH_4, and N_2O by integrated path differential absorption lidar: a sensitivity analysis, Appl. Phys. B, 90, 593–608, 2008.

Eidhammer, T. and Deshler, T.: Technical Note: Evaporation of polar stratospheric cloud particles, in situ, in a heated inlet, Atmos. Chem. Phys., 5, 97–106. SRef–ID: 1680–7324 / acp / 2005–5–97, 2005.

Eidhammer, T., DeMott, P. J., Rogers, D. C., Prenni, A. J., Petters, M. D., Twohy, C. H., Rogers, D. C., Stith, J., Heymsfield, A., Wang, Z., Haimov, S., French, J., Pratt, K., Prather, K., Murphy, S., Seinfeld, J., Subramanian, R., and Kreidenweis, S. M.: Ice initiation by aerosol particles: Measured and predicted ice nuclei concentrations versus measured ice crystal concentrations in an orographic wave cloud, J. Atmos. Sci., paper in press, 2010.

Eisele, F. L., Mauldin, R., Tanner, D., Fox, J., Mouch, T., and Scully, T.: An inlet / sampling duct for airborne OH and sulfuric acid measurements, J. Geophys. Res. D: Atmos., 102, 27 993–28 001, 1997.

Emery, E., Miller, D., Plaskon, S., Strapp, J., and Lilie, L. E.: Ice particle impact on cloud water content Instrumentation, in 42nd AIAA Aerospace Sciences Meeting and Exhibit, Reno, Nevada, AIAA–2004–0731, 2004.

Engeln, R., von Helden, G., Berden, G., and Meijer, G.: Phase shift cavity ring–down absorption spectroscopy, Chem. Phys. Lett., 262, 105, 1996.

Engeln, R., Berden, G., Peeters, R., and Meijer, G.: Cavity enhanced absorption and cavity enhanced magnetic rotation spectroscopy, Rev. Sci. Instrum., 69, 3763–3769, 1998.

English, S.: Estimation of temperature and humidity profile information from microwave radiances over different surface types, J. App. Meteor., 38, 1526–1541, 1999.

English, S.: The Importance of Accurate Skin Temperature in Assimilating Radiances From Satellite Sounding Instruments, IEEE Transactions on Geoscience and Remote Sensing, 46, 403–408, 2008.

English, S., Guillou, C., Prigent, C., and Jones, D.: Aircraft measurements of water vapor continuum absorption at millimetre wavelengths, Quart. J. Roy. Meteor. Soc., 120, 603–625, 1994.

ESA: The four candidate Earth Explorer core missions–Atmospheric Dynamics Mission. ESA Report for Mission Selection, Tech. Rep. ESA SP–1233(4), European Space Agency, 145 pp., 1999.

ESA: WALES–Water Vapour Lidar Experiment in Space. The Five Candidate Earth Explorer Core Missions, Tech. Rep. ESA SP-1257(2), European Space Agency, report for Assessment, 2001.

Esposito, B. and Marrazzo, M.: Application of PDPA System with Different Optical Configuration to the IWT Calibration, AIAA, Reno, NV, 2007, aIAA 2007-1094, 2007.

Esselborn, M., Wirth, M., Fix, A., Tesche, M., and Ehret, G.: Airborne high spectral resolution lidar for measuring aerosol extinction and backscatter coefficients, App. Opt., pp. 346–358, 2008.

Esselborn, M., Wirth, M., Fix, A., Weinzierl, B., Rasp, K., Tesche, M., and Petzold, A.: Spatial distribution and optical properties of Saharan dust observed by airborne high spectral resolution lidar during SAMUM 2006, Tellus B, 61, 131–143, 2009.

Evans, K. and Vivekanandan, J.: Multiparameter radar and microwave radiative transfer modeling of nonspherical atmospheric ice particles, IEEE Transactions on Geoscience and Remote Sensing, 28, 423–437, 1990.

Evans, K., Wang, J., Racette, P., Heymsfield, G., and Li, L.: Ice cloud retrievals and analysis with data from the Compact Scanning Submillimeter Imaging Radiometer and the Cloud Radar System during CRYSTAL–FACE, J. Appl. Meteor., 44, 839–859, 2005.

Facchini, M., Mircea, M., Fuzzi, S., and Charlson, R.: Cloud albedo enhancement by surface–active organic solutes in growing droplets, Nature, 401, 257–259, 1999.

Fahey, D., Kelly, K., Ferry, G., Poole, L., Wilson, J., Murphy, D., Loewenstein, M., and Chan, K.: In situ measurements of total reactive nitrogen, total water, and aerosol in a polar stratospheric cloud in the Antarctic, J. Geophys. Res., 94, 299–315, 1989.

Fahey, D. W., Eubank, C. S., Hübler, G., and Fehsenfeld, F. C.: Evaluation of a Catalytic Reduction Technique for the Measurement of Total Reactive Odd–Nitrogen NO_y in the Atmosphere, J.Atmos. Chem., 3, 435–468, 1985.

Faloona, I. C., Tan, D., Lesher, R., Hazen, N., Frame, C., Simpas, J., Harder, H., Martinez, M., Carlo, P. D., Ren, X., and Brune, W.: A laser induced fluorescence instrument for detecting tropospheric OH and HO_2: Characteristics and calibration, J. Atmos. Chem., 47, 139–167, 2004.

Farman, J. C., Gardiner, B., and Shanklin, J.: Large Losses Of Total Ozone In Antarctica Reveal Seasonal ClO_x / NO_x Interaction, Nature, 315, 207–210, 1985.

Febvre, G., Gayet, J.-F., Minikin, A., Schlager, H., Shcherbakov, V., Jourdan, O., Busen, R., Fiebig, M., Kärcher, B., and Schumann, U.: On optical and microphysical characteristics of contrails and cirrus, J. Geophys. Res., 114, doi:10.1029/2008JD010184, 2009.

Fehsenfeld, F. C., Ancellet, G., Bates, T., Goldstein, A., Hardesty, R., Honrath, R., Law, K., Lewis, A., Leaitch, R., McKeen, S., Meagher, J., Parrish, D., Pszenny, A., Russel, P., Seinfeld, H. S. J., Talbot, R., and Zbinden, R.: International Consortium for Atmospheric Research on Transport and Transformation (ICARTT): North America to Europe–Overview of the 2004 summer field study, J. Geophys. Res., 111, doi:10.1029/2006JD007829, 2006.

Feigl, C., Schlager, H., Kuhn, M., Ziereis, H., Curtius, J., Arnold, F., and Schiller, C.: Observations of NO_y uptake by particles in the Arctic tropopause region at low temperatures, Geophys. Res. Lett., 26, 2215–2219, 1999.

Feingersh, T., Ben-Dor, E., and Filin, S.: Correction of reflectance anisotropy: a multi–sensor approach, International Journal of Remote Sensing, 31, 49–74, 2010.

Feingold, G. and Chuang, P. Y.: Analysis of the influence of film-forming compounds on droplet growth: Implications for cloud microphysical processes and climate, J. Atmos. Sci., 59, 2006–2018, 2002.

Feingold, G., Cotton, W., Kreidenweis, S., and Davis, J.: The impact of giant cloud condensation nuclei on drizzle formation in stratocumulus: Implications for cloud radiative properties, J. Atmos. Sci., 56, 4100–4117, 1999.

Feldpausch, P., Fiebig, M., Fritzsche, L., and Petzold, A.: Measurement of ultrafine aerosol size distributions by a combination of diffusion screen separators and condensation particle counters., J. Aerosol Sci., 37, 577–597, 2006.

Felt, E. P.: Dispersal of insects by air currents, New York State Mus. Bull., 274, 59–129, 1928.

Fernandez, D., Kerr, E., Castells, A., Carswell, J., Frasier, S., Chang, P., Black, P., and Marks, F.: IWRAP: the Imaging Wind and Rain Airborne Profiler for remote sensing of the ocean and the atmospheric boundary layer within tropical cyclones, IEEE Transactions on Geoscience and Remote Sensing, 43, 1775–1787, 2005.

Fiebig, M., Stein, C., Schröder, F., Feldpausch, P., and Petzold, A.: Inversion of data containing information on the aerosol particle size distribution using multiple instruments, J. Aerosol Sci., 36, 1353–1372, 2005.

Fiedler, L., Newman, S., and Bakan, S.: Correction of detector nonlinearity in Fourier transform spectroscopy with a low–temperature blackbody, App. Opt., 44, 5332–5340, 2005.

Fiedler, S. E., Hese, A., and Ruth, A.: Incoherent broad–band cavity–enhnaced absorption spectroscopy, Chem. Phys. Lett., 371, 284–294, 2003.

Field, P. and Heymsfield, A.: Aggregation and scaling of ice crystal size distributions, J. Atmos. Sci., 60, 544–560, 2003.

Field, P., Wood, R., Brown, P., Kaye, P., and E. Hirst, R. Greenaway, J. S.: Ice particle interarrival times measured with a Fast FSSP., J. Atmos. Oceanic Technol., 20, 249–261, 2003.

Field, P. R., Heymsfield, A., and Bansemer, A.: Shattering and Particle Interarrival Times Measured by Optical Array Probes in Ice Clouds, J. Atmos. Oceanic Technol., 23, 1357–1370, 2006.

Field, P. R., Heymsfield, A. J., and Bansemer, A.: Snow Size Distribution Parameterization for Midlatitude and Tropical Ice Clouds, J. Atmos. Sci., 64, 4346–4365, 2007.

Fierz, M., Vernooij, M. G. C., and Burtscher, H.: An improved low–flow thermodenuder, J. Aerosol Sci., 38, 1163–1168, 2007.

Finnegan, W. G. and Chai, S. K.: A New Hypothesis for the Mechanism of Ice Nucleation on Wetted AgI and Ag AgCl Particulate Aerosols, J. Atmos. Sci., 60, 1723–1731, 2003.

Fiore, A. M., Dentener, F., Wild, O., Cuvelier, C. Schultz, M., Hess, P., Textor, C., Schulz, M., Doherty, R., Horowitz, L., MacKenzie, I., Sanderson, M., Shindell, D., Stevenson, D., Szopa, S., Van Dingenen, R. Zeng, G., Atherton, C., Bergmann, D., Bey, I., Carmichael, G., Collins, W., Duncan, B., Faluvegi, G., Folberth, G., Gauss, M., Gong, S., Hauglustaine, D., Holloway, T., Isaksen, I., Jacob, D., Jonson, J., Kaminski, J., Keating, T., Lupu, A., Marmer, E., Montanaro, V., Park, R., Pitari, G., Pringle, K., Pyle, J., Schroeder, S., Vivanco, M., Wind, P., Wojcik, G., Wu, S., and Zuber, A.: Multimodel estimates of intercontinental source–receptor relationships for ozone pollution, J. Geophys. Res., 114, doi:10.1029/2008JD010816, 2009.

Fix, A., Ehret, G., Hoffstädt, A., Klingenberg, H. H., Lemmerz, C., Mahnke, P., Ulbricht, M., Wirth, M., Wittig, R., and Zirnig, W.: CHARM A helicopter–borne lidar system for pipeline monitoring, in 24th International Laser Radar Conference, ESA SP 561, pp. 45–48, 2004.

Flagan, R. C.: On differential mobility analyzer resolution, Aerosol Sci. Technol., 30, 556–570, 1999.

Flagan, R. C.: Opposed Migration Aerosol Classifier (OMAC), Aerosol Sci. Technol., 38, 890–899, 2004.

Flamant, C., Pelon, J., Flamant, P. H., and Durand, P.: On the determination of the entrainment zone thickness at the top of the unstable boundary layer in clear air by lidar and in–situ measurements, Boundary Layer Meteorol., 83, 247–284, 1997.

Flamant, C., Chaboureau, J.-P., Parker, D. J., Taylor, C. M., Cammas, J.-P., Bock, O., Timouck, F., and Pelon, J.: Airborne observations of the impact of a convective system on the planetary boundary layer thermodynamics and aerosol distribution in the inter–tropical discontinuity region of the West African Monsoon, Q. J. R. Meteorolog. Soc., 133, 1175–1189, 2007.

Flentje, H., Dörnbrack, A., Ehret, G., Fix, A., Kiemle, C., Poberaj, G., and Wirth, M.: Water vapor heterogeneity related to tropopause folds over the North Atlantic revealed by airborne water vapor differential absorption lidar, J. Geophys. Res., 110, 2005.

Flocke, F., Atlas, E., Madronich, S., Schauffler, S. M., Aikin, K., Margitan, J. J., and Bui, T. P.: Observations of methyl nitrate in the lower stratosphere during STRAT: Implications for its gas phase production mechanisms, Geophys. Res. Lett., 25, 1891–1894, 1998.

Flocke, F., Herman, R. L., Salawitch, R. J., Atlas, E., Webster, C. R., Schauffler, S. M., Lueb, R. A., May, R. D., Moyer, E. J., Rosenlof, K. H., Scott, D. C., Blake, D. R., and Bui, T. P.: An examination of chemistry and transport processes in the tropical lower stratosphere using observations of long–lived and short–lived compounds obtained during STRAT and POLARIS, J. Geophys. Res., 104, 26 625–2664, 1999.

Fontijn, A., Sabadell, A. J., and Ronco, R. J.: Homogeneous chemiluminescent measurement of nitric oxide with ozone. Implications for continuous selective monitoring of gaseous air pollutants, Anal. Chem., 42, 575–579, 1970.

Foody, G.: The significance of border training patterns in classification by a feed forward neural network using back propagation learning, International Journal of Remote Sensing, 20, 3549–3562, 1999.

Foot, J.: Improvements in pyrgeometers, UK Patent Office, No. 8515024, 1985.

Foot, J.: A new prygeometer, J. Atmos. Oceanic Technol., 3, 363–370, 1986.

Forgan, B.: General method for calibrating Sun photometers, Appl. Opt., 33, 4841–4850, 1994.

Formenti, P., Schuetz, L., Balkanski, Y., Desboeufs, K., Ebert, M., Kandler, K., Petzold, A., Scheuvens, D., Weinbruch, S., and Zhang, D.: Recent progress in understanding physical and chemical properties of mineral dust, Atmos. Chem. Phys. Discuss., 10, 31 187–31 251, 2011.

Forster, P., Ramaswamy, V., Artaxo, P., Berntsen, T., Betts, R., Fahey, D., Haywood, J., Lean, J., Lowe, D., Myhre, G., Nganga, J., Prinn, R., Raga, G., Schulz, M., and Dorland, R. V.: Climate Change 2007: The Physical Science Basis. Contribution of Working Group I to the Fourth Assessment Report of the Intergovernmental Panel on Climate Change, chap. Changes in Atmospheric Constituents and in Radiative Forcing, Cambridge University Press, editors: Solomon, S. and D. Qin and M. Manning and Z. Chen and M. Marquis and K.B. Averyt and M. Tignor and H.L. Miller, 2007.

Fortner, E., Zhao, J., and Zhang, R.: Development of ion drift–chemical ionization mass spectrometry, Anal. Chem., 76, 5436–5440, 2004.

Fortner, E. C. and Knighton, W. B.: Quantitatively resolving mixtures of isobaric compounds using chemical ionization mass spectrometry by modulating the reactant ion composition, Rapid Commun. Mass Spectrom., 22, 2597–2601, 2008.

Foster, S.: Accuracy requirements for airborne wind measurement in aerial application, ASAE / NAAA Technical Section, 37th Annual National Agricultural Aviation Association Convention, Reno, NV, 8 December 2003, pp. Paper Number AA03–0012, 2003.

Fox, N.: Post–launch calibration of satellite sensors, vol. 2 of *ISPRS Book Series*, chap. Validated data and removal of bias through traceability to SI, pp. 31–42, Taylor and Francis, London, 2004.

Francis, P., Jones, A., Saunders, A., Shine, K., Slingo, A., and Zhian, S.: An observational and theoretical study of the radiative properties of cirrus: Some results from ICE ’89, Quart. J. Roy. Meteor. Soc., pp. 809–848, 1994.

Franz, P. and Röckmann, T.: High–precision isotope measurements of $H_2^{16}O$, $H_2^{17}O$, $H_2^{18}O$, and the $D^{17}O$–anomaly of water vapour in the southern lowermost stratosphere, Atmos. Chem. Phys., 5, 2949–2959, 2005.

Fried, A., Lee, Y., Frost, G., Wert, B., Henry, B., Drummond, J., Hu, G., and Jobson, T.: Airborne CH_2O measurements over the North Atlantic during the 1997 NARE campaign: Instrument comparisons and distributions, J. Geophys. Res., 107, 4039, doi: 10.1029 / 2000JD000260, 2002.

Fried, A., Crawford, J., Olson, J., Walega, J., Potter, W., Wert, B., Jordan, C., Anderson, B., Shetter, R., Lefer, B., Blake, D., Blake, N., Meinardi, S., Heikes, B., O’Sullivan, D., Snow, J., Fuelberg, H., Kiley, C. M., Sandholm, S., Tan, D., Sachse, G., Singh, H., Faloona, I., Harward, C. N., and Carmichael, G. R.: Airborne tunable diode laser measurements of formaldehyde during TRACE–P: Distributions and box–model comparisons, J. Geophys. Res., 108, 8798, doi:10.1029 / 2003JD003451, 2003.

Friedlander, S. K.: Smoke, Dust and Haze, Wiley, 1977.

Friehe, C., Grossman, R., and Pann, Y.: Calibration of an airborne Lyman–Alpha hygrometer and measurement of water vapor flux using a thermoelectric hygrometer, J. Atmos. Oceanic Technol., 3, 299–304, 1986.

Friehe, C. A. and Khelif, D.: Fast–response aircraft temperature sensors., J. Atmos. Oceanic Technol., 9, 784–795, 1992.

Friehe, C. A., Burns, S. P., Khelif, D., and Song, X.: Meteorological and Flux Measurements from the NOAA WP3D Aircraft in TOGA COARE, in 8^{th} Conference on Air–Sea Interaction, pp. J42–J45, AMS, 1996.

Frisch, A. S., Fairall, C. W., and Snider, J. B.: Measurement of stratus cloud and drizzle parameters in ASTEX with a K–alpha–band Doppler radar and a microwave radiometer, J. Atmos. Sci., 52, 2788–2799, 1995.

Fritz, S.: The albedo of the ground and atmosphere, Bull. Amer. Meteor. Soc., 29, 303–312, 1949.

Frost, G. J., Fried, A., Lee, Y., Wert, B., Henry, B., Drummond, J. R., Evans, M. J., Fehsenfeld, F. C., Goldan, P. D., Holloway, J. S., Hübler, G., Jakoubek, R., Jobson, B. T., Knapp, K., Kuster, W. C., Parrish, D. D., Roberts, J., Rudolph, J., Ryerson, T. B., Stohl, A., Stroud, C., Sueper, D. T., Trainer, M., and Williams, J.: Comparisons of box model calculations and measurements of formaldehyde from the 1997 North Atlantic Regional Experiment, J. Geophys. Res., 107, 4060, doi: 10.1029/2001JD000896, 2002.

Froyd, K. D., Murphy, D. M., Sanford, T. J., Thomson, D. S., Wilson, J. C., Pfister, L., and Lait, L.: Aerosol composition of the tropical upper troposphere, Atmos. Chem. Phys., 9, 4363–4385, 2009.

Fu, Q.: An accurate parameterization of the solar radiative properties of cirrus clouds for climate models, J. Climate, 9, 2058–2082, 1996.

Fuchs, H., Dubé, W., Ciciora, S., and Brown, S.: Determination of Inlet Transmission and Conversion Efficiencies for in Situ Measurements of the Nocturnal Nitrogen Oxides, NO_3, N_2O_5 and NO_2, via Pulsed Cavity Ring–Down Spectroscopy, Anal. Chem., 80, 6010–6017, doi: 10.1021/ac8007253, 2008.

Fuchs, H., Ball, S., Bohn, B., Brauers, T., Cohen, R., Dorn, H.-P., Dubé, W., Fry, J., Häseler, R., Heitmann, U., Jones, R., Kleffmann, J., Mentel, T., Müsgen, P., Rohrer, F., Rollins, A., Ruth, A., Kiendler–Scharr, A., Schlosser, E., Shillings, A., Tillmann, R., Varma, R., Venables, D., Villena Tapia, G., Wahner, A., Wegener, R., Wooldridge, P., and Brown, S.: Intercomparison of measurements of NO_2 concentrations in the atmospheric simulation chamber SAPHIR during the NO_3COMP campaign, Atmos. Meas. Tech., 3, 21–37, 2010.

Fuchs, N. A.: On the stationary charge distribution of aerosol particles in bipolar ionic atmospheres, Geofis. Pura. Appl., 56, 185–193, 1963.

Fugal, J. and Shaw, R.: Cloud particle size distributions measured with an airborne digital in–line holographic instrument, Atmos. Meas. Tech., 2, 259–271, 2009.

Fugal, J., Shaw, R., Saw, E., and Sergeyev, A.: Airborne digital holographic system for cloud particle measurements, Appl. Opt., 43, 5987–5995, 2004.

Fugal, J., Schulz, T., and Shaw, R.: Practical methods for automated reconstruction and characterization of particles in digital in–line holograms, Meas. Sci. Technol., 20, 075 501, doi:10.1088/0957–0233/20/7/075501, 2009.

Fukuta, N. and Saxena, V.: A horizontal thermal gradient cloud condensation nucleus spectrometer, J. Appl. Meteorol., 18, 1352–1362, 1979.

Gal–Chen, T.: Errors in fixed and moving grame of references–applications for conventional and Doppler radar analysis, J. Atmos. Sci., 39, 2279–2300, 1982.

Galloway, J., Pazmany, A., Mead, J., McIntosh, R., Leon, D., French, J., Kelly, R., and Vali, G.: Detection of ice hydrometeror alignment using an airborne W–band polarimetric radar, J. Atmos. Oceanic Technol., 14, 3–12, 1997.

Gamache, J., Marks, F., and Roux, F.: Comparison of 3 airborne Doppler sampling techniques with airborne in–situ wind observations in Hurricane Gustav (1990), J. Atmos. Oceanic Technol., 12, 171–181, 1995.

Gamero-Castano, M. and de la Mora, J. F.: A condensation nucleus counter (CNC) sensitive to singly charged sub–nanometer particles, J. Aerosol. Sci., 31, 757–772, 2000.

Gao, B. and Goetz, F.: Column atmospheric water vapor and vegetation liquid water retrievals from airborne imaging spectrometer data, J. Geophys. Res., 95, 3549–3564, 1990.

Gao, B. and Goetz, F.: Retrieval of equivalent water thickness and information related to biochemical components of vegetation canopies from AVIRIS data CAREFUL:in word reference list the year 1994 was also given, assuming 1995 is correct, Remote Sensing of Environment, 52, 155–162, 1995.

Gao, B., Goetz, A., and Wiscombe, W.: Cirrus cloud detection from Airborne Imaging Spectrometer data using the 1.38 μm water vapor band, Geophysical Research Letters, 20, 301–304, 1993.

Gao, B., Davis, C., Montes, M., and Ahmad, Z.: Atmospheric correction algorithm for hyperspectral remote sensing of ocean color from space, Applied Optics, 39, 887–896, 2000.

Gao, B., Montes, M., Davis, C., and Goetz, A.: Atmospheric correction algorithms for hyperspectral remote sensing data of land and ocean, Remote Sens. Environ., 113, 17–24, 2007.

Gao, R., Keim, E., Woodbridge, E., Ciciora, S., Proffitt, M., Thompson, T., Mclaughlin, R., and Fahey, D.: New photolysis system for NO_2 measurements in the lower stratosphere, J. Geophys. Res., 99, 673–681, 1994.

Gardiner, B. and Hallett, J.: Degradation of in–cloud forward scattering spectrometer probe measurements in the presence of ice particles., J. Atmos. Oceanic Technol., 2, 171–180, 1985.

Garnier, A. and Chanin, M. L.: Description of a Doppler Rayleigh LIDAR for measuring winds in the middle atmosphere, Appl. Phys. B, 55, 35–40, 1992.

Garrett, T.: Comment on "Effective radius of ice cloud particle populations derived from aircraft probes" by Heymsfield et al., Atmos. Oceanic. Technol., 24, 1495–1503, doi:10.1175 / JTECH2075.1, 2007.

Garrett, T.: Observational quantification of the optical properties of cirrus cloud, in Light Scattering Reviews 3, Springer, Berlin, 2008.

Garrett, T., Hobbs, P., and Gerber, H.: Shortwave, single–scattering properties of arctic ice clouds, J. Geophys. Res., 106, 15 155–15 172, 2001.

Garrett, T., Gerber, H., Baumgardner, D., Twohy, C., and Weinstock, E.: Small, highly reflective ice crystals in low–latitude cirrus, Geophys. Res. Lett., 30, 2132, doi:10.1029 / 2003GL018 153, 2003.

Garrett, T., Navarro, B., Twohy, C., Baumgardner, E. J. D., Bui, P., Gerber, H., Herman, R., Heymsfield, A., Lawson, P., Minnis, P., Nguyien, L., Poellot, M., Pope, S., Valero, F., and Weinstock, E.: Evolution of a Florida cirrus anvil, J. Atmos. Sci., 62, 2352–2372, 2005.

Gasso, S., Hegg, D. A., Covert, D. S., Collins, D., Noone, K. J., Ostrom, E., Schmid, B., Russell, P. B., Livingston, J. M., Durkee, P. A., and Jonsson, H.: Influence of humidity on the aerosol scattering coefficient and its effect on the upwelling radiance during ACE-2, Tellus Ser. B, 52, 546–567, 2000.

Gayet, J.-F., Febvre, G., and Larsen, H.: The reliability of the PMS FSSP in the presence of small ice crystals, J. Atmos. Oceanic Techn., 13, 1300–1310, 1996.

Gayet, J.-F., Crépel, O., Fournol, J.-F., and Oshchepkov, S.: A new airborne Polar Nephelometer for the measurements of optical and microphysical cloud properties. Part I: Theoretical design, Annales Geophysicae, 15, 451–459, 1997.

Gayet, J.-F., Auriol, F., Oshchepkov, S., Schröder, F., Duroure, C., Febvre, G., Fournol, J.-F., Crépel, O., Personne, P., and Daugeron, D.: In situ measurements of the scattering phase function of stratocumulus, contrails and cirrus, Geophys. Res. Lett., pp. 971–974, 1998.

Gayet, J.-F., Asano, S., Yamazaki, A., Uchiyama, A., Sinyuk, A., Jourdan, O., and Auriol, F.: Two case studies of continental-type water and maritime mixed-phased stratocumuli over the sea. Part I : Microphysical and Optical properties, J. Geophys. Res., 107, doi: 10.1029 / 2001JD1106, 2002.

Gayet, J.-F., Stachlewska, I., Jourdan, O., Shcherbakov, V., Schwarzenboeck, A., and Neuber, R.: Microphysical and optical properties of precipitating drizzle and ice particles obtained from alternated Lidar and in situ measurements, Annales Geophys., 25, 1487–1497, 2007.

Gayet, J.-F., Mioche, G., Shcherbakov, V., Gourbeyre, C., Busen, R., and Minikin, A.: Optical properties of pristine ice crystals in mid–latitude cirrus clouds: a case study during CIRCLE–2 experiment, Atmos. Chem. Phys., 11, 2537–2544, doi:10.5194 / acp–11–2537–2011, 2011.

Gege, P., Fries, J., Haschberger, P., Schötz, P., Schwarzer, H., Strobl, P., Suhr, B., Ulbrich, G., and Vreeling, W.: Calibration facility for airborne imaging spectrometers, ISPRS Journal of Photogrammetric and Remote Sensing, 64, 387–397, 2009.

Geist, J. and Blevin, W.: Chopper–stabilized null radiometer based upon an electrically calibrated pyroelectic detector, Appl. Opt., 12, 2532–2535, 1973.

Geller, A. S., Rader, D., and Kempka, S.: Calculation of particle concentration around aircraft–like geometries, J. Aerosol Sci., 24, 823–634, 1993.

George, I. and Abbatt, J.: Chemical evolution of secondary organic aerosol from OH–initiated heterogeneous oxidation, Atmos Chem Phys, 10 (12), 5551–5563, 2010.

Gerber, H.: Direct measurement of suspended particulate volume concentration and far–infrared extinction coefficient with a laser–diffraction instrument, Appl. Opt., 30, 4824–4831, 1991a.

Gerber, H.: Standards for measuring fog liquid water content, QC929.F7157, pp. 1–4, 1^{st} Intern. Conf. On Fog and Fog Collection, 1998.

Gerber, H.: Comment on "Effective radius of ice cloud particle populations derived from aircraft probes" by Heymsfield et al, J. Atmos. Oceanic Technol., 25, 1504–1510, 2007.

Gerber, H., Arends, B., and Ackerman, A.: New microphysics sensor for aircraft use, Atm. Res., 31, 235–252, 1994.

Gerber, H., Takano, Y., Garrett, T. J., and Hobbs, P.: Nephelometer measurements of the asymmetry parameter, volume extinction coefficient and backscatter ratio in Artic clouds, J. Atmos. Sci., 57, 3021–3034, 2000.

Gerber, H., Jensen, J., Davis, A., Marshak, A., and Wiscombe, W.: Spectral density of liquid water content at high frequencies, J. Atmos. Sci., 58, 497–503, 2001.

Gerber, H., Garrett, T., Heymsfield, A., Poellot, M., and Twohy, C.: Nephelometer measurements in Florida thunderstorms, in Proc. 14th Int. Conf. On Clouds and Precip., pp. 1092–1094, Bologna, Italy, 2004.

Gerber, H., Frick, G., Malinowski, S., Brenguier, J.-L., and Burnet, F.: Holes and entrainment in stratocumulus, J. Atmos. Sci., 62, 443–459, 2005.

Gerber, H., Frick, G., Jensen, J., and Hudson, J.: Entrainment, mixing, and microphysics in trade–wind cumulus, J. Meteor. Soc. Japan, 86a, 87–106, 2008.

Gerber, H. E.: A saturation hygrometer for the measurement of relative humidity between 95 and 105 %, J. Appl. Meteor., 19, 1196–1208, 1980.

Gerber, H. E.: Supersaturation and droplet spectral evolution in fog, J. Atmos. Sci., 48, 2569–2588, 1991b.

Gerbig, C., Kley, D., Volz–Thomas, A., Kent, J., Dewey, K., and McKenna, D.: Fast response resonance fluorescence CO measurements aboard the C–130: Instrument characterization and measurements made during North Atlantic Regional Experiment 1993, J. Geophys. Res., 101, 229–238, 1996.

Gerbig, C., Schmitgen, S., Kley, D., Volz-Thomas, A., Dewey, K., and Haaks, D.: An improved fast–response vacuum–UV resonance fluorescence CO instrument, J. Geophys Res., 104, 1699–1704, 1999.

Gersman, R., Ben–Dor, E., Beyth, M., Avigad, D., Abraha, M., and Kibreab, A.: Mapping of hydrothermally altered rocks by the EO–1 Hyperion sensor, Northern Danakil Depression, Eritrea, International Journal of Remote Sensing, 29, 3911–3936, 2008.

Geyer, A., Alicke, B., Mihelcic, D., Stutz, J., and Platt, U.: Comparison of tropospheric NO_3 radical measurements by differential optical absorption spectroscopy and matrix isolation electron spin resonance, J. Geophys. Res., 104, 26 097–26 105, 1999.

Ghan, S., Rissman, T., Elleman, R., Ferrare, R., Turner, D., Flynn, C., Wang, J., Ogren, J., Hudson, J., Jonsson, H., VanReken, T., Flagan, R., and Seinfeld, J.: Use of in situ cloud condensation nuclei, extinction and aerosol size distribution measurements to test a method for retrieving cloud condensation nuclei profiles from surface measurements, J. Geophys. Res., 111, 2006.

Gherman, T., Venables, D., Vaughan, S., Orphal, J., and Ruth, A.: Incoherent broadband cavity–enhanced absorption spectroscopy in the near–ultarviolet: application to HONO and NO_2, Environ. Sci. Technol., 42, 890–895, 2008.

Giangrande, S. E. and Ryzhkov, A. V.: Estimation of rainfall based on the results of polarimetric echo classification, J. Appl. Meteorol. Climatol., 47, 2445–2462, 2008.

Gibert, F., Flamant, P. H., Bruneau, D., and Loth, C.: $2\,\mu$m heterodyne differential absorption lidar measurements of the atmospheric CO_2 mixing ratio in the boundary layer, Appl. Opt., 45, 4448–4458, 2006.

Giez, A., Ehret, G., Schwiesow, R. L., Davis, K. J., and Lenschow, D. H.: Water vapor flux measurements from groundbased vertically pointed water vapor differential absorption and Doppler lidars, J. Atmos. Oceanic Technol., 16, 237–250, 1999.

Gleason, S. and Gebre–Egziabher, D.: GNSS applications and methods, Artech House, Boston, MA, 2009.

Glickman, T.: Glossary of Meteorology, Second Edition, American Meteorological Society, Boston, MA, 2000.

GloPac: http://www.nasa.gov/centers/dryden/research/GloPac/index.html, 2010.

Glover, A., Skippon, S., and Boyle, R.: Interferometric laser imaging for droplet sizing : a method for droplet–size measurement in sparse spray systems, Appl. Opt., 34, 8409, 1995.

Goetz, A.: Three decades of hyperspectral remote sensing of the Earth: A personal view, Remote Sens. Environ., 113, Imaging Spectroscopy Special Issue, 5–16, 2009.

Goetz, A., ed.: Present the Art, Science and Applications of Reflectance Spectroscopy Symposium, Boulder, Colorado, U.S.A., http://www.asdi.com/remote-sensing/articles, 2010.

Goetz, A. and Wellman, J.: Airborne Imaging Spectrometer: A new tool for remote sensing, IEEE Trans. Geosciences Remote Sensing, 22, 546–550, 1984.

Goetz, A., Preining, O., and Kallai, T.: The metastability of natural and urban aerosols, Pure Appl. Geophys., 50, 67–80, 1961.

Goetz, A., Vane, G., Solomon, J., and Rock, B.: Imaging spectrometry for Earth remote sensing, Science, 228, 1147–1153, 1985.

Goetz, F.: HIRS, High Resolution Imaging Spectrometer: Science Opportunities of the 1990, Earth Observation System, Tech. Rep. Volume IIc, Instrument Panel Report to NASA, 74 p., 1987.

Goldstein, R. J., ed.: Fluid mechanics measurements, Taylor & Francis, Washington, D. C., USA, 712 p., 1996.

Golitzine, N.: Method for Measuring the Size of Water Droplets in Clouds, Fogs and Sprays, Tech. Rep. Report ME–177, National Research Council, Ottawa, Canada, also published as Note 6 (1951), National Aeronautical Establishment, Ottawa, Canada, 1950.

Good, N., Coe, H., and McFiggans, G.: Instrumentational operation and analytical methodology for the reconciliation of aerosol water uptake under sub- and supersaturated conditions, Atmos. Meas. Tech., 3, 1241–1254, 2010.

Goodman, J.: Introduction to Fourier Optics, McGraw Hill, Boston, 2nd Ed., 1996.

Gorgucci, E., Scarchilli, G., Chandrasekar, V., and Bringi, V. N.: Measurement of Mean Raindrop Shape from Polarimetric Radar Observations, J. Atmos. Sci., 57, 3406–3413, 2000.

Gorgucci, E., Chandrasekar, V., and Baldini, L.: Rainfall estimation from X–band dual polarization radar using reflectivity and differential reflectivity, Atmos. Res., 82, 164–172, 2006.

Gossard, E., Snider, J., Clothiaux, E. E., Martner, B., Gibson, J., Kropfli, R., and Frisch, A.: The potential of 8 mm radars for remotely sensing cloud drop size distributions, J. Atmos. Oceanic Technol., 14, 76–87, 1997.

Govind, P.: Dropwindsonde instrumentation for weather reconnaissance aircraft, J. Appl. Meteorol., pp. 1512–1520, 1975.

Gower, J. F. R. and Borstad, G. A.: Phytoplankton remote sensing with the FLI imaging spectrometer, Advanc. Space Res., 9, 461, 1989.

Grace, J., Nichol, C., Disney, M., Lewis, P., Qquaife, T., and Bowyer, P.: Can we measure terrestrial photosynthesis from space directly, using spectral reflectance and fluorescence?, Global Change Biology11, pp. 1484–1497, 2007.

Gracey, W.: Measurement of static pressure on aircraft, Tech. Rep. NACA Report 1364, National Advisory Committee for Aeronautics NACA, 1956.

Graham, B., Mayol–Bracero, O. L., Guyon, P., Roberts, G. C., Decesari, S., Facchini, M. C., Artaxo, P., Maenhaut, W., Köll, P., and Andreae, M. O.: Water–soluble organic compounds in biomass burning aerosols over Amazonia, J. Geophys. Res., 107, 8047, 2002.

Green, R.: Measuring the spectral expression of carbon dioxide in the solar reflected spectrum with AVIRIS, in Proceedings of the 11th Annual Airborne Earth Science Workshop, Jet 442 Propulsion Laboratory, Pasadena, CA, 2001.

Green, R. and Pavri, B.: AVIRIS in–flight calibration experiment, sensitivity analysis, and intraflight stability, in Proceedings of the 9th Airborne Visible / Infrared Imaging Spectrometer (AVIRIS) Workshop, JPL Publ. 00-18, pp. 207–221, Jet Propulsion Laboratory, Pasadena, CA, 2000.

Green, R. and Shimada, M.: On–orbit calibration of a multi–spectral satellite sensor using a high altitude airborne imaging spectrometer, Advances in Space Research, 19, 1387–1398, 1997.

Green, R., Estwood, M., Sarture, C., Chrien, T., Arnonsson, M., Chippendale, B., Faust, J., Pavri, B., Chovit, C., Soils, M., Olaha, M., and Williams, O.: Imaging Spectroscopy and the airborne visible / infrared imaging spectrometer (AVIRIS), Remote Sensing of Environment, 65, 227–248, 1998.

Green, R., Pavri, B., and Chrien, T.: On–orbit radiometric and spectral calibration characteristics of EO–1 Hyperion derived with an under flight of AVIRIS and in situ measurements at Salar de Arizaro, Argentina, IEEE Transactions on Geoscience and Remote Sensing, 42, 1194–1203, 2003a.

Green, T., Brough, N., Reeves, C., Edwards, G., Monks, P., and Penkett, S.: Airborne measurements of peroxy radicals using the PERCA technique, J. Environ. Monit., 5, 75–83, 2003b.

Green, T. J., Reeves, C., Fleming, Z., Brough, N., Rickard, R. A., Bandy, B., Monks, P., and Penkett, S.: An improved dual channel PERCA instrument for atmospheric measurements of peroxy radicals, J. Environ. Monit., 8, 530–536, doi: 10.1039 / b514630e, 2006.

Griffiths, P. and de Haseth, J.: Fourier transform infrared spectrometry, Chem. Anal., 83, 1986.

Grody, N.: Classification of snow cover and precipitation using the Special Sensor Microwave / Imager (SSM / I), J. Geophys. Res., 96, 7423–7435, 1991.

Grossman, R. L.: Bivariate Conditional Sampling of Moisture Flux over a Tropical Ocean, J. Atmos. Sci., 41, 3238–3252, 1984.

Grossman, R. L.: Sampling Errors in the Vertical Fluxes of Potential Temperature and Moisture Measured by Aircraft During FIFE, J. Geophys. Res., 97, 18 439–18 443, 1992.

Grund, C. J., Banta, M., George, J., Howell, J., Post, M., Richter, R., and Weickmann, A.: High–resolution Doppler lidar for boundary layer research, J. Atmos. Oceanic Technol., 18, 376–393, 2001.

Guan, H., Schmid, B., Bucholtz, A., and Bergstrom, R.: Sensitivity of shortwave radiative flux density, forcing, and heating rate to the aerosol vertical profile, J. Geophys. Res., 11, D06 209, doi:10.1029 / 2009JD012 907, 2010.

Guanter, L., Estellés, V., and Moreno, J.: Spectral calibration and atmospheric correction of ultra–fine spectral and spatial resolution remote sensing data. Application to CASI–1500 data, Remote Sens. Environ., 109, 54–65, 2006.

Guildner, L. A., Johnson, D. P., and Jones, F. E.: Vapor pressure of water at its triple point, J. Res. Natl. Bur. Stand., 80, 1976.

Guilfoyle, K., Althouse, M. L., and Chang, C.: A quantitative and comparative analysis of linear and nonlinear spectral mixture models using radial basisi function neural network, Remote Sens. Environ., 39, 2314–2318, 2001.

Gunthe, S. S., King, S. M., Rose, D., Chen, Q., Roldin, P., Farmer, D. K., Jimenez, J. L., Artaxo, P., Andreae, M. O., Martin, S. T., and Pöschl, U.: Cloud condensation nuclei in pristine tropical rainforest air of Amazonia: size–resolved measurements and modeling of atmospheric aerosol composition and CCN activity, Atmos. Chem. Phys., 9, 7551–7575, 2009.

Gurlit, W., Zimmermann, R., Giesemann, C., Fernholz, T., Ebert, V., Wolfrum, J., Platt, U., and Burrows, J.: Lightweight diode laser spectrometer CHILD (Compact High–altitude In–situ Laser Diode) for balloonborne measurements of water vapor and methane, Appl. Opt., 44, 91–102, 2005.

Haddad, Z. S., Short, D., Durden, S. L., Im, E., Hensley, S., Grable, M., and Black, R.: A new parameterization of the rain drop size distribution, IEEE Transactions on Geoscience and Remote Sensing, 35, 532–539, 1997.

Haering, E. A.: Airdata Calibration of a High–Performance Aircraft for Measuring Atmospheric Wind Profiles, Tech. Mem. NASA–TM–101714, NASA, 24 pp, 1990.

Haering, E. A.: Airdata Measurement and Calibration, Tech. Mem. 104316, NASA, 19 pp, 1995.

Haggerty, J. and Curry, J.: Variability of sea ice emissivity estimated from airborne passive microwave measurements during FIRE SHEBA, J. Geophys. Res., 106, 15 265–15 277, 2001.

Hair, J. W., Hostetler, C. A., Cook, A. L., Harper, D. B., Ferrare, R. A., Mack, T. L., Welch, W., Izquierdo, L. R., and Hovis, F. E.: Airborne high spectral resolution lidar for profiling aerosol optical properties, Appl. Opt., 47, 6734–6752, 2008.

Hallett, J., Arnott, W., Purcell, R., and Schmidt, C.: A technique for characterizing aerosol and cloud particles by real time processing, in Proceedings of an International Specialty Conference, vol. 1, pp. 318–325, Air & Waste Manage. Assoc., Long Beach, California, Long Beach, California, 1998.

Halthore, R.: Sun photometric measurements of atmospheric water vapor column abundance in the 940 nm band, J. Geophys. Res., 102, 4343–4352, 1997.

Haman, K. E., Makulski, A., Malinowski, S. P., and Busen, R.: A new ultrafast thermometer for airborne measurements in clouds, J. Atmos. Oceanic Technol., 14, 217–227, 1997.

Haman, K. E., Malinowski, S. P., Struś, B. D., Busen, R., and Stefko, A.: Two new types of ultrafast aircraft thermometer, J. Atmos. Oceanic Technol., 18, 117–134, 2001.

Haman, K. E., Malinowski, S. P., Kurowski, M. J., Gerber, H., and Brenguier, J.-L.: Small–scale mixing processes at the top of a marine stratocumulus – A case-study, Q. J. R. Meteorol. Soc., 133, 213–226, 2007.

Hammer, P., Valero, F., and Kinne, S.: The 27–28 October 1986 FIRE cirrus case study: Retrieval of cloud particle sizes and optical depths from comparative analyses of aircraft and satellite–base infrared measurements, M. Wea. Rev., 119, 1673–1692, 1991.

Hancock, G. and Orr–Ewing, A.: Cavity ring–down spectroscopy: techniques and applications, chap. Applications of cavity ring–down spectroscopy in atmospheric chemistry, pp. 181–212, Blackwell Publishing Limited, iSBN 978–1–4051–7688–0, 2009.

Hänel, G.: Single–scattering albedo of atmospheric aerosol particles as a function of relative humidity, Journal of the Atmospheric Sciences, 33, 1120–1124, 1976.

Hanke, M., Uecker, J., Reiner, T., and Arnold, F.: Atmospheric peroxy radicals: ROXMAS, a new mass–spectrometric methodology for speciated measurements of HO_2 and ΣRO_2 and first results, Int. J. Mass Spectrom., 213, 91–99, 2002a.

Hanke, M., Uecker, J., Reiner, T., and Arnold, F.: Atmospheric peroxy radicals: ROXMAS, a new mass–spectrometric methodology for speciated measurements of HO_2 and ΣRO_2 and first results, Int. J. Mass Spec., 213, 91–99, 2002b.

Hansel, A., Singer, W., Wisthaler, A., Schwarzmann, M., and Lindinger, W.: Energy dependencies of the proton transfer reactions $H_3O^+ + CH_2O \not\Leftrightarrow CH_2OH^+ + H_2O$, Int. J. Mass Spectrom., 167, 697–703, 1997.

Hansen, A. D. A., Rosen, H., and Novakov, T.: The aethalometer–an instrument for the real–time measurement of optical absorption by aerosol particles, Sci. Total Environ., 36, 191–196, 1984.

Hansen, J., Sato, M., and Ruedy, R.: Radiative forcing and climate response, J. Geophys. Res., 102, 6831–6864, 1997.

Hansford, G., Freshwater, R., Eden, L., Turnbull, K., Hadaway, D., Ostanin, V., and Jones, R.: Lightweight dew–/frost–point hygrometer based on a surface–acoustic–wave sensor for balloon–borne atmospheric water vapor profile sounding, Rev. Sci. Instrum., 77, 2006.

Hanson, D. R., Koppes, M., Stoffers, A., Harsdorf, R., and Edelen, K.: Proton transfer mass spectrometry at 11 hPa with a circular glow discharge: Sensitivities and applications, Int. J. Mass Spectrom., 282, 28–37, 2009.

Harlow, R.: Millimeter microwave emissivities and effective temperatures of snow covered surfaces: Evidence for Lambertian surface scattering, IEEE Transactions on Geoscience and Remote Sensing, 37, 1957–1970, 2009.

Harlow, R.: Can millimeter–wave data be used to improve snow water equivalent estimates?, in Microwave Signatures 2010, Florence, Italy, submitted to Rivista Italiana di Telerilevamento, 2011a.

Harlow, R.: Estimation of snow water equivalent from cm to mm wavelength microwave data: Impacts of layering and partial penetration within tundra snow packs, in preparation, 2011b.

Harlow, R.: Sea ice emissivities and effective temperatures at AMSU–B frequencies: An analysis of airborne microwave data measured during two Arctic campaigns, IEEE Transactions on Geoscience and Remote Sensing, 49, 1223–1237, 2011c.

Harrison, L., Michalsky, J., and Berndt, J.: Automated multifilter rotating shadowband radiometer: An instrument for optical depth and radiation measurements, Appl. Opt., 33, 5118–5125, 1994.

Harsanyi, J. and Chang, C.: Hyperspectral image classification and dimensionality reduction: An orthogonal subspace projection, IEEE Transaction in Geoscience and Remote Sensing, 32, 779–785, 1994.

Hastie, D., Weissenmayer, M., Burrows, J., and Harris, G.: Calibrated chemical amplifier for atmospheric RO_x measurements, Anal. Chem., 63, 2048, 1991.

Hauf, T.: Turbulenzmessungen mit dem Forschungsflugzeug Falcon, Meteorol. Rdsch., 37, 163–176, 1984.

Hayasaka, T., Kikuchi, N., and Tanaka, M.: Absorption of solar radiation by stratocumulus clouds: arcraft measurements and theoretical calculations, J. Appl. Meteorol., 34, 1047–1055, 1995.

Hayward, S., Hewitt, C. N., Sartin, J. H., and Owen, S. M.: Performance characteristics and applications of a proton transfer reaction–mass spectrometer for measuring volatile organic compounds in ambient air, Environ. Sci. Technol., 36, 1554–1560, 2002.

Haywood, J. and Boucher, O.: Estimates of the direct and indirect radiative forcing due to tropospheric aerosols: A review, Rev. Geophys., 38, 513–543, 10.1029 / 1999RG000078, 2000.

Haywood, J. M. and Shine, K. P.: The effect of anthropogenic sulfate and soot aerosol on the clear sky planetary radiation budget, Geophys. Res. Lett., 22, 603–606, 1995.

Heard, D.: Analytical Techniques for Atmospheric Measurement, Blackwell Publishing Ltd, 528 pp., 2006.

Hegg, D., Larson, T., and Yuen, P. F.: A theoretical study of the effect of relative humidity on light.scattering by trospopsheric aerosols, J. Geophys. Res., 98, 18 435–18 439, 1993.

Hegg, D., Covert, D., Jonsson, H., and Covert, P.: Determination of the Transmission Efficiency of an Aircraft Aerosol Inlet, Aerosol Sci. Technol., 39, 966–971 DOI:10.1080 / 02786820500377814, 2005.

Hegg, D., Covert, D., Jonsson, H., and Woods, R.: Differentiating natural and anthropogenic cloud condensation nuclei in the California coastal zone, Tellus, 61b, 669–676, 2009.

Hegg, D. A., Gao, S., Hoppel, W., Frick, G., Caffrey, P., Leaitch, W., Shantz, N., Ambrusko, J., and Albrechcinski, T.: Laboratory studies of the efficiency of selected organic aerosols as CCN, Atmos. Res., 58, 155–166, 2001.

Heidt, L. E., Vedder, J. F., Pollock, W. H., Lueb, R. A., and Henry, B. E.: Trace Gases in the Antarctic Atmosphere, J. Geophys. Res., 94, 11 599–11 611, 1989.

Heikes, B., Lee, M., Jacob, D., Talbot, R., Bradshaw, J., Singhs, H., Blake, D., Anderson, B., Fuelberg, H., and Thompson, A.: Ozone, hydroperoxides, oxides of nitrogen, and hydrocarbon budgets in the marine boundary layer over the South Atlantic, J. Geophys. Res., 101, 221–234, 1996.

Heikes, B., Snow, J., Ergli, P., O'Sullivan, D., Crawford, J., Orlson, J., Chen, G., Davis, D., Blakes, N., and Blake, D.: Formaldehyde over the central Pacific during PEM–Tropics B, J. Geophys. Res., 106, 717, 2001.

Heinemann, G.: Aircraft–Based Measurements of Turbulence Structures in the Katabatic Flow over Greenland, Boundary Layer Meteorol., 103, 49–81, 2002.

Heintzenberg, J.: The SAMUM–1 experiment over Southern Morocco: overview and introduction, Tellus Ser. B, 61, j.1600-0889.2008.7 00403, 2009.

Heintzenberg, J., Wiedensohler, A., Tuch, T. M., Covert, D. S., Sheridan, P., Ogren, J. A., Gras, J., Nessler, R., Kleefeld, C., Kalivitis, N., Aaltonen, V., Wilhelm, R. T., and Havlicek, M.: Intercomparisons and aerosol calibrations of 12 commercial integrating nephelometers of three manufacturers, J. Atmos. Oceanic Technol., 23, 902–914, 2006.

Heinz, D. and Chang, C.: Fully constrained least squares linear mixture analysis for material quantification in hyperspectral imagery, IEEE Transaction on Geoscience and Remote Sensing, 39, 529–545, 2001.

Helmig, D., Boulter, J., David, D., Cullen, J. B. N., Steffen, K., Johnson, B., and Oltmans, S.: Ozone and meteorological Summit, Greenland, boundary–layer conditions at during 3–21 June 2000, Atmos. Env., 36, 2595–2608, 2002.

Helmig, D., Tanner, D., Honrath, R., Owen, R., and Parrish, D.: Nonmethane hydrocarbons at Pico Mountain, Azores: 1. Oxidation chemistry in the North Atlantic region, J. Geophys. Res., 113, 2008.

Helten, M., Smit, H. G. J., Straeter, W., Kley, D., Nedelec, P., Zöger, M., and Busen, R.: Calibration and performance of automatic compact instrumentation for the measurement of relative humidity from passenger aircraft, J. Geophys. Res., 103, 25 643–25 652, 1998.

Helten, M., Smit, H., Kley, D., Ovarlez, J., Schlager, H., Baumann, R., Schumann, U., Nedelec, P., and Marenco, A.: In–flight intercomparison of MOZAIC and POLINAT water vapor measurements, J. Geophys. Res., 104, 26 087–26 096, 1999.

Henderson, S., Suni, P., Hale, C., Hannon, S., Bruns, J. M. D., and Yuen, E.: Coherent laser radar at 2 μm using solid–state lasers, IEEE Transactions on Geoscience and Remote Sensing, 31, 4–15, 1993.

Hendricks, J., Karcher, B., Dopelheuer, A., Feichter, J., Lohmann, U., and Baumgardner, D.: Simulating the global atmospheric black carbon cycle: a revisit to the contribution of aircraft emissions, Atmos. Chem. Phys., 4, 2521–2541, 2004.

Hengstberger, F.: Thermal Detectors of Optical Radiation, in Absolute Radiometry, edited by F. Hengstberger, Academic Press, Inc., San Diego, Calif., 1989.

Hering, S., Appel, B., Cheng, W., Salaymeh, F., Cadle Mulawa, S., Cahill, T., Eldred, A., Surovik, M., Fitz, D., Howes, J., Knapp, K., Stockburger, L., Turpin, B., Huntzicker, J., Zhang, X.-Q., and McMurry, P.: Comparison of Sampling Methods for Carbonaceous Aerosols in Ambient Air, Aerosol Sci. Tech., 12, 200–213, 1990.

Hering, S. V. and Stolzenburg, M. R.: A method for particle size amplification by water condensation in a laminar, thermally diffusive flow, Aerosol Sci. Tech., 39, 42–8–436, 2005.

Hermann, M.: private communication, 2010.

Hermann, M. and Wiedensohler, A.: Counting efficiency of condensation particle counters at low–pressures with illustrative data from the upper troposphere, J. Aerosol Sci., 32, 975–991, 2001.

Hermann, M., Stratmann, F., and Wiedensohler, A.: Calibration of an aircraft–borne aerosol inlet system for fine particle measurements., J. Aerosol Sci., 30, S153–S154, 1999.

Hermann, M., Stratmann, F., Wilck, M., and Wiedensohler, A.: Sampling characteristics of an aircraft–borne aerosol inlet system, J. Atmos. Oceanic Technol., 18, 7–19, 2001.

Hermann, M., Adler, S., Caldow, R., Stratmann, F., and Wiedensohler, A.: Pressure–dependent efficiency of a condensation particle counter operated with FC–43 as working fluid, J. Aerosol Sci, 36, 1322–1337, 2005a.

Hermann, M., Brenninkmeijer, C., Heintzenberg, J., Martinsson, B., Nguyen, H., Reichelt, M., Slemr, F., Wiedensohler, A., and Zahn, A.: CARIBIC–Next generation: An airborne measurement platform for the global distribution of aerosol particles, presentation at the European Aerosol Conference (EAC), Ghent, Belgium, 28. August–2. September, winner of the INTROP poster award by ESF, 2005b.

Herold., M., Roberts, D., Noronha, V., and Smadi, O.: Imaging spectrometry and asphalt road surveys, Transportation Research Part C: Emerging Technologies, 2008.

Hess, M., Koepke, P., and Schult, I.: Optical Properties of Aerosols and Clouds: The Software Package OPAC, Bull. Am. Met. Soc., 79, 831–844, 1998.

Heue, K.-P., Wagner, T., Broccardo, S. P., Walter, D., Piketh, S. J., Ross, K. E., Beirle, S., and Platt, U.: Direct observation of two dimensional trace gas distributions with an airborne Imaging DOAS instrument, Atmos. Chem. Phys., 8, 6707–6717, 2008.

Hewison, T.: Airborne Measurements of Forest and Agricultural Land Surface Emissivity at Millimetre Wavelengths, IEEE Transactions on Geoscience and Remote Sensing, 39, 393–400, 2001.

Hewison, T.: Aircraft validation of clear air absorption models at millimeter wavelengths (89–183 GHz), J. Geophys. Res., 111, doi:10.1029/2005JD006719, 2006.

Hewison, T. and English, S.: Airborne Retrievals of Snow and Ice Surface Emissivity at Millimetre Wavelengths, IEEE Transactions on Geoscience and Remote Sensing, 37, 1871–1879, 1999.

Hewitt, C. N., Hayward, S., and Tani, A.: The application of proton transfer reaction–mass spectrometry (PTR–MS) to the monitoring and analysis of volatile organic compounds in the atmosphere, J. Environ. Monit., 5, 1–7, 2003.

Heymsfield, A.: On measurements of small ice particles in clouds, Geoph. Res. Lett., 34, doi:10.1029/2007GL030951, 2007a.

Heymsfield, A. and McFarquhar, G.: High albedos of cirrus in the tropical Pacific warm pool: Microphysical interpretations from CEPEX and from Kwajalein, Marshall Islands, J. Atmos. Sci., 53, 2424–2451, 1996.

Heymsfield, A. and Miloshevich, L.: Evaluation of liquid water measuring instruments in cold cloud sampled during FIRE, J. Atmos. Oceanic Technol., 6, 378–388, 1989.

Heymsfield, A., Kennedy, P., Massie, S., Schmitt, C., Wang, Z., Haimov, S., and Rangno, A.: Aircraft–Induced Hole Punch and Canal Clouds: Inadvertent Cloud Seeding, Bull. Amer. Meteor. Soc., p. doi:10.1175/2009BAMS2905.1, 2010.

Heymsfield, A. J.: Precipitation Development in Stratiform Ice Clouds: A Microphysical and Dynamical Study, J. Atmos. Sci., 34, 367–381, 1977.

Heymsfield, A. J.: On measurements of small ice particles in clouds, Geophys. Res. Lett., 34, 2007b.

Heymsfield, A. J. and Westbrook, C. D.: Advances in the Estimation of Ice Particle Fall Speeds Using Laboratory and Field Measurements, J. Atmos. Sci., 67, 2469–2482, 2010.

Heymsfield, A. J., Protat, A., Austin, R. T., Hogan, R., Delanoë, J., Okamoto, H., Sato, K., van Zadelhoff, G.-J., Donovan, D. P., and Wang, Z.: Testing IWC retrieval methods using radar and ancillary measurements with in situ data, J. Appl. Meteorol. Climatol., 47, 135–163, 2008.

Heymsfield, G., Bidwell, S., Caylor, I., Ameen, S., Nicholson, S., Boncyk, W., Miller, L., Vandemark, D., Racette, P., and Dod, L.: The EDOP radar system on the high–altitude NASA ER–2 aircraft, J. Atmos. Oceanic Technol., 13, 795–809, 1996.

Hignett, P., Taylor, J., Francis, P., and Glew, M.: Comparison of observed and modeled direct aerosol forcing during TARFOX, J. Geophys. Res., 104, 2279–2287, 1999.

Hildebrand, P. H., Lee, W.-C., Walter, C. A., Frush, C., Randall, M., Loew, E., Neitzel, R., Parsons, R., Testud, J., Baudin, F., and LeCornec, A.: The ELDORA–ASTRAIA airborne Doppler weather radar: high resolution observations from TOGA–COARE, Bull. Amer. Met. Soc., 77, 213–232, 1996.

Hindman, E.: A 'Cloud Gun' Primer, J. Atmos. Oceanic Technol., 4, 736–741, 1987.

Hinds, W. C.: Aerosol Technology, Properties, Behavior and Measurement of Airborne Particles, 2nd Edition, John Wiley and Sons, New York, 504 pp., 1999.

Hiranuma, N., Kohn, M., Pekour, M. S., Nelson, D. A., Shilling, J. E., and Cziczo, D. J.: Droplet activation, separation, and compositional analysis: laboratory studies and atmospheric measurements, Atmos. Meas. Tech. Discuss., 4, 691–713, 2011.

Hirleman, E., Oechsle, V., and Chigier, N.: Response characteristics of laser diffraction particle size analyzers: optical volume extent and lens effects, Opt. Eng., 23, 610–619, 1984.

Hirst, E., Kaye, P., Greenaway, R., Field, P., and Johnson, D.: Discrimination of micrometre-sized ice and supercooled droplets in mixed phase clouds, Atmos. Environm., 35, 33–47, 2001.

Hitschfeld, W. and Bordan, J.: Errors inherent in the radar measurement of rainfall at attenuating wavelengths, J. Meteorol., 11, 58–67, 1954.

Hlao, N. and Wong, F.: Hyperspectral Imagery Market Forcast: 2000–2005, Tech. rep., Contract No F4701–c–0009 for Space and Missile System Center Air Force Materiek Comman US Air Force, 2000.

Hock, T. and Franklin, J.: The NCAR GPS dropwindsonde, Bull. Am. Meteorol. Soc., 80, 407–420, 1999.

Hodges, J., Presser, C., Gupta, A., and Avedisian, C.: Analysis of Droplet Arrival Statistics in a Pressure–Atomized Spray Flame, in 25^{th} International Symposium on Combustion, pp. 353–361, The Combustion Institute, 1994.

Hoffmann, T., Huang, R.-J., and Kalberer, M.: Atmospheric Analytical Chemistry, Anal. Chem., doi: 10.1021 / ac2010718, in press, 2011.

Hofmann, D. J., Rosen, J. M., Pepin, T. J., and Pinnick, R. G.: Particles in the polar stratospheres, Nature, 245, 369–371, 1973.

Hofmann–Wellenhof, B., Lichtenegger, H., and Collins, J.: Global Positioning System: Theory and practice, Fifth Edition, Springer–Verlag, Wien, 2001.

Hofzumahaus, A.: Analytical Techniques for Atmospheric Measurement, chap. Measurement of photolysis frequencies in the atmosphere, pp. 406–500, Blackwell Publishing, 2006.

Hofzumahaus, A., Kraus, A., and Müller, M.: Solar actinic flux spectroradiometry: a technique for measuring photolysis frequencies in the atmosphere, Appl. Opt., 38, 4443–4460, 1999.

Hofzumahaus, A., Kraus, A., Kylling, A., and Zerefos, C.: Solar actinic radiation (280–420 nm) in the cloud–free troposphere between ground and 12 km altitude: Measurements and model results, J. Geophys. Res., 107, doi:10.1029 / 2001JD900142, 2002.

Hogan, R., Donovan, D., and Tinel, C.: Independent evaluation of the ability of spaceborne radar and lidar to retrieve the microphysical and radiative properties of ice clouds, J. Atmos. Oceanic Technol., 23, 211–227, 2003a.

Hogan, R. J., Francis, P. N., Flentje, H., Illingworth, A. J., Quante, M., and Pelon, J.: Characteristics of mixed phase clouds. I: Lidar, radar and aircraft observations from CLARE'98, Q. J. R. Meteorolog. Soc., 129, 2089–2116, 2003b.

Hogan, R. J., Gaussiat, N., and Illingworth, A. J.: Stratocumulus Liquid Water Content from Dual–Wavelength Radar, J. Atmos. Oceanic Technol., 22, 1207–1218, 2005.

Hogan, R. J., Brooks, M., Illingworth, A., Donovan, D., Tinel, C., Bouniol, D., and Baptista, J.: Independent Evaluation of the Ability of Spaceborne Radar and Lidar to Retrieve the Microphysical and Radiative Properties of Ice Clouds, J. Atmos. Oceanic Technol., 23, 211–217, 2006a.

Hogan, R. J., Mittermaier, M. P., and Illingworth, A. J.: The retrieval of ice water content from radar reflectivity factor and temperature and its use in evaluating a mesoscale model, J. Appl. Meteorol. Climatol., 45, 301–317, 2006b.

Holben, B. N., Eck, T. I., Slutsker, I., Tar, D., Buis, J., Setxer, A., Vemte, E., Reagan, J., Kaufman, Y. J., Nakajima, T., Lavenu, F., Jankowiak, I., and Smirnozjt, A.: AERONET–A federated instrument network and data archive for aerosol characterization, Remote Sens. Environ., 66, 1–16, 1998.

Holloway, J., Jakoubek, R., Parrish, D., Gerbig, C., Volz–Thomas, A., Schmitgen, S., Fried, A., Wert, B., Henry, B., James, R., and Drummond, J.: Airborne intercomparison of vacuum ultraviolet fluorescence and tunable diode laser absorption measurements of tropospheric carbon monoxide, J. Geophys Res., 105, 251–261, 2000.

Holzapfel, E. P.: Transoceanic airplane sampling for organisms and particles, Pacific Insects, 18, 169–189, 1978.

Holzinger, R., Williams, J., Salisbury, G., Klupfel, T., de Reus, M., Traub, M., Crutzen, P. J., and Lelieveld, J.: Oxygenated compounds in aged biomass burning plumes over the Eastern Mediterranean: evidence for strong secondary production of methanol and acetone, Atmos. Chem. Phys., 5, 39–46, 2005.

Holzwarth, S., Müller, A., Habermeyer, M., Richter, R., Hausold, A., Thiemann, S., and Strobl, P.: HySens-DAIS 7915 / ROSIS Imaging Spectrometers at DLR, in Proceedings of the 3rd EARSeL Workshop on Imaging Spectroscopy, pp. 3–14, Herrsching, 2003.

Homan, C. D., Volk, C., Kuhn, A., Werner, A., Baehr, J., Viciani, S., Ulanovski, A., and Ravegnani, F.: Tracer measurements in the tropical tropopause layer during the AMMA / SCOUT–O_3 aircraft campaign, Atmos. Chem. Phys., 10, 3615–3627, 2010.

Hopkins, J., Jones, I., Lewis, A., McQuaid, J., and Seakins, P.: Non–methane hydrocarbons in the Arctic boundary layer, Atmos. Environm., 36, 3217–3229, 2002.

Horrak, U., Mirme, A., Salm, J., Tamm, E., and Tammet, H.: Air ion measurements as a source of information about atmospheric aerosols, Atmos. Res., 46, 233–242, 1998.

Horstjann, M., Andrés Hernández, M., and Burrows, J.: Development of a novel optical feedback and cavity enhanced absorption spectroscopy (OF–CEAS) detector for airborne measurements of nitrogen dioxide, Atmos. Meas. Tech., to be submitted, 2011.

Horvath, H.: Atmospheric light absorption-A review, Atmos. Environm., 27, 293–317, 1993.

Hovenac, E. and Hirleman, E.: Use of rotating pinholes and reticles for calibrations of cloud droplet instrumentation, J. Atmos. Oceanic Technol., 8, 166–171, 1991.

Howell, J. F. and Mahrt, L.: Multiresolution flux decomposition, Boundary-Layer Meteorol., 83, 117–137, 1997.

Hubert, K.: Beobachtungen über die Verbreitung des Gelbrostes bei künstlichen Feldinfektionen, Fortschr. Landw., 7, 1932.

Hudson, J.: An instantaneous CCN spectrometer, J. Atmos. Oceanic Technol., 6, 1055–1065, 1989.

Hudson, J. and Squires, P.: An improved continuous flow diffusion cloud chamber, J. Appl. Meteorol., 15, 776–782, 1976.

Hudson, J., Noble, S., and Jha, V.: Stratus cloud supersaturations, Geophys. Res. Lett., 37, 2010.

Hudson, J. G., Jha, V., and Noble, S.: Drizzle correlations with giant nuclei, Geophys. Res. Lett., www.agu.org/journals/gl/papersinpress/html#id2010GL046207, Accepted January 25, 2011.

Huebert, B., Howell, S., Covert, D., Bertram, T., Clarke, A., Anderson, J., Lafleur, B., Seebaugh, W., Wilson, J., Gesler, D., Blomquist, B., and Fox, J.: PELTI: Measuring the passing efficiency of an airborne low turbulence aerosol inlet, Aerosol Sci. Technol., 38, 803–826, 2004.

Huebert, B. J., Lee, G., and Warren, W.: Airborne aerosol inlet passing efficiency measurements, J. Geophys. Res., 95, 16 369–16 381, 1990.

Huey, L. G.: Measurement of trace atmospheric species by chemical ionization mass spectrometry: Speciation of reactive nitrogen and future directions, Mass Spectrom. Rev., 26, 166–184, 2007.

Huey, L. G., Hanson, D. R., and Howard, C. J.: Reactions of SF^{-6} and I^- with Atmospheric Trace Gases, J. Phys. Chem., 99, 5001–5008, 1995.

Huey, L. G., Dunlea, E., Lovejoy, E., Hanson, D., Norton, R., Fehsenfeld, F., and Howard, C.: Fast time response measurements of HNO_3 in air with a chemical ionization mass spectrometer, J. Geophys. Res., 103, 3355–3360, 1998.

Huffaker, R. M. and Hardesty, R. M.: Remote sensing of atmospheric wind velocities using solid–state and CO_2 coherent laser systems, Proc. IEEE, 84, 181–204, 1996.

Huffman, J. A., Docherty, K. S., Aiken, A. C., Cubison, M. J., Ulbrich, I. M., DeCarlo, P. F., Sueper, D., Jayne, J. T., Worsnop, D. R., Ziemann, P. J., and Jimenez, J. L.: Chemically-resolved aerosol volatility measurements from two megacity field studies, Atmos. Chem. Phys., 9, 7161–7182, 2009.

Huffman, P. and Thursby, W.: Light scattering by ice crystals, J. Atmos. Sci., 26, 1073–1077, 1969.

Hunt, G. and Salisbury, J.: Visible and near infrared spectra of minerals and rocks–I: Silicate minerals., Modern Geology, pp. 283–300, 1970.

Hunt, G. and Salisbury, J.: Visible and near infrared spectra of minerals and rocks–II: Carbonates, Modern Geology, pp. 23–30, 1971.

Hunt, G., Salisbury, J., and Lenhoff, C.: Visible and near infrared spectra of minerals and rocks–III: Oxides and hydroxides, Modern Geology, 2, 195–205, 1971a.

Hunt, G., Salisbury, J., and Lenhoff, C.: Visible and near infrared of minerals and rocks: Halides, phosphates, arsenates, vanates and borates, Modern Geology, 3, 121–132, 1971b.

Hunter, E. P. L. and Lias, S. G.: Evaluated gas phase basicities and proton affinities of molecules: An update, J. Phys. Chem. Ref. Data, 27, 413–656, 1998.

Hunton, D., Ballenthin, J. O., Borghetti, J. F., Federico, G. S., Miller, T. M., Thorn, F., Viggiano, A. A., Anderson, B. E., Cofer, W. R., McDougal, D. S., and Wey, C. C.: Chemical ionization mass spectrometric measurements of SO_2 emissions from jet engines in flight and test chamber operations, J. Geophys. Res., 105, 26 841–26 855, 2000.

Huntrieser, H., Schlager, H., Roiger, A., Schumann, U., Höller, H., Kurz, C., Brunner, D., Schwierz, C., Richter, A., and Stohl, A.: Lightning–produced NO_x over Brazil during TROCCINOX: airborne measurements in tropical and subtropical thunderstorms and the importance of mesoscale convective systems, Atmos. Chem. Phys., 7, 2987–3013, 2007.

Huntrieser, H., Schlager, H., Lichtenstern, M., Roiger, A., Stock, P., Minikin, A., Höller, H., Schmidt, K., Betz, H.-D., Allen, G., Viciani, S., Ulanovsky, A., Ravegnani, F., and Brunner, D.: NO_x production by lightning in Hector: first airborne measurements during SCOUT–O_3 / ACTIVE, Atmos. Chem. Phys., 9, 8377–8412, 2009.

Hyson, P. and Hicks, B.: A single beam infrared hygrometer for evaporation measurement, J. Appl. Meteorol., 14, 301–307, 1975.

Iaquinta, J., Isaka, H., and Personne, P.: Scattering phase function of bullet rosette ice crystals, J. Atmos. Sci., 52, 1401–1413, 1995.

Ide, R.: Comparison of Liquid Water Content Measurement Techniques in an Icing Wind Tunnel, Tech. Mem. TM-1999-209643, NASA, aRL-TR-2134, 24 pp., 1999.

Ide, R. and Oldenburg, J.: Icing cloud calibration of the NASA Glenn Icing Research Tunnel, 39th Aerospace Sciences Meeting and Exhibit, aIAA–2001–0234, 2001.

Illingworth, A. and Marsh, S.: Static charging of aircraft by collisions with ice crystals, Revue Phys. Appl., 21, 803–808, 1986.

Illingworth, A. J., Hogan, R. J., O'Connor, E. J., Bouniol, D., Brooks, M. E., Delanoë, J., Donovan, D. P., Eastment, J. D., Gaussiat, N., Goddard, J. W. F., Haeffelin, M., Baltink, H. K., Krasnov, O. A., Pelon, J., Piriou, J.-M., Protat, A., Russchenberg, H. W. J., Seifert, A., Tompkins, A. M., van Zadelhoff, G.-J., Vinit, F., Willen, U., Wilson, D. R., and Wrench, C. L.: Cloudnet–Continuous evaluation of cloud profiles in seven operational models using ground–based observations, Bull. Am. Meteorol. Soc., 88, 883–898, 2007.

Inomata, S., Tanimoto, H., Aoki, N., Hirokawa, J., and Sadanaga, Y.: A novel discharge source of hydronium ions for proton transfer reaction ionization: design, characterization, and performance, Rapid Commun. Mass Spectrom., 20, 1025–1029, 2006.

Intrieri, J. M., Stephens, G. L., Eberhard, W. L., and Uttal, T.: A Method for Determining Cirrus Cloud Particle Sizes Using Lidar and Radar Backscatter Technique, J. Appl. Meteor., 32, 1074–1082, 1993.

Inverarity, G. W.: Correcting airborne temperature data for lags introduced by instruments with two–time–constant responses., J. Atmos. Oceanic Technol., 17, 176–184, 2000.

Iqbal, M.: An Introduction to Solar Radiation, Academic Press, Inc., 1983.

Iribarne, J. and Godson, W.: Atmospheric Thermodynamics. 2nd Ed., D. Reidel, Dordrecht, Holland, 1981.

Irons, J., Weismiller, R., and Petersen, G.: Theory and Application of Optical Remote Sensing, chap. Soil reflectance, pp. 66–106, Willey Series in Remote Sensing, John Wiley and Sons, New York, 1989.

Irshad, H., McFarland, A., Landis, M., and Stevens, R.: Wind tunnel evaluation of an aircraft–borne sampling system, Aerosol Sci. Technol., 38, 311–321, 2004.

Isaac, G., Korolev, A., Strapp, J., Cober, S., Boudala, F., Marcotte, D., and Reich, V.: Assessing the collection efficiency of natural cloud particles impacting the Nevzorov total water content probe, in AIAA 44^{th} Aerospace Sciences Meeting and Exhibit, Reno, Nevada, AIAA–2006–1221, 2006.

Isaac, P. R., Mcaneney, J., Leuning, R., and Hacker, J. M.: Comparison of Aircraft and Ground–Based Flux Measurements during OASIS95, Boundary Layer Meteorol., 110, 39–67, 2004.

Ismail, S., Koch, G., Abedin, N., Refaat, T., Rubio, M., and Singh, U.: Development of Laser, Detector, and Receiver Systems for an atmospheric CO_2 Lidar Profiling System, in Proc. IEEE Aerospace Conference, pp. 1–7, 2008.

ISO: International Organization for Standardization, 1975: Standard atmosphere (identical with the ICAO and WMO Standard Atmospheres from - 2 to 32 km), International Organization for Standardization., Geneva, Switzerland, 1975.

Itten, K., Meyer, P., Staenz, K., Kellenberger, T., and Schaepman, M.: Evaluation of AVIRISwiss' 91 Campaign Data, in Proc. of the Third Annual JPL Airborne Remote Sensing Workshop, JPL Publication 92-41, pp. 108-110, 1992.

Itten, K., Dell Endice, F., Hueni, A., Kneubühler, M., Schläpfer, D., Odermatt, D., Seidel, F., Huber, S., Schopfer, J., and Kellenberger, T.: APEX–the hyperspectral ESA airborne prism experiment, Sensors, 8, 6235–6259, 2008.

Itten, K. I.: The emergence of imaging spectrometry in Europe Remote Sensing Laboratories, in Proceedings of the 5th EARSEL SIG IS Workshop, Bruges, 2007.

Jackson, T.: Liquid Particle Size Measurements, vol. 2nd, chap. Droplet Sizing Interferometry, ASTM, Philadelphia, PA, edited by D.E. Hirleman, W.D. Bachalo and P.G. Felton, 1990.

Jacobson, M., Hansson, H., Noone, K., and Charlson, R.: Organic atmospheric aerosols: Review and state of the science, Rev. Geophys., 38, 267–294, doi: 10.1029/1998RG000045, 2000.

Jaegle, L., Jacob, D., Brune, W., Faloona, I., Tan, D., Heikes, B., Kondo, Y., Sachse, G., Anderson, B., Gregory, G., Singh, H., Ferry, R. P. G., Blake, D., and Shetter, R.: Photochemistry of HO_x in the upper troposphere at northern midlatitudes, J. Geophys. Res. D: Atmos., 105, 3877–3892, 2000.

Jaegle, L., Jacob, D. J., Brune, W. H., and Wennberg, P. O.: Chemistry of HO_x radicals in the upper troposphere, Atmos. Environ., 35, 469–489, 2001.

Jäkel, E., Wendisch, M., Kniffka, A., and Trautmann, T.: Airborne system for fast measurements of upwelling and downwelling spectral actinic flux densities, Appl.Opt., 44, 434–444, 2005.

Jäkel, E., Wendisch, M., and Lefer, B.: Parameterization of ozone photolysis frequency in the lower troposhere using data from photodiode array detector spectrometers, J. Atmos. Chem., 54, 67–87, 2006.

Jarecke, P. and Yokoyama, K.: Radiometric calibration of the Hyperion imaging spectrometer instrument From primary standards to end–to–end calibration, in Proceedings of SPIE, vol. 4135, pp. 254–263, 2000.

Jayne, J. T., Leard, D. C., Zhang, X. F., Davidovits, P., Smith, K. A., Kolb, C. E., and Worsnop, D. R.: Development of an aerosol mass spectrometer for size and composition analysis of submicron particles, Aerosol Sci. Technol., 33, 49–70, 2000.

Jenkin, M. and Clemitshaw, K.: Ozone and other secondary photochemical pollutants: Chemical processes governing their formation in the planetary boundary layer, Atmos. Environm., 34, 2499, 2000.

Jennings, S. G. and O'Dowd, C. D.: Volatility of aerosol at Mace Head, on the west coast of Ireland, J. Geophys. Res., 95, 13 937–13 948, 1990.

Jennings, S. G., O'Dowd, C. D., Cooke, W. F., Sheridan, P. J., and Cachier, H.: Volatility of elemental carbon, Geophys. Res. Lett., 21, 1719–1722, 1994.

Jensen, E., Lawson, P., Baker, B., Pilson, B., Mo, Q., Heymsfield, A. J., Bansemer, A., Bui, T. P., McGill, M., Hlavka, D., Heymsfield, G., Platnick, S., Arnold, G. T., and Tanelli, S.: On the importance of small ice crystals in tropical anvil cirrus, Atmos. Chem. Phys., 9, 5519–5537, 2009.

Jensen, J. and Granek, H.: Optoelectronic Simulation of the PMS 260X Optical Array Probe and Application to Drizzle in a Marine Stratocumulus, J. Atmos. Oceanic Technol., 19, 568–585, 2002.

Jimenez, J. L., Jayne, J., Shi, Q., Kolb, C., Worsnop, D., Yourshaw, I., Seinfeld, J., Flagan, R., Zhang, X., Smith, K., Morris, J., and Davidovits, P.: Ambient aerosol sampling using the Aerodyne Aerosol Mass Spectrometer, J. Geophys. Res., 108, 2003.

Jimenez, J. L., Canagaratna, M. R., Donahue, N. M., Prevot, A. S. H., Zhang, Q., Kroll, J. H., DeCarlo, P. F., Allan, J. D., Coe, H., Ng, N. L., Aiken, A. C., Docherty, K. S., Ulbrich, I. M., Grieshop, A. P., Robinson, A. L., Duplissy, J., Smith, J. D., Wilson, K. R., Lanz, V. A., Hueglin, C., Sun, Y. L., Tian, J., Laaksonen, A., Raatikainen, T., Rautiainen, J., Vaattovaara, P., Ehn, M., Kulmala, M., Tomlinson, J. M., Collins, D. R., Cubison, M. J., E., J. D., Huffman, J. A., Onasch, T. B., Alfarra, M. R., Williams, P. I., Bower, K., Kondo, Y., Schneider, J., Drewnick, F., Borrmann, S., Weimer, S., Demerjian, K., Salcedo, D., Cottrell, L., Griffin, R., Takami, A., Miyoshi, T., Hatakeyama, S., Shimono, A., Sun, J. Y., Zhang, Y. M., Dzepina, K., Kimmel, J. R., Sueper, D., Jayne, J. T., Herndon, S. C., Trimborn, A. M., Williams, L. R., Wood, E. C., Middlebrook, A. M., Kolb, C. E., Baltensperger, U., and Worsnop, D. R.: Evolution of Organic Aerosols in the Atmosphere, Science, 326, 1525–1529, 2009.

Jobson, B., Niki, H., Yokouchi, Y., Bottenheim, J., Hopper, F., and Leaitch, R.: Measurements of C_2–C_6 Hydrocarbons During the Polar Sunrise 1992 Experiment: Evidence for Cl Atom and Br Atom Chemistry, J. Geophys. Res., 99, 25 355–25 368, 1994.

Jobson, B., Parrish, D., P., G., Kuster, W., Fehsenfeld, F., Blake, D., Blake, N., and Niki, H.: Spatial and temporal variability of nonmethane hydrocarbon mixing ratios and their relation to photochemical lifetime, J. Geophys. Res., 103, 13 557–13 567, 1998.

Jobson, B. T. and McCoskey, J. K.: Sample drying to improve HCHO measurements by PTR–MS instruments: laboratory and field measurements, Atmos. Chem. Phys. Discuss., 9, 19 845–19 877, 2009.

Joe, P. and List, R.: Testing and performance of of two–dimensional Optical Array Spectrometer with greyscale, J. Atmos. Oceanic Technol., 4, 139–150, 1987.

John, W., Hering, S., Reischl, G., Sasaki, G., and Goren, S.: Characteristics of Nuclepore filters with large pore size. 2. Filtration properties, Atmos. Environm., 17, 373–382, 1983.

Johnson, C., Rice, J., and Brown, S.: The establishment and verification of traceability for remote sensing radiometry, with an eye towards intercomparison of results, in 2004 CEOS / IVOS Calibration Workshop, ESA / ESTEC, Noordwijk, The Netherlands, 2004.

Johnson, D. G., Jucks, K. W., Traub, W. A., and Chance, K. V.: Isotopic composition of stratospheric water vapour: Measurements and photochemistry, Atmos. Chem. Phys., 106, 12 211–12 217, 2001.

Johnston, P. S. and Lehmann, K.: Cavity enhanced absorption spectroscopy using a broadband prism cavity and a supercontinuum source, Opt. Express, 16, 15 013–15 023, 2008.

Jones, J.: Electric charge acquired by airplanes penetrating thunderstorms, J. Geophys. Res., 95(D10), 16 589–16 600, 1990.

Jonsson, H. H., Wilson, J., Brock, C., Knollenberg, R., Newton, R., Dye, J., Baumgardner, D., Borrmann, S., Ferry, G., Pueschel, R., Woods, D., and Pitts, M.: Performance of a focused cavity aerosol spectrometer for measurements in the stratosphere of particle size in the 0.06–2.0 μm-Diameter range, J. Atmos. Oceanic Technol., 12, 115–129, 1995.

Jordan, A., Haidacher, S., Hanel, G., Hartungen, E., Herbig, J., Mark, L., Schottkowsky, R., Seehauser, H., Sulzer, P., and Mark, T. D.: An online ultra–high sensitivity Proton–transfer–reaction mass–spectrometer combined with switchable reagent ion capability (PTR+SRI–MS), Int. J. Mass Spectrom., 286, 32–38, 2009a.

Jordan, A., Haidacher, S., Hanel, G., Hartungen, E., Mark, L., Seehauser, H., Schottkowsky, R., Sulzer, P., and Mark, T. D.: A high resolution and high sensitivity proton–transfer–reaction time–of–flight mass spectrometer (PTR–TOF–MS), Int. J. Mass Spectrom., 286, 122–128, 2009b.

Jorgensen, D., Hildebrand, P. H., and Frush, C.: Feasibility test of an airborne pulse–Doppler meteorological radar, J. Clim. Appl. Meteorol., 22, 744–757, 1983.

Jorgensen, D. P., Matejka, T., and Dugranrut, J. D.: Multi–beam techniques for deriving wind fields from airborne Doppler radars, Meteorol. Atmos. Phys., 59, 83–104, 1996.

Josset, D., Pelon, J., Protat, A., and Flamant, C.: New approach to determine aerosol optical depth from combined CALIPSO and CloudSat ocean surface echoes, Geophys. Res. Lett., 35, 2008.

Jourdan, O., Oshchepkov, S., Gayet, J.-F., Shcherbakov, V., and Isaka, H.: Statistical analysis of cloud light scattering and microphysical properties obtained from airborne measurements, J. Geophys. Res., 2003.

Junge, C. E.: Vertical Profiles of Condensation Nuclei in the Stratosphere, J. Meteorol., 18, 501–509, 1961.

Junge, C. E., Chagnon, C. W., and Manson, J. E.: A world–wide stratospheric aerosol layer, Science, 133, 1478–1479, 1961.

Kahle, A. and Goetz, A.: Mineralogic information from a new airborne Thermal Infrared Multispectral Scanner, Science, 222, 24–27, 1983.

Kaimal, J. C. and Finnigan, J. J.: Atmospheric Boundary Layer Flows–Their Structure and Measurement, Oxford University Press, 289 pp., 1994.

Kaimal, J. C., Wyngaard, J. C., and Haugen, D. A.: Deriving power spectra from a three–component sonic anemometer, J. Appl. Meteor., 7, 827–837, 1968.

Kalnajs, L. E. and Avallone, L.: Frost flower influence on springtime boundary–layer ozone depletion events and atmospheric bromine levels, Geophys. Res. Letts., 33, 1–3, 2006.

Kalogiros, J. and Wang, Q.: Aerodynamic effects on wind turbulence measurements with research aircraft, J. Atmos. Oceanic Technol., 19, 1567–1576, 2002.

Kampe, H.: Visibility and liquid water content in clouds in the free atmosphere, J. Meteorology, 7, 54–57, 1950.

Kanaya, Y., Matsumoto, J., Kato, S., and Akimoto, H.: Behaviors of OH and HO_2 radicals during the observations at a remote island of Okinawa (ORION99) field campaign. 1. Observation using a laser–induced fluorescence instrument, J. Geophys. Res., 106, 24 197–24 208, 2001.

Karbou, F.: Two microwave land emissivity parameterizations suitable for AMSU observations, IEEE Transactions on Geoscience and Remote Sensing, 43, 1788–1795, 2005.

Karl, T., Spirig, C., Rinne, J., Stroud, C., Prevost, P., Greenberg, J., Fall, R., and Guenther, A.: Virtual Disjunct Eddy Covariance Measurements of Organic Compound Fluxes from a Subalpine Forest using Proton Transfer Reaction Mass Spectrometry, Atmos. Chem. Phys, 2, 279–291, 2002.

Karl, T., Potosnak, M., Guenther, A., Clark, D., Walker, J., Herrick, J., and Geron, C.: Exchange processes of volatile organic compounds above a tropical rain forest: Implications for modeling tropospheric chemistry above dense vegetation, J. Geophys. Res., 109, 2004.

Karl, T., Guenther, A., Yokelson, R. J., Greenberg, J., Potosnak, M., Blake, D. R., and Artaxo, P.: The tropical forest and fire emissions experiment: Emission, chemistry, and transport of biogenic volatile organic compounds in the lower atmosphere over Amazonia, J. Geophys. Res. D: Atmos., 112, 2007.

Karl, T., Apel, E., Hodzic, A., Riemer, D. D., Blake, D. R., and Wiedinmyer, C.: Emissions of volatile organic compounds inferred from airborne flux measurements over a megacity, Atmos. Chem. Phys., 9, 271–285, 2009.

Kartal, D., Andrés–Hernández, M., Reichert, L., Schlager, H., and Burrows, J.: Technical Note: Characterisation of a DUALER instrument for the airborne measurement of peroxy radicals during AMMA 2006, Atmos. Chem. Phys., 10, 3047–3062, 2010.

Kasten, F. and Young, A.: Revised optical air mass tables and approximation formula, Appl. Opt., 28, 4735–4738, 1989.

Katz, J. and Mirabel, P.: Calculation of supersaturation profiles in thermal diffusion cloud chambers, J. Atmos. Sci., 32, 646–652, 1975.

Kaufman, Y. and Tanré, D.: Strategy for direct and indirect methods for correction the aerosol effect on remote sensing: From avhrr to eos–modis, Remote Sens. Environ., 55, 65–79, 1996.

Kaufman, Y. J., Tanré, D., Léon, J.-F., and Pelon, J.: Retrievals of profiles of fine and coarse aerosols using lidar and radiometric space measurements, IEEE Transactions on Geoscience and Remote Sensing, 41, 1743–1754, 2003.

Kawamura, K., Umemoto, N., Mochida, M., Howell, T. B. S., and Huebert, B.: Water–soluble dicarboxylic acids in the tropospheric aerosols collected over east Asia and western North Pacific by ACE–Asia C–130 aircraft, J. Geophys. Res. D: Atmos., 108, 2003.

Kebabian, P., Wood, E., Herndon, S., and Freedman, A.: A practical alternative to chemiluminescence–based detection of nitrogen dioxide: cavity attenuated phase shift spectroscopy, Environ. Sci. Technol., 42, 6040–6045, 2008.

Keck, L., Oeh, U., and Hoeschen, C.: Corrected equation for the concentrations in the drift tube of a proton transfer reaction–mass spectrometer (PTR–MS), Int. J. Mass Spectrom., 264, 92–95, 2007.

Keck, L., Hoeschen, C., and Oeh, U.: Effects of carbon dioxide in breath gas on proton transfer reaction–mass spectrometry (PTR–MS) measurements, Int. J. Mass Spectrom., 270, 156–165, 2008.

Keeler, R. J., Serafin, R. J., Schwiesow, R. L., Lenschow, D. H., Vaughan, J. M., and Woodfield, A. A.: An airborne laser air motion sensing system. Part I: Concept and preliminary experiment, J. Atmos. Ocean. Tech., 4, 113–127, 1987.

Kelly, K., Tuck, A., Murphy, D., Proffitt, M., Fahey, D., Jones, R., McKenna, D., Loewenstein, M., Podolske, J., Strahan, S., Ferry, G., Chan, K., Vedder, J., Gregory, G., Hypes, W., McCormick, M., Browell, E., and Heidt, L.: Dehydration in the Lower Antarctic Stratosphere During Late Winter and Early Spring, 1987, J. Geophys. Res., 94(D9), 11 317–11 357, 1989.

Kempter, T. and Sommer, S.: Mapping and monitoring of residual heavy metal contamination and acidification risk after the Aznalcóllar mining accident (Andalusia, Spain) using field and airborne hyperspectral data, in Proceedings of the 3rd EARSeL Workshop on Imaging Spectroscopy, edited by M. Habermeyer, A. Müller, and S. Holzwarth, pp. 333–343, Herrsching, Germany, 2003.

Keramitsoglou, I., Harries, J., Colling, D., Barker, R., and Foot, J.: A study of the theory and operation of a resonance fluorescence water vapor sensor for upper tropospheric humidity measurements, Meteorol. Appl., 9, 443–453, 2002.

Kerstel, E., Iannone, R., Chenevier, M., Kassi, S., Jost, H., and Romanini, D.: A water isotope (^{2}H, ^{1}7O, and ^{1}8O) spectrometer based on optical feedback cavity enhanced absorption for in–situ airborne applications, Appl. Phys. B, 85, 397–406, 2006.

Keshava, N. and Mustard, J.: Spectral unmixing, IEEE Signal Processing Magazine, 19, 44–57, 2002.

Khelif, D., Burns, S. P., and Friehe, C. A.: Improved Wind Measurements on Research Aircraft, J. Atmos. Oceanic Technol., 16, 860–875, 1999.

Kieffera, H., Stone, T., Barnes, R., Benderc, S., Eplee, R., J.Mendenha, and Ong, L.: On–orbit Radiometric Calibration Over Time and Between Spacecraft Using the Moon, in Proceedings of SPIE, vol. 4881, pp. 287–298, 2003.

Kiemle, C., Brewer, W., Ehret, G., Hardesty, R., Fix, A., Senf, C., Wirth, M., Poberaj, G., and LeMone, M.: Latent Heat Flux Profiles from Collocated Airborne Water Vapour and Wind Lidars during IHOP_2002, J. Atmos. Oceanic Technol., 2007.

Kindel, B., Schmidt, K., Pilewskie, P., Baum, B., Yang, P., and Platnick, S.: Observations and modeling of ice cloud shortwave spectral albedo during the Tropical Composition, Cloud and Climate Coupling Experiment, J. Geophys. Res., p. doi:10.1029 / 2009JD013127, 2010.

King, L.: On the Convection of Heat from Small Cylinders in a Stream of Fluid: Determination of the Convective Constants of Small Platinum Wires with Applications to Hot Wire Anemometry, Proc. R. Society London, 90, 563–570, 1914.

King, M., Byrne, D., Herman, B., and Reagan, J.: Aerosol size distributions obtained by inversion of spectral optical depth measurements, J. Atmos. Sci., 35, 2153–2167, 1978a.

King, W.: Air flow and particle trajectories around aircraft fuselages. I: Theory, J. Atmos. Oceanic Technol., 1, 5–13, 1984.

King, W. and Handsworth, R.: Total droplet concentration and average droplet sizes from simultaneous liquid water content and extinction measurements, J. Appl. Meteorol., 18, 940–944, 1979.

King, W. and Turvey, D.: A thermal device for aircraft measurement of the solid water content of clouds, J. Atmos. Oceanic Technol., 3, 356–362, 1986.

King, W., Parkin, D., and Handsworth, R.: A hot–wire water device having fully calculable response characteristics, J. Appl. Meteor., 17, 1809–1813, 1978b.

King, W., Turvey, D., Williams, D., and Llewellyn, D.: Air flow and particle trajectories around aircraft fuselages. II: Measurements, J. Atmos. Ocean. Tech., 1, 14–21, 1984.

King, W., Dye, J., Strapp, J., Baumgardner, D., and Huffman, D.: Icing wind tunnel tests on the CSIRO liquid water probe, J. Atmos. Oceanic Technol., 2, 340–353, 1985.

Kipp and Zonen: CMP series Pyranometer Instruction Manual, The Netherlands, 2010.

Klein, H., Haunold, W., Bundke, U., Nillius, B., Wetter, T., Schallenberg, S., and Bingemer, H.: A new method for sampling of atmospheric ice nuclei with subsequent analysis in a static diffusion chamber, Atmos. Res., 2009.

Kleindienst, T. E., Hudgens, E., Smith, D., McElroy, E., and Bufalini, J.: Comparison of chemiluminescence and ultraviolet ozone monitor responses in the presence of humidity and photochemical pollutants, J. Air Waste Manage. Assoc., 43, 213–222, 1993.

Kleinman, L. I., Daum, P. H., Lee, Y.-N., Senum, G. I., Springston, S. R., Wang, J., Berkowitz, C., Hubbe, J., Zaveri, R. A., Brechtel, F. J., Jayne, J., Onasch, T. B., and Worsnop, D.: Aircraft observations of aerosol composition and ageing in New England and Mid–Atlantic States during the summer 2002 New England Air Quality Study field campaign, J. Geophys. Res., 112, 2007.

Klett, J. D.: Lidar Inversion with Variable Backscatter/Extinction Ratios, Appl.Opt., 24, 1638–1643, 1985.

Kley, D. and Stone, E.: Measurement of water vapor in the stratosphere by photodissociation with Ly–α (1216 Å), Rev. Sci. Instrum., 49, 691–697, 1978.

Kley, D., Stone, E., Henderson, W., Drummond, J., Harrop, W., Schmeltekopf, A., Thompson, T., and Winkler, R.: In situ measurements of the mixing ratio of water vapor in the strato-sphere, J. Atmos. Sci., 36, 2513–2524, 1979.

Kliner, D. A. V., Daube, B. C., Burley, J. D., and Wofsy, S. C.: Laboratory investigation of the catalytic reduction technique for measurement of atmospheric NO_y, J. Geophys. Res., 102, 759–776, 1997.

Klobuchar, J.: Ionospheric effects on GPS. In Global Positioning Systems: Theory and Applications, Parkinson, B., et al. (eds.), American Institute of Aeronautics and Astronautics, 1996.

Knighton, W. B., Fortner, E. C., Midey, A. J., Viggiano, A. A., Herndon, S. C., Wood, E. C., and Kolb, C. E.: HCN detection with a proton transfer reaction mass spectrometer, Int. J. Mass Spectrom., 283, 112–121, 2009.

Knollenberg, R.: The Optical Array: An alternative to scattering or extinction for airborne particle size determination, J. Appl. Meteorol., 9, 86–103, 1970.

Knollenberg, R.: Three new instruments for cloud physics measurements: The 2–D spectrometer probe, the forward scattering spectrometer probe and the active scattering aerosol spectrometer, in International Conference on Cloud Physics, pp. 554–561, American Meteorological Society, 1976.

Knollenberg, R.: Clouds, Their Formation, Optical Properties and Effects, chap. Techniques for probing cloud microstructure, p. 495, Academic Press, edited by P.V. Hobbs and A. Deepak, 1981.

Knox, R., Green, R., Middleton, E., Turner, W., Hook, S., and Ungar, S.: The Hyperspectral Infrared Imager (HyspIRI) mission: A new capability for global ecological research and applications, in Proceedings of the 95th ESA Annual Meeting, PS–79–114, Pittsburg, Pennsylvania, 2010.

Kobayashi, T., Kawaguchi, T., and Maeda, M.: Measurement of spray flow by an improved Interferometric Laser Imaging Droplet Sizing (ILIDS), in Proc. 10th. Int. Symp. Applications of Laser Techniques to Fluid Mechanics, Lisbon, Portugal, 2000.

Kojima, T., Buseck, P., Wilson, J., Reeves, J., and Mahoney, M.: Aerosol particles from tropical convective systems: Cloud tops and cirrus anvils, J. Geophys. Res., 109 (D12), D12 201 doi:10.1029 / 2003JD004 504, 2004.

Köler, H.: The nucleus in and the growth of hygroscopic droplets, Trans. Faraday Soc., 32, 1152–1161, 1936.

Kollias, P., Albrecht, B. A., Lhermitte, R., and Savtchenko, A.: Radar observations of updrafts, downdrafts, and turbulence in fair–weather cumuli, J. Atmos. Sci., 58, 1750–1766, 2001.

Kollias, P., Albrecht, B. A., and Marks, F.: Why Mie? Accurate Observations of Vertical Air Velocities and Raindrops Using a Cloud Radar, Bull. Am. Meteorol. Soc., 83, 1471–1483, 2002.

Kollias, P., Albrecht, B. A., and Marks, F. D.: Cloud Radar Observations of Vertical Drafts and Microphysics in Convective Rain, J. Geophys. Res. Atmos., 108, 2003.

Kollias, P., Jo, I., and Albrecht, B. A.: High–resolution observations of mammatus in Tropical Anvils, Mon. Wea. Rev., 133, 2105–2112, 2005.

Komabayasi, M., Gonda, T., and Isono, K.: Life time of water drops before breaking and size distribution of fragment drops, J. Met. Soc. Japan, 42, 330–340, 1964.

Kondo, Y., Ziereis, H., Koike, M., Kawakami, S., Gregory, G., Sachse, G., Singh, H., Davis, D., and Merrill, J.: Reactive nitrogen over the Pacific Ocean during PEM–West A, J. Geophys. Res., 101, 1809–1828, 1996.

König, G., Anders, K., and Frohn, A.: A new light–scattering technique to measure the diameter of periodically generated moving droplets, J. Aerosol Sci., p. 157, 1986.

Korb, C. L., M.Gentry, B., and Li, S.: Edge technique Doppler lidar wind measurements with high vertical resolution, Appl. Opt., 36, 5976, 1997.

Kormann, R., Fischer, H., de Reus, M., Lawrence, M., Bruhl, C., von Kuhlmann, R., Holzinger, R., Williams, J., Lelieveld, J., Warneke, C., de Gouw, J., Heland, J., Ziereis, H., and Schlager, H.: Formaldehyde over the eastern Mediterranean during MINOS: comparison of airborne in–situ measurements with 3D–model results, Atmos. Chem. Phys., 3, 851–861, 2003.

Korolev, A.: Reconstruction of the Sizes of Spherical Particles from Their Shadow Images. Part I: Theoretical Considerations, J. Atmos. Oceanic Technol., 24, 376–389, 2007.

Korolev, A. and Isaac, G.: Shattering during sampling by OAPs and HVPS. Part 1: Snow particles., J. Atmos. Oceanic Technol., 22, 528–542, 2005.

Korolev, A., Kuznetsov, S. V., Makarov, Y., and Novikov, V. S.: Evaluations of measurements of particle size and sample area from optical array probes, J. Atmos. Oceanic Technol., 8, 514–522, 1991.

Korolev, A., Strapp, J., Isaac, G., and Nevzorov, A.: The Nevzorov Airborne Hot–wire LWC–TWC Probe: Principle of operation and performance characteristics, J. Atmos. Oceanic Technol., 15, 1495–1510, 1998a.

Korolev, A., Isaac, G., Mazin, I., and Barker, H.: Microphysical properties of continental clouds from in situ measurements, Q. J. R. Meteorol. Soc., 127, 2117–2151, 2001.

Korolev, A., Strapp, J., Isaac, G. A., and Emery, E.: Improved Airborne Hot–Wire Measurements of Ice Water Content in Clouds, in 15th Int. Conf. on Clouds and Precipitation, Cancun, Mexico, CD P13.4, 2008.

Korolev, A., Emery, E., Strapp, J., Cober, S., Isaac, G., Wasey, M., and Marcotte, D.: Small ice particles in tropospheric clouds: fact or artifact? Airborne Icing Instrumentation Evaluation Experiment, Bull. Amer. Meteor. Soc., 92, 967–973, 2011.

Korolev, A. V., Strapp, J. W., and Isaac, G. A.: Evaluation of accuracy of PMS Optical Array Probes, J. Atmos. Oceanic Technol., 15, 708–720, 1998b.

Kosarev, A., Mazin, I., Nevzorov, A., and Shugaev, V.: Optical density of clouds, Trans. Cent. Aerol. Obs., 124, 44–110, 1976.

Kostkowski, H.: Reliable spectroradiometry, Spectroradiometry consulting, La Plata, MD, USA., 609 pp., 1997.

Kotchenruther, R. A., Hobbs, P. V., and Hegg, D. A.: Humidification factors for atmospheric aerosols off the mid–Atlantic coast of the United States, J. Geophys. Res., 104, 2239–2251, 1999.

Kourtidis, K., Ziomas, I., Zerefos, C., Gousopoulos, A., Balis, D., and Tzoumaka, P.: Benzene and toluene levels measured with a commercial DOAS system in Thessaloniki, Greece, Atmos. Environm., 34, 1471–1480, 2000.

Kovalev, V. A. and Eichinger, W. E.: Elastic Lidar, Wiley, New York, 2004.

Kowol–Santen, J. and Ancellet, G.: Mesoscale analysis of transport across the subtropical tropopause, Geophys. Res. Lett., 27, 3345–3348, 2000.

Kozikowska, A., Haman, K., and Supronowicz, J.: Preliminary results of an investigation of the spatial distribution of fog droplets by a holographic method, Q. J. R. Meteorol. Soc., 110, 65–73, 1984.

Krämer, M. and Afchine, A.: Sampling characteristics of inlets operated at low U/Uo ratios: new insights from computational fluid dynamics (CFX) modelling, J. Aerosol Sci., 35, 683–694, 2004.

Kreidenweis, S. M., Chen, Y., DeMott, P. J., and Rogers, D. C.: Isolating and identifying atmospheric ice–nucleating aerosols: A new technique, Atmos. Res., 46, 263–278, 1998.

Kritten, L., Butz, A., Dorf, M., Deutschmann, T., Kühl, S., Prados–Roman, C., Pukite, J., Rozanov, A., Schofield, R., and Pfeilsticker, K.: Balloon–borne limb measurements of the diurnal variation of UV / vis absorbing radicals–a case study on NO_2 and O_3, Atmos. Meas. Tech., submitted, 2010.

Kropfli, R. A. and Kelly, R. D.: Meteorological research applications of MM–wave radar, Meteorol. Atmos. Phys., 59, 105–121, 1996.

Krüger, G., Erzinger, H., and Kaufmann, H.: Laboratory and airborne reflectance spectrometric analyses of lignite overburden dumps. 4th ISEG Symp., Vail, CO, USA, Journal of Geochem. Res, 64, 47–65, 1998.

Kruse, F.: Use of Airborne Imaging Spectrometer data to map minerals associated with hydrothermally altered rocks in the northern Grapevine Mountains, Nevada and California, Remote Sens. Environ., 24, 31–51, 1988.

Kruse, F., Lefkoff, A., Boardman, J., Heidebrecht, K., Sapiro, A., Barloon, P., and Goetz, A.: The spectral image processing system (SIPS)–Interactive Visualization and analysis of imaging spectrometer data, Remote Sens. Environ., 44, 145–168, 1993.

Kruse, F. A., Boardman, J., Lefkoff, A., Young, J., Kierein–Young, K., Cocks, T., Jenssen, R., and Cocks, P.: HyMap: An Australian Hyperspectral Sensor Solving Global Problems–Results from USA HyMap Data Acquisitions, in Proceedings of the 10th Australasian Remote Sensing and Photogrammetry Conference, Causal Productions (www.causalproductions.com), Adelaide, Australia, 2000.

Kuhn, P. and Suomi, V.: Airborne observations of albedo with a beam reflector, J. Meteor., 15, 172–174, 1958.

Kuhn, P. and Suomi, V.: Passive Broadband and Spectral Radiometric Measurements Available on NSF / NCAR Research Aircraft, NCAR RAF Technical Bulletin No. 25, 2003.

Kulkarni, P. and Wang, J.: New fast integrated mobility spectrometer for real–time measurement of aerosol size distribution–I: Concept and theory, J. Aerosol Sci., 37, 1303–1325, 2006a.

Kulkarni, P. and Wang, J.: New fast integrated mobility spectrometer for real–time measurement of aerosol size distribution: II. Design, calibration, and performance characterization, J. Aerosol Sci., 37, 1326–1339, 2006b.

Kumala, W., Haman, K. E., Kopec, M., and Malinowski, S.: Ultrafast Thermometer UFTM: High Resolution Temperature Measurements during Physics of Stratocumulus Top (POST)., J. Atmos. Oceanic Technol., in preparation, 2010.

Kunkel, B., Blechinger, F., Viehmann, D., van der Piepen, H., and Doerffer, R.: ROSIS imaging spectrometer and its potential for ocean parameter measurements (airborne and space-borne), Int. J. Remote Sens., 12, 753, 1991.

Kuwata, M. and Kondo, Y.: Measurements of particle masses of inorganic salt particles for calibration of cloud condensation nuclei counters, Atmos. Chem. Phys., 9, 5921–5932, 2009.

Kyle, T.: The measurement of water content by an evaporator, J. Appl. Meteor., 14, 327–332, 1975.

Kylling, A., Webb, A., Kift, R., Gobbi, G., Ammannato, L., Barnaba, F., Bais, A., Kazadzis, S., Wendisch, M., Jäkel, E., Schmidt, S., Kniffka, A., Thiel, S., Junkermann, W., Blumthaler, M., Silbernagl, R., Schallhart, B., Schmitt, R., Kjeldstad, B., Thorseth, T., Scheirer, R., and Mayer, B.: Spectral actinic flux in the lower troposphere: measurement and 1–D simulations for cloudless, broken cloud and overcast situations, Atm. Chem. Phys., 5, 1975–1997, 2005.

Lala, G. G. and Juisto, J. E.: An automatic light scattering CCN counter, J. Appl. Meteorol., 16, 413–418, 1977.

Lämmerzahl, P., Röckmann, T., Brenninkmeijer, C. A. M., Krankowsky, D., and Mauersberger, K.: Oxygen isotope composition of stratospheric carbon dioxide, Atmos. Chem. Phys., 29, 1582, 2002.

Lance, S., Medina, J., Smith, J. N., and Nenes, A.: Mapping the operation of the DMT Continuous Flow CCN counter, Aerosol Sci. Technol., 40, 242–254, 2006.

Landgrebe, D.: Signal Theory Methods in Multispectral Remote Sensing, John Wiley and Sons, New York, 508 pp, 2003.

Lang–Yona, M., Rudich, Y., Segre, E., Dinar, E., and Abo–Riziq, A.: Complex Refractive Indices of Aerosols Retrieved by Continuous Wave–Cavity Ring Down Aerosol Spectrometer, Anal. Chem., 81, 1762–1769, 2009.

Langer, G.: Evaluation of NCAR ice nucleus counter, Part I: Basic operation, J. Appl. Meteorol., 12, 1000–1011, 1973.

Langer, G. and Rogers, J.: An experimental study of the detection of ice nuclei on membrane filters and other substrata, J. Appl. Meteorol., 14, 560–570, 1975.

Langley, S.: The "Solar Constant" and related problems, Astrophysical Journal, 17, 89–99, 1903.

Langridge, J. L., Laurila, T., Watt, R., Jones, R., Kaminski, C., and Hult, J.: Cavity enhanced absorption spectroscopy of multiple trace gas species using a supercontinuum radiation source, Opt. Express, 16, 10 178–10 188, 2008a.

Langridge, J. M., Ball, S., Shillings, A., and Jones, R.: A broadband absorption spectrometer using light emitting diodes for ultra–sensitive in situ trace gas detection, Rev. Sci. Instrum., 79, 2008b.

Lappe, U. O. and Davidson, B.: On the range of validity of Taylor's Hypothesis and the Kolmogoroff Spectral Law, J. Atmos. Sci., 20, 569–576, 1963.

Lary, D. J.: Gas phase atmospheric bromine photochemistry, J. Geophys. Res. D: Atmos., 101, 1505–1516, 1996.

Laube, J. C., Engel, A., Bonisch, H., Mobius, T., Sturges, W. T., Brass, M., and Röckmann, T.: Fractional release factors of long–lived halogenated organic compounds in the tropical stratosphere, Atmos. Chem. Phys., 10, 1093–1103, 2010a.

Laube, J. C., Martinerie, P., Witrant, E., Blunier, T., Schwander, J., Brenninkmeijer, C. A. M., Schuck, T. J., Bolder, M., Röckmann, T., van der Veen, C., Bonisch, H., Engel, A., Mills, G. P., Newland, M. J., Oram, D. E., Reeves, C. E., and Sturges, W. T.: Accelerating growth of HFC–227ea (1,1,1,2,3,3,3–heptafluoropropane) in the atmosphere, Atmos. Chem. Phys., 10, 5903–5910, 2010b.

Laucks, M. L. and Twohy, C.: Size–dependent collection efficiency of an airborne counterflow virtual impactor, Aerosol Sci. Technol., 28, 40–61, 1998.

Lawson, C. L. and Hanson, R. J.: Solving Least Square Problems, Prentice-Hall, 1974.

Lawson, R. and Cormack, R.: Theoretical design and preliminary tests of two new particle spectrometers for cloud microphysics research, Atmos. Res., 35, 315–348, 1995.

Lawson, R., O'Connor, D., Zmarzly, P., Weaver, K., Baker, B., Mo, Q., and Jonsson, H.: The 2D–S (Stereo) Probe: Design and Preliminary Tests of a New Airborne, High Speed, High–Resolution Particle Imaging Probe, J. Atmos. Oceanic Technol., 23, 1462–1477, 2006.

Lawson, R. P. and Cooper, W. A.: Performance of some airborne thermometer in clouds, J. Atmos. Oceanic Technol., 7, 480–494, 1990.

Lawson, R. P. and Rodi, A. R.: A new airborne thermometer for atmospheric and cloud physics research. Part I: Design and preliminary flight tests, J. Atmos. Oceanic Technol., 9, 556–574, 1992.

Lazrus, A., Fong, K., and Lind, J.: Automated Fluorometric Determination of Formaldehyde in Air, Anal. Chem., 1088, 1074–1078, 1988.

Lebel, T., Parker, D., Flamant, C., Bourles, B., Marticorena, M., Mougin, E., Peugeot, C., Diedhiou, A., Haywoodand, J., Ngaminiand, J., Polcher, J., Redelsperger, J.-L., and Thorncroft, C.: The AMMA field campaigns: Multiscale and multidisciplinary observations in the West African region, Q. J. R. Meteorolog. Soc., 136, 8–33, 2010.

Lee, M., Noone, B., O'Sullivan, D., and Heikes, B.: Method for the collection and HPLC analysis of hydrogen peroxide and C1–C2 hydroperoxides in the atmosphere, J. Atmos. Oceanic Technol., 12, 1060–1070, 1995.

Lee, M., Heikes, B., Jacod, D., Sachse, G., and Anderson, B.: Hydrogen peroxide, organic hydroperoxide, and formaldehyde as primary pollutants from biomass burning, J. Geophys. Res., 102, 1301–1309, 1997.

Lee, M., Heikes, B., and O'Sullivan, D.: Hydrogen peroxide and organic hydroperoxide in the troposphere: a review, Atmos. Environm., 34, 3475–3494, 2000.

Lee, Y., Zhou, X., Leaitch, W., and Banic, C.: An aircraft measurement technique for formaldehyde and soluble carbonyl compounds, J. Geophys. Res., 101, 75–80, 1996.

Lefer, B., Shetter, R., Hall, S., Crawford, J., and Olson, J.: Impact of clouds and aerosols on photolysis frequencies and photochemistry during TRACE–P, PartI: Analysis using radiative transfer and photochemical box models, J. Geophys. Res., 108, doi:10.1029/2002JD003171, 2003.

Leibrock, E. and Huey, L. G.: Ion chemistry for the detection of isoprene and other volatile organic compounds in ambient air, Geophys. Res. Lett., 27, 1719–1722, 2000.

Lelieveld, J., Butler, T., Crowley, J., Dillon, T., Fischer, H., Ganzeveld, L., Harder, H., Lawrence, M., Martinez, M., Taraborrelli, D., and Williams, J.: Atmospheric oxidation capacity sustained by a tropical forest, Nature, 452, 737–740, 2008.

Lemaitre, P., Porcheron, E., and Nuboer, A.: Development of Rainbow refractometry and out–of–focus imaging to characterize heat and mass transfers in two–phase flow and aerosol collection processes by droplets, in 15th International Conference on Nuclear Engineering, Nagoya, 2007.

Lemke, H. and Quante, M.: Backscatter characteristics of nonspherical ice crystals: Assessing the potential of polarimetric radar measurements, J. Geophys. Res., 104, 729–751, 1999.

Lemonis, G., Schmücker, M., and Struck, H.: A Fast Response Probe System for In-Flight Measurements of Atmospheric Turbulence, Aerospace Sci. Tech., 6, 233–243, 2002.

Lenschow, D.: Measurement of Air Velocity and Temperature using the NCAR Buffalo Aircraft Measurement System, Tech. Note NCAR/EDD–74, National Center for Atmos. Res., Boulder, CO, 1972.

Lenschow, D.: Estimating Updraft Velocity from an Airplane Response, Mon. Wea. Rev., 104, 618–627, 1976.

Lenschow, D.: Probing the atmospheric boundary layer, American Meteorological Society, Boston, MA, 1986.

Lenschow, D., Savic–Jovcic, V., and Stevens, B.: Divergence and vorticity from aircraft air motion measurements, J. Atmos. Oceanic Technol., 24, doi: 10.1175/2007JTECHA940.1, 2062–2072, 2007.

Lenschow, D. H. and Pennell, W. T.: On the measurementof in–cloud and wet–bulb temperature from aircraft, Mon. Wea. Rev., 102, 447–454, 1974.

Lenschow, D. H. and Spyers–Duran, P.: Measurement Techniques: Air Motion Sensing, National Center for Atmospheric Research, Bulletin No. 23, available at: http://raf.atd.ucar.edu/Bulletins/bulletin23.html, 1989.

Lenschow, D. H. and Stankov, B. B.: Length scales in the convective boundary layer, J. Atmos. Sci., 43, 1198–1209, 1986.

Lenschow, D. H., Friehe, C. A., and Larue, J. C.: The development of an airborne hot–wire anemometer system, in Symposium on Meteorological Observations and Instrumentation, 4^{th}, Denver, Colo., April 10–14, 1978, Preprints. (A79–21901 07–35) Boston, Mass., American Meteorological Society, pp. 463–466, 1978.

Lenschow, D. H., Mann, J., and Kristensen, L.: How Long Is Long Enough When Measuring Fluxes and Other Turbulence Statistics, J. Atmos. Oceanic Technol., 11, 661–673, 1994.

Leon, D. and Vali, G.: Retrieval of three–dimensional particle velocity from airborne Doppler radar data, J. Atmos. Oceanic Technol., 15, 860–870, 1998.

Leon, D., Vali, G., and Lothon, M.: Dual–Doppler analysis in a single plane from an airborne platform, J. Atmos. Oceanic Technol., 23, 3–22, 2006.

Leon, D. C., Wang, Z., and Liu, D.: Climatology of drizzle in marine boundary layer clouds based on 1 year of data from CloudSat and Cloud–Aerosol Lidar and Infrared Pathfinder Satellite Observations (CALIPSO), J. Geophys. Res., 113, 2008.

Lewis, A., Evans, M., Methven, J., Watson, N., Lee, J., Hopkins, J., Purvis, R., Arnold, S., McQuaid, J., Whalley, L., Pilling, M., Heard, D., Monks, P., Parker, A., Reeves, C., Oram, D., Mills, G., Bandy, B., and Coe, H.: Chemical composition observed over the mid–Atlantic and the detection of pollution signatures far from source regions, J. Geophys. Res., 112, doi:10.1029/2006JD007584, 2007.

Lewis, J. M.: The Lettau–Schwerdtfeger balloon experiment: measurement of turbulence via Austausch Theory, Bull. Amer. Meteorol. Soc., 78, 2619–2635, 1997.

Lewtas, J., Pang, Y., Booth, D., Reimer, S., Eatough, D. J., and Gundel, L. A.: Comparison of sampling methods for semi–volatile organic carbon associated with PM2.5, Aerosol Sci. Technol., 34, 9–22, 2001.

Lhermitte, R.: Attenuation and Scattering of Millimeter Wavelength Radiation by Clouds and Precipitation, J. Atmos. Oceanic Technol., 7, 464–479, 1990.

Lhermitte, R.: Centimeter and milllimeter wavelength radars in meteorology, Lhermitte Publications, Miami, FL, USA, 550 pp., 2002.

Lhermitte, R. M.: Probing of Atmospheric Motion by Airborne Pulse–Doppler Radar Techniques, J. Appl. Meteorol., 10, 234–246, 1971.

Li, L., Sekelsky, S. M., Reising, S. C., Swift, C. T., Durden, S. L., Sadowy, G. A., Dinardo, S., Li, F. K., Huffman, A., Stephens, G., Babb, D. M., and Rosenberger, H. W.: Retrieval of Atmospheric Attenuation Using Combined Ground–Based and Airborne 95 GHz Cloud Radar Measurements, J. Atmos. Oceanic Technol., 18, 1345–1353, 2001.

Li, L., Heymsfield, G. M., Tian, L., and Racette, P. E.: Measurements of Ocean Surface Backscattering Using an Airborne 94 GHz Cloud Radar–Implication for Calibration of Airborne and Spaceborne W–Band Radars, J. Atmos. Oceanic Technol., 22, 1033–1045, 2005.

Li, Z., Lemmerz, C., Paffrath, U., Reitebuch, O., and Witschas, B.: Airborne Doppler lidar investigation of sea surface reflectance at a 355–nm ultraviolet wavelength, J. Atmos. Oceanic Techn., 27, 693–704, 2010.

Liebe, H. J., Manabe, T., and Hufford, G. A.: Millimeter–wave attenuation and delay rates due fog / cloud conditions, IEEE Trans. Antenn. Prop., 37, 1617–1623, 1989.

Lightfoot, P., Cox, R., Crowley, J., Destriau, M., Hayman, G., Jenkin, M., Moortgat, G., and Zabel, F.: Organic peroxy radicals: Kinetics, spectroscopy and tropospheric chemistry, Atmos. Environm., 26A, 1805, 1992.

Lilie, L., Emery, E., Strapp, J., and Emery, J.: A Multiwire Hot–Wire Device for Measurement of Icing Severity, Total Water Content, Liquid Water Content, and Droplet Diameter, in 43rd AIAA Aerospace Sciences Meeting, Reno, Nevada, AIAA–2005–0860, 2004.

Lindinger, W., Hansel, A., and Jordan, A.: On–line monitoring of volatile organic compounds at pptv levels by means of proton–transfer–reaction mass spectrometry (PTR–MS)–Medical applications, food control and environmental research, Int. J. Mass Spectrom., 173, 191–241, 1998.

Lipton, A., Moncet, J.-L., and Uymin, G.: Approximations of the Planck function for models and measurements into the submillimeter range, IEEE Geosc. Rem. Sens. Lett., 6, 433–437, 2009.

Liu, C.-L. and Illingworth, A.: Toward more accurate retrievals of ice water content from radar measurements of clouds, J. Appl. Meteorol., 39, 1130–1146, 2000.

Liu, G. S.: Approximation of single scattering properties of ice and snow particles for high microwave frequencies, J. Atmos. Sci., 61, 2441–2456, 2004.

Liu, H. W. and Chandrasekar, V.: Classification of hydrometeors based on polarimetric radar measnurements: Development of fuzzy–logic and neurologic systems and in–situ verification, J. Atmos. Oceanic Technol., 7, 140–164, 2000.

Liu, P. S. K., Leaitch, W. R., Wasey, J. W., and Wasey, M. A.: The response of the Particle Measuring Systems airborne ASAP and PCASP to NaCl and latex particles, Aerosol Sci. Technol., 16, 83–95, 1992.

Liu, Y., Morales Cueto, R., Hargrove, J., Medina, D., and Zhang, J.: Measurements of peroxy radicals using chemical amplification–cavity ringdown spectroscopy, Environ. Science Tech., 43, 7791–7796, 2009.

Livingston, J., Schmid, B., Russell, P., Eilers, J., Kolyer, R., Redemann, J., Ramirez, S., Yee, J.-H., Swartz, W., Trepte, C., Thomason, L., Pitts, M., Avery, M., Randall, C., Lumpe, J., Bevilacqua, R., Bittner, M., Erbertseder, T., McPeters, R., Shetter, R., Browell, E., Kerr, J., and Lamb, K.: Retrieval of ozone column content from airborne Sun photometer measurements during SOLVE II: Comparison with coincident satellite and aircraft measurements Atmospheric Chemistry and Physics Special Issue on the SOLVE II / VINTERSOL campaign, Atmos. Chem. Phys., 5, 2035–2054, 2005.

Lobl, E., Aonashib, K., Griffith, B., Kummerow, C., Liu, G., Murakami, M., and Wilheit, T.: Wakasa Bay: An AMSR precipitation validation campaign, Bull. Amer. Meteor. Soc., 88, 551–558, 2007.

Lohmann, U. and Feichter, J.: Global indirect aerosol effects: a review, Atmos. Chem. Phys., 5, 715–37, 2005.

Long, C., Bucholtz, A., Jonsson, H., Schmid, B., Vogelmann, A., and Wood, J.: A method of correcting for tilt from horizontal in downwelling shortwave irradiance measurements on moving platforms, The Open Atmospheric Science Journal, 4, 78–87, 2010.

Low, R.: A generalized equation for the solution effect in droplet growth, J. Atmos. Sci., 26, 608–611, 1969.

Lu, J., Fugal, J., Nordsiek, H., Saw, E., Shaw, R., and Yang, W.: Lagrangian particle tracking in three dimensions via single–camera in–line digital holography, New J. Phys., 10, 125 015, doi: 10.1088 / 1367–2630 / 10 / 12 / 125013, 2008.

Luftfahrtnorm: LN 9300, Blatt 1, Flugmechanik, Normenstelle Luftfahrt, Leinfelden, Germany, 42 pp., 1970.

Lumley, L. and Panofsky, H.: The Structure of Atmospheric Turbulence, John Wiley & Sons, New York, 239 pp., 1964.

Ma, Y., Weber, R. J., Maxwell–Meier, K., Orsini, D. A., Lee, Y. N., Huebert, B. J., Howell, S. G., Bertram, T., Talbot, R. W., Dibb, J. E., and Scheuer, E.: Intercomparisons of airborne measurements of aerosol ionic chemical composition during TRACE–P and ACE–Asia, J. Geophys. Res., 109, 2004.

MacCready, P.: Standardization of gustiness values from aircraft, J. Appl. Meteorol., 3, 439–449, 1964.

MacDonald, J., Ustin, S., and Schaepman, M.: The contributions of Dr. Alexander F.H. Goetz to imaging spectrometry, Remote Sens. Environ., 113, S2–S4, 2009.

Mace, G. G., Deng, M., Soden, B., and Zipser, E.: Association of Tropical Cirrus in the 10–15 km Layer with Deep Convective Sources: An Observational Study Combining Millimeter Radar Data and Satellite–Derived Trajectories, J. Atmos. Sci., 63, 480–503, 2006.

Mace, G. G., Zhang, Q., Vaughan, M., Marchand, R., Stephens, G., Trepte, C., and Winker, D.: A description of hydrometeor layer occurrencestatistics derived from the first year of merged Cloudsat and CALIPSO data, J. Geophys. Res., 114, 2009.

Macke, A.: Scattering of light by polyhedral ice crystals, Appl. Opt., 32, 2780–2788, 1993.

Macke, A., Mueller, J., and Raschke, E.: Single scattering properties of atmospheric ice crystals, J. Atmos. Sci., 53, 2812–2825, 1996.

MacPherson, J. and Baumgardner, D.: Airflow about King Air wingtip-mounted cloud particle measurement probes, J. Atmos. Ocean. Tech., 5, 259–273, 1988.

Magnusson, L. E., Koropchak, J. A., Anisimov, M. P., Poznjakovskiy, V. M., and de la Mora, J. F.: Correlations for vapor nucleating critical embryo parameters, Journal of Physical and Chemical Reference Data, 32, 1387–1410, 2003.

Mahrt, L.: Surface heterogeneity and vertical structure of the boundary layer, Boundary Layer Meteorol., 96, 33–62, 2000.

Mahrt, L., Vickers, D., and Sun, J.: Spatial Variations of Surface Moisture Flux from Aircraft Data, Adv. Water Res., 24, 1133–1141, 2001.

Malkus, J. S.: Some results of a trade–cumulus cloud investigation, J. Atmos. Sci., 11, 220–237, 1954.

Malley, D., Martin, P., and Ben–Dor, E.: Near Infrared Spectroscopy in Agriculture, chap. 26: Application in Analysis of Soils, to be completed, edited by R. Craig R. Windham and J. Workman, 2004.

Mann, J. and Lenschow, D. H.: Errors in Airborne Flux Measurements, J. Geophys. Res., D 99, 14 519–14 526, 1994.

Mao, J., Ren, X., Brune, W. H., Olson, J. R., Crawford, J. H., Fried, A., Huey, L. G., Cohen, R. C., Heikes, B., Singh, H. B., Blake, D. R., Sachse, G. W., Diskin, G. S., Hall, S. R., and Shetter, R. E.: Airborne measurement of OH reactivity during INTEX–B, Atmos. Chem. Phys., 9, 163–173, 2009.

Mapes, B. and Houze Jr., R.: Cloud clusters and superclusters over the oceanic warm pool, Monthly Weather Review, 121, 1398–1415, 1993.

Marcy, T. P., Gao, R. S., Northway, M. J., Popp, P. J., Stark, H., and Fahey, D. W.: Using chemical ionization mass spectrometry for detection of HNO_3, HOl, and $CIONO_2$ in the atmosphere, Int. J. Mass Spectrom., 243, 63–70, 2005.

Maring, H., Savoie, D., Izaguirre, M., and Custals, L.: Vertical distribution of dust and sea–salt aerosols over Puerto Rico during PRIDE measured from a light aircraft, J. Geophys. Res., 108, 8587, doe:10.1029 / 2002JD002 544, 2003.

Markowski, G. R.: Improving Twomey's algorithm for inversion of aerosol measurement data, Aerosol Sci. Technol., 7, 127–141, 1987.

Marks, F. and Houze, R.: Inner core structure of Hurricane Alicia from airborne Doppler radar observations, J. Atmos. Sci., 44, 1296–1317, 1987.

Marticorena, B., Chatenet, B., Traoré, J. R. S., Diallo, M. C. A., Koné, I., Maman, A., Diaye, T., and Zakou, A.: Temporal variability of mineral dust concentrations over West Africa: Analyses of a pluriannual monitoring from the AMMA Sahelian Dust Transect, Atmos. Chem. Phys., 10, 8899–8915, 2010.

Martinez, M., Harder, H., Kubistin, D., Rudolf, M., Bozem, H., Eerdekens, G., Fischer, H., Gurk, C., Klüpfel, T., Königstedt, R., Parchatka, U., Schiller, C., Stickler, J., Williams, J., and Lelieveld, J.: Hydroxyl radicals in the tropical troposphere over the Suriname rainforest: airborne measurements, Atmos. Chem. Phys. Discuss., 8, 15 491–15 536, 2008.

Martinez, M., Andujar, J., and Enrique, J.: A new and inexpensive pyranometer for the visible spectral range, Sensors, pp. 4615–4634, doi:10.3390 / s90604 615, 2010a.

Martinez, M., Harder, H., Kubistin, D., Rudolf, M., Bozem, H., Eerdekens, G., Fischer, H., Klupfel, T., Gurk, C., Konigstedt, R., Parchatka, U., Schiller, C. L., Stickler, A., Williams, J., and Lelieveld, J.: Hydroxyl radicals in the tropical troposphere over the Suriname rainforest: airborne measurements, Atmos. Chem. Phys., 10, 3759–3773, 2010b.

Maser, R., Franke, H., Preiss, M., and Jaeschke, W.: Methods provided and applied on a research aircraft for the study of cloud physics and chemistry, Beitr. Phys. Atmosph., 67, 321–334, 1994.

Massoli, P., Kebabian, P. L., Onasch, T. B., Hills, F. B., and Freedman, A.: Aerosol Light Extinction Measurements by Cavity Attenuated Phase Shift (CAPS) Spectroscopy: Laboratory Validation and Field Deployment of a Compact Aerosol Particle Extinction Monitor, Aerosol Sci. Technol., 44, 428–435, 2010.

Mastenbrook, H.: Water vapor distribution in the stratosphere and high troposphere, J. Atmos. Sci., 25, 299–311, 1968.

Matejka, T. and Lewis, S. A.: Improving research aircraft navigation by incorporating INS and GPS information in a variational solution, J. Atmos. Oceanic Technol., 14, 495–511, 1997.

Matrosov, S. Y.: Prospects for the Measurement of Ice Cloud Particle Shape and Orientation with Elliptically Polarized Radar Signals, Radio Sci., 26, 847–856, 1991.

Matrosov, S. Y.: Modeling backscatter properties of snowfall at millimeter wavelengths, J. Atmos. Sci., 64, 1727–1736, 2007.

Matrosov, S. Y., Korolev, A. V., and Heymsfield, A. J.: Profiling Cloud Ice Mass and Particle Characteristic Size From Doppler Radar Measurements, J. Atmos. Oceanic Technol., 19, 1003–1018, 2002.

Matrosov, S. Y., Shupe, M. D., and Djalalova, I. V.: Snowfall Retrievals Using Millimeter–Wavelength Cloud Radars, J. Appl. Meteorol. Climatol., 47, 769–777, 2008.

Matsumoto, J. and Kajii, Y.: Improved analyzer for nitrogen dioxide by laser induced fluorescence technique, Atmos. Environ., 37, 4847–4851, 2003.

Matsumoto, T., Russell, P., Mina, C., van Ark, W., and Banta, V.: Airborne tracking sunphotometer, J. Atmos. Oceanic Tech., 4, 336–339, 1987.

Matthew, B. M., Middlebrook, A. M., and Onasch, T. B.: Collection efficiencies in an Aerodyne Aerosol Mass Spectrometer as a function of particle phase for laboratory generated aerosols, Aerosol Sci. Technol., 42, 884–898, 2008.

Mätzler, C.: On the determination of surface emissivity from satellite observations, IEEE Geosci. Remote Sens. Lett., 2, 160–163, 2005.

Mätzler, C.: Dependence of Microwave Brightness Temperature on Bistatic Scattering: Model Functions and Application to AMSU–A, IEEE Transactions on Geoscience and Remote Sensing, 45, 2130–2138, 2007.

Mauldin, R., Tanner, D., and Eisele, F.: A new chemical ionization mass spectrometric technique for the fast measurements of gas–phase nitric acid in the atmosphere, J. Geophys. Res., 103, 3361–3367, 1998.

Mauldin, R., Eisele, F., Cantrell, C., Kosciuch, E., Ridley, B., Lefer, B., Tanner, D., Nowak, J., Chen, G., Wang, L., and Davis, D.: Measurements of OH aboard the NASA P–3 during PEM–Tropics B, J. Geophys. Res., 106, 32 657–32 666, 2001.

Mauldin, R., Kosciucha, E., Henry, B., Eiselea, F., Shetter, R., Lefer, B., Chen, G., Davis, D., Huey, G., and Tanner, D.: Measurements of OH, HO_2+RO_2, H_2SO_4, and MSA at the South Pole during ISCAT 2000, Atmos. Environm., 38, 5423–5437, 2004.

May, R. D.: Open–path, near–infrared tunable diode laser spectrometer for atmospheric measurements of H_2O, J. Geophys. Res., 103, 19 161–19 172, 1998.

Mayer, J.-C., Korbinian, H., Rummel, U., Meixner, F. X., and Foken, T.: Moving measurement platforms–specific challenges and corrections, Meteorologische Zeitschrift, 18, 477–488, 2009.

Mayol–Bracero, O. L., Guyon, P., Graham, B., Roberts, G., Andreae, M. O., Decesari, S., Facchini, M. C., Fuzzi, S., and Artaxo, P.: Water–soluble organic compounds in biomass burning aerosols over Amazonia, 2, Apportionment of the chemical composition and importance of the polyacidic fraction, J. Geophys. Res., 107, 8091, 2002.

Mazin, I., Korolev, A., Heymsfield, A., Isaac, G., and Cober, S.: Thermodynamics of icing cylinder for measurements of liquid water content in super cooled clouds, J. Atmos. Oceanic Technol., 18, 543–558, 2001.

McBratney, A. M. B. and Rossel, R. V.: Spectral soil analysis and inference system: A powerful combination for solving soil data crisis, Geoderma, pp. 272–278, 2006.

McCarthy, J.: A Method for Correcting Airborne Temperature Data for Sensor Response Time, J. Appl. Meteorol., 12, 211–214, 1973.

McElroy, M. B., Salawitch, R., Wofsy, S., and Logan, J.: Reductions Of Antarctic Ozone Due To Synergistic Interactions Of Chlorine And Bromine, Nature, 32, 759–762, 1986.

McFarquhar, G. M., Um, J., Freer, M., Baumgardner, D., Kok, G., and Mace, G.: The importance of small ice crystals to cirrus properties: Observations from the Tropical Warm Pool International cloud Experiment (TWP–ICE), Geophys. Res. Lett., 57, doi:10.1029 / 2007GL029 865, 2007.

McGill, M. J., Hlavka, D. L., Hart, W. D., Spinhirne, J. D., Scott, V. S., and Schmid, B.: The Cloud Physics Lidar: Instrument description and initial measurement results, Appl. Opt., 41, 3725–3734, 2002.

McGill, M. J., Li, L., Hart, W. D., Hlavka, G. H. D., Vaughan, M., and Winker, D.: Combined lidar–radar remote sensing: Initial results from CRYSTAL–FACE, J. Geophys. Res. Atmos., 109, 2004.

McGrath, A. and Hewison, T.: Measuring the accuracy of MARSS–An airborne microwave radiometer, J. Atmos. Oceanic Technol., 18, 2003–2012, 2001.

McKenna, D., Konopka, P., Grooss, J., Gunther, G., Muller, R., Spang, R., Offermann, D., and Orsolini, Y.: A new Chemical Lagrangian Model of the Stratosphere (CLaMS)–1. Formulation of advection and mixing, J. Geophys. Res. D: Atmos., 107, 2002a.

McKenna, D. S., Grooss, J., Gunther, G., Konopka, P., Muller, R., Carver, G., and Sasano, Y.: A new Chemical Lagrangian Model of the Stratosphere (CLaMS)–2. Formulation of chemistry scheme and initialization, J. Geophys. Res. D: Atmos., 107, 2002b.

McMurry, P. H.: The history of condensation nucleus counters, Aerosol Sci. Tech., 33, 297–322, 2000.

Measures, R. M.: Laser Remote Sensing, Krieger, Malabar, FA, 1984.

Mees, J., Crewell, S., Nett, H., de Lange, G., van de Stadt, H., Kuipers, J., and Panhuyzen, R. A.: ASUR–An airborne SIS–receiver for atmospheric measurements at 625 to 720 GHz, IEEE Transactions on Microwave Theory and Technique, 43, 2453–2458, 1995.

Merceret, F. and Schricker, T.: A new hot–wire liquid water meter, J. Appl. Meteor., 14, 319–326, 1975.

Merceret, F. J.: Measuring atmospheric turbulence with airborne hot–film anemometers, J. Appl. Meteor., 15, 482–490, 1976a.

Merceret, F. J.: Airborne hot–film measurements of the small–scale structure of atmospheric turbulence during GATE, J. Atmos. Sci., pp. 1739–1746, 1976b.

Mertes, S., Schroder, F., and Wiedensohler, A.: The Particle–Detection Efficiency Curve of the Tsi–3010 Cpc as a Function of the Temperature Difference between Saturator and Condenser, Aerosol Sci. Tech., 23, 257–261, 1995.

Mertes, S., Verheggen, B., Walter, S., Connolly, P., Ebert, M., Schneider, J., Bower, K., Cozic, J., Weinbruch, S., Baltensperger, U., and Weingartner, E.: Counterflow virtual impactor based collection of small ice particles in mixed–phase clouds for the physico–chemical characterization of tropospheric ice nuclei: sampler description and first case study, Sci. Technol., 41, 848–864, 2007.

Möhler, O., DeMott, P., Stetzer, O., and the ICIS-2007 team, eds.: The Fourth International Ice Nucleation Workshop ICIS-2007: Methods and Instruments, Proceedings, 15th International Conference on Clouds and Precipitation, Cancun, Mexico, 2008.

Michalsky, J., Harrison, L., and Berkheiser, W.: Cosine response characteristics of some radiometric and photometric sensors, Solar Energy, 54, 397–402, 1995.

Mie, G.: Beiträge zur Optik trüber Medien, speziell kolloidaler Metallösungen, Annalen der Physik, 25, 377–445, 1908.

Mielke, L. H., Erickson, D. E., McLuckey, S. A., Muller, M., Wisthaler, A., Hansel, A., and Shepson, P. B.: Development of a Proton–Transfer Reaction–Linear Ion Trap Mass Spectrometer for Quantitative Determination of Volatile Organic Compounds, Anal. Chem., 80, 8171–8177, 2008.

Mihele, C. and Hastie, D.: The sensitivity of the radical amplifier to ambient water vapour, Geophys. Res. Lett., 25, 1911, 1998.

Mihele, C. and Hastie, D.: Optimized operation and calibration procedures for radical amplifier–type detectors, J. Atmos. Oceanic Technol., 17, 788, 2000.

Mihele, C., Mozurkewich, M., and Hastie, D.: Radical loss in a chain reaction of CO and NO in the presence of water: Implications for the radical amplifier and atmospheric chemistry, Int. J. Chem. Kinet., 31, 145, 1999.

Miles, R. E. H., Rudic, S., Orr–Ewing, A. J., and Reid, J. P.: Measurements of the wavelength dependent extinction of aerosols by cavity ring down spectroscopy, Phys. Chem. Chem. Phys., 12, 3914–3920, 2010.

Miller, T., Ballenthin, J., Meads, R., Hunton, D., Thorn, W., Viggiano, A., Kondo, Y., Koike, M., and Zhao, Y.: Chemical ionization mass spectrometric technique for the measurements of HNO_3 in air traffic corridors in the upper troposphere during the SONEX campaign, J. Geophys. Res., 105, 3701–3707, 2000.

Millet, D. B., Jacob, D. J., Custer, T. G., de Gouw, J. A., Goldstein, A. H., Karl, T., Singh, H. B., Sive, B. C., Talbot, R. W., Warneke, C., and Williams, J.: New constraints on terrestrial and oceanic sources of atmospheric methanol, Atmos. Chem. Phys., 8, 6887–6905, 2008.

Mirme, S., Mirme, A., Minikin, A., Petzold, A., Horrak, U., Kerminen, V. M., and Kulmala, M.: Atmospheric sub-3 nm particles at high altitudes, Atmos. Chem. Phys., 10, 437–451, 2010.

Mishchenko, M. and Travis, L.: T–matrix computations of light scattering by large spheroidal particles, Opt. Commun., 109, 16–21, 1994.

Miyazaki, K., Parker, A. E., Fittschen, C., Monks, P. S., and Kajii, Y.: A new technique for the selective measurement of atmospheric peroxy radical concentrations of HO_2 and RO_2 using a denuding method, Atmos. Meas. Tech., 3, 1547–1554, 2010.

Moisseev, D. N., Unal, C. M. H., Russchenberg, H. W. J., and Ligthart, L. P.: Improved Polarimetric Calibration for Atmospheric Radars, J. Atmos. Oceanic Technol., 19, 1968–1977, 2002.

Moisseev, D. N., Chandrasekar, V., Unal, C. M. H., and Russchenberg, H. W. J.: Dual–Polarization Spectral Analysis for Retrieval of Effective Raindrop Shapes, J. Atmos. Oceanic Technol., 23, 1682–1695, 2006.

Molina, L. T. and Molina, M.: Production Of Cl_2O_2 From The Self–Reaction Of The ClO Radical, J. Phys. Chem., 91, 433–436, 1987.

Monks, P.: Gas–phase radical chemistry in the troposphere, Chem. Soc. Rev., 34, 376–395, 2005.

Montgomery, R. B.: Vertical Eddy Flux of Heat in the Atmosphere, J. Meteorol., 1948.

Moore, K. G., Clarke, A., Kapustin, V., McNaughton, C., Anderson, B., Winstead, E., Weber, R., Ma, Y., Lee, Y., Talbot, R., Dibb, J., Anderson, T., Doherty, S., Covert, D., and Rogers, D.: A comparison of similar aerosol measurements made on the NASA P3–B, DC–8, and NSF C–130 aircraft during TRACE–P and ACE–Asia, J. Geophys. Res., 109 (D15), D15S15, doi:10.1029/2003JD003543, 2004.

Moore, R. H. and Nenes, A.: A Scanning Flow CCN Analysis–A Method for Fast Measurements of CCN Spectra, Aerosol Sci. Technol., 43, 1192–1207, 2009.

Moore Jr., S., Brown, K. E., Hall, W. M., Barnes, J. C., Edwards, W. C., Petway, L. B., Little, A. D., Luck Jr., W. S., Jones, I. W., Antill Jr., C. W., Browell, E. V., and Ismail, S.: Advances in Atmospheric Remote Sensing with Lidar, chap. Development of the Lidar Atmospheric Sensing Experiment (LASE), an advanced airborne DIAL instrument, pp. 281–288, Springer–Verlag, Berlin, editors: A. Ansmann and R. Neuber and P. Rairoux and U. Wandinger, 1997.

Moosmüller, H., Chakrabarty, R. K., and Arnott, W. P.: Aerosol light absorption and its measurement: A review, J. Quant. Spectrosc. Radiat. Transfer, 110, 844–878, 2009.

Morgan, W. T., Allan, J. D., Bower, K. N., Capes, G., Crosier, J., Williams, P. I., and Coe, H.: Vertical distribution of sub–micron aerosol chemical composition from North–Western Europe and the North–East Atlantic, Atmos. Chem. Phys., 9, 5389–5401, 2009.

Moteki, N., Kondo, Y., Miyazaki, Y., Takegawa, N., Komazaki, Y., Kurata, G., Shirai, T., Blake, D. R., Miyakawa, T., and Koike, M.: Evolution of mixing state of black carbon particles: Aircraft measurements over the western Pacific in March 2004, Geophys. Res. Lett., 34, 2007.

Moteki, N., Kondo, Y., Takegawa, N., and Nakamura, S.: Directional dependence of thermal emission from nonspherical carbon particles, J. Aerosol Sci., 40, 790–801, 2009.

Mounaïm-Rousselle, C. and Pajot, O.: Droplet Sizing by Mie Scattering Interferometry in a Spark Ignition Engine, Part. & Part. Syst. Charact., 16, 160, 1999.

Moyer, E. J., Irion, F. W., Yung, Y. L., and Gunson, M. R.: ATMOS stratospheric deuterated water and implications for troposphere stratosphere transport, Geophys. Res. Lett., 23(17), 2385–2388, 1996.

Mozurkewich, M.: Mechanisms for the Release of Halogens from Sea–salt Particles by Free Radicals Reactions, J. Geophys. Res., 100, 14 199–14 207, 1995.

Müller, D., Wandinger, U., Althausen, D., Mattis, I., and Ansmann, A.: Retrieval of physical particle properties from lidar observations of extinction and backscatter at multiple wavelengths, Appl. Opt., 37, 2260–2263, 1998.

Müller, S., Kämpfer, N., Feist, D., Haefele, A., Milz, M., Sitnikov, N., Schiller, C., Kiemle, C., and Urban, J.: Validation of stratospheric water vapor measurements from the airborne microwave radiometer AMSOS, Atmos. Chem. Phys. Discuss., 8, 1635–1671, 2008.

Munson, M. S. B. and Field, F. H.: Chemical Ionization Mass Spectrometry–I. General Introduction, J. Am. Chem. Soc., 88, 2621–2630, 1966.

Murphy, D. and Koop, T.: Review of the vapor pressures of ice and supercooled water for atmospheric applications, Quart. J. Roy. Meteorol. Soc., 131, 1539–1565, 2005.

Murphy, D., Cziczo, D., Hudson, P., Thomson, D., Wilson, J., Kojima, T., and Buseck, P.: Particle generation and resuspension in aircraft inlets when flying in clouds, Aerosol Sci. Technol., 38, 400–408, 2004.

Murphy, D. M.: The design of single particle mass spectrometers, Mass Spectrom. Rev., 26, 150–165, 2007.

Murphy, D. M. and Schein, M. E.: Wind tunnel tests of a shrouded aircraft inlet, Aerosol Sci. Technol., 28, 33–39, 1998.

Murphy, D. M., Cziczo, D. J., Froyd, K. D., Hudson, P. K., Matthew, B. M., Middlebrook, A. M., Peltier, R. E., Sullivan, A., Thomson, D. S., and Weber, R. J.: Single–particle mass spectrometry of tropospheric aerosol particles, J. Geophys. Res., 111, 2006.

Muschinski, A. and Wode, C.: First In–Situ Evidence for Co–Existing Sub–Meter Temperature and Humidity Sheets in the Lower Free Troposphere, J. Atmos. Sci., 55, 2893–2906, 1998.

National Research Council: Earth science and its applications from space: National imperatives for the next decade and beyond, Tech. rep., NRC, The National Academies Press, 500 Fifth Street, N.W., Washington, DC 20001, 455 pp, 2007.

Nedelec, P., Cammas, J., Thouret, V., Athier, G., Cousin, J., Legrand, C., Abonnel, C., Lecoeur, F., Cayez, G., and Marizy, C.: An Improved Infra–Red Carbon Monoxide Analyser for Routine Measurements aboard Commercial Airbus Aircraft : Technical Validation and First Scientific Results of the MOZAIC III Program, Atmos. Chem. And Phys., 3, 1551–1564, 2003.

Neel, C.: A heated–wire liquid–water–content instrument and results of initial flight tests in icing conditions, Tech. rep., NASA Research Memo., RM A54123, 33 pp., 1955.

Neel, C.: Measurement of cloud liquid–water content with a heated wire, in Proc. 19th Intl. Aerospace Symp., edited by B. Washburn, p. 301, Instrument Society of America, Pittsburgh, PA, 1973.

Nemarich, J., Wellman, R. J., and Lacombe, J.: Backscatter and attenuation by falling snow and rain at 96, 140, and 225 GHz, IEEE Transactions on Geoscience and Remote Sensing, 26, 319–329, 1988.

Nenes, A., Chuang, P., Flagan, R., and Seinfeld, J.: A theoretical analysis of cloud condensation nucleus (CCN) instruments, J. Geophys. Res., 106, 3449–3474, 2001.

Neuman, J., Huey, L., Ryerson, T., and Fahey, D.: Study of inlet materials for sampling atmospheric nitric acid, Environ. Science Tech., 33, 1133–1136, doi: 10.1021 / es980767f, 1999.

Neumann, J., Gao, R., Schein, M., Ciciora, S., Holecek, J., Thompson, T., Winkler, R., McLaughlin, R., Northway, M., Richard, E., and Fahey, D.: A fast response chemical ionization mass spectrometer for in–situ measurements of HNO_3 in the upper troposphere and lower stratosphere, Rev. Sci. Instrum., 71, 3886–3894, 2000.

Nevzorov, A.: Aircraft cloud water content meter, in Comm. a la 8eme conf int. sur la phys. des nuages, vol. II, pp. 701–703, Clermont–Ferrand, France, 1980.

Nevzorov, A. and Shugaev, V.: The use of integral parameters for study of cloud microstructure (in Russian), Trans. Cent. Aerol. Obs., 101, 32–47, 1972.

Nevzorov, A. and Shugaev, V.: Aircraft cloud extinction meter, Trans. of Cent. Aerol. Obs., 106, 3–10, 1974.

Nicholls, S., Leighton, J., and Barker, R.: A New Fast Response Instrument for Measuring Total Water Content from Aircraft, J. Atmos. Oceanic Technol., 7, 706–718, 1990.

Nicodemus, F., Richmond, J., Hsia, J., Ginsberg, I., and Limperis, T.: Geometrical considerations and nomenclature for reflectance, Tech. rep., Institute for Basic Standards, National Bureau of Standards, 1977.

Nieke, J., Schwarzer, H., Neumann, A., and Zimmermann, G.: Imaging Spaceborne and Airborne Sensor Systems in the Beginning of the Next Century, presented at The European Symposium on Aerospace Remote Sensing (IEE), in Conference on Sensors, Systems and Next Generation Satellites III, vol. 3221, SPIE, London, UK, 1997.

Nieke, J., Itten, K., Meuleman, K., Gege, P., Del'Endice, F., Hueni, A., Alberti, E., Ulbrich, G., and Meynart, R.: Supporting facilities of the Airborne Imaging Spectrometer APEX, in Proceedings of IGARSS 2008, pp. V–502–V–505, IEEE, 2008.

Nielson–Gammon, J., Powell, C., Mahoney, M., Angevine, W., Senff, C., White, A., Berkowitz, C., Doran, J., and Knupp, K.: Multi–sensor estimation of mixing heights over coastal city, J. Appl. Meteor. Clim., 47, 27–43, 2008.

Noël, V., Chepfer, H., Ledanois, G., Delaval, A., and Flamant, P.: Classification of particle effective shape ratio in cirrus clouds based on the lidar depolarization ratio, Appl. Opt., 41, 4245–4257, 2002.

Noël, V., Winker, D. M., McGill, M., and Lawson, P.: Classification of particle shapes from lidar depolarization ratio in convective ice clouds compared to in situ observations during CRYSTAL–FACE, J. Geophys. Res., 109, 2004.

Noel, V., Winker, D., Garrett, T., and McGill, M.: Extinction coefficients retrieved in deep tropical ice clouds from lidar observations using a CALIPSO–like algorithm compared to in–situ measurements from the cloud integrating nephelometer during CRYSTAL–FACE, Atmos. Chem. Phys., 7, 1415–1422, 2007.

Noomem, M., Meer, F., and Skidmore, A.: Hyperspectral remote sensing for detecting the effects of three hydrocarbon gases on maize reflectance, in Proceedings: 31th International Symposium of Remote Sensing of Environment, Saint Petersburg, 2005.

Noone, K., Noone, K., Heintzenberg, J., Strom, J., and Ogren, J.: In Situ Observations using the Counterflow Virtual Impactor, J. Atmos. Oceanic Technol., 10, 294–303, 1993.

Noone, K. J., Ogren, J., Heintzenberg, J., Charlson, R., and Covert, D.: Design and Calibration of a Counterflow Virtual Impactor for Sampling of Atmospheric Fog and Cloud Droplets, Aerosol Sci. Tech., 8, 235–244, 1988.

Norment, H.: Calculation of water drop trajectories to and about arbitrary three dimensional lifting and non-lifting bodies in potential airflow, Tech. rep., National Aeronautics and Space Administration, NTIS N87-11694 / 3 / GAR, 1985.

Norment, H.: Three–Dimensional Trajectory Analysis of Two Drop Sizing instruments: PMS* OAP and PMS* FSSP, J. Atmos. Oceanic Technol., 5, 743–756, 1988.

Novelli, P.: CO in the Atmosphere: Measurement Techniques and Related Issues, Chemosphere, 1, 115–126, doi:10.1016 / S1465–9972, 1999.

Nunnermacker, L. J., Weinstein–Lloyd, J. B., Hillery, B., Giebel, B., Kleinman, L. I., Springston, S. R., Daum, P. H., Gaffney, J., Marley, N., and Huey, G.: Aircraft and ground–based measurements of hydroperoxides during the 2006 MILAGRO field campaign, Atmos. Chem. Phys., 8, 7619–7636, 2008.

Ochou, A. D., Nzeukou, A., and Sauvageot, H.: Parametrization of drop size distribution with rain rate, Atmos. Res., 84, 58–66, 2007.

O'Connor, E. J., Hogan, R. J., and Illingworth, A. J.: Retrieving Stratocumulus Drizzle Parameters Using Doppler Radar and Lidar, J. Appl. Meteorol., 44, 14–27, 2005.

O'Donnell, C.: Inertial navigation; analysis and design, McGraw–Hill, New York, 1964.

Oebel, A., Broch, S., Raak, D., Bohn, B., Rohrer, F., Hofzumahaus, A., Holland, F., and Wahner, A.: In–situ measurements of vertical profiles of chemical tracers in the PBL using the airship Zeppelin NT, ISARS meeting, 2010.

Ogren, J., Heintzenberg, J., and Charlson, R.: In-situ sampling of clouds with a droplet to aerosol converter, Geophys. Res. Lett., 12, 121–124, 1985.

Ogren, J. A.: Aerosol Forcing of Climate, chap. A systematic approach to in situ observations of aerosol properties, pp. 215–226, John Wiley, eds.: R. J. Charlson and J. Heintzenberg, 1995.

Ogren, J. A.: Comment on Calibration and Intercomparison of Filter–Based Measurements of Visible Light Absorption by Aerosolso, Aerosol Sci. Technol., 44, 589–591, 2010.

Oguchi, T.: Electromagnetic wave propagation and scattering in rain and other hydrometeors, in Proceedings of the IEEE, vol. 71, pp. 1029–1078, 1983.

Ohtaki, E. and Matsui, T.: Infrared device for simultaneous measurement of fluctuations of atmospheric carbon dioxide and water vapor, Boundary Layer Meteorol., 24, 109–119, 1982.

Okamoto, H., Iwasaki, S., Yasui, M., Horie, H., Kuroiwa, H., and Kumagai, H.: An algorithm for retrieval of cloud microphysics using 95 GHz cloud radar and lidar, J. Geophys. Res. Atmos., 108, 2003.

Okamoto, K., Kubokawa, T., Tamura, A., and Ushio, T.: Long term trend ofocean surface normalized radar cross section observed by TRMM precipitation radar, in Proc. Second Global Precipitation Mission (GPM) Int. Planning Workshop, vol. 9, http://ams.confex.com/ams/pdfpapers/96443.pdf, shinagawa, Japan, 2002.

O'Keefe, A. and Deacon, D.: Cavity ring–down optical spectrometer for absorption measurements using pulsed laser sources, Rev. Sci. Instrum., 59, 2544–2551, 1988.

Olfert, J. S. and Wang, J.: Dynamic Characteristics of a Fast–Response Aerosol Size Spectrometer, Aerosol Sci. Technol., 43, 97–111, 2009.

Olfert, J. S., Kulkarni, P., and Wang, J.: Measuring aerosol size distributions with the fast integrated mobility spectrometer, J. Aerosol Sci., 39, 940–956, 2008.

Oppelt, N. and Mauser, W.: The Airborne Visible / Infrared Imaging Spectrometer AVIRIS: Design, characterization and calibration, Sensors, 7, 1934–1953, 2007.

Orr, B. W. and Kropfli, R. A.: A method for estimating particle fall velocities from vertically pointing Doppler radar, J. Atmos. Oceanic Technol., 16, 29–37, 1999.

Orsini, D. A., Wiedensohler, A., Stratmann, F., and Covert, D. S.: A new volatility tandem differential mobility analyzer to measure the volatile sulfuric acid aerosol fraction, J. Atmos. Oceanic Technol., 16, 760–772, 1999.

Orsini, D. A., Ma, Y. L., Sullivan, A., Sierau, B., Baumann, K., and Weber, R. J.: Refinements to the particle–into–liquid sampler (PILS) for ground and airborne measurements of water soluble aerosol composition, Atmos. Environm., 37, 1243–1259, 2003.

Owens, G.: Wind Tunnel Calibrations of Three Instruments Designed for Measurements of the Liquid–Water Content of Clouds, Technical Note 10, U. Chicago Cloud Physics Laboratory, 1957.

Paffrath, U., Lemmerz, C., Reitebuch, O., Witschas, B., Nikolaus, I., and Freudenthaler, V.: The airborne demonstrator for the direct–detection Doppler wind lidar ALADIN on ADM–Aeolus: II. Simulations and Rayleigh radiometric performance, J. Atmos. Oceanic Techn., 26, 2516–2530, 2009.

Paldus, B. A., Harb, C., Spence, T., Wilke, B., Xie, J., and Harris, J.: Cavity–locked cavity ring–down spectroscopy, J. Appl. Phys., 83, 3991–3997, 1998.

Pan, G. and Meng, H.: Digital holography of particle fields: reconstruction by use of complex amplitude, Appl. Opt., 42, 827–833, 2003.

Parish, T., Matthew, R., Burkhart, D., and Rodi, A.: Determination of the horizontal pressure gradient force using global positioning system on board an instrumented aircraft, J. Atmos. Oceanic Technol., 24, 521–528, 2007.

Parrish, D. and Fehsenfeld, F.: Methods for gas–phase measurements of ozone, ozone precursors and aerosol precursors, Atmos. Environ., 34, 1921–1957, 2000.

Parrish, D., Holloway, J., and Fehsenfeld, F.: Routine, continuous measurement of carbon monoxide with parts per billion precision, Environ. Sci. Technol., 28, 1615, 1994.

Parrish, D. D., Allen, D., Bates, T., Estes, M., Fehsenfeld, F., Feingold, G., Ferrare, R., Hardesty, R., Meagher, J., Nielsen–Gammon, J., Pierce, R., Ryerson, T., Seinfeld, J., and Williams, E.: Overview of the Second Texas Air Quality Study (TexAQS II) and the Gulf of Mexico Atmospheric Composition and Climate Study (GoMACCS), J. Geophys. Res., 114, doi:10.1029/2009JD011842, 2008.

Patent Application, 2009: Probe Tips For Airborne Instruments Used to Measure Cloud Microphysical Parameters, United States Patent Application No. 12/415,314; Canadian Patent Application No. 2660753, 2009.

Pawlowska, H., Brenguier, J.-L., and Salut, G.: Optimal non-linear estimation for cloud particle measurements, J. Atmos. Oceanic Tech., 14, 88–104, 1997.

Payne, F. R. and Lumley, J. L.: One-dimensional spectra derived from an airborne hot-wire anemometer, Q. J. R. Meteorol. Soc., 92, 397 – 401, 1965.

Pazmany, A. L., McIntosh, R. E., Kelly, R. D., and Vali, .: An airborne 95 GHz dual–polarized radar for cloud studies, IEEE Transactions on Geoscience and Remote Sensing, 32, 731–739, 1994.

Pearlman, J., Barry, P., Segal, C., Shepanski, J., Beiso, D., and Carman, S.: Hyperion, a space–based imaging spectrometer, IEEE Transactions in Geosciences and Remote Sensing, 41, 1160–1173, 2003.

Pelon, J., Flamant, C., Chazette, P., Léon, J.-F., Tanré, D., Sicard, M., and Sathees, S. K.: Characterization of aerosol spatial distribution and optical properties over the Indian Ocean from airborne lidar and radiometry during INDOEX’99, J. Geophys. Res., 107, 8029, 2002.

Peltier, R. E., Weber, R. J., and Sullivan, A. P.: Investigating a liquid-based method for online organic carbon detection in atmospheric particles, Aerosol Sci. Technol., 41, 1117–1127, 2007.

Penkett, S., Blake, N., Lightman, P., Marsh, A., and Anwyl, P.: The Seasonal Variation of Non–Methane Hydrocarbons in the Free Troposphere Over the North Atlantic Ocean: Possible Evidence for Extensive Reaction of Hydrocarbons with the Nitrate Radical, J. Geophys. Res., 98, 2865–2885, 1993.

Penner, J. E., Charlson, R. J., Schwartz, S. E., Hales, J. M., Laulainen, N. S., Travis, L., Leifer, R., Novakov, T., Ogren, J., and Radke, L. F.: Quantifying and Minimizing Uncertainty of Climate Forcing by Anthropogenic Aerosols, Bull. Am. Met. Soc., 75, 375–400, 1994.

Perner, D., Arnold, T., Crowley, J., Kluepfel, T., Martinez, M., and Seuwen, R.: The measurement of active chlorine in the atmosphere by chemical amplification, J. Atmos. Chem., 34, 1999.

Petropavlovskikh, I., Froidevaux, L., Shetter, R., Hall, S., Ullmann, L., Bhartia, P., Kroon, M., and Levelt, P.: In–flight validation of Aura MLS ozone with CAFS partial ozone columns, J. Geophys. Res., 113, doi:10.1029/2007JD008690, 2008.

Petters, M. D. and Kreidenweis, S. M.: A single parameter representation of hygroscopic growth and cloud condensation nucleus activity, Atmos. Chem. Phys., 7, 1961–1971, 2007.

Peturson, B.: Rept. Dominion Botanist for the year 1930, chap. Epidemiology of cereal rusts, pp. 44–46, Div. of Botany, Canada Dept. of Agric., 1931.

Petzold, A. and Schönlinner, M.: Multi-angle absorption photometry - A new method for the measurement of aerosol light absorption and atmospheric black carbon, J. Aerosol Sci., 35, 421–441, 2004.

Petzold, A., Fiebig, M., Flentje, H., Keil, A., Leiterer, U., Schröder, F., Stifter, A., Wendisch, M., and Wendling, P.: Vertical variability of aerosol properties observed at a continental site during the Lindenberg Aerosol Characterization Experiment (LACE 98), J. Geophys. Res., 107, 2002.

Petzold, A., Schloesser, H., Sheridan, P. J., Arnott, W. P., Ogren, J. A., and Virkkula, A.: Evaluation of multiangle absorption photometry for measuring aerosol light absorption, Aerosol Sci. Technol., 39, 40–51, 2005a.

Petzold, A., Schloesser, H., Sheridan, P. J., Arnott, W. P., Ogren, J. A., and Virkkula, A.: Particle emissions from aircraft engines - a survey of the European project PartEmis, Meteorol. Z., 14, 465–476, 2005b.

Petzold, A., Weinzierl, B., Huntrieser, H., Stohl, A., Real, E., Cozic, J., Fiebig, M., Hendricks, J., Lauer, A., Law, K., Roiger, A., Schlager, H., and Weingartner, E.: Perturbation of the European free troposphere aerosol by North American forest fire plumes during the ICARTT–ITOP Experiment in summer 2004, Atmos. Chem. Phys., 7, 105–5127, 2007.

Petzold, A., Rasp, K., Weinzierl, B., Esselborn, M., Hamburger, T., Dörnbrack, A., Kandler, K., Schütz, L., Knippertz, P., Fiebig, M., and Virkkula, A.: Saharan dust refractive index and optical properties from aircract-based observations during SAMUM 2006, Tellus, 61B, 118–130, 2009.

Petzold, A., Veira, A., Mund, S., Esselborn, M., and. Weinzierl, C. K., Hamburger, T., and Ehret, G.: Mixing of mineral dust with urban pollution aerosol over Dakar (Senegal)–Impact on dust physico–chemical and radiative properties, Tellus, 63B, in press, 2011.

Pfau, A., Schlienger, J., Kalfas, A. I., and Abhari, R. S.: Virtual Four Sensor Fast Response Aerodynamic Probe (FRAP), in 16th Symposium on Measuring Techniques in Transonic and Supersonic Flow in Cascades and Turbomachines, Cambridge, UK, 2002.

Pfeilsticker, K. and Platt, U.: Airborne Measurements during the Arctic Stratospheric Experiment: Observation of O_3 and NO_2, Geophys. Res. Lett., 21, 1375, 1994.

Philipona, R., Fröhlich, and Betz, C.: Characterisation of pyrgeometers and the accuracy of atmospheric long–wave radiation measurements, Appl. Opt., 34, 1598–1605, 1995.

Pieters, C., Boardman, J., Buratti, B., Chatterjee, A., Clark, R., Glavich, T., Green, R., Head, J., Isaacson, P., Malaret, E., McCord, T., Mustard, J., Petro, N., Runyon, C., Staid, M., Sunshine, J., Taylor, L., Varanasi, S. T. P., and White, M.: The Moon Mineralogy Mapper (M3) on Chandrayaan–1, Current Science, 96, 500–505, 2009a.

Pieters, C., Goswami, J., Clark, R., Annadurai, M., Boardman, J., Buratti, B., Combe, J.-P., Dyar, M., Green, R., Head, J., Hibbitts, C., Hicks, M., Isaacson, P., Klima, R., Kramer, G., Kumar, S., Livo, E., Lundeen, S., Malaret, E., McCord, T., Mustard, J., Nettles, J., Petro, N., Runyon, C., Staid, M., Sunshine, J., Taylor, L., Tompkins, S., and Varanasi, P.: Character and Spatial Distribution of OH/H_2O on the surface of the Moon seen by M3 ON Chandrayaan–1, Science, 326, 568, 2009b.

Pilch, M. and Erdman, C.: Use of breakup time data and velocity history data to predict the maximum size of stable fragments for acceleration-induced breakup of a liquid drop, Int. J. Multiphas. Flow, 13, 741–757, 1987.

Pilewskie, P. and Valero, F.: Optical depths and haze particle sizes during AGASP III, Atmos. Environ., 27A, 2895–2899, 1993.

Pilewskie, P., Pommier, J., Bergstrom, R., Gore, W., Howard, S., Rabbette, M., Schmid, B., Hobbs, P. V., and Tsay, S. C.: Solar spectral radiative forcing during the Southern African Regional Science Initiative, J. Geophys. Res., 108, doi:10.1029/2002JD002411, 2003.

Pilewskie, P., Rottman, G., and Richard, E.: An overview of the disposition of solar radiation in the lower atmosphere: Connections to the SORCE mission and climate change, Sol. Phys., 230, 55–69, 2005.

Pinnick, R. G., Jennings, S. G., and Fernandez, G.: Volatility of aerosols in the arid southwestern United States, J. Atmos. Sci., 44, 562–576, 1987.

Pinnick, R. G., Pendleton, J. D., and Videen, G.: Response Characteristics of the Particle Measuring Systems Active Scattering Aerosol Spectrometer Probes, Aerosol Sci. Technol., 33, 334–352, 2000.

Platnick, S., Li, J., King, M., Gerber, H., and Hobbs, P.: A solar reflectance method for retrieving the optical thickness and droplet size of liquid water clouds over snow and ice surfaces, J. Geophys. Res., 106, 15,185–15,200, doi:10.1029/2000JD900441, 2001.

Platt, C., Young, S. A., Manson, P. J., Patterson, G. R., Marsden, S. C., Austin, R. T., and Churnside, J. H.: The Optical Properties of Equatorial Cirrus from Observations in the ARM Pilot Radiation Observation Experiment, J. Atmos. Sci., 55, 1977–1996, 1998.

Platt, C., Austin, R. T., Young, S. A., and Heymsfield, A. J.: LIRAD observations of tropical cirrus clouds in MCTEX. Part II: Optical properties and base cooling in dissipating storm anvil clouds, J. Atmos. Sci., 59, 3163–3177, 2002.

Platt, U.: Air Monitoring by Spectroscopic Techniques, chap. Differential Optical Absorption Spectroscopy (DOAS), pp. 27–84, John Wiley and Sons, New York, 1994.

Platt, U. and Stutz, J.: Differential Optical Absorption Spectroscopy, Principles and Applications, Series: Physics of Earth and Space Environments, Springer Verlag, ISBN: 3540211934, 2008.

Plaza, A. and Chang, C., eds.: High performance Computing in Remote Sensing, Taylor & Francis, Chapman & Hall CRC publications, Boca Raton, 496 pp., 2007.

Plaza, A., Martinez, P., Perez, R., and Plaza, J.: A quantitative and comparative analysis of endmember extraction algorithms from hyperspectral data, IEEE Transaction on Geoscience and Remote Sensing, 42, 650–663, 2004.

Plaza, A., Benediktsson, A., Boardamn, J., Brazile, J., Bruzzone, L., CapsValls, G., Chanussot, J., Fauvel, M., Gampa, P., Gulatiri, J., Marconcini, M., Tilton, J., and Trianni, G.: Recent advances in techniques for hyperspectral image processing, Remote Sens. Environ., 113, 110–122, 2009.

Poberaj, G., Fix, A., Assion, A., Wirth, M., Kiemle, C., and Ehret, G.: Airborne all–solid–state DIAL for water vapour measurements in the tropopause region: system description and assessment of accuracy, Appl. Phys. B, 75, 165–172, 2002.

Pokharel, B. and Vali, G.: Evaluation of co-located measurements of radar reflectivity and particle sizes in ice clouds, J. Appl. Meteorol. Climatol., 2011.

Porter, J., Clarke, A., Ferry, G., and Pueschel, R.: Aircraft studies of size-dependent aerosol sampling through inlets, J. Geophys. Res., 97, 3815–3824, 1992.

Porter, J., Clarke, A., Reid, J., Shaw, G., Maring, H., Reid, E., and Kress, D.: Handheld Sun photometer measurements from light aircraft, J. Atmos. Oceanic Tech., 24, 1588–1597, 2007.

Poschl, U.: Atmospheric Aerosols: Composition, Transformation, Climate and Health Effects, Angew. Chem. Int. Ed., 44, 7520–7540, 2005.

Prados–Roman, R., Butz, A., Deutschmann, T., Dorf, M., Kritten, L., Minikin, A., Theys, N., Schlager, H., Platt, U., Roozendael, M. V., and Pfeilsticker, K.: BrO profiling in the arctic troposphere during spring 2007, Geophys. Res. Lett., in prep., 2010.

Pratt, K., Mayer, A., Holecek, J. C., Moffet, R. C., Sanchez, R. O., Rebotier, T. P., Furutani, H., Gonin, M., Fuhrer, K., Su, Y. X., Guazzotti, S., and Prather, K. A.: Development and Characterization of an Aircraft Aerosol Time–of–Flight Mass Spectrometer, Anal. Chem., 81, 1792–1800, 2009a.

Pratt, K. A., DeMott, P. J., French, J. R., Wang, Z., Westphal, D. L., Heymsfield, A. J., Twohy, C. H., Prenni, A. J., and Prather, K. A.: In situ detection of biological particles in cloud ice–crystals, Nat. Geosci., 2, 397–400, 2009b.

Prazeller, P., Palmer, P. T., Boscaini, E., Jobson, T., and Alexander, M.: Proton transfer reaction ion trap mass spectrometer, Rapid Commun. Mass Spectrom., 17, 1593–1599, 2003.

Prenni, A. J., Petters, M. D., Kreidenweis, S. M., Heald, C. L., Martin, S. T., Artaxo, P., Garland, R. M., Wollny, A. G., and Pöschl, U.: Relative roles of biogenic emissions and Saharan dust as ice nuclei in the Amazon basin, Nat. Geosci., 2, 401–404, 2009.

Prigent, C., Chevallier, F., Karbou, F., Bauer, P., and Kelly, G.: AMSU–A land surface emissivity estimation for numerical weather prediction assimilation schemes, J. Appl. Meteor., 44, 416–426, 2005.

Proctor, B. E. and Parker, B. W.: An improved apparatus and technique for upper air investigations, J. Bacteriol., 36, 175–186, 1938.

Proffitt, M. H. and McLaughlin, R.: Fast–response dual beam UV absorption ozone photometer suitable for use on stratospheric balloons, Rev. Sci. Inst., 54, 1719–1728, 1983.

Protat, A., Lemaitre, Y., and Scialom, G.: Retrieval of kinematic fields using a single–beam airborne Doppler radar performing circular trajectories, J. Atmos. Oceanic Technol., 14, 769–791, 1997.

Protat, A., Lemaitre, Y., and Bouniol, D.: Terminal fall velocity and the FASTEX cyclones, Q. J. R. Meteorolog. Soc., 129, 1513–1535, 2003.

Protat, A., Pelon, J., Testud, J., Grand, N., Delville, P., Laborie, P., Vinson, J.-P., Bouniol, D., Bruneau, D., Chepfer, H., Delanoë, J., Haeffelin, M., Noël, V., and Tinel, C.: Etude des nuages faiblement précipitants par télédétection active, La Météorologie, 47, 2004.

Protat, A., Armstrong, A., Haeffelin, M., Morille, Y., Pelon, J., Delanoë, J., and Bouniol, D.: Impact of conditional sampling and instrumental limitations on the statistics of cloud properties derived from cloud radar and lidar at SIRTA, Geophys. Res. Lett., 33, 2006.

Protat, A., Delanoe, J., Bouniol, D., Heymsfield, A. J., Bansemer, A., and Brown, P.: Evaluation of ice water content retrievals from cloud radar reflectivity and temperature using a large airborne in situ microphysical database, J. Appl. Meteorol. Climatol., 46, 557–572, 2007.

Protat, A., Bouniol, D., Delanoe, J., May, P. T., Plana-Fattori, A., Hasson, A., O'Connor, E., Görsdorf, U., and Heymsfield, A. J.: Assessment of Cloudsat Reflectivity Measurements and Ice Cloud Properties Using Ground–Based and Airborne Cloud Radar Observations, J. Atmos. Oceanic Technol., 26, 1717–1741, 2009.

Pruppacher, H. and Klett, J.: Microphysics of Clouds and Precipitation, D. Reidel Publishing Company, Boston, 714 pp., 1980.

Pu, S., Allano, D., Patte–Rouland, B., Malek, M., Lebrun, D., and Chen, K. F.: Particle field characterization by digital in–line holography: 3D location and sizing, Exp. Fluids, 39, 1–9, 2005.

Purcell, E. and Pennypacker, C. R.: Scattering and Absorption of Light by Nonspherical Dielectric Grains, Astrophys. J., 186, 705–714, 1973.

Purvis, R., Lewis, A., Carney, R., McQuaid, J., Arnold, S., Methven, J., Barjat, H., Dewey, K., Kent, J., Monks, P., Carpenter, L., Brough, N., Penkett, S., and Reeves, C.: Rapid uplift of nonmethane hydrocarbons in a cold front over central Europe, J. Geophys. Res., 108, 1–14, doi:10.1029/2002JD002521, 2003.

Puxbaum, H., Caseiro, A., Sánchez–Ochoa, A., Kasper–Giebl, A., Claeys, M., Gelencsér, A., Legrand, M., Preunkert, S., and Pio, C.: Levoglucosan levels at background sites in Europe for assessing the impact of biomass combustion on the European aerosol background, J. Geophys. Res., 112, 2007.

Qu, Z., Goetz, A., and Heidbrecht, K.: high accuracy atmosphere correction for hyperspectral data (HAATCH), in Proceedings of the Ninth JPL Airborne Earth Science Workshop, JPL–Pub 00-18, pp. 373–381, 2001.

Quérel, A., Lemaitre, P., Brunel, M., Porcheron, E., and Grëhan, G.: Real–time global interferometric laser imaging for the droplet sizing (ILIDS) algorithm for airborne research, Meas. Sci. Technol., 21, 2010.

Quinn, P. K. and Coffman, D. J.: Local closure during the First Aerosol Characterization Experiment (ACE 1): Aerosol mass concentration and scattering and backscattering coefficients, J. Geophys. Res., 16, 575–596, 1998.

Racette, P., Adler, R., Gasiewski, A., Jackson, D., Wang, J., and Zacharias, D.: An airborne millimeter–wave imaging radiometer for cloud, precipitation, and atmospheric water vapor studies, J. Atmos. Oceanic Technol., 13, 610–619, 1996.

Radney, J. G., Bazargan, M. H., Wright, M. E., and Atkinson, D. B.: Laboratory Validation of Aerosol Extinction Coefficient Measurements by a Field-Deployable Pulsed Cavity Ring–Down Transmissometer, Aerosol Sci. Technol., 43, 71–80, 2009.

Ram, M., Cain, S., and Taulbee, D.: Design of a shrouded probe for airborne aerosol sampling in a high velocity airstream, J. Aerosol Sci., 26, 945–962, 1995.

Ramana, M., Ramanathan, V., Kim, D., Roberts, G., and Corrigan, C.: Albedo, atmospheric solar absorption and heating rate measurements with stacked UAVs, Q. J. R. Meteorol. Soc., 133, doi: 10.1002 / qj.172, 1913–1931, 2007.

Ranz, W. and Wong, J.: Jet impactors for determining the particle size distribution of aerosols, Arch Ind. Hyg. Occ. Med., 5, 464–477, 1952.

Raupach, S.: Cascaded adaptive–mask algorithm for twin–image removal and its application to digital holograms of ice crystals, Appl. Opt., 42, 287–301, 2009.

Raupach, S., Vossing, H., Curtius, J., and Borrman, S.: Digital crossed-beam holography for in situ imaging of atmospheric particles, J. Optic. Pure Appl. Optic., 8, 796–806, 2006.

Rawlins, F.: Aircraft measurements of the solar absorption by broken cloud fields: A case study, Q. J. R. Meteorol. Soc., 115, 365–382, 1989.

Read, K., Lewis, A., Salmon, R., Jones, A., and Bauguitte, S.: OH and halogen atom influence on the variability of non–methane hydrocarbons in the Antarctic boundary layer, Tellus, 59, 22–38, 2006.

Read, K., Mahajan, A., Carpenter, L., Evans, M., Faria, B., Heard, D., Hopkins, J., Lee, J., Moller, S., Lewis, A., Mendes, L., McQuaid, J., Oetjen, H., Saiz–Lopez, A., Pilling, M., and Plane, J.: Extensive halogen–mediated ozone destruction over the tropical Atlantic Ocean, Nature, 453, 1232–1235, 2008.

Read, W. G., L. A., Bacmeister, J., Cofield, R. E., Christensen, L. E., Cuddy, D. T., Daffer, W. H., Drouin, B. J., Fetzer, E., Froidevaux, L., Fuller, R., Herman, R., Jarnot, R. F., Jiang, J. H., Jiang, Y. B., Kelly, K., Knosp, B. W., Kovalenko, L. J., Livesey, N. J., Liu, H.-C., Manney, G. L., Pickett, H. M., Pumphrey, H. C., Rosenlof, K. H., Sabounchi, X., Santee, M. L., Schwartz, M. J., Snyder, Stek, W. V. P. C., Su, H., Takacs, L. L., Thurstans, R. P., Voemel, H., Wagner, P. A., Waters, J. W., Webster, C. R., Weinstock, E. M., and Wu, D. L.: Aura Microwave Limb Sounder upper tropospheric and lower stratospheric H2O and relative humidity with respect to ice validation, J. Geophys.Res., 112, D24S35, doi:10.1029 / 2007JD008752, 2007.

Redemann, J., Schmid, B., Eilers, J., Kahn, R., Levy, R., Russell, P., Livingston, J., Hobbs, P., Smith Jr., W., and Holben, B.: Suborbital measurements of spectral aerosol optical depth and its variability at subsatellite grid scales in support of CLAMS, 2001, J. Atmos. Sci., 62, 993–1007,doi:10.1175 / JAS3387.1, 2005.

Redemann, J., Pilewskie, P., Russell, P., Livingston, J., Howard, S., Schmid, B., Pommier, J., Gore, W., Eilers, J., and Wendisch, M.: Airborne measurements of spectral direct aerosol radiative forcing in the Intercontinental chemical Transport Experiment / Intercontinental Transport and Chemical Transformation of anthropogenic pollution, 2004, J. Geophys. Res., 111, 2006.

Reeves, C. and Penkett, S.: Measurements of Peroxides and What They Tell Us, Chem. Rev., 103, 5199–5218, 2003.

Reiche, C. and Lasher–Trapp, S.: The minor importance of giant aerosol to precipitation development within small trade wind cumuli observed during RICO, Atmos. Res., 95 (4), 386–399, 2010.

Reichert, L., Andrés Hernández, M., Stöbener, D., Burkert, J., and Burrows, J. P.: Investigation of the effect of water complexes in the determination of peroxy radical ambient concentrations: implications for the atmosphere, J. Geophys. Res., 9, 4017–4032, 2003.

Reid, J. S., Jonsson, H. H., Maring, H. B., Smirnov, A., Savoie, D. L., Cliff, S. S., Reid, E. A., Livingston, J. M., Meier, M. M., Dubovik, O., and Tsay, S. C.: Comparison of size and morphological measurements of coarse mode dust particles from Africa, J. Geophys. Res., 108, 2003.

Reiner, T., Hanke, M., and Arnold, F.: Atmospheric peroxy radical measurements by ion molecule reaction mass spectrometry: A novel analytical method using amplifying chemical conversion to sulfuric acid, J. Geophys. Res. D: Atmos., 102, 1311–1326, 1997.

Reiner, T., Hanke, M., Arnold, F., Ziereis, H., and Schlager, H.: Aircraft–Borne Measurements of Peroxy Radicals by Chemical Conversion / Ion Molecule Reaction Mass Spectrometry: Calibration, Diagnostics and Results, J. Geophys. Res., 104, 18 647–18 659, 1999.

Reitebuch, O., Werner, C., Leike, I., Delville, P., P. H. Flamant, A. C., and Engelbart, D.: Experimental Validation of Wind Profiling Performed by the Airborne 10 μm–Heterodyne Doppler Lidar WIND, J. Atmos. Oceanic Technol., pp. 1331–1344, 2001.

Reitebuch, O., Volkert, H., Werner, C., Dabas, A., Delville, P., Drobinski, P., Flamant, P. H., and Richard, E.: Determination of air flow across the alpine ridge by a combination of airborne Doppler lidar, routine radio–sounding and numerical simulation, Q. J. R. Meteorol. Soc., 128, 715–728, 2003.

Reitebuch, O., Lemmerz, C., Nagel, E., Paffrath, U., Durand, Y., Endemann, M., Fabre, F., and Chaloupy, M.: The Airborne Demonstrator for the Direct-Detection Doppler Wind Lidar ALADIN on ADM–Aeolus. Part I: Instrument Design and Comparison to Satellite Instrument, J. Atmos. Oceanic Technol., 26, 2501–2515, 2009.

Rempe, H.: Untersuchungen über die Verbreitung des Blütenstaubes durch die Luftströmungen, Planta, 27, 93–147, 1937.

Ren, X., Brune, W., Cantrell, C., Edwards, G., Shirley, T., Metcalf, A., and Lesher, R. L.: Hydroxyl and Peroxy Radical Chemistry in a Rural Area of Central Pennsylvania: Observations and Model Comparisons, J. Atmos. Chem., 52, 231–257, 2005.

Ren, X., Olson, J. R., Crawford, J. H., Brune, W. H., Mao, J., Long, R. B., Chen, Z., Chen, G., Avery, M. A., Sachse, G. W., Barrick, J. D., Diskin, G. S., Huey, L. G., Fried, A., Cohen, R. C., Heikes, B., Wennberg, P. O., Singh, H. B., Blake, D. R., and Shetter, R. E.: HO_x chemistry during INTEX–A 2004: Observation, model calculation, and comparison with previous studies, J. Geophys. Res. D: Atmos., 113, doi:10.1029 / 2007JD009166, 2008.

Reuter, A. and Bakan, S.: Improvements of cloud particle sizing with a 2D–Grey probe, J. Atmos. Oceanic Technol., 15, 1196–1203, 1998.

Rice, A. L., Gotoh, A. A., Ajie, H. O., and Tyler, S. C.: High–precision continuous–flow measurement of delta C–13 and delta D of atmospheric CH_4, Anal. Chem., 73, 4104–4110, 2001.

Richard, E., Flamant, C., Bouttier, F., Baelen, J. V., Champollion, C., Argence, S., Arnault, J., Barthlott, C., Behrendt, A., Bosser, P., Brousseau, P., Chaboureau, J.-P., Corsmeier, U., Cuesta, J., DiGirolamo, P., Hagen, M., Kottmeier, C., Limnaios, P., Masson, F., Pigeon, G., Pointin, Y., Seiti, Y., and Wulfmeyer, V.: La campagne COPS: initiation et cycle de vie de la convection en région montagneuse, La Météorologie, 8, 32–42, 2009.

Richards, J. and Jia, X.: Remote Sensing Digital Image Analysis, An Introduction, Springer, Berlin, 4th edn., 3–540–25128–6, 2006.

Richardson, M.: Making Real Time Measurements of Ice Nuclei Concentrations at Upper Tropospheric Temperatures: Extending the Capabilities of the Continuous Flow Diffusion Chamber, Ph.D. thesis, Colorado State University, Fort Collins, 268 pp., 2009.

Richardson, M. S., DeMott, P. J., Kreidenweis, S. M., Petters, M. D., and Carrico, C. M.: Observations of ice nucleation by ambient aerosol in the homogeneous freezing regime, Geophys. Res. Lett., in press, 2010.

Richter, R. and Muller, A.: De–shadowing of satellite / airborne imagery, International Journal of Remote Sensing, 26, 3137–3148, 2005.

Richter, R. and Schläpfer, D.: Geo–atmospheric processing of airborne imaging spectrometry data. part 2: Atmospheric / topographic correction, International Journal of Remote Sensing, 23, 3137–3148, 2002.

Ridley, B., Grahek, F., and Walega, J.: A small, high–sensitivity, medium–response ozone detector suitable for measurements from light aircraft, J. Atmos. Oceanic Technol., 9, 142–148, 1992.

Rinne, H., Delany, A., Greenberg, J., and Guenther, A.: A True Eddy Accumulation System for Trace Gas Fluxes Using Disjunct Eddy Sampling Method, J. Geophys. Res., 105, 24 791–24 798, 2000.

Rinne, H., Guenther, A., Warneke, C., De Gouw, J., and Luxembourg, S.: Disjunct Eddy Covariance Technique for Trace Gas Flux Measurements, Geophysical Research Letters, 28, 3139–3142, 2001.

Roach, W.: Some aircraft observations of fluxes of solar radiation in the atmosphere, Q. J. R. Meteorol. Soc., 87, 346–363, 1961.

Roberts, D., Bradley, E., Cheung, R., Leifer, I., Dennison, P., and Margolis, J.: Mapping methane emissions from a marine geological deep source using imaging spectrometry, Remote Sens. Environ., 114, 592–606, 2010.

Roberts, G. and Nenes, A.: A continuous–flow streamwise thermal–gradient CCN chamber for atmospheric measurements, Aerosol Sci. Technol., 39, 206–221, 2005.

Roberts, G. C., Artaxo, P., Zhou, J., Swietlicki, E., and Andreae, M. O.: Sensitivity of CCN spectra on chemical and physical properties of aerosol: A case study from the Amazon Basin, J. Geophys. Res., 107, 2002.

Roberts, J., Hutte, R., Fehsenfeld, F., Albritton, D., and Sievers, R.: Measurements of Anthropogenic Hydrocarbon Concentration Ratios in the Rural Troposphere–Discrimination Between Background and Urban Sources, Atmos. Environm., 19, 1945–1950, 1985.

Roberts, P. and Hallett, J.: A laboratory study of the ice nucleating properties of some mineral particulates, Q. J. R. Meteorolog. Soc., 94, 25–34, 1968.

Robertson, S. D.: Targets for microwave radar navigation, Bell System Technical Journal, 26, 852–869, 1947.

Robinson, J. K., Bollinger, M., and Birks, J.: Luminol / H_2O_2 chemiluminescence detector for the analysis of nitric oxide in exhaled breath, Anal. Chem., 71, 5131–5136, 1999.

Röckmann, T., Brass, M., Borchers, R., and Engel, A.: The isotopic composition of methane in the stratosphere: High–altitude balloon sample measurements, Atm. Chem. Phys. Disc., manuscript in preparation, 2011.

Rodgers, C.: Inverse methods for atmospheric sounding, World Scientific, 2000.

Rodi, A. and Parish, T.: Aircraft measurement of mesoscale pressure gradients and ageostrophic winds, J. Atmos. Oceanic Technol., 5, 91–101, 1988.

Rodi, A. R. and Spyers-Duran, P. A.: Analysis of time response of airborne temperature sensors., J. Appl. Meteor., 11, 554–556, 1972.

Rogers, D.: Detecting ice nuclei with a continuous flow diffusion chamber–some exploratory tests of instrument response, J. Atmos. Oceanic Technol., 11, 1042–1047, 1994.

Rogers, D., DeMott, P., Kreidenweis, S., and Chen, Y.: A continuous-flow diffusion chamber for airborne measurements of ice nuclei, J. Atmos. Oceanic Technol., 18, 725–741, 2001.

Rogers, D. C.: Development of a Continuous Flow Thermal Gradient Diffusion Chamber for Ice Nucleation Studies, Atmos. Res., 22, 149–181, 1988.

Rogers, R. and Yau, M.: A Short Course in Cloud Physics, Pergamon Press, Oxford, third edition edn., 1989.

Rogge, D., Rivard, B., Zhang, J., and Feng, J.: Iterative spectral unmixing for optimization per–pixel endmeber sets, IEEE Transaction on Geoscience and Remote and Sensing, 44, 3725–3736, 2006.

Roiger, A., Aufmhoff, H., Stock, P., Arnold, F., and Schlager, H.: An aircraft-borne chemical ionization–ion trap mass spectrometer (CI–ITMS) for fast PAN and PPN measurements, Atmos. Meas. Tech., 4, 173–188, 2011a.

Roiger, A., Schlager, H., Schäfler, A., Huntrieser, H., Scheibe1, M., Aufmhoff, H., Cooper, O. R., Sodemann, H., Stohl, A., Burkhart, J., andC. Schiller, M. L., Law, K. S., and Arnold, F.: In–situ observation of Asian pollution transported into the Arctic lowermost stratosphere, Atmos. Chem. Phys., accepted, 2011b.

Romay, F., Pui, D., Smith, T., Ngo, N., and Vincent, J.: Corona discharge effects on aerosol sampling efficiency, Atmos. Environ., 30, 2607–2613, 1996.

Rosa, B., Bajer, K., Haman, K., and Szoplik, T.: Theoretical and experimental characterization of the ultrafast aircraft thermometer: reduction of aerodynamic disturbances and signal processing, J. Atmos. Oceanic Technol., 22, 1727–1738, 2005.

Rose, D., Gunthe, S., Mikhailov, E., Frank, G., Dusek, U., Andreae, M., and Pöschl, U.: Calibration and Measurement Uncertainties of a Continuous-Flow Cloud Condensation Nuclei Counter (DMT-CCNC): CCN Activation of Ammonium Sulfate and Sodium Chloride Aerosol Particles in Theory and Experiment, Atmos. Chem. Phys., pp. 1153–1179, 2008.

Rosemount: Model 858 Flow Angle Sensors, Rosemount Inc., bulletin 1014, 1982.

Rothermel, J., Cutten, D. R., Hardesty, R. M., Menzies, R. T., Howell, J. N., Johnson, S. C., Tratt, D. M., Olivier, L. D., and Banta, R. M.: The Multi–center Airborne Coherent Atmospheric Wind Sensor, Bull. Am. Meteorol. Soc., 79, 581–599, 1998.

Rotta, J. C.: Turbulente Strömungen. Eine Einführung in die Theorie und ihre Anwendung, Teubner, Stuttgart, 267 pp., 1972.

Rudolph, J. and Ehhalt, D.: Measurements of C_2–C_5 Hydrocarbons Over the North Atlantic, J. Geophys. Res., 86, 11 959–11 964, 1981.

Ruehl, C. R., Chuang, P. Y., and Nenes, A.: Distinct CCN activation kinetics above the marine boundary layer along the California coast, Geophys. Res. Lett., 36, 2009.

Ruskin, R.: Measurements of Water–Ice Budget Changes at -5 C in AgI Seeded Tropical Cumulus, J. Appl. Meteor., 6, 72–81, 1965.

Russel, P., Swissler, T., and McCormick, M.: Methodology for error analysis and simulation of lidar aerosol measurements, Appl. Opt., 18, 3783–3797, 1979.

Russell, L. M., Flagan, R. C., and Seinfeld, J. H.: Asymmetric instrument response resulting from mixing effects in accelerated DMA–CPC measurements, Aerosol Sci. Technol., 23, 491–509, 1995.

Russell, P., Livingston, J., Dutton, E., Pueschel, R., Reagan, J., DeFoor, T., Box, M., Allen, D., Pilewskie, P., Herman, B., Kinne, S., and Hofmann, D.: Pinatubo and pre–Pinatubo optical–depth spectra: Mauna Loa measurements, comparisons, inferred particle size distributions, radiative effects, and relationship to Lidar data, J. Geophys. Res., 98, 22 969–22 985, 1993.

Russell, P., Livingston, J., Pueschel, R., Pollack, J., Brooks, S., Hamill, P., Hughes, J., Thomason, L., Stowe, L., Deshler, T., Dutton, E., and Bergstrom, R.: Global to microscale evolution of the Pinatubo volcanic aerosol, derived from diverse measurements and analyses, J. Geophys. Res., 101, 18 745–18 763, 1996.

Russell, P. B., Bergstrom, R. W., Shinozuka, Y., Clarke, A. D., DeCarlo, P. F., Jimenez, J. L., Livingston, J. M., Redemann, J., Dubovik, O., and Strawa, A.: Absorption Angstrom exponent in AERONET and related data as an indicator of aerosol composition, Atmos. Chem. Phys., 10, 1155–1169, doi:10.5194 / acp–10–1155–2010, 2010.

Ryerson, T. B., Buhr, M., Frost, G., Goldan, P., Holloway, J., Hubler, G., Jobson, B., Kuster, W., McKeen, S., Parrish, D., Roberts, J., Sueper, D., Trainer, M., Williams, J., and Fehsenfeld, F.: Emissions lifetimes and ozone formation in power plant plumes, J. Geophys. Res., 103, 569–584, doi:10.1029 / 98JD01620, 1998.

Ryerson, T. B., Huey, L. G., Knapp, K., Neuman, J. A., Parrish, D. D., Sueper, D. T., and Fehsenfeld, F. C.: Design and initial characterization of an inlet for gas–phase NO_y measurements from aircraft, J. Geophys. Res., 104, 5483–5492, 1999.

Ryerson, T. B., Williams, E. J., and Fehsenfeld, F. C.: An efficient photolysis system for fast–response NO_2 measurements, J. Geophys. Res., 105, 447–461, 2000.

Ryzhkov, A. V., Giangrande, S., and Schuurand, V. M. T. J.: Calibration issues of dual–polarization radar measurements, J. Atmos. Oceanic Technol., 22, 1138–1155, 2005.

Sadanaga, Y., Yoshino, A., Watanabe, K., Yoshioka, A., Wakazono, Y., Kanaya, Y., and Kajii, Y.: Development of a measurement system of peroxy radicals using a chemical amplification / laser–induced fluorescence technique, Rev. Sci. Instrum., 75, 864–872, 2004.

Sagalyn, R. C. and Faucher, G.: Investigation of charged nuclei in the free atmosphere, Geofisica Pura e Applicata, 31, 182, 1955.

Saito, T., Yokouchi, Y., and Kawamura, K.: Distributions of C_2–C_6 hydrocarbons over the western North Pacific and eastern Indian Ocean, Atmos. Environm., 34, 4373–4381, 2000.

Salisbury, G., Monks, P. S., Bauguitte, S., Bandy, B. J., and Penkett, S. A.: A Seasonal Comparison of the Ozone Photochemistry in Clean and Polluted Air Masses at Mace Head, Ireland, J. Atmos. Chem., 41, 163–187, 2002.

Sander, S., Friedl, R. R., Golden, D. M., Kurylo, M. J., Moortgat, G. K., Keller-Rudek, H., Wine, P. H., Ravishankara, A. R., Kolb, C. E., Molina, M. J., Finlayson-Pitts, B. J., Huie, R. E., and Orkin, V.: Chemical kinetics and photochemical data for use in atmospheric studies, Jet Propulsion Laboratory Publ. 06–2, evaluation No. 15, 2006.

Sankar, S. and Bachalo, W.: Trajectory Dependent Scattering in Phase Doppler Interferometry: Minimizing and Eliminating Sizing Errors, in Proceedings of the Sixth Annual Symposium on Applications of Laser Techniques to Fluid Mechanics, Lisbon, Portugal, 1992.

Sankar, S., Weber, B., Kamemoto, D., and Bachalo, W.: Sizing Fine Particles with the Phase Doppler Interferometric Technique, in 2nd International Congress on Optical Particle Sizing, Arizona State University, Tempe, Arizona, 1990.

Sarabandi, K., Oh, Y., and Ulaby, F. T.: Measurement and calibration of differential Muller matrix of distributed targets, IEEE Trans. Antenn. Prop., 40, 1524–1532, 1992.

Sassen, K.: The Polarization Lidar Technique for Cloud Research–A Review and Current Assessment, Bull. Am. Meteorol. Soc., 72, 1848–1866, 1991.

Sassen, K. and Cho, B. S.: Subvisual Thin Cirrus LIDAR Dataset for Satellite Verification and Climatological Research, J. Appl. Meteor., 31, 1275–1285, 1992.

Sassen, K. and Liao, L.: Estimation of cloud content by W–band radar, J. Appl. Meteor., 35, 932–938, 1996.

Sassen, K. and Liou, K.: Scattering of polarized laser light by water droplet, mixed–phase and ice crystal clouds. Part I: Angular scattering patterns, J. Atmos. Sci., 5, 838–851, 1979.

Sassen, K., Mace, G. G., Wang, Z., Poellot, M. R., Sekelsky, S. M., and McIntosh, R. E.: Continental stratus clouds: A case study using coordinated remote sensing and aircraft measurements, J. Atmos. Sci., 56, 2345–2358, 1999.

Sato, K. Okamoto, H., Yamamoto, M. K., Fukao, S., Kumagai, H., Ohno, Y., Horie, H., and Abo, M.: 95 GHz Doppler radar and lidar synergy for simultaneous ice microphysics and in–cloud vertical air motion retrieval, J. Geophys. Res. Atmos., 114, 2009.

Sato, K. and Okamoto, H.: Characterization of Ze and LDR of nonspherical and inhomogeneous ice particles for 95 GHz cloud radar: Its implication to microphysical retrievals, J. Geophys. Res., 111, 2006.

Saunders, R., Brogniez, G., Buriez, J., Meerkötter, R., and Wendling, P.: A comparison of measured and modeled broadband fluxes from aircraft data during the ICE ’89 field experiment, J. Atmos. Oceanic Technol., 9, 391–406, 1992.

Sauvageot, H.: Radar Meteorology, Artech House, 1992.

Savitzky, A. and Golay, M. J. E.: Smoothing and Differentiation of Data by Simplified Least Squares Procedures, Analytical chemistry, 36, 1627–1639, 1964.

Saw, E. W., Shaw, R. A., Ayyalasomayajula, S., Chuang, P. Y., and Gylfason, A.: Inertial clustering of particles in high-Reynolds-number turbulence, Phys. Rev. Lett., 100, 214 501, 2008.

Saxena, V. K. and Carstens, J. C.: On the operation of cylindrical thermal diffusion cloud chambers, Journal de Recherches Atmospheriques, 5, 11–23, 1971.

Sayres, D., Moyer, E. J., Hanisco, T. F., Clair, J. M. S., Keutsch, F. N., Brien, A. O., Allen, N. T., Lapson, L., Demusz, J. N., Rivero, M., Martin, T., Greenberg, M., Tuozzolo, C., Engel, G. S., Kroll, J. H., Paul, J. B., and Anderson, J. G.: A new cavity based absorption instrument for detection of water isotopologues in the upper troposphere and lower stratosphere, Rev. Sci. Instrum., 80, doi:10.1063 / 1.3117 349, 2009a.

Sayres, D. S., Moyer, E. J., Hanisco, T. F., St Clair, J. M., Keutsch, F. N., O’Brien, A., Allen, N. T., Lapson, L., Demusz, J. N., Rivero, M., Martin, T., Greenberg, M., Tuozzolo, C., Engel, G. S., Kroll, J. H., Paul, J. B., and Anderson, J. G.: A new cavity based absorption instrument for detection of water isotopologues in the upper troposphere and lower stratosphere, Rev. Sci. Instrum., 80, 2009b.

Schaepman, M., Ustin, S., Plaza, A., Painter, T., Verrelst, J., and Liang, S.: Earth system science related imaging spectroscopy–An assessment, Remote Sens. Environ., 113, 123–137, 2009.

Schauffler, S. M., Atlas, E. L., Flocke, F., Lueb, R. A., Stroud, V., and Travnicek, W.: Measurements of bromine containing organic compounds at the tropical tropopause, Geophys. Res. Lett., 25, 317–320, 1998.

Scheuer, E., Talbot, R. W., Dibb, J. E., Seid, G. K., DeBell, L., and Lefer, B.: Seasonal distributions of fine aerosol sulfate in the North American Arctic basin during TOPSE, J. Geophys. Res., 108, 2003.

Schiller, C., Krämer, M., Afchine, A., Spelten, N., and Sitnikov, N.: The ice water content of Arctic, midlatitude and tropical cirrus, J. Geophys. Res., 113, doi:10.1029/2008JD010342, 2008.

Schkolnik, G. and Rudich, Y.: Detection and quantification of levoglucosan in atmospheric aerosols: a review, Anal. Bioanal. Chem., 385(1), 26–33, 2006.

Schlager, H. and Arnold, F.: Balloon–borne composition measurements of stratospheric negative ions and inferred sulfuric acid vapour abundances during the MAP/GLOBUS campaign, Planet. Space Sci., 35, 693–701, 1987a.

Schlager, H. and Arnold, F.: On stratospheric acetonitrile detection by passive chemical ionization mass spectrometry, Planet. Space Sci., 35, 715–725, 1987b.

Schlager, H., Konopka, P., Schulte, P., Schumann, U., Ziereis, H., Arnold, F., Klemm, M., Hagen, D., Whitefield, P., and Ovarlez, J.: In–Situ Observations of Air Traffic Emission Signatures in the North Atlantic Flight Corridor, J. Geophys. Res., 102, 10 739–10 750, 1997.

Schlager, H. e. a.: First East–Asian anthropogenic SO_2 detection in the lower stratosphere: CI–ITMS measurements aboard the research aircraft HALO, Geophys. Res. Lett., submitted, 2011.

Schläpfer, D. and Richter, R.: Geo–atmospheric processing of airborne imaging spectrometry data. part 1: Parametric ortho–rectification process, International Journal of Remote Sensing,, 23, 2609–2630, 2002.

Schläpfer, D., Borel, C., Keller, J., and Itten, K.: Atmospheric pre–corrected differential absorption techniques to retrieve columnar water vapor, Remote Sens. Environ., 65, 353–366, 1998.

Schläpfer, D., McCubbin, I., Kindel, B., Kaiser, J., and Ben–Dor, E.: Imaging Spectroscopy : New Quality in Environmental Studies, chap. Wildfire smoke analysis using the 760 nm oxygen absorption feature, pp. 423–435, N.A., edited by A. Zagajewski and M. Sobczak, 2006.

Schlienger, J., Pfau, A., Kalfas, A. I., and Abhari, R. S.: Single Pressure Transducer Probe for 3D Flow Measurements, in 16th Symposium on Measuring Techniques in Transonic and Supersonic Flow in Cascades and Turbomachines, Cambridge, UK, 2002.

Schmid, B. and Wehrli, C.: Comparison of Sun photometer calibration by use of the Langley technique and the standard lamp, Appl. Opt., 34, 4501–4512, 1995.

Schmid, B., Thome, K., Demoulin, P., Peter, R., Matzler, C., and Sekler, J.: Comparison of modeled and empirical approaches for retrieving columnar water vapor from solar transmittance measurements in the 0.94 μm region, J. Geophys. Res., 101, 9345–9358, 1996.

Schmid, B., Redemann, J., Russell, P., Hobbs, P., Hlavka, D., McGill, M., Holben, B., Welton, E., Campbell, J., Torres, O., Kahn, R., Diner, D., Helmlinger, M., Chu, D., Robles-Gonzalez, C., and deLeeuw, G.: Coordinated airborne, spaceborne, and ground–based measurements of massive, thick aerosol layers during the dry season in Southern Africa, J. Geophys. Res., 108, doi:10.1029/2002JD002297, 2003.

Schmidt, G.: INS/GPS technology trends. Paper 1. Low–Cost Navigation Sensors and Integration Technology, NATO Research and Technology Organisation, RTO–EN–SET–116(2010) AC/323(SET–116)TP/311,ISBN 978–92–837–0109–5., ftp://ftp.rta.nato.int//PubFullText/RTO/EN/RTO-EN-SET-116(2010)///EN-SET-116(2010)-01.pdf, 2010.

Schmidt, G. and Phillips, R.: "INS/GPS Integration Architectures," and "INS/GPS Integration Architecture Performance Comparisons", NATO Research and Technology Organisation, RTO–EN–SET–116, Low–Cost Navigation Sensors and Integration Technology, 2010.

Schmidt, K. S., Feingold, G., Pilewskie, P., Jiang, H., Coddington, O., and Wendisch, M.: Irradiance in polluted cumulus fields: Measured and modeled cloud–aerosol effects, Geophys. Res. Lett., 36, doi:10.1029/2008GL036848, 2009.

Schmidt, K. S., Pilewskie, P., Bergstrom, R., Coddington, O., Redemann, J., Livingston, J. M., Russell, P., Bierwirth, E., Wendisch, M., Gore, W., Dubey, M. K., and Mazzoleni, C.: A new method for deriving aerosol solar radiative forcing and its first application within MILAGRO/INTEX–B, Atmos. Chem. Phys., 10, 7829–7843, doi:10.5194/acp– 10–7829–2010, 2010.

Schmitt, C. and Heymsfield, A.: The size distribution and mass–weighted terminal velocity of low–latitude tropopause cirrus crystal populations, J. Atmos. Sci., 66, 2013–2028, 2009.

Schneider, T. L. and Stephens, G. L.: Theoretical Aspects of Modeling Backscattering by Cirrus Ice Particles at Millimeter Wavelengths, J. Atmos. Sci., 52, 4367–4385, 1995.

Schotland, R. M.: Errors in the lidar measurement of atmospheric gases by differential absorption, J. Appl. Meteor., 13, 71–77, 1974.

Schott, J.: Remote Sensing: The Image Chain Approach, 2nd Edition, Oxford University Press, New York, NY, 2007.

Schowengerdt, R.: Remote Sensing : Models and Methods for Image Processing, Academic Press, Elsevier Pub., New York, 2nd edn., 509 pp., 1997.

Schreder, J., Grobner, J., Los, A., and Blumthaler, M.: Intercomparison of monochromatic source facilities for the determination of the relative spectral response of erythemal broadband filter radiometers, Opt. Lett., 13, 1455–1457, 2004.

Schröder, F. and Ström, J.: Aircraft measurements of sub micrometer aerosol particles (> 7 nm) in the midlatitude free troposphere and tropopause region, Atmos. Res., 44, 333–356, 1997.

Schröter, M., Bange, J., and Raasch, S.: Simulated Airborne Flux Measurements in a LES Generated Convective Boundary Layer, Boundary Layer Meteorol., 95, 437–456, 2000.

Schultz, M., Heitlinger, M., Mihelcic, D., and Volz–Thomas, A.: A calibration source for peroxy radicals with built–in actinometry using H_2O and O_2 photolysis at 185 nm, J. Geophys. Res., 100, 811, 1995.

Schumann, U. and Huntrieser, H.: The global lightning-induced nitrogen oxides source rate, Atmos. Chem. Phys., 7, 3823–3907, 2007.

Schwab, J. J. and Anderson, J.: Oscillator–Strengths Of Cl(I) In The Vacuum Ultraviolet–The 2d–2p Transitions, J. Quant. Spectrosc. Radiat. Transfer, 27, 445–457, 1982.

Schwarz, J. P., Gao, R., Fahey, D., Thomson, D., Watts, L., Wilson, J., Reeves, J., Darbeheshti, M., Baumgardner, D., Kok, G., Chung, S., Schulz, M., Hendricks, J., Lauer, A., Kärcher, B., Slowik, J., Rosenlof, K., Thompson, T., Langford, A., Loewenstein, M., and Aikin, K.: Single–particle measurements of midlatitude black carbon and light–scattering aerosols from the boundary layer to the lower stratosphere, J. Geophys. Res., 111, doi:10.1029/2006JD007076, 2006.

Schwarz, J. P., Spackman, J. R., Fahey, D. W., Gao, R. S., Lohmann, U., Stier, P., Watts, L. A., Thomson, D. S., Lack, D. A., Pfister, L., Mahoney, M. J., Baumgardner, D., Wilson, J. C., and Reeves, J. M.: Coatings and their enhancement of black carbon light absorption in the tropical atmosphere, J. Geophys. Res., 113, 2008.

Schwarzenboeck, A., Mioche, G., Armetta, A., Herber, A., and Gayet, J.-F.: Response of the Nevzorov hot wire probe in clouds dominated by droplet conditions in the drizzle size range, Atmos. Meas. Tech., 2009.

Schwiesow, R. L. and Spowart, M. P.: The NCAR airborne infrared lidar system: Status and applications, J. Atmos. Oceanic Technol., 13, 4–15, 1996.

Scialom, G., Protat, A., and Lemaitre, Y.: Retrieval of kinematic fields from dual–beam airborne radar data gathered in circular trajectories during the FASTEX experiment, J. Atmos. Oceanic Technol., 20, 630–646, 2003.

Secker, J., Staenz, K., Gauthier, R., and Budkewitsch, P.: Vicarious calibration of airborne hyperspectral sensors in operational environments, Remote Sens. Environ., 76, 81–92, 2001.

Seebaugh, W. and Wilson, J.: High–volume low–turbulence inlet for aerosol sampling from aircraft, Tech. rep., Annual Report to the NSF, http://www.engr.du.edu/aerosol/ATM-9713408%20Progress%201999.pdf, 1999.

Seifert, M., Tiede, R., Schnaiter, M., Linke, C., Mohler, O., Schurath, U., and Strom, J.: Operation and performance of a differential mobility particle sizer and a TSI 3010 condensation particle counter at stratospheric temperatures and pressures, J. Aerosol Sci., 35, 981–993, 2004.

Seinfeld, J. H. and Pandis, S. N.: Atmospheric Chemistry and Physics: From Air Pollution to Climate Change, John Wiley & Sons, Inc, 1326 pp., 1998.

Seliga, T. A. and Bringi, V. N.: Potential use of radar differential reflectivity meanurements at orthogonal polarization for measuring precipitation, J. Appl. Meteor., 39, 1341–1372, 1976.

Sellar, R. G. and Boreman, G. D.: Classification of imaging spectrometers for remote sensing applications, Opt. Engineering, 44, 013 602–013 603, 2005.

Sellegri, K., Umann, B., Hanke, M., and Arnold, F.: Deployment of a ground–based CIMS apparatus for the detection of organic gases in the boreal forest during the QUEST campaign, Atmos. Chem. Phys., 5, 357–372, 2005.

Sellers, W.: Physical Climatology, The University of Chicago Press, Chicago, Illinois, 1965.

Shaw, G.: The vertical distribution of tropospheric aerosols at Barrow, Alaska, Tellus, 27, 39–49, 1975.

Shaw, G.: Sun photometry, Bull. Amer. Meteor. Soc., 64, 4–10, 1983.

Shcherbakov, V., Gayet, J.-F., Baker, B., and Lawson, P.: Light scattering by single natural ice crystals, J. Atmos. Sci., 63, 1513–1525, doi:10.1175/JAS3690.1, 2006.

Sheih, C. M., Tennekes, H., and Lumley, J. L.: Airborne hot–wire measurements of the small–scale structure of atmospheric turbulence, Phys. Fluids, 14, 201–215, 1971.

Sheridan, P., Arnott, W., Ogren, J., Andrews, E., Atkinson, D., Covert, D., Moosmüller, H., Petzold, A., Schmid, B., Strawa, A., Varma, R., and Virkkula, A.: The Reno aerosol optics study: An evaluation of aerosol absorption measurement methods, Aerosol Sci. Technol., 39, 1–16, 2005.

Shetter, R. and Müller, M.: Photolysis frequency measurements using actinic flux spectroradiometry during the PEM-Tropics mission: Instrumentation description and some results, J. Geophys. Res., 104, 5647–5661, 1999.

Shetter, R., Cinquini, L., Lefer, B., and Madronich, S.: Comparison of airborne measured and calculated spectral actinic flux and derived photolysis frequencies during the PEM Tropics B mission, J. Geophys. Res., 108, doi:10.1029/2001JD001320, 2003.

Shettle, P. E. and Fenn, R. W.: Models for the aerosols of the lower atmosphere and the effects of humidity variations on their optical properties, Tech. Rep. 79 0214, Research Papers No. 676, Air Force Cambridge Research Laboratory, Hanscom Airforce Base, MA., 100 pp., 1979.

Shifrin, K., Shifrin, Y., and Mikulinski, I.: Light scattering by an ensemble of large particles of arbitrary shape, Doklady Akad. Nauk SSSR, 227, 582, 1984.

Shimoni, M., Heremans, R., van der Meer, F., and Acheroy, M.: Measuring pollutant gases using VNIR and TIR imaging, in Proceedings 5^{th} EARSeL Workshop on Imaging Spectroscopy, p. 12, Bruges, Belgium, 2007.

Shiobara, M., Spinhirne, J., Uchiyama, A., and Asano, S.: Optical depth measurements of aerosol, cloud and water vapor using sun photometers during FIRE Cirrus IFO II, J. Appl. Meteor., 35, 36–46, 1991.

Shipley, S. T., Tracy, D. H., Eloranta, E. W., Trauger, J. T., Sroga, J. T., Roesler, F. L., and Weinman, J. A.: High spectral resolution lidar to measure optical scattering properties of atmospheric aerosols. 1: Theory and instrumentation, Appl. Opt., 22, 3716–3724, 1983.

Shiraiwa, M., Kondo, Y., Moteki, N., Takegawa, N., Sahu, L. K., Takami, A., Hatakeyama, S., Yonemura, S., and Blake, D. R.: Radiative impact of mixing state of black carbon aerosol in Asian outflow, J. Geophys. Res., 113, 2008.

Shulman, M., Jacobson, M., Charlson, R., Synovec, R., and Young, T.: Dissolution behavior and surface tension effects of organic compounds in nucleating cloud droplets, Geophys. Res. Lett., 23, 277–280, 1996.

Shupe, M. D., Daniel, J. S., de Boer, G., Eloranta, E., Kollias, P., Luke, E., Long, C., Turner, D., and Verlinde, J.: A Focus on Mixed–Phase Clouds The Status of Ground–Based Observational Methods, Bull. Am. Meteorol. Soc., 89, 1549, 2008.

Siebert, H. and Muschinski, A.: Relevance of a Tuning-Fork Effect for Temperature Measurements with the Gill Solent HS Ultrasonic Anemometer-Thermometer, J. Atmos. Oceanic Technol., 18, 1367–1376, 2001.

Siebert, H., Franke, H., Lehmann, K., Maser, R., Saw, E. W., Schell, D., Shaw, R. A., and Wendisch, M.: Probing finescale dynamics and microphysics of clouds with helicopter-borne measurements, Bull. Amer. Meteor. Soc., 87, 1727–1738, 2006a.

Siebert, H., Franke, H., Lehmann, K., Maser, R., Saw, E. W., Schell, D., Shaw, R. A., and Wendisch, M.: Probing Fine–Scale Dynamics and Microphysics of Clouds with Helicopter–Borne Measurements, Bull. Am. Meteor. Soc., 87, 1727 – 1738, 2006b.

Siebert, H., Lehmann, K., and Wendisch, M.: Observations of small scale turbulence and energy dissipation rates in the cloudy boundary layer., J. Atmos. Sci., 63, 1451 – 1466, 2006c.

Siebert, H., Lehmann, K., and Shaw, R.: On the use of a hot–wire anemometer for turbulence measurements in clouds, J. Atmos. Oceanic Technol., 24, 980–993, 2007.

Siebert, H., Shaw, R. A., and Warhaft, Z.: Statistics of small–scale velocity fluctuations and internal intermittency in marine stratocumulus clouds, J. Atmos. Sci., 67, 262–273, 2010.

Simoneit, B. R. T., Kobayashi, M., Mochida, M., Kawamura, K., Lee, M., Lim, H.-J., Turpin, B. J., and Komazaki, Y.: Composition and major sources of organic compounds of aerosol particulate matter sampled during the ACE-Asia campaign, J. Geophys. Res., 109, 2004.

Simpson, W. R., von Glasow, R., Riedel, K., Anderson, P., Ariya, P., Bottenheim, J., Burrows, J., Carpenter, L. J., Friess, U., Goodsite, M. E., Heard, D., Hutterli, M., Jacobi, H.-W., Kaleschke, L., Neff, B., Plane, J., Platt, U., Richter, A., Roscoe, H., Sander, R., Shepson, P., Sodeau, J., Steffen, A., Wagner, T., and Wolff, E.: Halogens and their role in polar boundary–layer ozone depletion, Atmos. Chem. Phys., 7, 4375–4418, 2007.

Sinkevich, A. A. and Lawson, R. P.: A survey of temperature measurements in convective clouds, J. Appl. Meteor., 44, 1133–1145, 2005.

Sinnerwalla, A. and Alofs, D.: A cloud nucleus counter with long available growth time, J. Appl. Meteorol., 12, 831–835, 1973.

Sipila, M., Lehtipalo, K., Kulmala, M., Petäjä, T., Junninen, H., Aalto, P. P., Manninen, H. E., Kyrö, E.-M., Asmi, E., Riipinen, I., Curtius, J., Kürten, A., Borrmann, S., and O'Dowd, C. D.: Applicability of condensation particle counters to measure atmospheric clusters, Atmos. Chem. Phys., 8, 4049–4060, 2008.

Sipila, M., Lehtipalo, K., Attoui, M., Neitola, K., Petaja, T., Aalto, P. P., O'Dowd, C. D., and Kulmala, M.: Laboratory Verification of PH–CPC's Ability to Monitor Atmospheric Sub–3 nm Clusters, Aerosol Sci. Tech., 43, 126–135, 2009.

Sipila, M., Berndt, T., Petaja, T., Brus, D., Vanhanen, J., Stratmann, F., Patokoski, J., Mauldin, R. L., Hyvarinen, A. P., Lihavainen, H., and Kulmala, M.: The Role of Sulfuric Acid in Atmospheric Nucleation, Science, 327, 1243–1246, 2010.

Skoog, D., West, D., Holler, J., and Crouch, S.: Fundamentals of Analytical Chemistry, vol. 8, Brooks / Cole Publishing Company, 2003.

Slusher, D., Slusher, D., Huey, L., Tanner, D., Flocke, F., and Roberts, J.: A thermal dissociation–chemical ionization mass spectrometry (TD–CIMS) technique for the simultaneous measurements of peroxyacyl nitrates and dinitrogen pentoxide, J. Geophys. Res., 109, doi:10.1029 / 2004JD004670, 2004.

Slusher, D. L., Pitteri, S. J., Haman, B. J., Tanner, D. J., and Huey, L. G.: A chemical ionization technique for measurement of pernitric acid in the upper troposphere and the polar boundary layer, Geophys. Res. Lett., 28, 3875–3878, 2001.

Smit, H., Volz–Thomas, A., Helten, M., Pätz, H., and Kley, D.: An in–flight calibration method for near real–time humidity measurements with the airborne MOZAIC sensor, J. Atmos. Oceanic Technol., 25, 656–666, 2008.

Smith, G. E.: The Invention of the CCD, Nuclear Instr. Methods Phys. Res., 471, 1–5, 2001.

Smith, M., Roberts, D., Shipman, H., Adams, J., Willis, S., and Gillespie, A.: Calibrating AIS images using the surface as a reference, in Proceedings of the 3rd Airborne Imaging Spectrometer Workshop, edited by R. Green, pp. 63–69, 1987.

Snider, J., Petters, M., Wechsler, P., and Liu, P.: Supersaturation in the Wyoming CCN Instrument, J. Atmos. Oceanic Technol., 23, 1323–1339, 2006.

Snider, J. R. and Brenguier, J.-L.: A comparison of cloud condensation nuclei and cloud droplet measurements obtained during ACE-2, Tellus, 52, 828–842, ser. B, 2000.

Snider, J. R., Guibert, S., Brenguier, J.-L., and Putaud, J.-P.: Aerosol activation in marine stratocumulus clouds: 2. Köhler and parcel theory closure studies, J. Geophys. Res., 108, 2003.

Soderman, P., Hazen, N., and Brune, W.: Aerodynamic design of gas and aerosol samplers for aircraft, http://ntrs.nasa.gov/, nASA Technical Memorandum 103854, Report Number: A–91110, NAS 1.15:103854, 1991.

Solberg, S., Dye, C., Schmidbauer, N., Herzog, A., and Gehrig, R.: Carbonyls and nonmethane hydrocarbons at rural European sites from the Mediterranean to the Arctic, J. Atmos. Chem., 25, 33–66, 1996a.

Solberg, S., Schmidbauer, N., Semb, A., and Hov, O.: Boundary layer ozone depletion as seen in the Norwegian Arctic spring, J. Atmos. Chem., 25, 301–322, 1996b.

Solomon, S., Borrmann, S., Garcia, R., Portmann, R., Thomason, L., Poole, L., Winker, D., and McCormick, M.: Heterogeneous chlorine chemistry in the tropopause region, J. Geophys. Res. D: Atmos., 102, 21 411–21 429, 1997.

Sonntag, D.: Advancements in the field of hygrometry, Meteorol. Z., N.F.3, 51–66, 1994.

Sorooshian, A., Brechtel, F. J., Ma, Y. L., Weber, R. J., Corless, A., Flagan, R. C., and Seinfeld, J. H.: Modeling and characterization of a particle–into–liquid sampler (PILS), Aerosol Sci. Technol., 40, 396–409, 2006.

Sorooshian, A., Lu, M. L., Brechtel, F. J., Jonsson, H., Feingold, G., Flagan, R. C., and Seinfeld, J. H.: On the source of organic acid aerosol layers above clouds, Environ. Science Tech., 41, 4647–4654, 2007.

Spanel, P., Dryahina, K., and Smith, D.: Microwave plasma ion sources for selected ion flow tube mass spectrometry: Optimizing their performance and detection limits for trace gas analysis, Int. J. Mass Spectrom., 267, 117–124, 2007.

Speidel, M., Nau, R., Arnold, F., Schlager, H., and Stohl, A.: Sulfur dioxide measurenments in the lower, middle and upper troposphere: deployment of an aircraft–based chemical ionization mass spectrometer with permanent in–flight calibration, Atmos. Environm., 41, 2427–2437, 2007.

Spek, A. L. J., Unal, C. M. H., Moisseev, D. N., Russchenberg, H., Chandrasekar, V., and Dufournet, Y.: A new technique to categorize and retrieve the microphysical properties of ice particles above the melting layer using radar dual–polarization spectral analysis, J. Atmos. Oceanic Technol., 25, 482–497, 2008.

Spinhirne, J., Hansen, M., and Caudill, L.: Cloud top remote sensing by airborne lidar, Appl. Opt., 21, 1564–1571, 1982.

Spinhirne, J., Boers, R., and Hart, W. D.: Cloud top liquid water from lidar observations of marine stratocumulus, J. Appl. Meteor., 28, 81–90, 1989.

Spinhirne, J., Hart, W., and Hlavka, D.: Cirrus infrared parameters and shortwave reflectance relations from observations, J. Atmos. Sci., 53, 1438–1458, 1996.

Spinhirne, J., Chudamani, S., Cavanaugh, J., and Bufton, J.: Aerosol and cloud backscatter at 1.06, 1.54, and 0.53 μm by airborne hard–target–calibrated Nd:YAG / methane Raman lidar, Appl. Opt., 36, 3475–3490, 1997.

Sprung, D., Jost, C., Reiner, T., Hansel, A., and Wisthaler, A.: Acetone and acetonitrile in the tropical Indian Ocean boundary layer and free troposphere: Aircraft–based intercomparison of AP–CIMS and PTR–MS measurements, J. Geophys. Res. D: Atmos., 106, 28 511–28 527, 2001.

Spuler, S., Richter, D., Spowart, M., and Rieken, K.: Optical fiber–based laser remote sensor for airborne measurement of wind velocity and turbulence, Appl. Opt., 50, 842–851, 2011.

Spyres–Duran, P.: Measuring the Size, Concentration, and Structural Properties of Hydrometeors in Clouds With Impactor and Replicating Devices, Atmospheric Technology, pp. 3–9, national Center for Atmospheric Research, Boulder, Colorado 80307-3000, 1976.

Squires, P. and Twomey, S.: A comparison of cloud nucleus measurements over central North America and the Caribbean Sea, J. Atmos. Sci., 22, 401–404, 1966.

Srivastava, R. C., Matejka, T. J., and Lorello, T. J.: Doppler Radar Study of the Trailing Anvil Region Associated with a Squall Line, J. Atmos. Sci., 43, 356–377, 1986.

St Clair, J., Hanisco, T., Weinstock, E., Moyer, E., Sayres, D., Keutsch, F., Kroll, J. H., Demusz, J. N., Allen, N. T., Smith, J., Spackman, J., and Anderson, J. G.: A new photolysis laser-induced fluorescence instrument for the detection of H2O and HDO in the lower stratosphere, Rev. Sci. Instr., 79, Art. No. 064 101, 2008.

Stackhouse, P. and Stephens, G.: A theoretical and observational study of the radiative properties of cirrus: Results from FIRE 1986, J. Atmos. Sci., 48, 2044–2059, 1991.

Staenz, K.: Terrestrial Imaging Spectroscopy, Some future perspectives, in Proceedings of the 6th EARSEL SIG IS, p. 12, Tel Aviv, 2009.

Stallabrass, J.: An appraisal of the single rotating cylinder method of liquid water content measurement, Tech. Rep. LTR–LT–92, NRC Canada, 1978.

Stankov, B., Cline, D., Weber, B., Gasiewski, A., and Wick, G.: High–resolution airborne polarimetric microwave imaging of snow cover during the NASA cold land processes experiment, IEEE Trans. Geosci. Remote Sens., 8, 1635–1671, 2008.

Stark, H., Lerner, B., Schmitt, R., Jakoubek, R., Williams, E., Ryerson, T., Sueper, D., Parrish, D., and Fehsenfeld, F.: Atmospheric in situ measurement of nitrate radical (NO_3) and other photolysis rates using spectroradiometry and filter radiometry, J. Geophys. Res., 112, doi:10.1029/2006JD007578, 2007.

Stedman, D. H., Daby, E. E., Stuhl, F., and Niki, H.: Analysis of Ozone and Nitric Oxide by a Chemiluminescent Method in Laboratory and Atmospheric Studies of Photochemical Smog, J. Air Pollut. Contr. Assoc., 22, 260–263, 1972.

Steeghs, M. M. L., Sikkens, C., Crespo, E., Cristescu, S. M., and Harren, F. J. M.: Development of a proton–transfer reaction ion trap mass spectrometer: Online detection and analysis of volatile organic compounds, Int. J. Mass Spectrom., 262, 16–24, 2007.

Steffenson, D. and Stedman, D.: Optimisation of the parameters of chemiluminescent nitric oxide detectors, Anal. Chem., 46, 1704–1709, 1974.

Steinbacher, M., Dommen, J., Ammann, C., Spirig, C., Neftel, A., and Prevot, A. S. H.: Performance characteristics of a proton–transfer–reaction mass spectrometer (PTR–MS) derived from laboratory and field measurements, Int. J. Mass Spectrom., 239, 117–128, 2004.

Stephens, M., Turner, N., and Sandberg, J.: Particle identification by laser–induced incandescence in a solid–state laser cavity, Appl. Opt., 42, 3726–3736, 2003.

Stetzer, O., Baschek, B., Lüönd, F., and Lohmann, U.: The Zurich Ice Nucleation Chamber (ZINC)–A New Instrument to Investigate Atmospheric Ice Formation, Aerosol Sci. Technol., 42, 64–74, 2008.

Stevens, A., van Wesemael, B., Bartholomeus, H., Rosillon, D., B., T., and Ben-Dor, E.: Laboratory, Field and Airborne Spectroscopy for monitoring Organic Carbon Content in Agricultural Soils, Geoderma, 144, 395–40, 2008.

Stevens, B., Lenschow, D., Vali, G., Gerber, H., Bandy, A., Blomquist, B., Brenguier, J.-L., Bretherton, C., Burnet, F., Campos, T., Chai, S., Faloona, I., Friesen, D., Haimov, S., Laursen, K., Lilly, D., Loehrer, S., Malinowski, S., Morley, B., Petters, M., Rogers, D., Russell, L., Savic-Jovcic, V., Snider, J., Straub, D., Szumowski, M., Takagi, H., Thornton, D., Tschudi, M., Twohy, C., Wetzel, M., and van Zanten, M.: Dynamics and chemistry of marine stratocumulus - DYCOMS-II, Bull. Amer. Meteorol. Soc., 84, 579–593, 2003.

Stewart, D. J., Taylor, C. M., Reeves, C. E., and McQuaid, J. B.: Biogenic nitrogen oxide emissions from soils: impact on NO_x and ozone over west Africa during AMMA (African Monsoon Multidisciplinary Analysis: observational study, Atmos. Chem. Phys., 8, 2285–2297, 2008.

Stickler, A., Fischer, H., Williams, J., de Reus, M., Sander, R., Lawrence, M., Crowley, J., and Lelieveld, J.: Influence of summertime deep convection on formaldehyde in the middle and upper troposphere over Europe, J. Geophys. Res., 111, doi:10.1029/2005JD007001, 2006.

Stickney, T., Shedlov, M., and Thompson, D.: Total temperature sensors, Tech. Rep. 5755, Revision C, Rosemount Aerospace, Eagan, MN, USA, 1994.

Stimpfle, R. M. and Anderson, J.: In–situ detection of oh in the lower stratosphere with a balloon borne high repetition rate laser system, Geophys. Res. Lett., 15, 1503–1506, 1988.

Stimpfle, R. M., Cohen, R., Bonne, G., Voss, P., Perkins, K., Koch, L., Anderson, J., Salawitch, R., Lloyd, S., Gao, R., Negro, L. D., Keim, E., and Bui, T.: The coupling of $ClONO_2$, ClO, and NO_2 in the lower stratosphere from in situ observations using the NASA ER–2 aircraft, J. Geophys. Res. D: Atmos., 104, 26 705–26 714, 1999.

Stimpfle, R. M., Wilmouth, D., Salawitch, R., and Anderson, J.: First measurements of ClOOCl in the stratosphere: The coupling of ClOOCl and ClO in the Arctic polar vortex, J. Geophys. Res. D: Atmos., 109, 2004.

Stolzenburg, M.: An ultrafine aerosol size distribution measuring system, Ph.D. thesis, Department of Mechanical Engineering, University of Minnesota, 1988.

Stolzenburg, M. R. and McMurry, P. H.: An ultrafine aerosol condensation nucleus counter, Aerosol Sci. Tech., 14, 48–65, 1991.

Stone, R., Herber, A., Vitale, V., Mazzola, M., Lupi, A., Schnell, R., Dutton, E., Liu, P., Li, S.-M., Dethloff, K., Lampert, A., Ritter, C., Stock, M., Neuber, R., and Maturilli, M.: A three-dimensional characterization of Arctic aerosols from airborne Sun photometer observations: PAN-ARCMIP, April 2009, J. Geophys. Res., D13203, doi:10.1029/2009JD013605, 2010.

Straka, J. M., Zrnic, D. S., and Ryzhkov, A. V.: Bulk Hydrometeor Classification and Quantification Using Polarimetric Radar Data: Synthesis of Relations, J. Appl. Meteor., 39, 1341–1372, 2000.

Strapp, J., Albers, F., Reuter, A., Korolev, A., Maixner, U., Rashke, E., and Vukovic, Z.: Laboratory Measurements of the Response of a PMS OAP–2DC, J. Atmos. Oceanic Technol., 18, 1150–1170, 2001.

Strapp, J., Oldenburg, J., Ide, R., Lilie, L., Bacic, S., Vukovic, Z., Oleskiw, M., Miller, D., Emery, E., and Leone, G.: Wind Tunnel Measurements of the Response of Hot–Wire Liquid Water Content Instruments to Large Droplets, J. Atmos. Oceanic Technol., 20, 791–806, 2002.

Strapp, J., Lilie, L., Emery, E., and Miller, D.: Preliminary Comparison of Ice Water Content as Measured by Hot Wire Instruments of Varying Configuration, in 43rd AIAA Aerospace Sciences Meeting, Reno, NV, AIAA-2005-0860, 2005.

Strapp, J., MacLeod, J., and Lilie, L.: Calibration of Ice Water Content in a Wind Tunnel/Engine Test Cell Facility, in 15th Intl. Conf. on Cloud and Precipitation, Cancun, Mexico, 2008.

Strapp, J. W., Leaitch, W. R., and Liu, P. S. K.: Hydrated and Dried Aerosol–Size–Distribution Measurements from the Particle Measuring Systems FSSP–300 Probe and the Deiced PCASP-100X Probe, J. Atmos. Oceanic Technol., 9, 548–555, 1992.

Stratmann, F., Hummes, D., Kauffeldt, T., and Fissan, H.: Convolution and its application to DMA transfer function measurements, J. Aerosol Sci., 26, S143–S144, 1995.

Strawa, A. W., Castaneda, R., Owano, T., Baer, D. S., and Paldus, B. A.: The measurement of aerosol optical properties using continuous wave cavity ring-down techniques, J. Atmos. Oceanic Technol., 20, 454–465, 2003.

Su, T. and Chesnavich, W. J.: Parametrization of the Ion–Polar Molecule Collision Rate–Constant by Trajectory Calculations, J. Chem. Phys., 76, 5183–5185, 1982.

Sugimoto, N. and Minato, A.: Long–path absorption measurement of CO_2 with a Raman–shifted tunable dye laser, Appl. Opt., 32, 6827–6833, 1993.

Sullivan, R. C., Moore, M. J. K., Petters, M. D., Kreidenweis, S. M., Roberts, G. C., and Prather, K. A.: Timescale for hygroscopic conversion of calcite mineral particles through heterogeneous reaction with nitric acid, Phys. Chem. Chem. Phys., 11, 7826–7837, 2009.

Sumner, D.: Calibration Methods for a Seven–Hole Pressure Probe, in Sixth Triennial International Symposium on Fluid Control, Measurement and Visualization (Flucome 2000), edited by A. Laneville, p. 6, Sherbrooke, Canada, 2000.

Super, A. B., Boe, B. A., Heimbach, J. A., McPartland, J. T., and Langer, G.: Comparison of silver iodide outputs from two different generators and solutions measured by acoustic ice nucleus counters, Journal of Weather Modification, in press, 2010.

Taipale, R., Ruuskanen, T. M., Rinne, J., Kajos, M. K., Hakola, H., Pohja, T., and Kulmala, M.: Technical Note: Quantitative long–term measurements of VOC concentrations by PTR–MS–measurement, calibration, and volume mixing ratio calculation methods, Atmos. Chem. Phys., 8, 6681–6698, 2008.

Takano, Y. and Liou, K.: Solar radiative transfer in cirrus clouds. Part I : single scattering and optical properties of hexagonal ice crystals, J. Atmos. Sci., 46, 3–19, 1989.

Takano, Y. and Liou, K.: Radiative transfer in cirrus clouds, J. Atmos. Sci., 52, 818–837, 1995.

Tammet, H., Mirme, A., and Tamm, E.: Electrical aerosol spectrometer of Tartu University, Atmos. Res., 62, 315–324, 2002.

Tanaka, M., Nakajima, T., and Shiobara, M.: Calibration of a sunphotometer by simultaneous measurements of direct–solar and circumsolar radiation, Appl. Opt., 25, 1170–1176, 1986.

Tanelli, S., Durden, S. L., Im, E., Pak, K., Reinke, D., Partain, P., Haynes, J., and Marchand, R.: Cloudsa's Cloud Profiling Radar after 2 years in orbit: Performance, external calibration, and processing, IEEE Transactions on Geoscience and Remote Sensing, 46, 3560–3573, 2008.

Tang, C. and Aydin, K.: Scattering from ice crystals at 94 and 220 GHz millimeter wave frequencies, IEEE Transactions on Geoscience and Remote Sensing, 33, 93–99, 1995.

Tanimoto, H., Aoki, N., Inomata, S., Hirokawa, J., and Sadanaga, Y.: Development of a PTR–TOFMS instrument for real–time measurements of volatile organic compounds in air, Int. J. Mass Spectrom., 263, 1–11, 2007.

Tanré, D., Herman, M., Deschamps, P., and Leffe, A.: Atmospheric modeling for space measurements of ground reflectances, including bidirectional properties, Appl. Opt, 18, 3587–3594, 1979.

Tanré, D., Deschamps, P., Duhaut, P., and Herman, M.: Adjacency effect produced by the atmospheric scattering in thematic mapper data, J. Geophys. Res., 92, 12 000–12 006, 1987.

Tanré, D., Haywood, J., Pelon, J., Léon, J., Chatenet, B., Formenti, P., Francis, P., Goloub, P., Highwood, E. J., and Myhre, G.: Measurement and modeling of the Saharan dust radiative impact : Overview of the Saharan Dust experiment (SHADE), J. Geophys. Res., 108, 8574, 2003.

Targ, R., Kavaya, M. J., Huffaker, R. M., and Bowles, R. L.: Coherent lidar airborne windshear sensor: performance evaluation, Appl. Opt., 30, 2013–2026, 1991.

Targ, R., Steakley, B. C., Hawley, J. G., Ames, L. L., Fomey, P., Swanson, D., Stone, R., Otto, R. G., Zarifis, V., Brockman, P., Calloway, R. S., Klein, S. H., and Robinson, P. A.: Coherent lidar airborne wind sensor II: flight–test results at 2 and 10 μm, Appl. Opt., 35, 7117–7127, 1996.

Tarnogrodzki, A.: Theoretical prediction of the critical Weber number, Int. J. Multiphas. Flow, 19, 329–336, 1993.

Telford, J. W. and Warner, J.: On the measurement from an aircraft of buoyancy and vertical air velocity in cloud, J. Atmos. Sci., 19, 415–423, 1962.

Testud, J., Hildebrand, P. H., and Lee, W.-C.: A procedure to correct airborne Doppler radar data for navigation errors using the echo returned from the Earth's surface, J. Atmos. Oceanic Tech., 12, 800–820, 1995.

Thomason, L., Herman, B., and Reagan, J.: The effect of atmospheric attenuators with structured vertical distributions on air mass determinations and Langley plot analyses, J. Atmos. Sci., 40, 1851–1854, 1983.

Thompson, B.: Holographic particle sizing techniques, J. Phys. E, 7, 781–788, 1974.

Thomson, D. S., Schein, M. E., and Murphy, D. M.: Particle analysis by laser mass spectrometry WB–57F instrument overview, Aerosol Sci. Technol., 33, 153–169, 2000.

Thornberry, T., Murphy, D. M., Thomson, D. S., de Gouw, J., Warneke, C., Bates, T. S., Quinn, P. K., and Coffman, D.: Measurement of Aerosol Organic Compounds Using a Novel Collection / Thermal–Desorption PTR–ITMS Instrument, Aerosol Sci. Technol., 43, 486–501, 2009.

Thornton, B. F., Toohey, D., Avallone, L., Harder, H., Martinez, M., Simpas, J., Brune, W., and Avery, M.: In situ observations of ClO near the winter polar tropopause, J. Geophys. Res. D: Atmos., 108, 2003.

Thornton, B. F., Toohey, D., Avallone, L., Hallar, A., Harder, H., Martinez, M., Simpas, J., Brune, W., Koike, M., Kondo, Y., Takegawa, N., Anderson, B., and Avery, M.: Variability of active chlorine in the lowermost Arctic stratosphere, J. Geophys. Res. D: Atmos., 110, 2005.

Thornton, J., Wooldridge, P., and Cohen, R.: Atmospheric NO_2: in situ laserinduced fluorescence detection at parts per trillion mixing ratios, Anal. Chem., 72, 528–539, 2000.

Thurai, M., Huang, G. J., and Bringi, V. N.: Drop shapes, model comparisons, and calculations of polarimetiric radar parameters in rain, J. Atmos. Oceanic Tech., 24, 1019–1032, 2007.

Tian, L., Heymsfield, G. M., Li, L., and Srivastava, R.: Properties of light stratiform rain derived from 10 and 94 GHz airborne Doppler radars measurements, J. Geophys. Res., 112, 2007.

Timko, M., Yu, Z., Kroll, J., Jayne, J., Worsnop, D., Miake–Lye, R., Onasch, T., Liscinsky, D., Kirchstetter, T., Destaillats, H., Holder, A., Smith, J., , and Wilson, K.: Sampling artifacts from Conductive Silicone Tubing, Aerosol Sci. Technol., 43, 855–865, doi:10.1080/02786820902984811, 2009.

Tinel, C., Testud, J., Pelon, J., Protat, R. H. A., Delanoë, J., and Bouniol, D.: The retrieval of ice–cloud properties from cloud radar and lidar synergy, J. Appl. Meteorol., 44, 860–875, 2005.

Tokay, A., Hartmann, P., Battaglia, A., Gage, K. S., Clark, W. L., and Williams, C. R.: A Field Study of Reflectivity and Z–R Relations Using Vertically Pointing Radars and Disdrometers, J. Atmos. Oceanic Technol., 26, 1120–1134, 2009.

Toohey, D. W., Avallone, L., Allen, N., Demusz, J., Hazen, J., Hazen, N., and Anderson, J.: The Performance of a New Instrument For In–Situ Measurements of ClO in the Lower Stratosphere, Geophys. Res. Lett., 20, 1791–1794, 1993.

Torgeson, W. L. and Stern, S.: An aircraft impactor for determining the size distributions of tropospheric aerosol, J. Appl. Meteo., 5, 205–210, 1966.

Trolinger, J.: Particle field holography, Opt. Eng., 14, 383–392, 1975.

Turner, D., Caddedu, M., Löhnert, U., Crewell, S., and Vogelmann, A.: Modifications to the water vapor continuum in the microwave suggested by ground–based 150 GHz observations, IEEE Geosc. Rem. Sens., 47, 3326–3337, DOI10.1109 / TGRS.2009.2022262, 2009.

Twohy, C.: Model calculations and wind tunnel testing of an isokinetic shroud for high-speed sampling, Aerosol Sci. Technol., 29, 261–280, 1998.

Twohy, C. and Rogers, D.: Airflow and water drop trajectories at instrument sampling points around the Beechcraft King Air and Lockheed Electra, J. Atmos. Oceanic Technol., 10, 566–578, 1993.

Twohy, C., Schanot, A., and Cooper, W.: Measurement of condensed water content in liquid and ice clouds using an airborne counterflow virtual impactor, J. Atmos. Oceanic Technol., 14, 197–202, 1997.

Twohy, C., Strapp, J., and Wendisch, M.: Performance of a Counterflow Virtual Impactor in the NASA Icing Research Tunnel, J. Atmos. Oceanic Technol., 20, 781–790, 2003.

Twomey, S.: The influence of cloud nucleus population on the microstructure and stability of convective clouds, Tellus, 11, 408–411, 1959.

Twomey, S.: On the composition of cloud nuclei in North–Eastern United States, J. Rech. Atmos., 4, 281–285, 1968.

Twomey, S.: Pollution and the planetary albedo, Atmos. Environm., 8, 1251–1256, 1974.

Twomey, S.: Comparison of constrained linear inversion and an iterative nonlinear algorithm applied to the indirect estimation of particle size distributions, J. Comput. Phys., 18, 188–200, 1975.

Twomey, S. and Wojciechowski, T.: Observations of the geographic variations of cloud nuclei, J. Atmos. Sci., 26, 684–688, 1969.

Uchiyama, A., Yamazaki, A., Matsuse, K., and Kobayashi, E.: Broadband shortwave calibration results for East Asian Regional Experiment 2005, J. Geophys. Res., 112, D22S34, doi:10.1029 / 2006JD008110, 2007.

Uhlig, E., Borrmann, S., and Jaenicke, R.: Holographic in–situ measurements of the spatial droplet distribution in stratiform clouds, Tellus, 50B, 377–387, 1998.

Ulaby, F. T., Moore, R. K., and Fung, K.: Microwave Remote Sensing: Active and Passive, vol. 1 and 2, Addison–Wesley, Advanced Book Program, Reading, Massachusetts, 456 pp., 1981.

Ulanowski, Z., Hesse, E., Kaye, P., and Baran, A.: Light scattering by complex ice-analogue crystals, J. Quant. Spectrosc. Radiat. Transfer, 100, 382–392, 2006.

Ungar, S., Middleton, E., Ong, L., and Campbell, L. P.: EO–1 Hyperion onboard performance over eight years: Hyperion calibration, in Proceedings of the 6th EARSeL SIG IS, p. 7, Tel Aviv, 2009.

Ustin, S., Roberts, D., Gamon, J., Asner, G., and Green, R.: Using Imaging Spectroscopy to Study Ecosystem Processes and Properties, BioScience, pp. 523–534, 2008.

Valero, F., Gore, W., and Giver, L.: Radiative flux measurements in the troposphere, Appl. Opt., 21, 831–838, 1982.

Valero, F., Ackerman, T., and Gore, W.: The effects of the Arctic haze as determined from airborne radiometric measurements during AGASP II, J. Atmos. Chem., 9, 225–244, 1989.

Valero, F., Bucholtz, A., Bush, B., Pope, S., Collins, W., and Flatau, P.: Atmospheric Radiation Measurements Enhanced Shortwave Experiment (ARESE): Experimental and data details, J. Geophys. Res., 102, 29 929–29 937, 1997a.

Valero, F., Bucholtz, A., Bush, B., Pope, S., Collins, W., Flatau, P., Strawa, A., and Gore, W.: Atmospheric Radiation Measurements Enhanced Shortwave Experiment (ARESE): Experimental and data details, J. Geophys. Res., 102(D25), 29 929–29 937, 1997b.

Valero, F., Pope, S., Bush, B., Nguyen, Q., Marsden, D., Ces, R., Leitner, A., Bucholtz, A., and Udelhofen, P.: Absorption of solar radiation by the clear and cloudy atmosphere during the Atmosphereic Radiation Measurement Enhanced Shortwave Experiments (ARESE) I and II: Observations and models, J. Geophys. Res., 108, doi:10.1029 / 2001JD001384, 2003.

Vali, G.: Nucleation terminology, J. Aerosol Sci., 16, 575–576, 1985.

Vali, G. and Haimov, S.: Observed extinction by clouds at 95 GHz, IEEE Transactions on Geoscience and Remote Sensing, 39, 190–193, 2001.

Vali, G., Kelly, R. D., Pazmany, A., and McIntosh, R. E.: Airborne RADAR and in-situ observations of a shallow stratus with drizzle., Atmos. Res., 38, 361–380, 1995.

Van Baelen, J., Tridon, F., and Pointin, Y.: Simultaneous X–band and K–band study of precipitation to derive specific $Z - R$ relationships, Atmos. Res., 94, 596–605, 2009.

van de Hulst, H.: Light Scattering by Small Particles, Wiley, New York, 1957.

van de Hulst, H.: Light scattering by small particles, Dover Publications, pp.13-249, 1981.

van den Kroonenberg, A. C.: Airborne Measurement of Small–Scale Turbulence with special regard to the Polar Boundary Layer, no. 2009-11 in ZLR-Forschungsbericht, Sierke Verlag, Technische Universität Braunschweig, ISBN 13: 978–3–86844–216-8, 136 pp., 2009.

van den Kroonenberg, A. C., Martin, T., Buschmann, M., Bange, J., and Vörsmann, P.: Measuring the Wind Vector Using the Autonomous Mini Aerial Vehicle M^2AV, J. Atmos. Oceanic Technol., 25, 1969–1982, 2008.

van der Meer, F. and Jong, S. D.: Imaging Spectrometry: Basic Principles and Prospective Applications, Kluwer Academic Publishers, Dordrecht, The Netherlands, 451 pp, 2001.

van Overeem, M. A.: A sampling apparatus for aeroplankton, in Proceedings, vol. 39, pp. 1–11, Koninklijke Akademie van Wetenschappen te Amsterdam, 1936.

Vane, G., ed.: Airborne Imaging Spectrometry, Special Issue, vol. 44 (117–356), check appearance of this reference, different entry type may be neccessary, 1993.

Vane, G. and Goetz, A.: Terrestrial imaging spectroscopy, Remote Sens. Environ., 1, 3–15, 1988.

Varma, R. M., Venables, D., Ruth, A., Heitmann, U., Schlosser, E., and Dixneuf, S.: Long optical cavities for open–path monitoring of atmospheric trace gases and aerosol extinction, Appl. Opt., 48, B159–B171, 2009.

Vay, S. A., Anderson, B., Thornhill, H., and Hudgins, C.: An assessment of aircraft-generated contamination on in situ trace gas measurements: determinations from empirical data acquired aloft, J. Atmos. Oceanic Technol., 20, 1478–1487, 2003.

Veres, P., Roberts, J. M., Warneke, C., Welsh-Bon, D., Zahniser, M., Herndon, S., Fall, R., and de Gouw, J.: ment of negative–ion proton–transfer chemical–ionization mass spectrometry (NI–PT–CIMS) for the measurement of gas–phase organic acids in the atmosphere, Int. J. Mass Spectrom., 274, 48–55, 2008.

Vermote, E., Tanré, D., Deuzé, J., Herman, M., Morcette, J., and Kotchenova, S.: Second simulation of the satellite signal in the solar spectrum–vector (6sv), Tech. rep., Dept. of Geography, Univ. of Maryland, 2006.

Vidaurre, G. and Hallett, J.: Particle impact and breakup in aircraft measurements, J. Atmos. Oceanic Technol., 26, 972–983, doi:10.1175/2008JTECHA1147.1, 2009a.

Vidaurre, G. and Hallett, J.: Ice and water content of stratiform mixed phase cloud, Quarterly Journal of the Royal Meteorological Society, 135, 1292–1306, 2009b.

Viggiano, A.: In–situ mass spectrometry and ion chemistry in the stratosphere and troposphere, Mass Spectrom. Rev., 12, 115–137, 1993.

Villani, P., Picard, D., Marchand, N., and Laj, P.: Design and validation of a Volatility Tandem Differential Mobility Analyzer (VTDMA), Aerosol Sci. Technol, 41, 898–906, 2007.

Vincent, J. H.: Aerosol Sampling–Science, Standards, Instrumentation and Applications, John Wiley and Sons, New York, 636 pp., 2007.

Virkkula, A.: Correction of the Calibration of the 3–wavelength Particle Soot Absorption Photometer (3 PSAP), Aerosol Sci. Technol., 44, 706–712, 2010.

Virkkula, A., Ahlquist, N. C., Covert, D. S., Arnott, W. P., Sheridan, P. J., Quinn, P. K., and Coffman, D. J.: Modification, Calibration and a Field Test of an Instrument for Measuring Light Absorption by Particles, Aerosol Sci. Technol., 39, 68–83, 2005.

Vivekanandan, J., Oye, R., Zrnic, D. S., Ellis, S. M., Ryzhkov, A., and Straka, J.: Cloud microphysics retrival using S–band dual–polarization radar measurements, Bull. Am. Meteorol. Soc., 80, 381–388, 1999.

Voigt, C., Schlager, H., Luo, B., Dornbrack, A., Roiger, A., Stock, P., Curtius, J., Vossing, H., Borrmann, S., Davies, S., Konopka, P., Schiller, C., Shur, G., and Peter, T.: Nitric Acid Trihydrate (NAT) formation at low NAT supersaturation in Polar Stratospheric Clouds (PSCs), Atmos. Chem. Phys., pp. 1371–1380, 2005.

Volz, A. and Kley, D.: A resonance fluorescence instrument for the in–situ measurement of atmospheric carbon monoxide, J. Atmos. Chem., 2, 345–357, 1985.

Volz–Thomas, A., Arnold, T., Behmann, T., Borrell, P., Borrell, P., Burrows, J., Cantrell, C., Carpenter, L., Clemitshaw, K., Gilge, S., Heitlinger, M., Kluepfel, T., Kramp, F., Mihelcic, D., Muesgen, P., Paetz, H., Penkett, S., Perner, D., Schultz, M., Shetter, R., Slemr, J., and Weissenmayer, M.: Peroxy Radical InterComparison Exercise. A formal comparison of methods for ambient measurements of peroxy radicals, Berichte des Forschungszentrums Juelich, Institute fuer Chemie und Dynamik der Geosphaere–2, iSSN 0944–2952, 1998.

Volz–Thomas, A., Berg, M., Heil, T., Houben, N., Lerner, A., Petrick, W., Raak, D., and Pätz, H.-W.: Measurements of total odd nitrogen (NO_y aboard MOZAIC in–service aircraft: instrument design, operation and performanc, Atmos. Chem. Phys., 5, 583–595, 2005.

Volz-Thomas, A., Lerner, A., Paetz, H.-W., Schultz, M., McKenna, D., Schmitt, R., Madronich, S., and Roeth, E.: Airborne measurements of the photolysis of NO_2, J. Geophys. Res., 101, 18 613–18 627, 1996.

von der Weiden, S.-L., Drewnick, F., and Borrman, S.: Particle Loss Calculator– a new software tool for the assessment of the performance of aerosol inlet system, Atmos. Meas. Tech., 2, 479–494, 2009.

Von Hobe, M., Grooss, J., Muller, R., Hrechanyy, S., Winkler, U., and Stroh, F.: A re–evaluation of the ClO / Cl_2O_2 equilibrium constant based on stratospheric in–situ observations, Atmos. Chem. Phys., 5, 693–702, 2005.

Von Hobe, M., Ulanovsky, A., Volk, C., Grooss, J., Tilmes, S., Konopka, P., Gunther, G., Werner, A., Spelten, N., Shur, G., Yushkov, V., Ravegnani, F., Schiller, C., Muller, R., and Stroh, F.: Severe ozone depletion in the cold Arctic winter 2004–05, Geophys. Res. Lett., 33, 2006.

Von Hobe, M., Grooss, J.-U., Günther, G., Konopka, P., Gensch, I., Krämer, M., Spelten, N., Afchine, A., Schiller, C., Ulanovsky, A., Sitnikov, N., Shur, G., Yushkov, V., Ravegnani, F., Cairo, F., Roiger, A., Voigt, C., Schlager, H., Weigel, R., Frey, W., Borrmann, S., Müller, R., and Stroh, F.: Evidence for heterogeneous chlorine activation in the tropical UTLS, Atmos. Chem. Phys., 11, 241–256, 2011.

Voutilainen, A., Kolehmainen, V., and Kaipio, J. P.: Statistical inversion of aerosol size measurement data, Inverse Problems in Engineering, 9, 67–94, 2001.

Wahner, A., Callies, J., Dorn, H.-P., Platt, U., and Schiller, C.: Near UV atmospheric absorption measurements of column abundances during airborne arctic stratospheric expedition, January–February 1989: 1. Technique and NO_2 observations, Geophys. Res. Lett., pp. 497–500, 1990.

Wallington, T. and Nielsen, O.: The Chemistry of Free Radicals. Peroxyl Radicals, chap. Peroxy radicals and the atmosphere, pp. 457–481, John Wiley, 1997.

Wang, J.: A fast integrated mobility spectrometer with wide dynamic size range: Theoretical analysis and numerical simulation, J. Aerosol Sci., 40, 890–906, 2009.

Wang, J. and Chang, C.: Applications of independent component analysis in endmember extraction and aboundance quantification for hyperspetrcal imagery, IEEE Transaction in Geoscience and Remote Sensing, pp. 2601–2616, 2006.

Wang, J., Flagan, R., and Seinfeld, J.: Diffusional losses in particle sampling systems containing bends and elbows, Aerosol Sci. Technol., 33, 843–857, 2002a.

Wang, J., Flagan, R. C., and Seinfeld, J. H.: Diffusional losses in particle sampling systems containing bends and elbows, J. Aerosol Sci., 33, 843–857, 2002b.

Wang, J., Racette, P., Piepmeier, J., Monosmith, B., and Manning, W.: Airborne CoSMIR observations between 50 and 183 GHz over snow-covered Sierra mountains, IEEE Trans. Geosci. Remote Sens., 55–61, doi: 10.1109/TGRS.2006.885410, 2007.

Wang, P., Richter, A., Bruns, M., Rozanov, V. V., Burrows, J. P., Heue, K.-P., Wagner, T., Pundt, I., and Platt, U.: Measurements of tropospheric NO_2 with an air-borne multi–axis DOAS instrument, Atmos. Chem. Phys., pp. 337–343, 2005a.

Wang, S. C. and Flagan, R. C.: Scanning electrical mobility spectrometer, Aerosol Sci. Technol., 13, 230–240, 1990.

Wang, Z.: A refined two-channel microwave radiometer liquid water path retrieval for cold regions by using multiple–sensor measurements, IEEE Geosc. & Remote Sens. Lett., 4, 2007.

Wang, Z. and Sassen, K.: Cloud type and macrophysical property retrieval using multiple remote sensors, J. Appl. Meteorol., 40, 1665–1682, 2001.

Wang, Z. and Sassen, K.: Cirrus cloud microphysical property retrieval using lidar and radar measurements. Part I: Algorithm description and comparison with in situ data, J. Atmos. Sci., 41, 218–229, 2002.

Wang, Z., Sassen, K., Whiteman, D. N., and Demoz, B.: Studying Altocumulus with ice virga using ground–based active and passive remote sensors, J. Appl. Meteor., 43, 449–460, 2004.

Wang, Z., Heymsfield, G., and Li., L.: Retrieving optically thick ice cloud microphysical properties by using airborne dual-wavelength radar measurements, J. Geophys. Res., 110, D19 201, 2005b.

Wang, Z. E., Wechsler, P., Kuestner, W., French, J., Rodi, A., Glover, B., Burkhart, M., and Lukens, D.: Wyoming cloud lidar: Instrument description and applications, Opt. Express, 17, 13 576–13 587, 2009.

Warhaft, Z.: Passive scalars in turbulent flows, Annu. Rev. Fluid Mech., 32, 203–240, 2000.

Warneck, P. and Zerbach, T.: Synthesis of peroxyacetyl nitrate in air by acetone photlysis, Environ. Science Tech., 26, 74–79, 1992.

Warneke, C., van der Veen, C., Luxembourg, S., de Gouw, J. A., and Kok, A.: Measurements of benzene and toluene in ambient air using proton–transfer–reaction mass spectrometry: calibration, humidity dependence, and field intercomparison, Int. J. Mass Spectrom., 207, 167–182, 2001.

Warneke, C., de Gouw, J. A., Lovejoy, E. R., Murphy, P. C., Kuster, W. C., and Fall, R.: Development of proton–transfer ion trap–mass spectrometry: On–line detection and identification of volatile organic compounds in air, J. Am. Soc. Mass. Spectrom., 16, 1316–1324, 2005a.

Warneke, C., Kato, S., De Gouw, J. A., Goldan, P. D., Kuster, W. C., Shao, M., Lovejoy, E. R., Fall, R., and Fehsenfeld, F. C.: Online volatile organic compound measurements using a newly developed proton–transfer ion–trap mass spectrometry instrument during New England Air Quality Study–Intercontinental Transport and Chemical Transformation 2004: Performance, intercomparison, and compound identification, Environ. Science Tech., 39, 5390–5397, 2005b.

Warneke, C., McKeen, S. A., de Gouw, J. A., Goldan, P. D., Kuster, W. C., Holloway, J. S., Williams, E. J., Lerner, B. M., Parrish, D. D., Trainer, M., Fehsenfeld, F. C., Kato, S., Atlas, E. L., Baker, A., and Blake, D. R.: Determination of urban volatile organic compound emission ratios and comparison with an emissions database, J. Geophys. Res. D: Atmos., 2007.

Washenfelder, R. A., Langford, A., Fuchs, H., and Brown, S.: Measurement of glyoxal using an incoherent broadband cavity enhanced absorption spectrometer, Atmos. Chem. Phys., 8, 7779–7793, 2008.

Wayne, R.: Chemical Instrumentation, Oxford University Press, 1994.

Wayne, R.: Chemistry of Atmospheres–Third Edition, Oxford University Press, ISBN 0 19 850375 X, 1999.

Weber, R., Clarke, A., Litchy, M., Li, J., Kok, G., Schillawski, R., and McMurry, P. H.: Spurious aerosol measurements when sampling from aircraft in the vicinity of clouds, J. Geophys. Res., 103, 28,337–28,346, 1998.

Weber, R., McMurry, P., Bates, T., Clarke, A., Covert, D., Brechtel, F., and Kok, G.: Intercomparison of airborne and surface-based measurements of condensation nuclei in the remote marine troposphere during ACE 1, J. Geophys. Res., pp. 21 673–21 683, 1999.

Weber, R. J., Orsini, D., Daun, Y., Lee, Y. N., Klotz, P. J., and Brechtel, F.: A particle–into–liquid collector for rapid measurement of aerosol bulk chemical composition, Aerosol Sci. Technol., 35, 718–727, 2001.

Webster, C. and Heymsfield, A.: Water Isotope Ratios D / H, $^{18}O\,/\,^{16}O$, $^{17}O\,/\,^{16}O$ in and out of clouds map dehydration pathways, Science, 302, 1742–1745, 2003.

Weckwerth, T., Parsons, D. B., Koch, S., Moore, J. A., LeMone, M. A., Demoz, B. B., Flamant, C., Geerts, B., Wang, J., and Feltz, W. F.: An overview of the International H_2O Project (IHOP_2002) and some preliminary highlights, Bull. Am. Meteorol. Soc., pp. 253–277, 2003.

Wehner, B., Philippin, S., and Wiedensohler, A.: Design and calibration of a thermodenuder with an improved heating unit to measure the size-dependent volatile fraction of aerosol particles, J. Aerosol Sci., 33, 1087–1093, 2002.

Weickman, H.: Formen und Bildung atmosphärischer Eiskristalle, Beitr. Physik. fr. Atmos., pp. 12–52, 1945.

Weickmann, H.: Die Eisphase in der Atmosphäre, Berichte des Deutschen Wetterdienstes in der US–Zone, Nr. 6, 1949.

Weickmann, H. and Kampe, H.: Physical properties of cumulus clouds, J. Meteorol., 10, 204–211, 1953.

Weigel, R., Hermann, M., Curtius, J., Voigt, C., Walter, S., Bottger, T., Lepukhov, B., Belyaev, G., and Borrmann, S.: Experimental characterization of the Condensation Particle counting System for high altitude aircraft–borne application, Atmos. Meas. Tech., 2, 243–258, 2009.

Weinheimer, A. and Schwiesow, R.: A two–path, two wavelength ultraviolet hygrometer, J. Atmos. Oceanic Technol., 9, 407–419, 1992.

Weinman, J. A. and Kim, M. J.: A simple model of the millimeter–wave scattering parameters of randomly oriented aggregates of finite cylindrical ice hydrometeors, J. Atmos. Sci., 64, 634–644, 2007.

Weinstock, E., Smith, J., Sayres, D., Spackman, J., Pittman, J., Allen, N., Demusz, J., Greenberg, M., Rivero, M., Solomon, L., and Anderson, J. G.: Measurements of the Total Water Content of Cirrus Clouds. Part I: Instrument Details and Calibration, J. Atmos. Oceanic Technol., 23, 1397–1409, 2006.

Weinstock, E. M., Hintsa, E. J., Dessler, A. E., Oliver, J. F., Hazen, N. L., Demusz, J. N., Allen, N. T., Lapson, L. B., and Anderson, J. G.: New fast response photofragment fluorescence hygrometer for use on the NASA ER-2 and the Perseus remotely piloted aircraft, Rev. Sci. Instrum., 65, 3544—3554, 1994.

Weinstock, E. M., Smith, J. B., Sayres, D. S., Pittman, J. V., Spackman, J. R., Hintsa, E. J., Hanisco, T. F., Moyer, E. J., Clair, J. M. S., Sargent, M. R., and Anderson, J. G.: Validation of the Harvard Lyman-α in situ water vapor instrument: Implications for the mechanisms that control stratospheric water vapor, J. Geophys. Res., 114, doi:10.1029/2009JD012427, 2009.

Weinzierl, B., Petzold, A., Esselborn, M., Wirth, M., Rasp, K., Kandler, K., Schütz, L., Koepke, P., and Fiebig, M.: Airborne measurements of dust layer properties, particle size distribution and mixing state of Saharan dust during SAMUM 2006, Tellus, 61B, 96–117, 2009.

Weiß, S.: Comparing Three Algorithms for Modeling Flush Air Data Systems, in AIAA Aerospace Sciences Meeting and Exhibit, 40th, AIAA–2002–535, Reno, NV, USA, 2002.

Weiß, S. and Leißling, D.: Flush Air Data System Verfahren zur Luftdatenbestimmung und Fehlererkennung, in DGLR Jahrestagung, Hamburg, Germany, 2001.

Weiß, S., Thielecke, F., and Harders, H.: Ein neuer Ansatz zur Modellierung von Luftdatensystemen, in Deutscher Luft– und Raumfahrtkongress / DGLR Jahrestagung, p. 7, Berlin, Germany, 1999.

Weissmann, M. and Cardinali, C.: Impact of airborne Doppler lidar observations on ECMWF forecasts, Quart. J. Roy. Meteorol. Soc., 133, 1107–116, 2007.

Weissmann, M., Busen, R., Dörnbrack, A., Rahm, S., and Reitebuch, O.: Targeted observations with an airborne wind lidar, J. Atmos. Oceanic Technol., 22, 1706–1719, 2005.

Weitkamp, C., ed.: Range–resolved optical remote sensing of the atmosphere, Springer, New York, 2005.

Wendel, G., Stedman, D., Cantrell, C., and Damrauer, L.: Luminol–based nitrogen dioxide detector, Anal. Chem., 55, 937, 1983.

Wendisch, M. and Keil, A.: Discrepancies between measured and modeled solar and UV radiation within polluted boundary layer clouds, J. Geophys. Res., 104, 27 373–27 385, 1999.

Wendisch, M. and Yang, P.: Theory of Atmospheric Radiative Transfer – A Comprehensive Introduction, Wiley–VCH Verlag GmbH & Co. KGaA, Weinheim, Germany, 2012.

Wendisch, M., Müller, D., Schell, D., and Heintzenberg, J.: An airborne spectral albedometer with active horizontal stabilization, J. Atmos. Oceanic Technol., 18, 1856–1866, 2001.

Wendisch, M., Garrett, T., and Strapp, J.: Wind tunnel tests of the airborne PVM–100A response to large droplets, J. Atmos. Oceanic Technol., 19, 1577–1584, 2002.

Wendisch, M., Coe, H., Baumgardner, D., Brenguier, J.-L., Dreiling, V., Fiebig, M., Formenti, P., Hermann, M., Krämer, M., Levin, Z., Maser, R., Mathieu, E., Nacass, P., Noone, K., Osborne, S., Schneider, J., Schütz, L., Schwarzenböck, A., Stratmann, F., and C., W. J.: Aircraft particle inlets: State-of-the-art and future needs, Bull. Amer. Meteorol. Soc., 85, 89–91, 2004.

Wennberg, P., Salawitch, R., Donaldson, D., Hanisco, T., Lanzendorf, E., Perkins, K., Lloyd, S., Vaida, V., Gao, R., Hintsa, E., Cohen, R., Swartz, W., Kusterer, T., and Anderson, D.: Twilight observations suggest unknown sources of HO_x, Geophys. Res. Lett., 26, 1373, 1999.

Wennberg, P. O., Cohen, R., Hazen, N., Lapson, L., Allen, N., Hanisco, T., Oliver, J., Lanham, N., Demusz, J., and Anderson, J.: Aircraft–borne, laser–induced fluorescence instrument for the in situ detection of hydroxyl and hydroperoxyl radicals, Rev. Sci. Instrum., 65, 1994a.

Wennberg, P. O., Cohen, R., Stimpfle, R., Koplow, J., Anderson, J., Salawitch, R., Fahey, D., Woodbridge, E., Keim, E., Gao, R., Webster, C., May, R., Toohey, D., Avallone, L., Proffitt, M., Podolske, J., Chan, K., and Wofsy, S.: Removal of stratospheric O_3 by radicals in–situ measurements of OH, HO_2, NO, NO_2, CLO, and BRO, Science, 266, 398–404, 1994b.

Wennberg, P. O., Hanisco, T., Cohen, R., Stimpfle, R., Lapson, L., and Anderson, J.: In–situ measurements of OH and HO_2 in the upper troposphere and stratosphere, J. Atmos. Sci., 52, 1995.

Werner, C., Flamant, P. H., Reitebuch, O., Köpp, F., Streicher, J., Rahm, S., Nagel, E., Klier, M., Hermann, H., Loth, C., Delville, P., Drobinski, P., Romand, B., Boitel, C., Oh, D., Lopez, M., Meissonnier, M., Bruneau, D., and Dabas, A. M.: Wind Infrared Doppler Lidar Instrument, Opt. Eng., 40, 115–125, 2001.

Wert, B. P., Fried, A., Henrym, B., and Cartier, S.: Evaluation of inlets used for the airborne measurement of formaldehyde, J. Geophys. Res., 107, doi: 0.1029 / 2001JD001072, 2002.

Westwater, E., Crewell, S., and Mätzler, C.: Surface–based microwave and millimeter wave radiometric remote sensing of the troposphere: a tutorial, IEEE Geosc. Rem. Sens. Lett., 2005.

Whalley, L., Lewis, A., McQuaid, J., Purvis, R., Lee, J., Stemmler, K., Zellweger, C., and Ridgeon, P.: Two high–speed, portable GC systems designed for the measurement of non–methane hydrocarbons and PAN: Results from the Jungfraujoch High Altitude Observatory, J. Environ. Monitor., 6, 234–241., 2004.

Whitmore, S., Lindsey, W. T., Curry, R., and Gilyard, G.: Experimental characterization of the effects of pneumatic tubing on unsteady pressure measurements, NASA Technical Memorandum 4171, 1990.

Wiedensohler, A.: An approximation of the bipolar charge distribution for particles in the submicron size range, J. Aerosol Sci., 19, 387–389, 1988.

Wiedensohler, A., Orsini, D., Covert, D. S., Coffmann, D., Cantrell, W., Havlicek, M., Brechtel, F. J., Russell, L. M., Weber, R. J., Gras, J., Hudson, J. G., and Litchy, M.: Intercomparison study of the size-dependent counting efficiency of 26 condensation particle counters, Aerosol Sci. Tech., 27, 224–242, 1997.

Wiederhold, P.: Water vapor measurement: methods and instrumentation, Marcel Dekker Inc., New York, 357 pp., 1997.

Wielicki, B., Suttles, J., Heymsfield, A., Welch, R., Spinhirne, J., Wu, M.-L., O'Starr, D., Parker, L., and Arduini, R.: The 27–28 October 1986 FIRE IFO cirrus case study: Comparison of radiative transfer theory with observations by satellite and aircraft, Mon. Wea. Rev., 118, 2356–2376, 1990.

Wieringa, J.: Roughness–Dependent Geographical Interpolation of Surface Wind Speed Averages, Q. J. R. Meteorol. Soc., 112, 867–889, 1986.

Williams, A. and Marcotte, D.: Wind Measurements on a Maneuvering Twin-Engine Turboprop Aircraft Accounting for Flow Distortion, J. Atmos. Oceanic Technol., 17, 795–810, 2000.

Williams, J.: Analytical Technique for Atmospheric Measurements, chap. Mass spectrometric methods for atmospheric trace gases, Blackwell Publishing Ltd., ISBN–13: 978–1–4051–2357–0, 2006.

Williams, J., Poschl, U., Crutzen, P. J., Hansel, A., Holzinger, R., Warneke, C., Lindinger, W., and Lelieveld, J.: An atmospheric chemistry interpretation of mass scans obtained from a proton transfer mass spectrometer flown over the tropical rainforest of Surinam, J. Climate, 38, 133–166, 2001.

Wilson, J., Lafleur, B., Hilbert, H., Seebaugh, W., Fox, J., Gesler, D., Brock, C., Huebert, B., and Mullen, J.: Function and performance of a low turbulence inlet for sampling supermicron particles from aircraft platforms, Aerosol Sci. Technol., 38, 790–802, 2004.

Wilson, J. C., Hyun, J. H., and Blackshear, E. D.: The Function and Response of an Improved Stratospheric Condensation Nucleus Counter, Journal of Geophysical Research-Oceans and Atmospheres, 88, 6781–6785, 1983.

Wilson, J. C., Stolzenburg, M., Loewenstein, W. C. M., Ferry, G., Chan, K. R., and Kelly, K. K.: Stratospheric sulfate aerosol in and near the northern–hemisphere polar vortex–the Morphology of the sulfate layer, multimodal size distributions, and the effect of denitrification, J. Geophys. Res., 97, 7997–8013, 1992.

Wilson, K. and Birks, J.: Mechanism and Elimination of a Water Vapour Interference in the Measurement of Ozone by UV Absorbance, Environ. Sci. Technol., 40, 6361–6367, 2006.

Wilson, S., Atkinson, N., and Smith, J.: The development of an airborne infrared interferometer for meteorological sounding studies, J. Atmos. Oceanic Technol., 16, 1912–1927, 1999.

Wirth, M., Fix, A., Mahnke, P., Schwarzer, H., Schrandt, F., and Ehret, G.: The airborne multi–wavelength water vapor differential absorption lidar WALES: system design and performance, Appl. Phys. B., 96, 201–213, 2009.

Wisthaler, A., Hansel, A., Dickerson, R. R., and Crutzen, P. J.: Organic trace gas measurements by PTR–MS during INDOEX 1999, J. Geophys. Res. D: Atmos., 107, 2002.

Wofsy, S.: HIAPER Pole–to–Pole Observations (HIPPO): fine–grained, global–scale measurements of climatically important atmospheric gases and aerosols, Phil. Trans. Royal Soc., A369, 2073–2086, dOI: 10.1098/rsta.2010.0313, 2011.

Wolde, M. and Vali, G.: Polarimetric signatures from ice crystals observed at 95 GHz in winter clouds: Part I. Dependence on crystal type, J. Atmos. Sci., 58, 828–841, 2001a.

Wolde, M. and Vali, G.: Polarimetric signatures from ice crystals observed at 95 GHz in winter clouds: Part II. Frequencies of occurrence, J. Atmos. Sci., 58, 842–849, 2001b.

Woodcock, A.: Atmospheric salt particles and raindrops, J. Meteorol., 9, 200–212, 1952.

Woodfield, A. A. and Vaughan, J. M.: Airspeed and wind shear measurements with an airborne CO_2 CW laser, Int. J. Aviation Safety, 1, 207–224, 1983.

World Meteorological Organization: SPARC Assessment of Upper Tropospheric and Stratospheric Water Vapor, Tech. Rep. WMO / TD–No.1043, World Climate Research Programme, Geneva, 2000.

World Meteorological Organization: Measurements of humidity. Guide to Meteorological Instruments and Methods of Observation, chap. 12. WMO No.8, World Meteorological Organization, Geneva, 7 edn., http://www.wmo.int/pages/prog/www/IMOP/publications/CIMO-Guide/CIMO_Guide-7th_Edition-2008.html, 2008.

Wörrlein, K.: Kalibrierung von Fünflochsonden, Tech. rep., Technische Universität Darmstadt, 1990.

Wu, J.: Mean square slopes of the wind-disturbed water surface, their magnitude, directionality, and composition, Radio Sci., 25, 37–48, 1990.

Wyche, K. P., Blake, R. S., Willis, K. A., Monks, P. S., and Ellis, A. M.: Differentiation of isobaric compounds using chemical ionization reaction mass spectrometry, Rapid Commun. Mass Spectrom., 19, 3356–3362, 2005.

Wyche, K. P., Blake, R. S., Ellis, A. M., Monks, P. S., Brauers, T., Koppmann, R., and Apel, E. C.: Technical note: Performance of Chemical Ionization Reaction Time–of–Flight Mass Spectrometry (CIR–TOF–MS) for the measurement of atmospherically significant oxygenated volatile organic compounds, Atmos. Chem. Phys., 7, 609–620, 2007.

Wylie, R., Davies, D., and Caw, W.: The basic process of the dew–point hygrometer, Humidity and Moisture, R.E. Ruskin, Ed., Reinhold, 1, 123–134, 1965.

Wyngaard, J. C.: Turbulence in the Atmosphere, Cambridge University Press, 408 p., 2010.

Wyngaard, J. T. and Zhang, S.-F.: Transducer–shadow effects on turbulence spectra measured by sonic anemometers, J. Atmos. Oceanic Technol., 2, 548–558, 1985.

Yang, P. and Liou, K.: Geometric–optics–integral–equation method for light scattering by nonspherical ice crystals, Appl. Opt., 35, 6568–6584, 1996.

Yang, P. and Liou, K.-N.: Single scattering properties of complex ice crystals in terrestrial atmosphere, Contr. Atmos. Phys., 71, 223–248, 1998.

Yarin, A.: Drop Impact Dynamics: Splashing, Spreading, Receding, Bouncing …, Annu. Rev. Fluid Mech., 38, 159–192, doi:10.1146/annurev.fluid.38.050304.092144, 2006.

Ye, J. and Hall, J.: Ultrasensitive detection in atomic and molecular physics: demonstration in molecular overtone spectroscopy, J. Opt. Soc. Am. B: Opt. Phys., 15, 6–15, 1998.

Yu, Y., Alexander, M., Perraud, V., Bruns, E., Johnson, S., Ezell, M., and Finlayson-Pitts, B.: Contamination from electrically conductive silicone tubing during aerosol chemical analysis, Atmos. Environ., 43, 2836–2839, doi: 10.1016/j.atmosenv. 2009.02.014, 2009.

Yum, S. and Hudson, J.: Maritime/continental microphysical contrasts in stratus, Tellus, 54B, 61–73, 2002.

Yushkov, V., Oulanovsky, A., Lechenuk, N., Roudakov, I., Arshinov, K., Tikhonov, F., Stefanutti, L., Ravegnani, F., Bonafe, U., and Georgiadis, T.: A chemiluminescent analyzer for stratospheric measurements of the ozone concentration (FOZAN), J. Atmos. Oceanic Technol., 16, 1345–1350, 1999.

Zabrodsky, G.: Measurements and some results of study of visibility in clouds. in "Study of clouds, precipitation and cloud electrification", Gidrometeizdat, 1957.

Zaer, A. and Gader, P.: Hyperspectral band selection and endmember detection using sparsity promoting priors, IEEE Transaction Geoscience and Remote Sensing Letters, 5, 256–260, 2008.

Zahn, A.: Constraints on 2–way transport across the Arctic tropopause based on O_3, stratospheric tracer (SF_6) ages, and water vapor isotope (D, T) tracers, J. Atmos. Chem., 39, 303–325, 2001.

Zahn, A., Barth, V., Pfeilsticker, K., and Platt, U.: Deuterium, oxygen–18, and tritium as tracers for water vapour transport in the lower stratosphere and tropopause region, J. Atmos. Chem., 30, 25–47, 1998.

Zahn, A., Brenninkmeijer, C., Crutzen, P., Parrish, D., Sueper, D., Heinrich, G., Güsten, H., Fischer, H., Hermann, M., and Heintzenberg, J.: Electrical discharge source for tropospheric 'ozone–rich transients', J. Geophys. Res., 107, (D22), 4638, doi: 10.1029/2002JD002345, 2002.

Zeng, T., Wang, Y., Chance, K., Blake, N., Blake, D., and Ridley, B.: Halogen–driven low–altitude O_3 and hydrocarbon losses in spring at northern high latitudes, J. Geophys. Res., 111, doi:10.1029/2005JD006706, 2006.

Zhang, N., Zhou, X., Shepson, P., Gao, H., Alaghmand, M., and Stirm, B.: Aircraft measurement of HONO vertical profiles over a forested region, Geophys. Res. Lett., 36, doi:10.1029/2009GL038999, 2009.

Zhang, S. H., Akutsu, Y., Russell, L. M., Flagan, R. C., and Seinfeld, J. H.: Radial differential mobility analyzer, Aerosol Sci. Technol., 23, 357–372, 1995.

Zhang, X. F., Smith, K. A., Worsnop, D. R., Jimenez, J., Jayne, J. T., and Kolb, C. E.: A numerical characterization of particle beam collimation by an aerodynamic lens–nozzle system: Part I. An individual lens or nozzle, Aerosol Sci. Technol., 36, 617–631, 2002.

Zhang, Z. Q. and Liu, B. Y. H.: Performance of Tsi 3760 Condensation Nuclei Counter at Reduced Pressures and Flow–Rates, Aerosol Sci. Tech., 15, 228–238, 1991.

Zhao, J. and Zhang, R. Y.: Proton transfer reaction rate constants between hydronium ion (H_3O_+) and volatile organic compounds, Atmos. Environm., 38, 2177–2185, 2004.

Ziereis, H., Schlager, H., Schulte, P., Köhler, I., Marquardt, R., and Feigl, C.: In situ observations of the NO_x distribution and variability over the eastern North Atlantic, J. Geophys. Res., 104, 16 021–16 032, 1999.

Ziereis, H., Schlager, H., Schulte, P., van Velthoven, P. F. J., and Slemr, F.: Distributions of NO, NO_x, and NO_y in the upper troposphere and lower stratospere between 28° and 61°N during POLINAT 2, J. Geophys. Res., 105, 3653–3664, 2000.

Ziereis, H., , Minikin, A., Schlager, H., Gayet, J.-F., Auriol, F., Stock, P., Baehr, J., Petzold, A., Schumann, U., Weinheimer, A., Ridley, B., and Ström, J.: Uptake of reactive nitrogen on cirrus cloud particles during INCA, Geophys. Res. Lett., 31, doi: 10.1029/2003GL018794, 2004.

Zimmermann, F., Ebert, M., Worringen, A., Schütz, L., and Weinbruch, S.: Environmental scanning electron microscopy (ESEM) as a new technique to determine the ice nucleation capability of individual atmospheric aerosol particles, Atmos. Environm., 41, 8219–8227, 2007.

Ziskind, G.: Particle resuspension from surfaces: Revisited and re–evaluated, Rev. Chem. Eng., 22, 1–123, 2006.

Zmarzly, P. and Lawson, R.: An Optical Extinctiometer for Cloud Radiation Measurements and Planetary Exploration. Final Report in fulfillment of Contract NAS5–98032, Tech. rep., NASA Goddard Space Flight Center, availablefromhttp://www.specinc.com/publications/Extinctiometer_Report.pdf, 131 pp., 2000.

Zöger, M., Afchine, A., Eicke, N., Gerhards, M.-T., Klein, E., McKenna, D., Mörschel, U., Schmidt, U., Tan, V., Tuitjer, F., Woyke, T., and Schiller, C.: Fast in situ stratospheric hygrometers: A new family of balloonborne and airborne Lyman–α photofragment fluorescence hygrometers, J. Geophys. Res., 104, 1807–1816, doi:10.1029/1998JD100025, 1999.

Zondlo, M., Mauldin, R., Kosciuch, E., Cantrell, C., and Eisele, F.: Development and characterization of an airborne–based instrument to measure nitric acid during the NASA Transport and Chemical Evolution over the Pacific field experiment, J. Geophys. Res., 108, 2003.

Zondlo, M., Paige, M., Massick, S., and Silver, J.: Vertical cavity laser hygrometer for the National Science Foundation Gulfstream-V aircraft, J. Geophys. Res., 115, D20309, doi:10.1029/2010JD014445, 2010.

Zuidema, P., Leon, D., Pazmany, A., and Cadeddu, M.: Aircraft millimeter-wave passive sensing of cloud liquid water and water vapor during VOCALS-REx, Atmos. Chem. Phys., 12, 355–369, 2012.

Index

Airborne Measurements for Environmental Research. Manfred Wendisch & Jean–Louis Brenguier
Copyright © 2012 copyright holder, location
ISBN: 3-527-XXXXX-X

10
Supplementary Material

10.1
Glossary

Atmospheric correction Compensation of the atmosphere influences by gases and aerosols from the radiometric signal at the airborne remote sensing instrument for retrieval of surface albedo, directional.

Boundary layer Layer of fluid in the immediate vicinity of a bounding surface (e.g. Earth's surface or aircraft skin). The aircraft boundary layer can be turbulent, which leads to strong particle losses on the aircraft skin.

Calibration The process of quantitatively defining the responses of a system to known, controlled signal inputs.

CFD modeling Computer simulation to solve and analyze problems that involve fluid flows. For this purpose, first the geometry of the body of interest and a surrounding domain (the fluid) is generated using software tools. Afterwards the fluid domain is filled with grid cells and the boundary conditions at the domain limits are defined. In the actual CFD simulation, the equations of fluid dynamics (Navier–Stokes) are solved iteratively.

Ice particle shattering and bouncing During sampling ice particles may impact a cloud probe's upstream tips or inlet, bounce away or shatter into small fragments.

Ram heating According to the energy conservation law for compressible fluids, an air flow which is deaccelerated adiabatically experiences a heating. In analogy to the static pressure of such a flow at zero velocity (ram pressure) the term ram heating is used for the heating process during declaration.

Airborne Measurements for Environmental Research. Manfred Wendisch & Jean–Louis Brenguier
Copyright © 2012 copyright holder, location
ISBN: 3-527-XXXXX-X

Reynolds number (Re) Dimensionless number that gives a measure of the ratio of inertial forces to viscous forces. A large Re indicates a turbulent flows, a low Re a laminar one.

Stokes number (Stk) Dimensionless number that gives a measure on how well particles or droplets can follow the gas flow streamlines, It is defined as the ratio of the stopping distance of a particle to a characteristic dimension of the obstacle.

Traceability Property of a measurement result relating the result to a stated metrological reference (free definition and not necessarily SI) through an unbroken chain of calibrations of a measuring system or comparisons, each contributing to the stated measurement uncertainty.

Turbulence intensity (TI) A measure of the strength of turbulence in a flow system. TI is defined as the ratio of the turbulent velocity fluctuation to the mean flow velocity and is usually expressed in percent. Laminar flow is indicated by TI values below 1%.

Uncertainty Parameter that characterizes the dispersion of the quantity values that are being attributed to a measured mean, based on the information used.

Validation The process of assessing, by independent means, the quality of the data products derived from the system outputs.

Vicarious calibration Vicarious calibration refers to techniques that make use of natural or artificial sites on the surface of the Earth for the post–launch calibration of sensors.

Weber number (We) Probability of drop breakup during high–speed sampling.

- monochromatic
- irradiance
- radiance
- actinic flux density
- broadband
- blackbody
- Planck function
- radiometer

- integrating sphere
- spectrometer
- Lambertian reflector
- albedo
- photolysis
- solar zenith angle
- pitch
- roll
- heading or yaw
- pyranometer
- pyrgeometer
- terrestrial radiation
- solar radiation
- interferometer
- interferogram
- optical thickness
- brightness temperature
- Rayleigh–Jeans approximation
- precipitation rate

Layer	Geopotential Height h_0 (gpkm)	Geometric Height z_0 (km)	Lapse Rate γ_0 (°C gpkm^{-1})	Temperature T_0 (°C)	Pressure P_0 (Pa)
0	0.0	0.0	-6.5	+15.0	101,325
1	11.000	11.019	+0.0	-56.5	22,632
2	20.000	20.063	+1.0	-56.5	5,474.9
3	32.000	32.162	+2.8	-44.5	868.02

Tab. 10.1 ISA standard atmosphere properties (base values) in the troposphere and stratosphere.

Variable	Accuracy
Latitude	1.5 km h^{-1} (50 % CEP)
Longitude	3.1 km h^{-1} (95 % CEP)
Ground Velocity	4.10 m s^{-1}
Vertical Velocity	0.15 m s^{-1} (baro–damped)
Pitch and Roll Angles	0.05°
True Heading	0.2°

Tab. 10.2 Accuracy of Unaided Navigation–Grade INS (Honeywell LaserRef2 SM after 6 hours). [ED: Needs ref.]

10.2 Thermodynamic Measurements

10.2.1 Aircraft State Parameters

10.2.2 Static Air Temperature

Radiative Probe

Air temperature may be derived from measurements of the emitted radiance in the TIR region. It is desirable that the weighting function of the detected radiation should be confined within a short distance (∼10–100 m) of the detector. This reduces the sensitivity to changes in aircraft attitude, when the viewing path of the instrument may be shifted from the horizontal and may, therefore, view through the vertical temperature gradient of the atmosphere. Suitable wavelengths for measurement are, therefore, strongly absorbed in the atmosphere and a typical choice is the 4.25 μm absorption band of CO_2 (Beaton, 2006).

Class	Position Performance	Gyro Technology	Accelerometer Technology	Gyro Bias	Acceleration Bias
Military Grade	1 nmi / 24 h	ESG, RLG FOG	Servo Accelerometer	$< 0.005°$ / h	30 μg
Navigation Grade	1 nmi / h	RLG FOG	Servo Accelerometer Vibrating Beam	0.01° / h	50 μg
Tactical Grade	>10 nmi / h	RLG FOG	Servo Accelerometer Vibrating Beam MEMS	1° / h	1 mg
AHRS	NA	MEMS, RLG FOG, Coriolis	MEMS	$1 - 10°$ / h	1 mg
Control System	NA	Coriolis	MEMS	$10 - 1000°$ / h	10 mg

Tab. 10.3 Performance of classes of unaided INS systems.

The brightness temperature, T_B, may be determined by inversion of the Planck function which describes the radiance exitance, $B_\lambda(\lambda, T)$, of a perfect blackbody, see Eq. (7.20):

$$T_\mathrm{B} = \frac{\mathrm{h} \cdot \mathrm{c}}{\lambda \cdot \mathrm{k_B}} \cdot \left[\log \left(\frac{2\,\pi \cdot \mathrm{c}^2 \cdot \mathrm{h}}{\lambda^5 \cdot B_\lambda(\lambda, T)} \right) \right]^{-1} , \tag{10.1}$$

with the Planck constant $\mathrm{h} = 6.6262 \times 10^{-34}\,\mathrm{J\,s}$, the Boltzmann constant: $\mathrm{k_B} = 1.3806 \times 10^{-23}\,\mathrm{J\,K^{-1}}$, T is the absolute temperature in Kelvin, and λ the wavelength in meter. When the atmospheric path is totally absorbing, and hence its emissivity is unity, the brightness temperature is equal to the temperature of the air.

A recent implementation of this principle is described by Beaton (2006), see Figure 10.1. The instrument consists of a filter radiometer, with a pass-band width of approximately 0.05 μm. A rotating chopper wheel allows the detector to view alternately the atmospheric radiance and the emission from an internal temperature–controlled black–body target. Measurement of the difference signal and the blackbody temperature allows the atmospheric brightness temperature to be determined.

The instrument housing has an external window that is transparent in the thermal infra-red. This allows the internal temperature and humidity of the instrument to be more easily stabilized. The window must be maintained free of any materials that are strongly absorbing at the detection wavelength. This includes liquid water which might form a thin film across the window when the instrument is in liquid-phase clouds or rain.

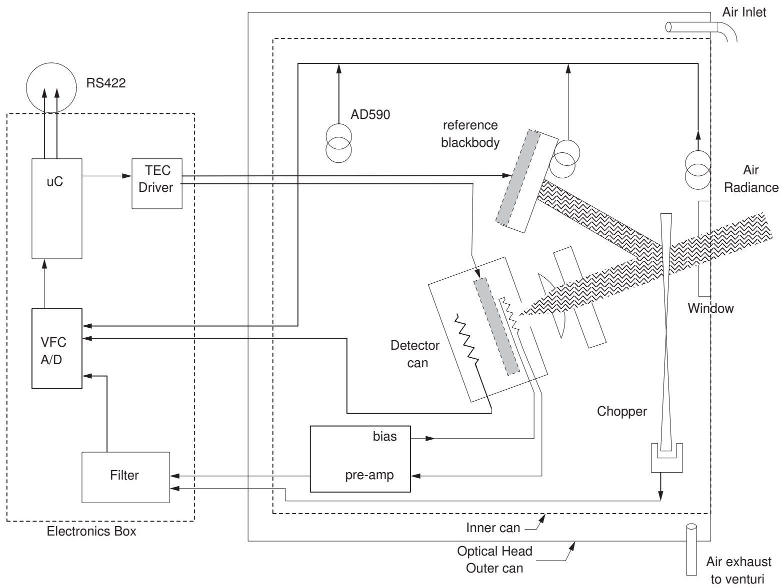

Fig. 10.1 A block diagram of the Ophir air temperature radiometer (Beaton, 2006). The external window is at the right. Behind it is the chopper wheel, the 4.3 μm interference filter, the focusing lens and then the detector can. Inside the detector can is the HgCdTe detector, the thermistor to monitor the detector temperature, and the thermoelectric cooler for the detector. The TEC driver supplies power to the thermoelectric coolers for the detector and controlled black body. The entire optical system is kept near the external air temperature by air circulating between the inner and outer cans of the optical head.

Liquid– and ice–phase clouds are both strongly absorbing at the 4.25 μm wavelength. The impact of this when making measurements in cloud is that the absorption within the wings of the pass–band of the filter is increased compared to that in clear air. This has the effect of decreasing the effective viewing path within cloud from $\sim$100 m to $\sim$20 m (Beaton, 2006). In principle, the instrument can be radiometrically calibrated to give an absolute true air temperature measurement. In practice, however, the stability of such calibrations is insufficient and they are normally calibrated against an immersion temperature sensor using cloud-free in–flight data. Such a calibration will typically exclude data from periods when the aircraft roll and pitch angles exclude certain limits. This ensures the rejection of any data obtained when the instrument may be viewing up or down the atmospheric vertical gradient of temperature.

The sample rate of such a radiometric temperature sensor is typically around 1 Hz. At typical flight speeds of 70–100 m s^{-1} this means that the along–track averaging length is comparable with the instrument viewing path length. Higher–frequency sampling is possible but will increase the noise level.

Ultrasonic Probe

Ultrasonic thermometry is based on the measurement of the speed of sound of the air which mainly is a function of temperature. The speed of sound is derived from the measurement of the transit time of a short sound pulse over a well known distance. A relative movement of the air with respect to the emitter of the sound pulse (e.g.wind) will be superimposed on the speed of sound. Measuring the transit time back and forth along the same path allows extraction of the speed of sound as well as the wind vector component along the sound propagation path. This principle is widely used for ground based measurements of 3D wind and temperature simultaneously. Due to the non–contact type of measurement a high time resolution is possible, making the method useful for measurement of temperature fluctuation. But its ability for absolute temperature measurement is strongly reduced by secondary effects in sound wave propagation theory based on the assumption that air is an ideal gas (Cruette et al., 2000). Up to now only a few ultrasonic temperature probes have been used for airborne measurement, mainly on slow flying aircraft or helicopters.

10.2.3 Three–Dimensional Wind Vector

Measuring the Flow Vector Using a Five–Hole Probe

Five-hole probes (FHP) do not provide very high temporal resolution (e.g., compared to a CTA) but are robust instruments that allow measurements up to about 100 Hz. The limit of temporal resolution is mainly due to limited response time of the connected pressure transducers and to due resonance effects in the connection tubes and in the cavities of the pressure transducers.

The following description mainly addresses FHP that measure (in addition to the static pressure) only differential pressures Lemonis et al. (2002). In larger probes (e.g., pressure holes in the aircraft fuselage as applied to the Space Shuttle or the F-18 High Angle of Attack Research Vehicle) the measurement of the individual, absolute pressures is possible and allows an even more accurate determination of the flow angles Weiß and Leißling (2001); Weiß (2002). Air flow systems involving more or less than five holes Crawford and Dobosy (1992); Sumner (2000); Pfau et al. (2002) can be treated more or less like a FHP.

The local wind vector in the aircraft coordinate system is determined from the dynamic pressure increment Δp_q and the pressure differences between opposite pressure holes in the FHP i.e., the pressure difference in the horizontal plane $\Delta p_\beta = p_2 - p_4$, and in the vertical plane $\Delta p_\alpha = p_1 - p_3$, where p_j denotes the individual holes of the FHP, with p_5 being the central hole (Figure 10.2). The pressure differences Δp_α and Δp_β increase when the angle of attack α and the sideslip β increase. But the pressure differences also depend on the airspeed (and therefore on the dynamic pressure increment Δp_q and on the Mach number) and on the air density ρ (and therefore on the altitude z). In general this can be expressed by

$$\varphi = F(\Delta p_\varphi, \Delta p_q, z) \quad \text{where } \varphi = \alpha, \beta\,, \tag{10.2}$$

where F denotes a functional relation.

Usually both the influence of the airspeed and the altitude can be considered by weighting the pressure difference with the dynamic pressure increment. The most simple assumption is therefore

$$\varphi = \frac{1}{K_{\mathrm{FHP}}}\,\frac{\Delta p_\varphi}{\Delta p_q}\,, \tag{10.3}$$

where the calibration coefficient K_{FHP} considers any disturbance of the air stream by the FHP (and also by the entire aircraft fuselage) and local stream effects directly at the pressure hole.

Actually the most difficult task is now the determination of the dynamic pressure increment Δp_q or the total pressure p_{tot} since the stagnation point is usually located somewhere between the holes of the FHP and can therefore not directly be measured. The approximation of the total pressure by the measured pressure p_5 at the central hole of the FHP would lead to a wind vector measurement that is very sensitive to the aircraft attitude, wind speed and wind direction Schlienger et al. (2002) and provides only small accuracy.

In the following some more sophisticated methods to estimate the correct sideslip and angle of attack are introduced Bange (2009). It is understood that any offset angles α_o or β_o due to bias in the pressure transducers or asymmetry of the FHP have to be quantified in a laboratory, a wind tunnel or in flight tests before. Calibration routines, both for wind-tunnel experiments and flight manoeuvres can be found in literature Haering (1990); Wörrlein (1990); Haering (1995); Barrick et al. (1996); Friehe et al. (1996); Khelif et al. (1999); Weiß

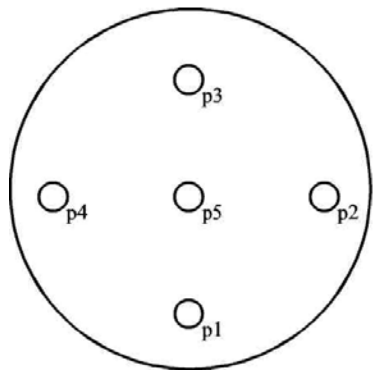

Fig. 10.2 Schematic illustration of a FHP showing the pressure ports p_1 to p_5 (head-on perspective, i.e., starboard is on the left side from this point of view). In the text, $p_0 = p_5$.

et al. (1999); Williams and Marcotte (2000); van den Kroonenberg et al. (2008); van den Kroonenberg (2009).

Rosemount Method

Providing an additional pressure–difference measurement

$$\Delta p_{\text{ref}} = p_0 - p_2 \tag{10.4}$$

between one of the horizontal holes and the central hole (Rosemount method), the dynamic pressure increment is estimated by

$$\Delta p_q \approx \Delta p_{\text{ref}} + \frac{1}{2}\,\Delta p_\beta\,. \tag{10.5}$$

The flow angles are determined by (10.3) with K_{FHP} set to 0.088 for airspeeds below 0.6 Ma Rosemount (1982). It has to be noted that the Δp_{ref} refers only to the horizontal plane i.e., the stagnation point is assumed to be located somewhere on the connecting line between the two opposite holes #2 and #4. This presupposes two items: 1) the FHP has to be mounted to the aircraft in a way that $\alpha = 0$ in the absence of vertical wind ($w = 0$); 2) the aircraft is not allowed to perform larger changes in both pitch Θ or roll Φ; i.e., this method is not suitable for highly dynamic systems.

An improvement requires an additional differential pressure measurement between the central hole and one of the holes in the vertical plane (#1 or #3), resulting in two disjunction equations of type (10.3):

$$\alpha = \frac{1}{K_{\mathrm{FHP},\alpha}} \frac{\Delta p_\alpha}{\Delta p_{\mathrm{ref},\alpha} + \frac{1}{2}\,\Delta p_\alpha} \tag{10.6}$$

$$\tilde{\beta} = \frac{1}{K_{\mathrm{FHP},\beta}} \frac{\Delta p_\beta}{\Delta p_{\mathrm{ref},\beta} + \frac{1}{2}\,\Delta p_\beta}\,. \tag{10.7}$$

It is obvious that this method represents no fundamental improvement compared to the usual Rosemount method, since no consistent dynamic pressure increment can be determined. This is mainly due to the general strategy to use a Cartesian approach to solve a rotationally symmetric problem.

Five–Differences Method and Calibration

More accurate results an be achieved using five pressure difference measurements: the difference between the central hole and each of the four remaining total pressure ports (ΔP_{01}, ΔP_{02}, ΔP_{03}, ΔP_{04}), and the difference between the static pressure and the central hole (ΔP_{0s}). These measurements are used to determine a total pressure difference

$$\Delta p = \left[\frac{1}{5}\sum_{i=0} 4\left(p_i - \frac{1}{5}\sum_{j=0} 4p_j\right)2\right]^{\frac{1}{2}} + \left[p_0 - \frac{1}{4}\sum_{i=1} 4p_i\right] \quad , \tag{10.8}$$

which uses the absolute pressures. Since the measurement of the absolute pressures is P_i is often not feasible, (10.8) can also be expressed by the pressure differences van den Kroonenberg et al. (2008):

$$\begin{aligned}\Delta p \;=\; & \left\{\frac{1}{125}\Big[\,(\Delta p_{01} + \Delta p_{02} + \Delta p_{03} + \Delta p_{04})\,2 + (-4\Delta p_{01} + \Delta p_{02} + \Delta p_{03} + \Delta p_{04})\,2\right. \\ & + (\Delta p_{01} - 4\Delta p_{02} + \Delta p_{03} + \Delta p_{04})\,2 + (\Delta p_{01} + \Delta p_{02} - 4\Delta p_{03} + \Delta p_{04})\,2 \\ & \left. + (\Delta p_{01} + \Delta p_{02} + \Delta p_{03} - 4\Delta p_{04})\,2\Big]\right\}^{0.5} \\ & + \frac{1}{4}\,(\Delta p_{01} + \Delta p_{02} + \Delta p_{03} + \Delta p_{04}) \quad .\end{aligned} \tag{10.9}$$

Next step is to calculate the dimensionless pressure coefficients

$$k_\alpha = \frac{\Delta p_{01} - \Delta p_{03}}{\Delta p} \quad , \tag{10.10}$$

$$k_\beta = \frac{\Delta p_{02} - \Delta p_{04}}{\Delta p} \quad . \tag{10.11}$$

Then, three functions are defined to calculate the airflow angles and the dimensionless coefficient k_q (later needed for the dynamic pressure)

$$\begin{aligned} \alpha &= f_1(k_\alpha, k_\beta) \quad , \\ \beta &= f_2(k_\alpha, k_\beta) \quad , \\ k_q &= f_3(k_\alpha, k_\beta) \quad , \end{aligned} \tag{10.12}$$

with the general calibration polynomial form Bohn and Simon (1975) with $x = \alpha, \beta, q$ and typically $m = n = 10$

$$f_x(k_\alpha, k_\beta) = \sum_{i=0}^{m} (k_\alpha)^i \left[\sum_{j=0}^{n} X_{ij} (k_\beta)^j \right] \quad . \tag{10.13}$$

Here, X_{ij} represents the individual calibration tensors for the angle of attack a_{ij} (f_α), sideslip b_{ij} (f_β), and dynamic pressure q_{ij} (f_q). Thus, the function (10.13) contains $m \times n$ unknown coefficients X_{ij} that have to be determined via a system of $m \times n$ independent equations (e.g., using a least-square method). The most accurate method to obtain these equations are measurements in a calibrated wind tunnel. Combinations of differential pressures with adjusted $x = \alpha, \beta, q$) can be achieved by varying the air speed and flow angles by turning the FHP in the wind tunnel. Preferably, the FHP is mounted on the aircraft (and not be removed between calibration and measurement flight). Of course, this is only feasible for very small aircraft like UAV and large wind tunnels. Finally the dynamic pressure q is given by

$$q = \Delta p_{0s} + \Delta p \cdot k_q \quad . \tag{10.14}$$

In–Flight Calibration

Lenschow Maneuvers

Regardless of where the air flow sensors are located on the aircraft and how carefully they are calibrated, errors are likely to be present in their measured outputs. Ground tests are not useful for calculating velocity-related errors. Wind tunnel tests are difficult and prohibitively expensive for exact simulation of flight conditions. Therefore, in–flight calibrations play an important role in estimating errors and correcting aircraft measurements.

Because of the airflow distortion ahead of the aircraft, the airflow angles (attack α and sideslip β) and airspeed U measured at the aircraft nose or the tip of a nose boom tip may differ considerably from the actual values that would be measured far away from the aircraft. The airflow distortion affects not only the sensitivity, but also the zero offset of angle measurements, which, therefore, must also be determined from in–flight calibrations.

Maneuvers used for this purpose involve changes in U and attitude angles. The following list summarizes several maneuvers used on NCAR aircraft equipped with an inertial navigation system (INS) and the information that can be obtained from them; examples of these maneuvers are shown in Figures 10.3 and 10.4 (Lenschow and Spyers–Duran, 1989).

Reverse heading maneuver: Fly at constant altitude and heading (usually in smooth air above the boundary layer) for several minutes. Then turn 180^o by first turning 90^o in one direction, then 270^o in the other direction at a constant rate so the aircraft flies through the same volume of air on its return track. This maneuver modulates errors in U and β, since they are measured in the aircraft coordinate system. The INS errors are not modulated, however, since they are measured in an inertial frame of reference. If the wind along the flight track is assumed to stay constant during this maneuver, differences in the two wind components between the two headings can be used to independently estimate errors in both U and β; U errors are associated with the longitudinal wind component and β errors with the lateral wind component.

Speed variation maneuver: Fly at constant altitude and heading ψ, and smoothly vary U from close to stall to close to maximum cruise speed. Since the lifting force on the aircraft is directly proportional to α and U^2, modulating U also modulates α. For level flight, the vertical aircraft velocity w_p is zero; if the air velocity w, is small, $\alpha = \theta$. Thus, α can be calibrated in flight by this technique, provided that θ is measured accurately. The attitude angle transducers, in contrast to airflow angle sensors, can be accurately calibrated in the laboratory.

If U is measured incorrectly, temperature may also be affected. Temperature recovery factors can also be measured or corrected with this maneuver, since U variations modulate the measured temperature because of dynamic heating effects. Any other measurements affected by either U or α variations are also modulated by this maneuver.

Pitch maneuver: Vary the aircraft elevator angle while holding the heading constant to obtain a sinusoidal pitching motion with a period of 10 to 20 s and a maximum rate of ascent and descent of 2.5 to 4 m s^{-1}. This maneuver modulates w_p, U, and, to a lesser extent, α. If any of these variables have significant errors, a periodic error in w should be evident. Since the terms do not have the same phase angle, in practice it is often possible to determine which of the variables is in error simply by determining the phase of the error in w and comparing it with the phase of w_p, θ, U, and α. This maneuver also can be used to detect dynamic errors in static pressure or rate-of-climb instruments by comparing their outputs with the integrated INS vertical acceleration.

Yaw maneuver: Vary the aircraft rudder angle while holding the roll and altitude constant to obtain a sinusoidal skidding or sideslip motion with a period of about 10 s and a maximum amplitude in β of about 2°. This maneuver

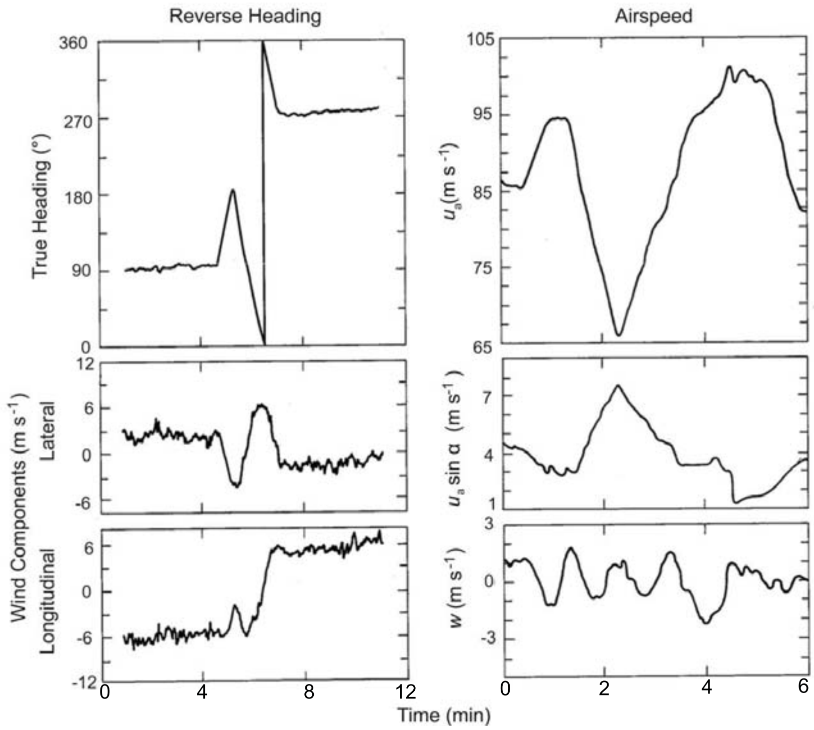

Fig. 10.3 Examples of reverse heading and airspeed maneuvers used to check the quality of air velocity measurements. The lateral and longitudinal velocity components are measured with respect to the aircraft; therefore, the measured wind should change sign, but not amplitude, after the 180° turn, if the wind field remains constant and is measured without error. An error in airspeed will result in a difference in the amplitude of only the longitudinal component before and after the turn, while an error in the sideslip angle will similarly affect only the lateral component, which simplifies correction procedures. The airspeed maneuver modulates α and θ; if θ is measured accurately, the error in α a can be determined by comparing the vertical wind component with respect to the aircraft ($U \sin \alpha$) with the vertical wind component with respect to the Earth. In this example, there is little correlation between the two, so the fluctuations in w are presumed to be due to turbulence rather than an inaccurate measurement of α. The airspeed maneuver can also be used to estimate airspeed–dependent errors in other variables and the temperature recovery factor.

modulates heading ψ, the longitudinal and lateral aircraft velocity components u_p and v_p, and β. As with the pitch maneuver, errors in any of these variables cause a periodic variation in the horizontal wind velocity.

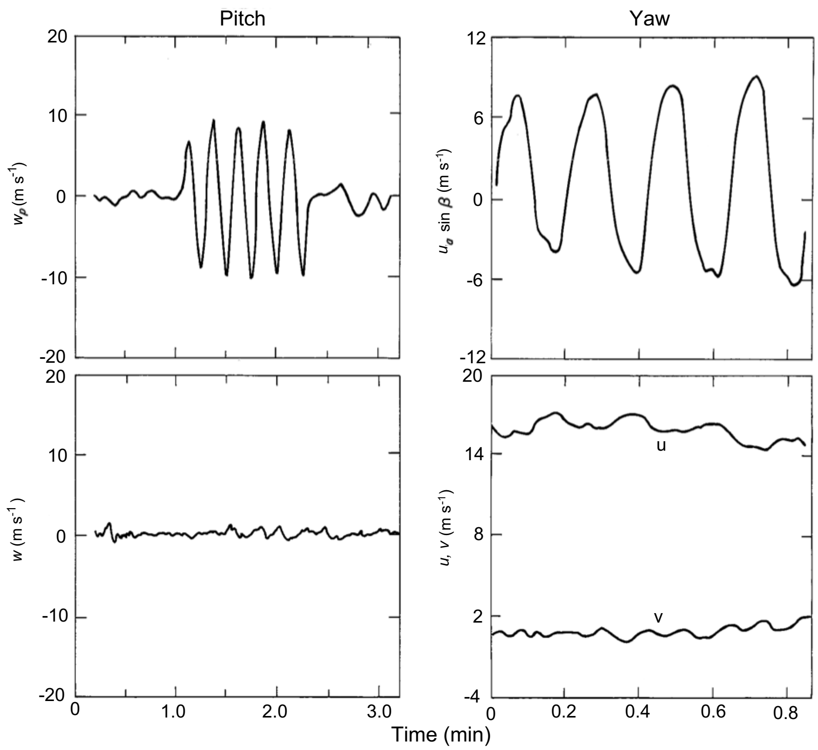

Fig. 10.4 Examples of pitch and yaw maneuvers. The pitch maneuver is used as an overall check on the accuracy of the w measurement; in this example, there is little modulation of w during the pitching maneuver, which implies that fluctuations in w are measured accurately. Similarly, the yaw maneuver is used as an overall check on the lateral (with respect to the aircraft) component; again there is little modulation of u and v (in geographic coordinates) by the yawing maneuver.

On the NCAR aircraft, the system performance is judged to be satisfactory if the w error is less than 10 % of w_p for the pitch maneuver, and v_p is less than 10 % of $U \sin\beta$ for the yaw maneuver.

Lenschow and Spyers–Duran (1989) estimate that short-term (i.e., not including long-term INS drift) velocity errors can be reduced to < 0.3 m s^{-1} by in–flight calibrations. An alternative technique for estimating the error coefficients in w, proposed by Khelif et al. (1999) is to iteratively vary the calibration coefficients of w to minimize the variance of w. This assumes that errors in the w measurement invariably increase the w variance. An advantage of this technique is that it can be done on research legs, without the requirement of dedicated maneuvers in non–turbulent air.

Rodi Maneuvers

An alternative approach developed at the University of Wyoming employs multiple regression analysis of data collected while maneuvering the aircraft while in a standard rate turn. While turning, the pilot induces sinusoidal sideslip variations of about 10 second period while maintaining constant altitude, resulting in sinusoidal flow angle and airspeed variation along both the lateral and vertical body axes. The motivation for the turning method is to induce flow angle changes that result in Earth-vertical speed fluctuations without large height variations and accelerations, all well within the envelope encountered during normal research operations. Further, in turns, the coordinate transformation matrix from aircraft body-axis to Earth coordinates changes rapidly allowing problems with time synchronization of the IMU and airspeed data can readily identified.

The assumptions in the analysis are: 1) the vertical component of the wind has zero mean; 2) that the horizontal wind components are steady during the turn; and 3) that the variability of the wind components is mainly random—i.e., no systematic spatial variability as would be caused by mountain waves, for example. The procedure finds constant coefficients and offsets which minimize a cost function expressed as $f = W * \mathrm{detrend}(M)$, where W is the vertical wind component and M is the horizontal wind magnitude. The procedure results in estimates of the upwash and sidewash factors, and the pitch, roll, and heading offsets that minimize f, evaluated using the full 3D wind equations in a non–linear least squares solver (such as Matlab "lsqnonlin").

The results of this calculation for the period shown in Figures 10.5 and 10.6 are tabulated in Table 10.4. Note that the upwash factor is consistent with the value estimated from attack-pitch analysis and also from aerodynamic considerations as discussed by Crawford et al. (1996). Figure 10.5 shows the pilot–induced inputs during the maneuver, and Figure 10.6 is the resulting winds during that period after application of the coefficients and offsets. One complicating factor is that the angle offset corrections are assumed to be constant factors caused by misalignment of the inertial measurement unit with the gust probe axis, but actually also include time-varying inertial errors. Applying IMU / GPS corrections first would alleviate this problem.

Upwash Factor	**Sidewash** Factor	**Angle Offsets [°]** Pitch	Roll	Heading
0.759	0.776	0.290	–0.534	0.126

Tab. 10.4 Results of least squares procedure.

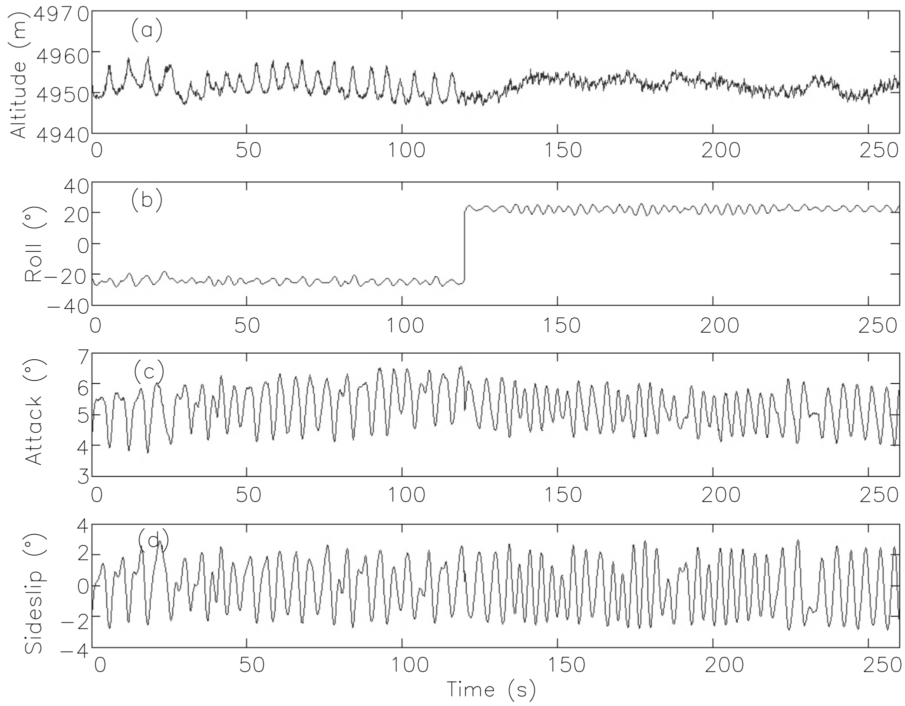

Fig. 10.5 Time series of 10–Hz data from University of Wyoming King Air flight on 19 March 2009. Shown are section from left turn concatenated with section from right turn. Period of induced sideslip oscillations is 10 seconds.

10.2.4 Small Scale Turbulence

Sampling and Sensor Resolution

The first question is how fast the sampling has to be to resolve a signal with frequencies f_{max}. The Nyquist theorem states that the sampling frequency f_s has to be at least two times f_{max} which reads mathematically $f_s \geq 2 \cdot f_{\mathrm{max}}$. If the signal is sampled with $f_s < 2 \cdot f_{\mathrm{max}}$, from the sampled values of the signal a waveform can be constructed with lower frequency. This effect is called "aliasing" and demonstrated in Figure 10.7 where a signal (solid black line) with f = 4 Hz is sampled with f_s = 5 Hz (red stars) which fits with a phase-shifted signal of 1 Hz (dashed black line). That is, in a Fourier spectrum one would expect a peak at 1 Hz which does not represent the frequency of the original signal.

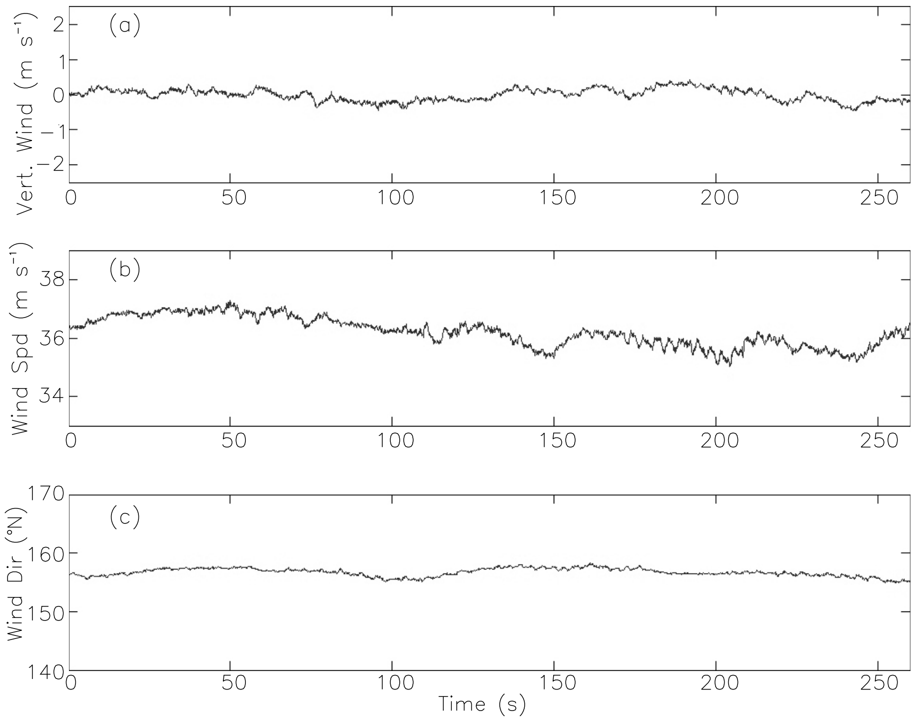

Fig. 10.6 Wind data after corrections from period as described in Fig. 10.5.

This effect can be solved by sufficient high sampling frequencies (e.g., $f_s \geq 2 \cdot f_{\mathrm{max}}$). Since the maximum frequency of a signal is often unknown and the temporal resolution mainly depends on the sensor design, a low-pass filter with a cut-off frequency $f_{\mathrm{cut}} < f_s/2$ should be applied, thereby removing the high frequency contributions which cannot be sufficiently resolved by the sensor.

Another point which has to be considered is the question about the required sensor resolution in combination as a function of sampling frequency. Therefore, this subsection deals with a few basic considerations concerning sensor resolution at a given TAS and degree of turbulence in terms of the mean energy dissipation rate. On small scales, turbulence is often described by the statistics and correlation of velocity increments $\delta u(x,r) = u'(x) - u'(x+r)$ where $u'(x)$ are the velocity fluctuations ($u'(x) = u(x) - \langle u \rangle_x$,where $\langle . \rangle_x$ denotes an average over the space parameter x). Here, we have simplified the problem to the longitudinal velocity component, x is the coordinate in flight

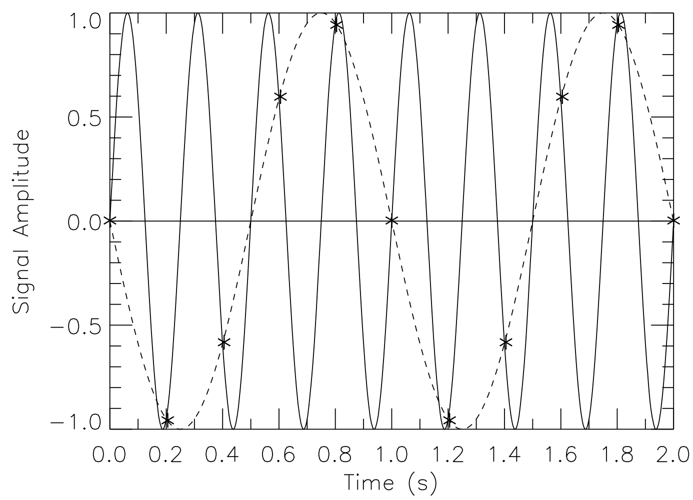

Fig. 10.7 The aliasing effect: A sinusoidal signal with a frequency $f = 4\,\mathrm{Hz}$ is sampled with a frequency of f_s = 5 Hz which violates the Nyquist theorem. The sampled points are represented as black stars and fit with a phase shifted signal with $f = 1\,\mathrm{Hz}$.

direction, and r is a spatial lag in the same direction. The second–order statistics of the velocity increments can be described by second–order structure functions and its scaling behavior in the inertial subrange $\eta \ll r \ll L$. Turbulence at sub-meter scale with $r \leq 1$ m down to about $10 \cdot \eta$ can be assumed to be safely within the inertial subrange under most turbulence conditions and $S^{(2)}$ reads:

$$S^{(2)}(r) = \left\langle (\delta u(x,r))^2 \right\rangle_x = 2(\varepsilon r)^{2/3}. \qquad (10.15)$$

Small corrections have to be applied to the scaling exponents (2 / 3) to consider internal intermittency effects in high Reynolds number flows which are negligible in this context, Note that Eq. (10.15) describes the same inertial subrange behavior as the famous $-5/3$–Kolmogorov law in the frequency domain since second-order structure functions and power spectra are a Fourier duality.

On an aircraft, a sensor signal is usually sampled as a function of time. Time increments δt can be transformed to spatial increments δr by applying Taylor's hypothesis of "frozen turbulence": $\delta r = TAS \cdot \delta r$. This transformation can be applied if the turbulence intensity $I = u_{\mathrm{rms}} / TAS$ is below a certain threshold - typically below $\sim 10\,\%$ which is fulfilled for most airborne applications due to the high TAS.

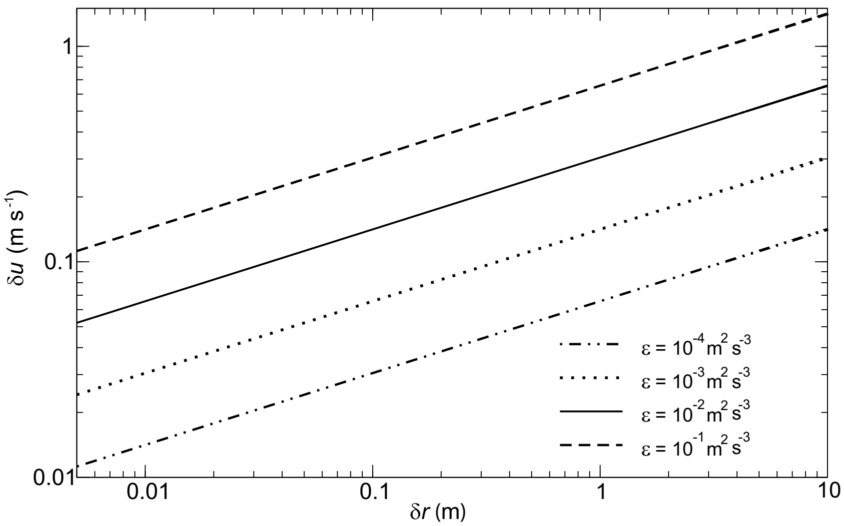

Fig. 10.8 Required sensor resolution δu for velocity measurements as a function of spatial resolution $\delta r = TAS/f_s$ and for different levels of turbulence described by the mean energy dissipation rate ε.

If we define the sensor resolution in such a way that the velocity increment $\delta u(r)$ in Eq.(10.15) can be resolved at given spatial resolution $\delta r \sim TAS/f_s$ and mean energy dissipation $\overline{\varepsilon}$ we can derive the following expression:

$$\delta u = \sqrt{2}\left(\overline{\varepsilon}\,\frac{TAS}{f_s}\right)^{1/3}. \tag{10.16}$$

Figure 10.8 shows the required resolution δu at given spatial resolution δ for four different $\overline{\varepsilon}$ typical for atmospheric conditions. For example, a spatial resolution of 0.1 m at given TAS = 100 m s^{-1} requires a sample frequency of at least 1 kHz and a sensor resolution of better than $\delta u = 3$ cm s^{-1} to resolve turbulence with $\varepsilon = 10^{-4}$ m^2 s^{-3} at given scale.

It has to be considered that this estimate is based on mean ε but atmospheric turbulence is highly variable in space and time. Locally, ε can vary a few orders of magnitude and it is more safe to estimate the sensor resolution based on a much smaller value (e.g., ε_{local} $\sim$1 % of $\bar{\varepsilon}$ results in a five times smaller δu).

In a similar way, the required sensor resolution for other passive scalars such as temperature or humidity can be estimated by replacing the factor “$2\varepsilon^{2/3}$" in Eq. (10.15) with the appropriate values Warhaft (2000).

In the following, we will introduce a couple of fast-response sensors for different parameters which are usually not part of the standard instrumentation of a research aircraft and which are going beyond the “standard” sensors introduced in the previous sections - although a few of them can be sampled fast enough to resolve sub-meter scales.

10.3 In Situ Measurements of Cloud and Precipitation Particles

10.3.1 Laser Doppler Velocimetry: Double–Doppler Shift and Beats

The physical principle underlying LDV is essentially the same as that responsible for Doppler broadening of spectral lines: the radiation source and detector can be considered stationary, with moving particles scattering light from the source to the detector. The motion of any given particle (for LDV the particle would be an aerosol or cloud particle) leads to a slight Doppler shift in the detected radiation. The general equation for the non–relativistic ($v \ll c$) Doppler effect is:

$$\nu' = \nu \left(\frac{c \pm v_{\text{observer}}}{c \mp v_{\text{source}}} \right) \approx \nu \left(1 \pm \frac{v_{\text{observer}}}{c} \pm \frac{v_{\text{source}}}{c} \right) , \tag{10.17}$$

where ν and ν' are the inherent and Doppler shifted frequencies, c is the propagation speed, and v_{source} and v_{observer} are the velocity components of the frequency source and observer, respectively, along the source-observer path. The derivations that follow are based on the more detailed treatment of Davis and Schweiger (2002).

In LDV there is a double Doppler shift because there are two ‘observers.’ First, light emitted from a stationary source (a laser) at frequency ν is observed by a moving particle as frequency ν'. Second, light scattered by the moving particle at frequency ν' is observed by a detector (e.g., a photomultiplier tube) as frequency ν''. The total resulting Doppler shift is therefore:

$$\frac{\nu'' - \nu}{\nu} \approx \frac{v}{c} \left(\cos\theta_1 + \cos\theta_2 \right) , \tag{10.18}$$

where v is the particle speed and again we have taken the limit $v/c \ll 1$. The angles describe the velocity components resulting from the system geometry: θ_1 is the angle between the source-particle vector and the velocity vector, and θ_2 is the angle between the particle-detector vector and the velocity vector. As should be expected, when the sum of θ_1 and θ_2 is 180°, meaning the particle lies on a straight path between the source and the detector, the double-Doppler shift is zero.

The basic physical mechanism is now clear, but because the relative Doppler shift $(\nu' - \nu)/\nu \propto v/c$ we must consider how such a small Doppler shift can be measured (assuming $v \sim 10$ m s^{-1}, we would expect relative Doppler shifts on the order of 10^{-7}). The elegant approach is do this via heterodyne detection, in other words, mixing two coherent signals to obtain an easily measurable beat frequency. In practice, this can be accomplished by splitting the laser beam and then crossing the two beams: The different source-detector geometry results in slightly different Doppler shifts from each beam, as illustrated in Figure 10.9. The beat frequency is equal to the difference of the two double-Doppler-shifted frequencies from sources A and B, $\Delta\nu'' \equiv \nu''_A - \nu''_B$. The two Doppler frequencies can be determined from Eq. (10.18) and, noting that θ_2 is the same for both, we obtain $\Delta\nu'' = \nu(v/c)(\cos\theta_{1A} - \cos\theta_{1B})$. Defining angle α as the beam crossing angle and angle β as that between the velocity vector and a perpendicular to the optical axis, these angles can be written as $\theta_{1A} = \pi/2 - \beta + \alpha/2$ and $\theta_{1B} = \pi/2 - \beta - \alpha/2$. Using the sine difference identity it follows that:

$$\Delta\nu'' = 2\nu\frac{v}{c}\cos(\beta)\sin\left(\frac{\alpha}{2}\right). \tag{10.19}$$

This result has several interesting implications. First, the beat frequency depends on the beam-crossing angle, so this is a parameter that must be accurately determined in the instrument setup. Second, the beat frequency is independent of the detector location, a perhaps non–intuitive result that is contrary to the single-source geometry (although the signal to noise ration may depend on detector location due to the angular dependence of light scattering. Third, the beat frequency is proportional to the component of the particle motion lying in the plane of the crossing beams and perpendicular to the optical axis.

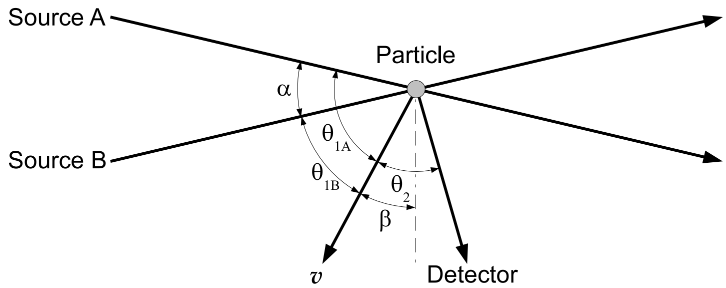

Fig. 10.9 Geometry of the heterodyne detection method for laser Doppler velocimetry. Two laser beams, denoted sources A and B, cross at their focal points with angle α. A particle passing through the beam–crossing region with velocity vector **v** scatters light from both beams to the detector. Other angles are defined in the text.

10.4 Scattering and Extinction of Light by Particles

10.4.1 Approximate Solutions of Light Scattering Problems as Used in the Processing Software of Modern Size Spectrometers

Light scattering methods are widely used in studies of turbid media such as atmospheric aerosol and clouds. They are based on the fact that the intensity and polarization of scattered light depends on the peculiarities of the object from which light has been scattered. The advantage of light scattering methods is due to the fact that they do not disturb the medium under study and enable investigations of dynamical processes in turbid media with high temporal resolution. The same applies to light extinction techniques where the attenuation of a direct beam is studied.

The shortcomings of the light scattering and extinction techniques for particle sizing as compared, e.g., to microscopy and digital imaging, are due to their indirect nature. For instance, if we limit ourselves to the case of single scattering by a unit volume filled with spherical particles (e.g., as those present in water clouds and fogs), the intensity of scattered light I_{sca} at the wavelength

λ in the direction specified by the scattering angle θ can be presented as:

$$I_{\text{sca}}(\lambda,\theta) \quad = \quad B\int_{a_1}^{a_2} I(\lambda,m,a,\theta)\cdot n(a)\ \mathrm{d}a\,, \tag{10.20}$$

where $I(\lambda,m,a,\theta)$ is the contribution to the detected signal by a single sphere with the radius a, m is the complex refractive index of particles, and $n(a)$ is the particle size distribution (PSD). It is assumed that only particles with radii between a_1 and a_2 are present in the scattering volume. The calibration constant B depends on the incident light intensity and also on a particular experimental setup. The value of $I(\lambda,m,a,\theta)$ can be presented via dimensionless Mie intensities i_1, i_2 (van de Hulst, 1981) as $I(\lambda,m,a,\theta) = \frac{i_1+i_2}{2}$. The parameter $C_{\text{sca}}(\lambda,m,a,\theta) = \frac{i_1+i_2}{2k^2}$ has a dimension of the area ($k = \frac{2\pi}{\lambda}$) and is called the differential scattering cross section (for a single particle). Clearly, it follows:

$$\int_{a_1}^{a_2} n(a)\ \mathrm{d}a \quad = \quad N\,, \tag{10.21}$$

where N is the number of particles of all sizes in the unit volume. The directional scattering coefficient is defined as $\beta_{\text{sca}} = N < C_{\text{sca}}(\theta) >$, where the brackets here and below mean averaging with respect to the size distribution $f(a) = \frac{n(a)}{N}$, namely:

$$\langle C_{\text{sca}}(\theta)\rangle \quad = \quad \int_{a_1}^{a_2} C_{\text{sca}}(\lambda,m,a,\theta)\cdot f(a)\ \mathrm{d}a\,. \tag{10.22}$$

Therefore, we conclude that for the determination of PSD $n(a)$, one needs to solve the integral Eq. (10.20) for a given set of measured functions $_{\text{sca}}$, e.g., at several angles θ. As a matter of fact this task belongs to a broad field of ill–posed problems and not always has a solution. Therefore, careful selection of the angular interval where measurements are performed is needed. In the case of large spherical particles such as fog and cloud droplets($a \gg \lambda$ in the VIS), there are several ranges of scattering angles, where the scattered light is most sensitive to the size of particles. They include the range of forward ($\theta \to 0$) and backscattering ($\theta \to \pi$) angles and also the scattering in the vicinity of the rainbow angle ($\theta 138°$) (van de Hulst, 1981). The single particle response function (SPRF) $I(\lambda,m,a,\theta)$ can be presented in a first approximation as (van de Hulst, 1981):

$$I(\lambda,m,a,\theta) \quad = \quad \left(\frac{x}{\theta}\right)^2\cdot J_1^2(x\cdot\theta)\,, \tag{10.23}$$

as $\theta \to 0$. Here $J_1^2(x\theta)$ is the Bessel function and $x = \frac{2\pi a}{\lambda}$ is the size parameter. The Bessel function $J_1^2(x\theta)$ is approximately equal to $\frac{x\theta}{\lambda}$ at small scattering angles. Therefore, we conclude that $I(\lambda, m, a, \theta) = \frac{x^4}{4}$ and the scattered energy is proportional to the squared geometrical cross section of the particle as $\theta \to 0$. It follows that the angular distribution of SPRF depends on the ratio of the size of a particle to the wavelength, the distribution being more narrow for larger particles. Generally, the Bessel function $J_1^2(x\theta)$ oscillates and the first minimum is located at $x\theta_{\min} \approx 3.832$. This gives for a typical droplet with: $x = 100 : \theta_{\min} = 0.03832$ or about $2.2°$. For larger droplets and crystals with the characteristic size parameter $x \sim 1000$, the value of $\theta_{\min}$ is about $0.2°$. Taking into account that most of the energy is concentrated within the first ring ($\theta < \theta_{\min}$) and the fact that the influence of the direct incident light must be eliminated, the construction of the corresponding measurement system is not trivial and powerful lenses with large focal lengths must be used.

Eq. (10.23) has a very limited range of applicability. For smaller spherical droplets, Mie theory (Mie, 1908) must be used. In particular, the refractive index of particles must be taken into account in calculations. In the case of large concentrations of scatterers, the small–angle, multiple scattering must be accounted for. Eq. (10.23) is also not valid for non–spherical particles. For instance, let us take the example of a single ellipsoidal particle. Then clearly, the diffraction pattern is not symmetrical with respect to the incident beam. The forward scattering pattern becomes symmetric with respect to the incident light only in the case of collections of randomly oriented particles.

In the case of a single crystal and at small scattering angles, the calculations of SPRF can be performed using the scalar Fraunhofer approximation:

$$I(u,v) \quad = \quad \Upsilon \cdot \left| \int\int \xi(x', y') \cdot \exp\left[-i \cdot k(u \cdot x' + v \cdot y')\right] \mathrm{d}x' \mathrm{d}y' \right|^2 \tag{10.24}$$

Here $\Upsilon = \frac{k^2}{2\pi}$, S is the geometrical cross section of the particle in the plane perpendicular to the incident beam, $\xi(x', y')$ is the aperture factor, $u = \frac{X}{R}$, $v = \frac{Y}{R}$ are angular coordinates in the observation plane located at the distance R from the particle. (X, Y) and (x', y') are coordinates in the observation and object planes, respectively. In the Fraunhofer approximation, a particle is substituted by an aperture having the same size and shape as the projection of a particle on the plane perpendicular to the incident beam direction. The aperture factor is equal to unity if it is assumed that the plane wave inside of the aperture is the same as in the free space. In particular, Eq. (10.23) follows from Eq. (10.24) under this assumption in the special case of spherical particles (van de Hulst, 1981). The generalization to account for the refractive index of particles (e.g., for small crystals) is also possible (van de Hulst, 1981). For collections of randomly oriented particles (e.g., hexagonal crystals in glaciated clouds), Eq. (10.24) must be averaged with respect to the corresponding Euler angles. Analytical calculations cannot be performed in this case and computer simulations are needed. An interesting result is that the Fraunhofer diffraction pattern of a single randomly oriented irregularly shaped particle (ISP) is equivalent to that of polydispersed spheres. The parameters of such a polydispersion depend on the parameters of ISP. The corresponding theory was developed by Shifrin et al. (1984).

The measurements of angular scattering $\beta(\lambda,\theta) = N\langle C_{\text{sca}}\rangle$ and extinction $\epsilon(\lambda) = N\langle C_{\text{ext}}\rangle$ (C_{ext} is the extinction cross section) coefficients of clouds are of importance not only for finding the size distributions and concentration of particles but also these are important quantities themselves. In particular, remote sensing of clouds is based on radiative transfer modeling, where $\beta(\lambda,\theta)$ and $\epsilon(\lambda)$ are considered as an input. In addition, the total scattering coefficient:

$$\sigma = 2\pi \int_0^{\pi} \beta(\lambda,\theta)\cdot \sin\theta \,\mathrm{d}\theta\,, \tag{10.25}$$

the phase function $p(\theta) = \frac{4\pi\beta(\theta)}{\sigma}$, the single scattering albedo $\omega_0 = \frac{\sigma}{\epsilon}$, and the absorption coefficient $k = \epsilon - \sigma$ are used. The phase function is normalized as follows:

$$\frac{1}{2} = \int_0^{\pi} p(\theta)\cdot \sin\theta \,\mathrm{d}\theta\,. \tag{10.26}$$

In radiative transfer studies, the asymmetry parameter:

$$g = \frac{1}{2}\int_0^{\pi} p(\theta)\ \sin\theta\cdot\cos\theta \,\mathrm{d}\theta\,, \tag{10.27}$$

is often used as well. The values of g depend on the size and shape of particles and they are often close to 0.75 for ice clouds and 0.85 for water clouds. This means that ice clouds generally are more reflective (in the VIS, where $k \approx 0$) as compared to water clouds of the same optical thickness:

$$\tau = \int_{l_1}^{l_2} \epsilon(z)\,\mathrm{d}z\,, \tag{10.28}$$

where z is the vertical coordinate, and l_1 and l_2 are corresponding cloud boundaries. It can be shown both using Mie theory and geometrical optics calculations that in the case of non–absorbing large ($a \gg \lambda$) particles as those, which exist in tropospheric clouds, it follows:

$$\sigma \;=\; 2\,N \cdot \langle S \rangle \;, \tag{10.29}$$

where S is the geometrical cross section of particles ($S = \pi \cdot a^2$ for spheres). The angular integration of the geometrical optics part of scattering field, as shown in Eq. (10.25), is somewhat involved. However, the diffraction part can be easily integrated resulting in:

$$\begin{aligned} C_{\mathrm{sca}}^{\mathrm{d}}(\lambda, m, a) \;&=\; 2\,\pi \cdot k^{-2} \int\limits_0^{\pi} \left(\frac{x}{\theta}\right)^2 \cdot J_1^2(x\theta) \cdot \sin\theta \; \mathrm{d}\theta \\ &\approx\; 2\,\pi \cdot a^2 \int\limits_0^{\infty} J_1^2(y) \cdot y^{-1} \; \mathrm{d}y \\ &=\; \pi \cdot a^2 \,, \end{aligned} \tag{10.30}$$

in the case of a single sphere with the radius a as it should be. Here we accounted for the property of Bessel functions (the orthogonality relation):

$$2 \int\limits_0^{\infty} J_1^2(y) \cdot y^{-1} \; \mathrm{d}y \;=\; 1\,. \tag{10.31}$$

The geometrical optics part of the scattering cross section is equal to πa^2 as well (for non–absorbing particles). The analytical integration can be performed till any scattering angle in the forward scattering region and not for the whole diffraction peak as in Eq. (10.30):

$$\begin{aligned} C_{\mathrm{sca}}^{\mathrm{d}}(\lambda, m, a, \theta_0) \;&\approx\; 2\,\pi \cdot a^2 \int\limits_0^{\mathrm{ka}\theta_0} J_1^2(y) \cdot y^{-1} \; \mathrm{d}y \\ &=\; \pi \cdot a^2 \cdot \Big[1 - J_0^2(k \cdot a \cdot \theta_0) - J_1^2(k \cdot a \cdot \theta_0)\Big] \,. \end{aligned} \tag{10.32}$$

In the calculation of this integral we employed the property:

$$\frac{J_1^2(y)}{y} \;=\; J_0(y) \cdot J_1(y) - J_1(y) \cdot J_1'(y)\,, \tag{10.33}$$

and the corresponding values of tabular integrals. Here J_1' is the derivative of the Bessel function. Therefore, it follows that the fraction of scattered energy

ΔC_{sca} in the angular range $\epsilon \in [\theta_1, \theta_2]$ is proportional to the following function:

$$\Delta C_{\text{sca}} = \pi \cdot a^2 \cdot \left[J_0^2(k \cdot a \cdot \theta_1) + J_1^2(k \cdot a \cdot \theta_1) - J_0^2(k \cdot a \cdot \theta_2) - J_1^2(ka\theta_2) \right] . \tag{10.34}$$

This equation (averaged with respect to the PSD) is the basis for the measurements of PSDs in a number of devices. Not only scattering but also light extinction can be used to determine the size distribution of particles. The extinction coefficient can be written as:

$$\epsilon = N \int_0^\infty C_{\text{ext}}(a) \cdot f(a) \, \mathrm{d}a . \tag{10.35}$$

Usually the spectral measurements of ϵ are used in the optics of turbid media to determine $f(a)$ solving Eq. (10.35). The value of C_{ext} is close to $2S$ for large particles (at the VIS wavelengths). It follows:

$$\epsilon_{\text{vis}} = 2\,N \cdot \langle S \rangle = 2\,\pi \cdot N \cdot \left\langle a^2 \right\rangle , \tag{10.36}$$

or $\epsilon_{\text{vis}} = \frac{1.5LWC}{a_{\text{ef}}\rho}$, where $LWC = N\rho \langle V \rangle$, ρ is the density of water, $\langle V \rangle$ is the average volume of particles, $a_{\text{ef}} = \frac{3\langle V \rangle}{4\langle S \rangle}$ is the effective radius of particles. The dimensionless volume concentration $C_{\text{v}} = N < V >$ is also often used in various theoretical calculations.

The measured extinction coefficient gives the total surface area of particles in unit volume $\Sigma = 4\pi N \left\langle a^2 \right\rangle$. Namely: $\Sigma = 2\epsilon$. The information on PSD is then lost. For thermal IR wavelengths (e.g., 12 μm) particles are highly absorbing and small as compared to the wavelength. Then one derives (van de Hulst, 1981) for the sphere of the volume V:

$$C_{\text{ext}} = \frac{9\,\alpha \cdot n \cdot V}{|m^2 + 2|^2} , \tag{10.37}$$

$$\epsilon_{\text{TIR}} = \varsigma \cdot N \cdot \langle V \rangle , \tag{10.38}$$

where:

$$\varsigma = \frac{9\,\alpha \cdot n}{|m^2 + 2|^2} , \qquad \alpha = \frac{4\,\pi \cdot \chi}{\lambda} , \tag{10.39}$$

$m = n - \mathrm{i} \cdot \chi$ is the complex refractive index of particles. It follows from Eqs. (10.35)) and (10.39) that the liquid water content can be obtained directly from ϵ_{TIR}. Namely, one derives:

$$LWC = \frac{\epsilon_{\mathrm{TIR}} \cdot \rho}{\varsigma} . \tag{10.40}$$

Also the effective radius of particles can be determined, see Eqs. (10.36)–(10.38):

$$a_{\mathrm{ef}} = \frac{3\,\epsilon_{\mathrm{TIR}}}{2\,\varsigma \cdot \epsilon_{\mathrm{vis}}} . \tag{10.41}$$

The application of theoretical results presented above in various optical instruments is given in Chapter 5.

10.4.2 Light Scattering Theory for Specific Spectrometers

The operating principle of the FSSP, CDP, CAS, CAS–DPOL, CPSD and SID is based on the concept of light scattering described above, i.e. that the intensity of scattered light depends on the particle size and can be predicted theoretically if the shape and refractive index of a particle is known, as well as the wavelength of the incident light, as was described in detail above. The important thing to remember is that the intensity of light scattered by a particle varies with the angle with respect to the incident light. If the particle is spherical and of homogeneous composition, the scattered intensity is symmetric around the axis parallel with the incident wave but varies in intensity from 0° to 180°, where 0° is the most forward scattering and 180° is directly backward. Figure 10.10 shows an example of the angular pattern of scattering. This angular dependency of the scattering around a spherical particle can be calculated using the equations that were developed by Mie (1908) for a specific diameter, refractive index and incident wavelength.

This theory is applied in optical particle counters (OPCs) by collecting scattered light from particles that pass through a light beam of controlled intensity and wavelength and converting the photons to an electrical signal whose amplitude can be subsequently related back to the size of the particle.

The property of a particle to interact with light is usually described by its scattering cross section, σ_{s}. This is the product of the scattering efficiency, θ_{s}, and cross sectional area, $\frac{\pi}{4}D^2$, where D is the particle diameter. If we have an optical system that collects light over a range of angles and we measure the intensity of scattered light collected from a particle, we can determine the particle size from the calculated scattering cross sections by integrating over the range of angles used in the instrument. The single particle light scattering spectrometers differ mostly in the collection angles that are used in each system.

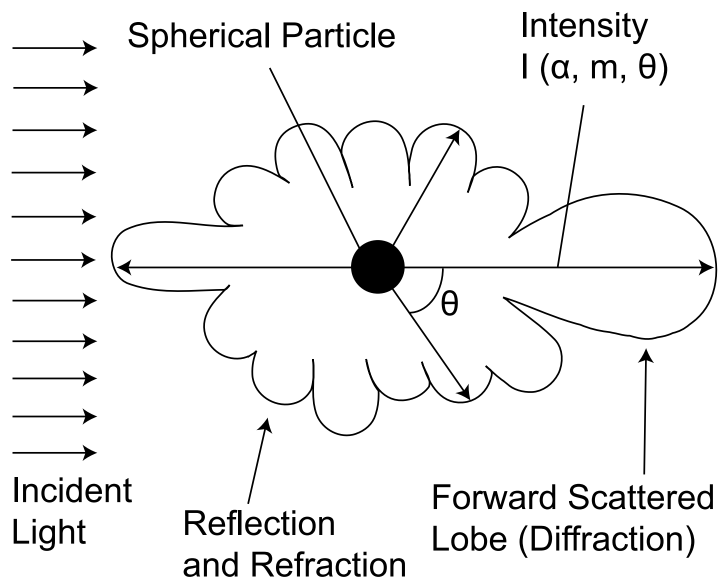

Fig. 10.10 This diagram demonstrates the intensity of scattered light as a function of angle with respect to the incident ray for a typical spherical particle.

10.4.3 Imaging Theory

Section 5.3.3 described the optical array probes (OAP) that capture images of cloud particles using optical imaging. Here we describe in greater detail the theory underlying the measurement.

Consider a plane wave that is incident, perpendicular to an opaque screen Figure 10.10. Following Babinet's principle, the amplitude of the diffracted wave at point Q can be presented as, e.g., Born and Wolf (1965, 2003):

$$U(Q) = U_{\mathrm{a}}(Q) + U_{\mathrm{b}}(Q)\,, \tag{10.42}$$

where $U_{\mathrm{a}}(Q)$ is the amplitude of the diffracted wave, if the opaque screen is in place and $U_{\mathrm{b}}(Q)$ is the diffracted wave when the aperture, with the same shape as the screen, is in place. In the frame of the Fresnel–Kirchhoff diffraction theory $U_{\mathrm{a}}(Q)$ and $U_{\mathrm{b}}(Q)$ can be written as (Baker and Copson, 1950):

$$U_{\mathrm{a}}(Q) = \begin{cases} \exp\left(\mathrm{i}\cdot K\vec{k}\cdot\vec{g}\right) & \text{if point} Q \text{is outside the geometrical shadow} \\ 0 & \text{if point} Q \text{is inside the geometrical shadow} \end{cases} \tag{10.43}$$

$$U_{\mathrm{b}} = -\frac{1}{4\pi}\oint_{\Gamma} \exp(\mathrm{i}\cdot K\cdot\vec{k}\cdot\vec{g})\,\frac{\exp(\mathrm{i}KS)(\vec{s}\times\vec{k})}{S(1+\vec{k}\cdot\vec{s})}\mathrm{d}\vec{l}, \qquad (10.44)$$

where $\vec{k}=\frac{\vec{K}}{|\vec{K}|}$ is a unit vector in the direction of the wave propagation; $K=\frac{2\pi}{\lambda}$ is the wave number, $\vec{p}$ is the radius vector of point P on the contour Γ, S is the differential element along the contour Γ, S is the distance between points P and Q, and $\vec{s}$ is the unit vector in the PQ direction.

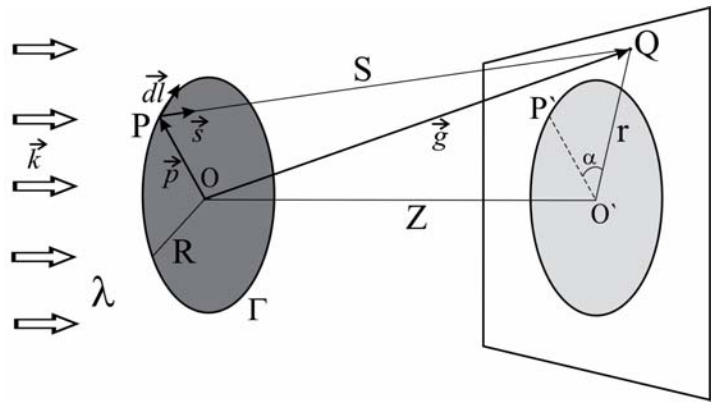

Fig. 10.11 A schematic explaining calculation of diffraction by an opaque disc.

Integration of $U_{\mathrm{b}}(Q)$ in Eq. (10.44) is carried along the contour of the boundary of the geometrical shadow. Eqs. (10.42)–(10.44) give a general description of the Fresnel diffraction by an opaque screen with an arbitrary shape. For the case of an opaque disc Eqs. (10.43) and (10.44) can be transformed into (Korolev et al., 1991)

$$U_{\mathrm{a}}(Q) = \begin{cases} \exp(\mathrm{i}\cdot k\cdot Z) & \text{if } r>R \\ 0 \text{ if } r\le R \end{cases} \qquad (10.45)$$

$$U_{\mathrm{b}}(Q) = -\frac{1}{4\pi}\int_0^{2\pi}\frac{\exp(\mathrm{i}\cdot k\cdot S)\cdot(R^2-R\cdot r\cdot\cos\alpha)}{S\cdot(S-Z)}\,\mathrm{d}\alpha, \qquad (10.46)$$

where $=\frac{r}{R}$, R is the radius of the opaque disc; r is the distance from the center of the image to point Q, $k=2$, is the wavelength, Z is the distance between the disc and its image; and S can be found as $S=(Z^2+R^2+r^2-3Rr\cos\alpha)^{\frac{1}{2}}$.

The intensity of the light at point Q Figure 10.11 is calculated as:

$$I(Q) = |U_a(Q) + U_b(Q)|^2 . \tag{10.47}$$

The analysis of Eqs. (10.45)–(10.47) yields the following properties of diffraction images by an opaque disc (Korolev et al., 1991):

1. The diffraction image can be presented as a function of only one dimensionless variable:

$$Z_d = \frac{\lambda \cdot |Z|}{R^2} . \tag{10.48}$$

2. Two droplets with different diameters give the same diffraction image if $\frac{|Z_1|}{|Z_2} = \frac{R_1^2}{R_2^2}$. The images for such droplets are different only by the scale factor $\frac{R_1}{R_2}$.

3. The diffraction image does not depend on the sign of Z. The diffraction image of the same droplet will be the same at equal distances on opposite sides of the object plane.

10.4.4 Holography Theory

For the purposes of providing a clear understanding of the holographic method it is useful to consider an analytical model for the hologram resulting from a single water droplet. Holograms recorded in a liquid cloud typically involve the interference of a reference beam and a wave scattered by transparent, order 10 to 100 μm diameter, spherical water droplets. This would suggest a complete solution using Mie theory to describe the electric field due to scattering from a sphere and its interference with the incident plane wave. However, we note that the particle size and scattering geometry allow for several useful approximations.

Because size parameters are large($\pi \cdot d/\lambda > 60$) and in–line holographic systems observe only forward–scattered light (scattering angle $< 10°$), to good approximation we may neglect the complexities of Mie theory and treat the scattered wave as diffraction from an opaque disk with the same diameter as the water droplet (Bohren and Huffman, 1983b). Furthermore, in the droplet size range considered, most holographic systems operate in the far field $(z \gg d^2/\lambda \sim 2$ to 20 mm), so we may treat the scattered wave with the Fraunhofer approximation. In practice, digital reconstruction of the holograms is normally carried out using more general approaches because actual conditions do not always satisfy the far–field constraint (for example, ice particles larger than 100 μm in extent).

To develop the analytical model, we consider an opaque disk of diameter d located at $z = 0$, and centered on the optical axis, where the z–coordinate is taken to be the optical axis. We use (x, y) as coordinates in the (far field) diffraction plane, also perpendicular to the optical axis. Making the foregoing assumptions (far–field, large size parameter, etc.), an analytical expression for the total electric field E_{H} can be obtained. Defining $r = (x^2 + y^2)^{1/2}$, $C = \pi \cdot d^2 / (4\,\lambda \cdot z)$, $Q(r) = 2\,J_1(\xi) / \xi$ with $\xi = \pi\, r \cdot d / (\lambda \cdot z)$, and $\Phi(r) = \pi\, r^2 / (\lambda \cdot z)$, the resultant field E_{H} and measured intensity $I_{\mathrm{H}}(r) = E_{\mathrm{H}}(r) \cdot E^*_H(r)$ has the form:

$$\begin{aligned} E_{\mathrm{H}} &= 1 - C \cdot Q \cdot \mathrm{i}^{-1} \cdot \exp\,(i\,\Phi) \\ I_{\mathrm{H}} &= 1 - 2\,C \cdot Q \cdot \sin\,(\Phi) + C^2 \cdot Q^2\,. \end{aligned} \tag{10.49}$$

The first term is the background intensity and $(C \cdot Q)^2$ is the negligible scattered intensity (diffraction) term. In the Fraunhofer limit, therefore, the hologram obtained from a population of cloud droplets may be approximated as the superposition of the fields, one for each particle, with r and d adjusted appropriately for droplet position and size, respectively. In practice the cloud of particles is sufficiently dilute that interference of waves from various particles can be neglected.

Eq. (10.49) demonstrates several important features of holography. First, the interference term $\Phi(r)$ depends only on the position of the particle along the optical axis, not on its diameter d. Hence, the spatial frequencies in this term alone contain sufficient information to provide the particle's position along the optical axis (the position in the (x, y) plane is easily determined). Also, the spatial frequency increases radially as $r = z$ so that the desired depth of field of the instrument places a constraint on the spatial resolution of the detector. Note also that the increasing spatial frequency with r suggests that the finite pixel size limits the maximum sharpness attainable in reconstructed images. Both of these conclusions can be obtained by considering in–line holography for a point particle, but the disk aperture model makes it clear that the interference fringe pattern described by the $\sin[\Phi(r)]$ term contains information on particle position, while the modulation of this pattern by the term $2\,C \cdot Q(r)$, depends on both z and d, as expected from common experience with diffraction by a circular aperture.

1 10.5 LIDAR and RADAR Observations

2 10.5.1 Overview of Airborne RADAR Systems

DESIGNATION:	NOAA P-3 Lower Fuselage Radar	NOAA P-3 Parabolic Antenna	NOAA P-3 French dual Flat plate	ELDORA
Full name of radar	Lower Fuselage Radar	Tail Doppler radar	Tail Doppler radar	Electra Doppler Radar
Aircraft(s) carrying the unit	NOAA WP-3D both N42RF and N43RF	NOAA WP-3D either N42RF or N43RF	NOAA WP-3D either N42RF or N43RF	NRL P3
Main purpose	precipitation, particularly in hurricanes but also in other weather such as severe storms	winds and precipitation, particularly in hurricanes but also in other weather such as severe storms	winds and precipitation, particularly in hurricanes but also in other weather such as severe storms	3D kinematic structures of precipitation systems and clear air boundary layer
Antenna configuration	parabolic antenna that rotates in a plane parallel to the ground, while being steerable up to 5 degrees up or down of plane parallel to the ground	parabolic antenna that rotates completely around the axis of the fuselage, while being steerable up to 25 degrees fore and aft of the plane normal to the fuselage	French-built dual flat-plane antennas that rotate completely around the axis along the fuselage, with beams 20 degrees fore or aft of a plane normal to the fuselage	dual- flat plate, slotted waveguide antenna, conical scan, dual-beam (15-19 deg FORE and AFT)
Year placed in service	1976	1976	1991	Jan 1993
Operating frequency (GHz)	5.37 (C-band)	9.315±0.0116 (X-band)	9.315±0.0116 (X-band)	9.3-9.8 (X-band)
Peak power (kW)	70	60	60	35-40
Usable signal level (best configuration)	0 dBZ	-10 dBZ at 10 km	-10 at 10 km	-12 dBZ at 10 km
Calibration accuracy (dBZ)	2	2	2	1.5
Best range resolution (m)	250	75	75	37.5
Beam width (degrees)	4.1 (vertical), 1.1 (horizontal)	1.35 perpendicular to scan direction, 1.90 along scan direction	2	1.8
Doppler capability yes/no	no	yes	yes	Yes
Polarization diversity yes/no	no	no	no	No
Special features				frequency diversity
Link to detailed information	http://www.aoml.noaa.gov/hrd/HRD-P3_radar.html	http://www.aoml.noaa.gov/hrd/HRD-P3_radar.html	http://www.aoml.noaa.gov/hrd/HRD-P3_radar.html	http://www.eol.ucar.edu/instrumentation/airborne-instruments/eldora/eldora

DESIGNATION:	EDOP	WCR	SPIDER	EC CPR	RASTA
Full name of radar	ER-2 Doppler Radar	Wyoming Cloud Radar	Super Polarimetri Ice-crystal Detection and Explication Radar	Environment Canada Cloud Profiling Radar	Radar SysTem Airborne
Aircraft(s) carrying the unit	NASA ER-2	University of Wyoming King Air 200T or NSF/NCAR C-130	Gulfstream II (operated by Diamond Air Service Co. Ltd.)	NRC Convair-580	Falcon 20, ATR-42
Main purpose	vertical structure of deep precipitation systems, hurricanes, and thunderstorms from high-altitude nadir viewing	atmospheric research: clouds, light precipitation	cloud microphysics	cloud microphysics	cloud microphysics and dynamics, light precipitation
Antenna configuration	two fixed beams: nadir and 35 deg forward looking	up to 5 single-polarization antennas, currently using 1 dual-pol and 3-single-pol antennas on the King Air and 3 single-pol antennas on the C-130	offset Gregorian type antenna, -40 to +95 degree scan across flight direction	Fixed zenith and nadir-looking single pol 30.5 cm antennas	Falcon 20 : 3 beams downward (45 cm antennas: nadir,), 2 beams upward. ATR42 : 2 beams downward
Year placed in service	Sept 1993	June 1995; Oct 2009	1998	1999	November 2000
Operating frequency (GHz)	9.6 (X-band)	94.92 (W-band)	95.04 (W-band)	35 (Ka-band)	95.04 (W-band)
Peak power (kW)	25 (split between two ports)	1.8 kW, 1% duty cycle	1.6	50 kW - split to 2 ports	1.8
Usable signal level (best configuration)	-20 dBZ at 10 km	-40 dBZ at 1 km	-30 dBZ at 5 km	-33 at 1 km	-35 dBZ at 1 km
Calibration accuracy (dBZ)	1	better than 2.5 dB (est.)	1		1
Best range resolution (m)	37.5	15 m	41.25	37.5	30
Beam width (degrees)	3	0.8 (max.)	0.6	2	0.5
Doppler capability yes/no	yes	yes	yes	No	yes
Polarization diversity yes/no	yes – receive LDR	yes, linear, up to 2 antennas	yes	No	no
Special features		pulse pair and full Doppler spectra acquisition modes; King Air also provides an external reflector for redirecting the side-pointing beam to upward-pointing for a total of 5 fixed-beam directions	pulse pair and FFT modes		pulse pair and FFT acquisition modes (2048 pts) - reflector will be implemented in 2010 to scan a +-15 degrees sector perpendicular to the aircraft heading
Link to detailed information	http://har.gsfc.nasa.gov	http://atmos.uwyo.edu/wcr			

DESIGNATION:	APR-2	NOAA IWRAP	CRS	NAWX		HIWRAP
Full name of radar	Airborne Precipitation Radar 2nd Generation	Imaging Wind and Rain Profiler	Cloud Radar System	NRC Airborne W and X-band Polarimetric Doppler Radar		High-altitude Imaging Rain and Wind Profiler
Aircraft(s) carrying the unit	NASA DC-8 & P-3	NOAA WP-3D either N42RF or N43RF	NASA ER-2	NRC Convair 580		NASA WB-57, Global Hawk
Main purpose	cloud and precipitation	winds and precipitation, particularly in hurricanes but also in other weather	vertical structure of clouds from high-altitude nadir viewing	atmospheric research		3D winds and reflectivity from precipitation and clouds, ocean surface winds
Antenna configuration	Dual-frequency horn, fixed collimating antenna and scanning flat plane to achieve +/- 25° scan angle in the cross-track plane	conical scan about nadir, quad-beam (30, 35,40 and 50 deg), dual-frequency	nadir	66 cm parabolic to side; 45 cm flat plate slotted waveguide for up and down	30 cm fixed to side and down; third beam to zenith or up to 40° from vertical or side via reflector plate	conical scan about nadir, dual-beam (30 and 40 deg off nadir), dual-frequency
Year placed in service	2001	2002	July 2002	May 2006	Jan 2007	Jan 2010
Operating frequency (GHz)	13.4 GHz (Ku), 35.6 GHz (Ka)	5.01-5.4 (C-band), 12.87-13.92 (Ku-band)	94.155 (W-band)	9.41 (X-band)	94.05 (W-band)	13.47, 13.91, 33.72, 35.56
Peak power (kW)	0.2 (Ku), 0.1 (Ka)	15.8	1.7	25 split between two ports	1.9	0.025 (Ku), 0.008 (Ka)
Usable signal level (best configuration)	10dBZ (Ku), 0 dBZ (Ka) at 10 km	0 dBZ at 1 km	-28 dBZ at 10 km	-20 dBZ at 1 km	-30 dBZ at 1 km	0 dBZ (Ku), -5 dBZ(Ka) at 10 km
Calibration accuracy (dBZ)	1.5	1	2	2	2	1
Best range resolution (m)	30	15	37.5	45	15	37.5
Beam width (degrees)	4	5-10 depending on frequency and incidence angle	0.6 x 0.8 (cross-track x along-track)	3.5 side / 5.5 nadir & zenith	0.7	3.0 (Ku), 1.2 (Ka)
Doppler capability yes/no	yes	yes	yes	yes	yes	yes
Polarization diversity yes/no	single pol TX, dual pol Rx (for LDR)	yes, linear HH, VV (C and Ku)	yes - receive LDR	yes – linear	yes -linear	no
Special features	pulse compression, cross-track scanning	pulse compression, frequency diversity		four identical receiver channels connected to four antenna ports; simultaneous transmit and receive Z, ZDR, Kdp	FM Chirp Mode option. Least Mean Squared (LMS) filters provide better than -30 dB range side lobe suppression	unpressurized low-power solid state power amplifier based transceivers; pulse compression; frequency diversity
Link to detailed information	"Development of an advanced airborne precipitation radar" by Sadowy et al., Microwave Journal, (2003)	http://mirsl.ecs.umass.edu/index.pl?iid=2469	http://har.gsfc.nasa.gov	http://www.nawx.nrc.gc.ca/		http://har.gsfc.nasa.gov

DESIGNATION:	G-IV Tail Doppler Radar	HCR	ACR	EXRad
Full name of radar	G-IV Tail Doppler radar	HIAPER Cloud Radar	Airborne Cloud Radar	ER-2 X-band Radar
Aircraft(s) carrying the unit	NOAA G-IV SP aircraft	NSF/NCAR G-V	NASA P-3	NASA ER-2
Main purpose	winds and precipitation, particularly in hurricanes but also in other weather	cloud microphysics	cloud and precipitation	3D winds and reflectivity from precipitation and clouds; ocean surface winds
Antenna configuration	dual-flat-plane antennas that rotate completely around the axis along the fuselage, with beams that point either a fixed 20 degrees fore or aft of the plane normal to the fuselage	lens coupled to rotating reflector positions beam anywhere between zenith and nadir	W-band lens antenna	dual-beam: conical or cross-track scan about nadir; fixed nadir
Year placed in service	2010	single-pol Jan. 2011, dual-pol July 2013	??	2010
Operating frequency (GHz)	9.3 (X-band)	94.04625 (W-band)	94.9 GHz	9,6
Peak power (kW)	7	2	1.4	9 kW, 2% duty cycle
Usable signal level (best configuration)	-12 dBZ at 10 km	-22 dBZ at 10 km	N/A	-15 dBZ at 10 km
Calibration accuracy (dBZ)	2	2	N/A	1
Best range resolution (m)	50	30	30	37,5
Beam width (degrees)	2.7	0.7	0.8	3
Doppler capability yes/no	yes	yes	yes	yes
Polarization diversity yes/no	no	yes - alternating H,V	yes	
				no
Special features	pulse compression		frequency diversity	
Link to detailed information	http://www.aoml.noaa.gov/hrd/tdr/index.htm	http://www.eol.ucar.edu/development/current-dev-proj/hcr/hiaper-cloud-radar/?searchterm=hcr	"The NASA DC-8 Airborne Cloud Radar: Design and Preliminary Results" by Sadowy at al., IGARSS Proc. (1997)	http://har.gsfc.nasa.gov/

Designation	NOAA P–3 Lower Fuselage Radar	NOAA P3–Parabolic Antenna	NOAA P3–French dual Flat plate	ELDORA	EDOP
Full name of RADAR	Lower Fuselage Radar	Tail Doppler RADAR	Tail Doppler RADAR	Electra Doppler Radar	ER–2 Doppler Radar
Aircraft(s) carrying the unit	NOAA WP–3D both N42RF and N43RF	NOAA WP–3D either N42RF or N43RF	NOAA WP–3D either N42RF or N43RF	NRL P3	NASA ER–2
Main purpose	precipitation, particularly in hurricanes but also in other weather such as severe storms	winds and precipitation, particularly in hurricanes but also in other weather such as severe storms	winds and precipitation, particularly in hurricanes but also in other weather such as severe storms	3D kinematic structures of precipitation systems and clear air boundary layer	vertical structure of deep precipitation systems, hurricanes, and thunderstorms from high–altitude nadir viewing
Antenna configuration	parabolic antenna that rotates in a plane parallel to the ground, while being steerable up to 5 degrees up or down of plane parallel to the ground	parabolic antenna that rotates completely around the axis of the fuselage, while being steerable up to 25 degrees fore and aft of the plane normal to the fuselage.	French–built dual flat–plane antennas that rotate completely around the axis along the fuselage, with beams 20 degrees fore or aft of a plane normal to the fuselage.	dual–flat plate, slotted waveguide antenna, conical scan, dual–beam (15–19 deg FORE and AFT).	two fixed beams: nadir and 35 deg forward looking
Year placed in service	1976	1976	1991	1993	1993
Operating frequency (GHz)	5.37 (C–band)	9.315±0.0116 (X–band)	9.315±0.0116 (X–band)	9.3–9.8 (X–band)	9.6 (X–band)
Peak power (kW)	70	60	60	35–40	25 (split between two ports)
Usable signal level (best configuration)	0 dBZ	-10 dBZ at 10 km	-10 dBZ at 10 km	-12 dBZ at 10 km	-20 dBZ at 10 km

Designation	NOAA P–3 Lower Fuselage Radar	NOAA P3–Parabolic Antenna	NOAA P3–French dual Flat plate	ELDORA	EDOP
Calibration accuracy (dBZ)	2	2	2	1.5	1
Best range resolution (m)	250	75	75	37.5	37.5
Beam width (degrees)	4.1 (vertical), 1.1 (horizontal)	1.35 perpendicular to scan direction, 1.90 along scan direction	2	1.8	3
Doppler capability	no	yes	yes	yes	yes
Polarization diversity	no	no	no	no	yes–receive LDR
Special features				frequency diversity	
Link to detailed information	http://www.aoml.noaa.gov/hrd/HRD-P3_radar.html	http://www.aoml.noaa.gov/hrd/HRD-P3_radar.html	http://www.aoml.noaa.gov/hrd/HRD-P3_radar.html	http://www.eol.ucar.edu/instrumentation/airborne-instruments/eldora/eldora	http://har.gsfc.nasa.gov

1

Designation	**WCR**	**SPIDER**	**EC CPR**	**RASTA**	**APR–2**
Full name of RADAR	Wyoming Cloud Radar	Super Polarimetri Ice–crystal Detection and Explication Radar	Environment Canada Cloud Profiling Radar	Radar SysTem Airborne	Airborne Precipitation Radar 2nd Generation
Aircraft(s) carrying the unit	University of Wyoming King Air 200T, NSF / NCAR C–130 Hercules	Gulfstream II (operated by Diamond Air Service Co. Ltd.)	NRC Convair–580	Falcon 20, ATR–42	NASA DC–8 & P–3
Main purpose	atmospheric research: clouds, light precipitation	cloud microphysics	cloud microphysics	cloud microphysics and dynamics, light precipitation	cloud and precipitation
Antenna configuration	up to 5 single–polarization antennas, currently using 1 dual–pol and 3–single-pol antennas on the King Air and 3 single–pol antennas on the C–130	offset Gregorian type antenna, -40 to +95 degree scan across flight direction	Fixed zenith and nadir–looking single pol 30.5 cm antennas	Falcon 20: 3 beams downward (45 cm antennas: nadir), 2 beams upward. ATR42: 2 beams downward	Dual–frequency horn, fixed collimating antenna and scanning flat plane to achieve $\pm 25°$ scan angle in the cross–track plane
Year placed in service	June 1995; Oct 2009	1998	1999	November 2000	2001
Operating frequency (GHz)	94.92 (W–band)	95.04 (W–band)	35 (Ka–band)	95.04 (W–band)	13.4 (Ku), 35.6 (Ka)
Peak power (kW)	1.8 kW, 1 % duty cycle	1.6	50 kW–split to 2 ports	1.8	0.2 (Ku), 0.1 (Ka)
Usable signal level (best configuration)	-40 dBZ at 1 km	-30 dBZ at 5 km	-33 dBZ at 1 km	-35 dBZ at 1 km	10 dBZ (Ku), 0 dBZ (Ka) at 10 km

Designation	WCR	SPIDER	EC CPR	RASTA	APR–2
Calibration accuracy (dBZ)	better than 2.5 dB (est.)	1		1	1.5
Best range resolution (m)	15	41.25	37.5	30	30
Beam width (degrees)	0.8 (max.)	0.6	2	0.5	4
Doppler capability	yes	yes	no	yes	yes
Polarization diversity	yes, linear, up to 2 antennas	yes	no	no	single pol TX, dual pol Rx (for LDR)
Special features	pulse pair and full Doppler spectra acquisition modes; King Air also provides an external reflector for redirecting the side-pointing beam to upward–pointing for a total of 5 fixed–beam directions	pulse pair and FFT modes		pulse pair and FFT acquisition modes (2048 pts)–reflector will be implemented in 2010 to scan a ± 15 degrees sector perpendicular to the aircraft heading	pulse compression, cross–track scanning
Link to detailed information	http://atmos.uwyo.edu/wcr				"Development of an advanced airborne precipitation RADAR" by Sadowy et al., Microwave Journal, (2003)

Designation	NOAA IWRAP	CRS	NAWX		HIWRAP
Full name of RADAR	Imaging Wind and Rain Profiler	Cloud Radar System	NRC Airborne W– and X–band Polarimetric Doppler Radar		High–altitude Imaging Rain and Wind Profiler
Aircraft(s) carrying the unit	NOAA WP–3D either N42RF or N43RF	NASA ER–2	NRC Convair 580		NASA WB–57, Global Hawk
Main purpose	winds and precipitation, particularly in hurricanes but also in other weather	vertical structure of clouds from high–altitude nadir viewing	atmospheric research		3D winds and reflectivity from precipitation and clouds, ocean surface winds
Antenna configuration	conical scan about nadir, quad-beam (30, 35,40 and 50 deg), dual–frequency	nadir	66 cm parabolic to side; 45 cm flat plate slotted waveguide for up and down	30 cm fixed to side and down; third beam to zenith or up to 40 ° from vertical or side via reflector plate	conical scan about nadir, dual–beam (30 and 40 deg off nadir), dual–frequency
Year placed in service	2002	July 2002	May 2006	Jan 2007	Jan 2010
Operating frequency (GHz)	5.01–5.4 (C–band), 12.87–13.92 (Ku-band)	94.155 (W–band)	9.41 (X–band)	94.05 (W–band)	13.47, 13.91, 33.72, 35.56
Peak power (kW)	15.8	1.7	25 split between two ports	1.9	0.025 (Ku), 0.008 (Ka)
Usable signal level (best configuration)	0 dBZ at 1 km	-28 dBZ at 10 km	-20 dBZ at 1 km	-30 dBZ at 1 km	0 dBZ (Ku), -5 dBZ(Ka) at 10 km

Designation	NOAA IWRAP	CRS	NAWX		HIWRAP
Calibration accuracy (dBZ)	1	2	2	2	1
Best range resolution (m)	15	37.5	45	15	37.5
Beam width (degrees)	5–10 depending on frequency and incidence angle	0.6×0.8 (cross–track×along–track)	3.5 side / 5.5 nadir & zenith	0.7	3.0 (Ku), 1.2 (Ka)
Doppler capability	yes	yes	yes	yes	yes
Polarization diversity	yes, linear HH, VV (C and Ku)	yes–receive LDR	yes–linear	yes–linear	no
Special features	pulse compression, frequency diversity		four identical receiver channels connected to four antenna ports; simultaneous transmit and receive Z, Z_{DR}, Kdp	FM Chirp Mode option. Least Mean Squared (LMS) filters provide better than -30 dB range side lobe suppression	unpressurized low-power solid state power amplifier based transceivers; pulse compression; frequency diversity
Link to detailed information	http://mirsl.ecs.umass.edu/index.pl?iid=2469	http://har.gsfc.nasa.gov	http://www.nawx.nrc.gc.ca/		http://har.gsfc.nasa.gov

Designation	G–IV Tail Doppler Radar	HCR	ACR	EXRad
Full name of RADAR	G–IV Tail Doppler RADAR	HIAPER Cloud Radar	Airborne Cloud Radar	ER–2 X–band Radar
Aircraft(s) carrying the unit	NOAA G–IV SP aircraft	NSF / NCAR G–V	NASA P–3	NASA ER–2
Main purpose	winds and precipitation, particularly in hurricanes but also in other weather	cloud microphysics	cloud and precipitation	3D winds and reflectivity from precipitation and clouds; ocean surface winds
Antenna configuration	dual–flat–plane antennas that rotate completely around the axis along the fuselage, with beams that point either a fixed 20 degrees fore or aft of the plane normal to the fuselage	lens coupled to rotating reflector positions beam anywhere between zenith and nadir	W–band lens antenna	dual–beam: conical or cross-track scan about nadir; fixed nadir
Year placed in service	2010	single–pol Jan. 2011, dual–pol July 2013	??	2010
Operating frequency (GHz)	9.3 (X–band)	94.04625 (W–band)	94.9	9.6
Peak power (kW)	7	2	1.4	9 kW, 2 % duty cycle
Usable signal level (best configuration)	-12 dBZ at 10 km	-22 dBZ at 10 km	N / A	-15 dBZ at 10 km
Calibration accuracy (dBZ)	2	2	N / A	1
Best range resolution (m)	50	30	30	37.5
Beam width (degrees)	2.7	0.7	0.8	3

Designation	G–IV Tail Doppler Radar	HCR	ACR	EXRad
Doppler capability	yes	yes	yes	yes
Polarization diversity	no	yes–alternating H,V	yes	no
Special features	pulse compression		frequency diversity	
Link to detailed information	http://www.aoml.noaa.gov/hrd/tdr/index.htm	http://www.eol.ucar.edu/development/current–dev–proj/hcr/hiaper–cloud–radar/?searchterm=hcr	"The NASA DC-8 Airborne Cloud Radar: Design and Preliminary Results" by Sadowy at al., IGARSS Proc. (1997)	http://har.gsfc.nasa.gov/

Lidar System	Emitted wavelengths Laser source	Application	Year placed in service	Laboratory Country	A/C
HSRL	532 nm Solid state Nd–Yag	Aerosols, clouds	2007	DLR Germany	F20, HALO
HSRL	532 nm Solid state Nd–Yag	Aerosols, clouds	2007	NASA / LaRC USA	B200
LNG HSRL + Backscatter	355 nm (dual polar), 532, 1064 nm	Aerosols, clouds	2011	LATMOS / IPSL	France F20, ATR42
CPL Backscatter	532, 1064 nm	Aerosols, clouds	2005	NASA / GSFC	ER2
SABL	1064 nm	Aerosols, clouds	1995	NCAR	C130
	355 nm	Aerosols, clouds	2010	UKMO	BAE 146
				U. WYOMING	King Air
WALES (DIAL)	815–930 nm	H20, O3, aerosols	2000	DLR, Germany	F20, HALO
LASE	820–940 nm	H2O, aerosols	1995	NASA / LARC	ER2, DC8
LEANDRE II	720–750 nm	H2O, aerosols	1999	LATMOS / IPSL	F20, ATR42
(Doppler)	2 μm	Wind, aerosols	2002	DLR, Germany	F20, HALO
	2 μm	Wind, aerosols	TBD	NASA / LARC	TBD
	2 μm	Wind, aerosols	TBD	NASA / GSFC	TBD
WIND (Doppler)	10,6 μm	Wind, aerosols	1999	DLR–CNRS Germany–France	F20, HALO
RALI	94 GHz Doppler RADAR and HSRL	Clouds, aerosols	2011 LATMOS / IPSL	F20, ATR42	
	94 GHz RADAR and backscatter LIDAR		2000	JAPAN	King Air
ALTO	266, 299, 316 nm	O3, aerosols	1993	LATMOS	F20, ATR42
	280–320 nm, 600 nm	O3, aerosols	1990	NASA / LaRC	Electra, DC8

1

Tab. 10.10 Overview of airborne RADARs operate in the K or W band, with X–band used less frequently.
Available from ftp://cat.uwyo.edu/pub/permanent/vali/suppl/rad_table_full.pdf

10.5.2 Results of Airborne RADAR Observations–Some Examples

Examples are presented on the following pages of the variety of observations possible with airborne RADAR systems. Figures 10.12 to 10.19 demonstrate the possibilities, and also the limitations, of what can be learned with the use of the airborne RADARs currently in use. The cases selected here demonstrate the use of different RADAR systems and platforms, applications in various projects, and the interpretations of observations making use of numerous RADAR parameters. Brief explanations of each case are presented in the figure captions.

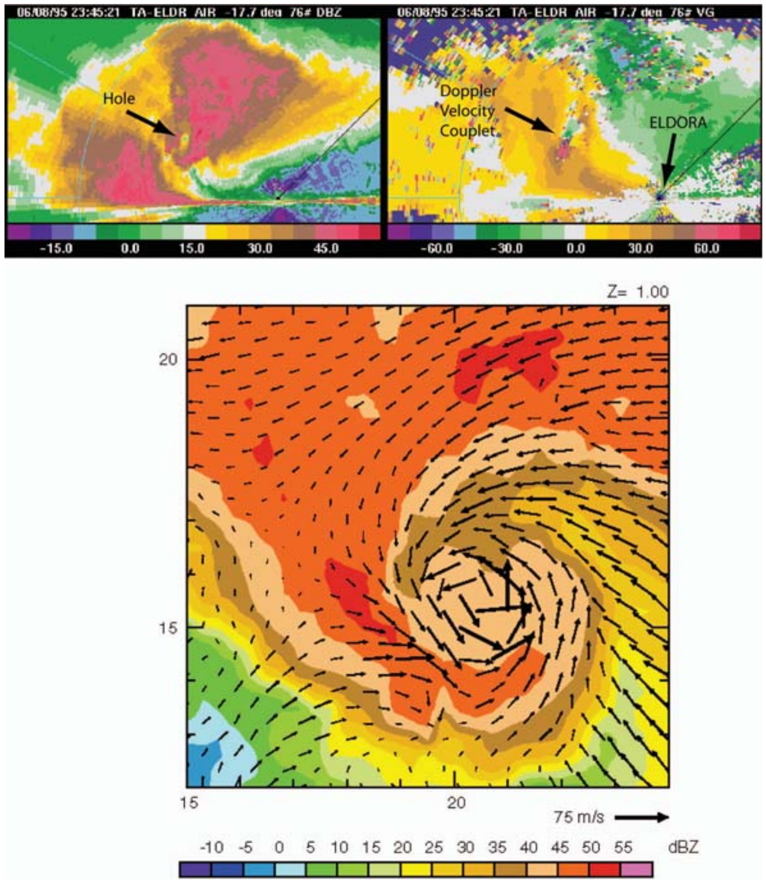

Fig. 10.12 (provided by Wen–Chao Lee): The NCAR/NSF Electra with ELDORA flew by a F5 tornado near Kellerville, TX on 8 June 1995. ELDORA's conical helix sliced through the vertically tilted tornado. Reflectivity and radial velocity are shown in the upper panels. Precipitation particles were centrifuged out by the tornado circulation to form a weak reflectivity "hole" (left panel). This was associated with an intense Doppler velocity couplet (right panel) with a > 30 m s^{-1} approaching wind (green) and $>$ 80 m s^{-1} receding wind (red) separated by $\sim$1 km. The anticyclonic rotation on this ELDORA scan inferred by the Doppler velocity couplet suggested that the tornado vortex was vertically tilted into the page with height. The speckles in the Doppler velocity display suggested highly turbulent winds within this supercell. Horizontal wind vectors and the reflectivity (in color) of the tornado are shown in the lower panel. The parent mesocyclone of the tornado associated with a "hook" RADAR reflectivity signature is clearly shown. With the 300 m resolution of the ELDORA data the actual tornado circulation on the scale of 500 m could not be resolved.
Available from
ftp://cat.uwyo.edu/pub/permanent/vali/suppl/10.17_eldora.tif

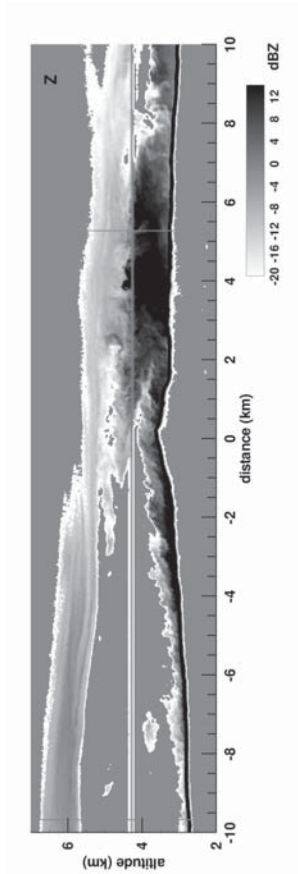

Fig. 10.13 (provided by G. Vali): Vertical section through a winter storm over the Medicine Bow Mountains of SE Wyoming (January 27, 2006, 22:02 UTC). The image consists of data collected by the 95 GHz WCR, see Table 10.10, onboard the Wyoming King Air as it flew at 4285 m altitude from west to East (left to right in the figure). Two antennas were used simultaneously, one pointing upward and one downward. The figure is very close to a 1:1 true proportions of the storm. The reflectivity scale is in dBZ. The image reveals an unexpected layer of shallow clouds right over the surface on the upwind side of the mountain range. The near–surface echo is very likely due to blowing snow. Due to its shallow depth and low reflectivity, it would have been very difficult to detect with ground–based RADARs. On the downwind side of the ridge, a deep cloud mass is seen as the result of the merger of wave clouds (5–6 km altitude), a cell forming there and the snow layer near the surface. Essentially all of the echo is due to ice crystals. Temperature at flight level was –15.5 °C and ice particle concentrations reached 80 L^{-1}.
Available from
ftp://cat.uwyo.edu/pub/permanent/vali/suppl/10.18_jan27-2222_bw.tif

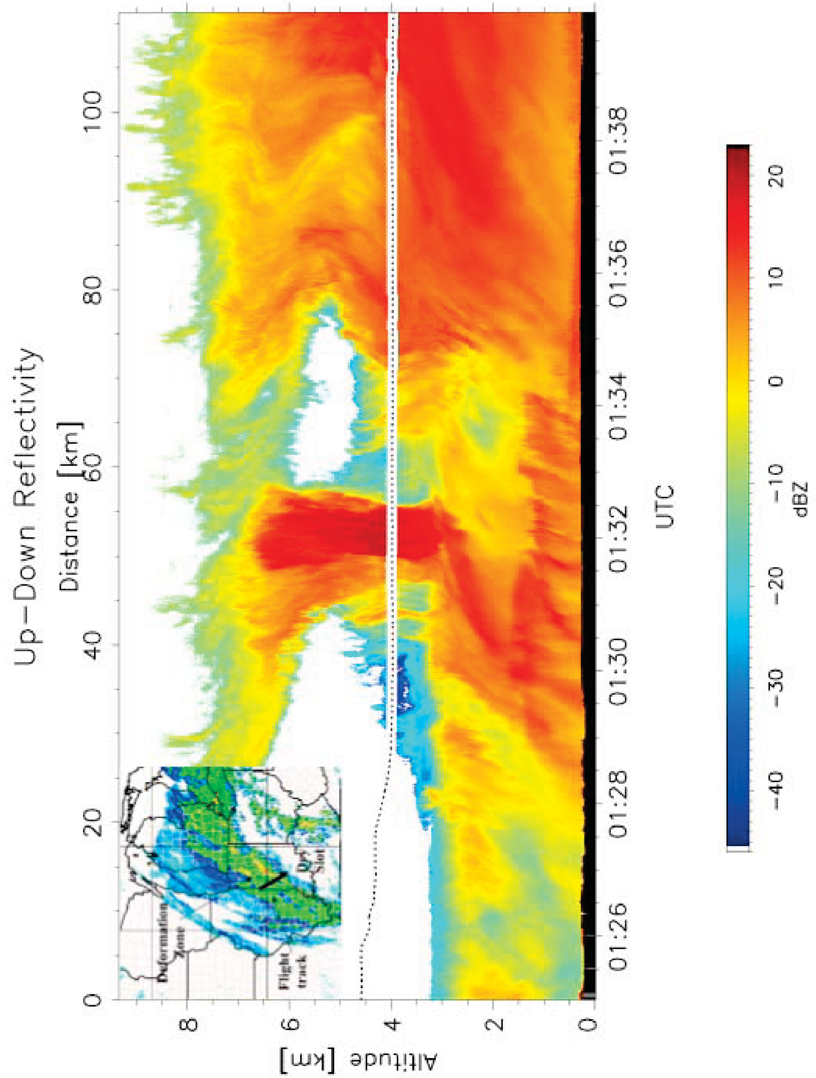

Fig. 10.14 (provided by Samuel Haimov and Bob Rauber): Wyoming Cloud RADAR reflectivity image, which was taken as the NCAR C–130 passed from the dry slot into the deformation zone north of the center of a continental cyclone, illustrates the triggering of convection along the dry slot-cloud interface. The data were collected during the U.S. NSF funded "Profiling of Winter Storms" or PLOWS experiment over the states of Illinois and Indiana on December 2, 2009.
Available from
ftp://cat.uwyo.edu/pub/permanent/vali/suppl/10.19_PLOWS09.20091203.012502_013956_nexrad.eps

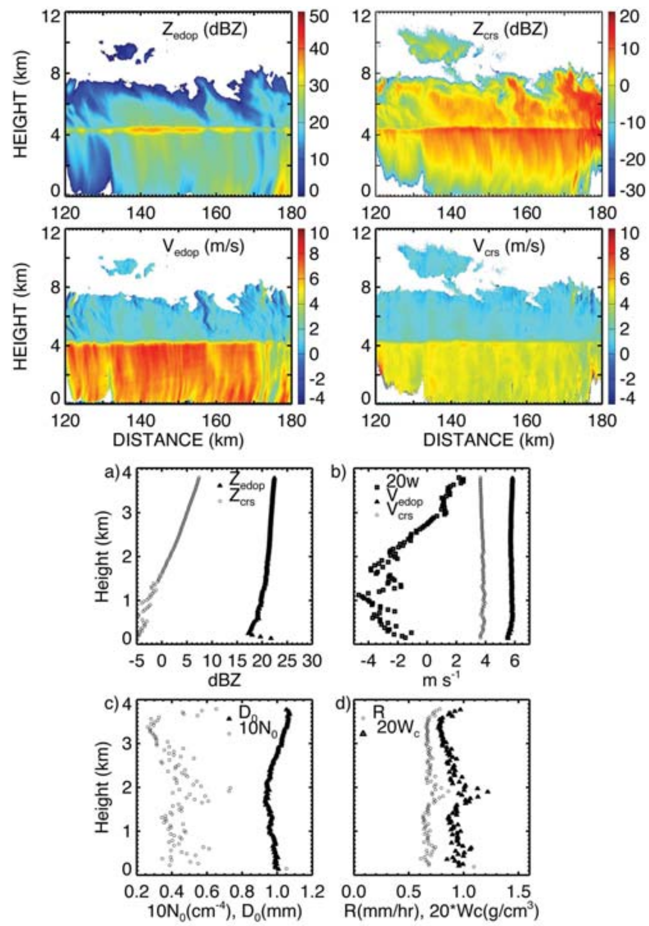

Fig. 10.15 Stratiform rain observed with EDOP (upper panels) and CRS (lower panels) in July 2002 over Florida. In the rain region below the melting band (4.3 km) scattering at 10 GHz is in the Rayleigh regime except for very large raindrops, the while at 94 GHz it is in the Mie regime except for the very small raindrops. The signal at 10 GHz is subject to little or no attenuation in light rain while the signal at 94 GHz is subject to significant attenuation by rain and water vapor. Consequently, the mean Doppler velocity and reflectivity measured at the two frequencies are quite different. These differences have been exploited to retrieve the parameters of an exponential raindrop size distribution, vertical air velocity, and attenuation by rain, melting band and water vapor for the entire rain fields. Graphs (lower panels) show the averages for the entire rain fields: median volume diameter, D_0, and the intercept parameter, N_0, rainfall rate R, and rain water content W.
Available from
ftp://cat.uwyo.edu/pub/permanent/vali/suppl/10.20_edop.tif

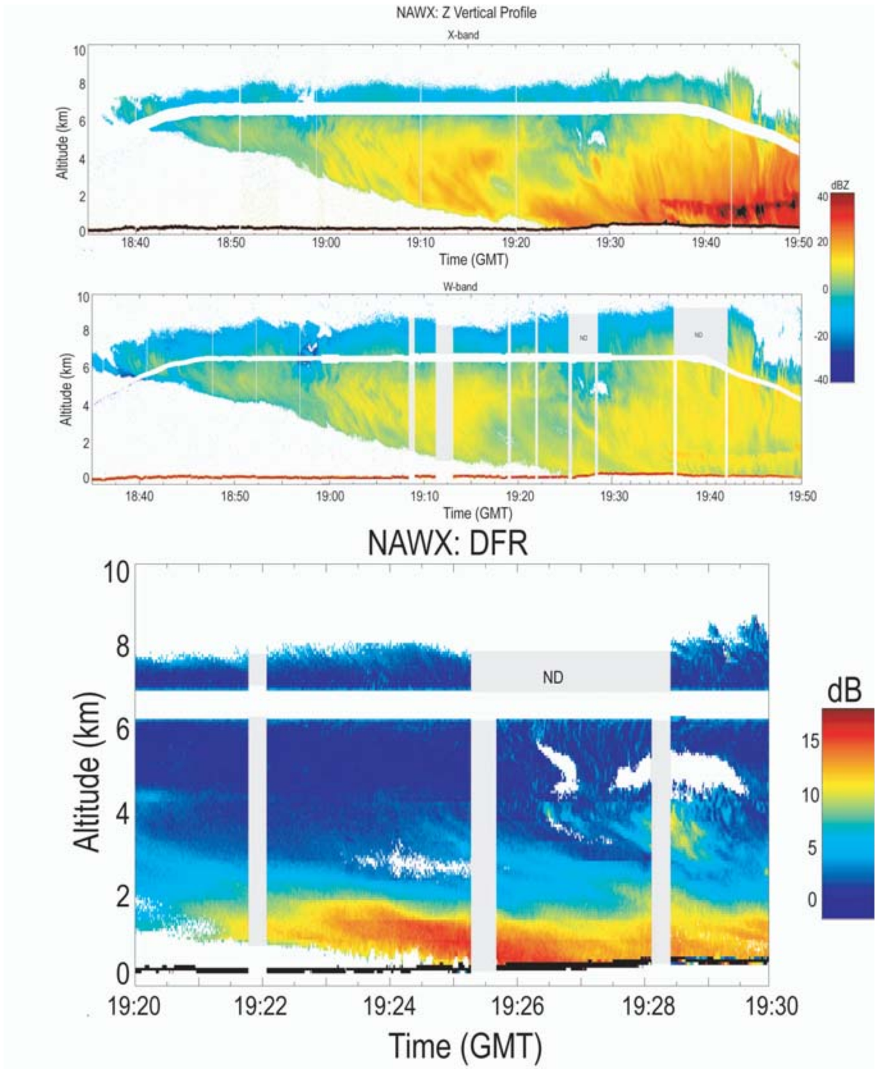

Fig. 10.16 (provided by Mengistu Wolde): During C3VP campaign, the Convair flew in large winter storms over eastern Ontario on March 01, 2007. Upper panels show simultaneous measurements of W and X–band reflectivity in vertical sections. The lowest panel shows the difference between the two, showing values near 0 dB for regions where ice crystals smaller than 1 mm were present (as per in situ data), close to 5 dB for the regions above the melting band ($\sim$ 2 km altitude) where larger crystals and aggregates were detected, and a significant drop by up to 15 dB in the W–band signal in the rain below the melting band due to attenuation and resonance effects.
Available from
ftp://cat.uwyo.edu/pub/permanent/vali/suppl/10.21_edop.tif

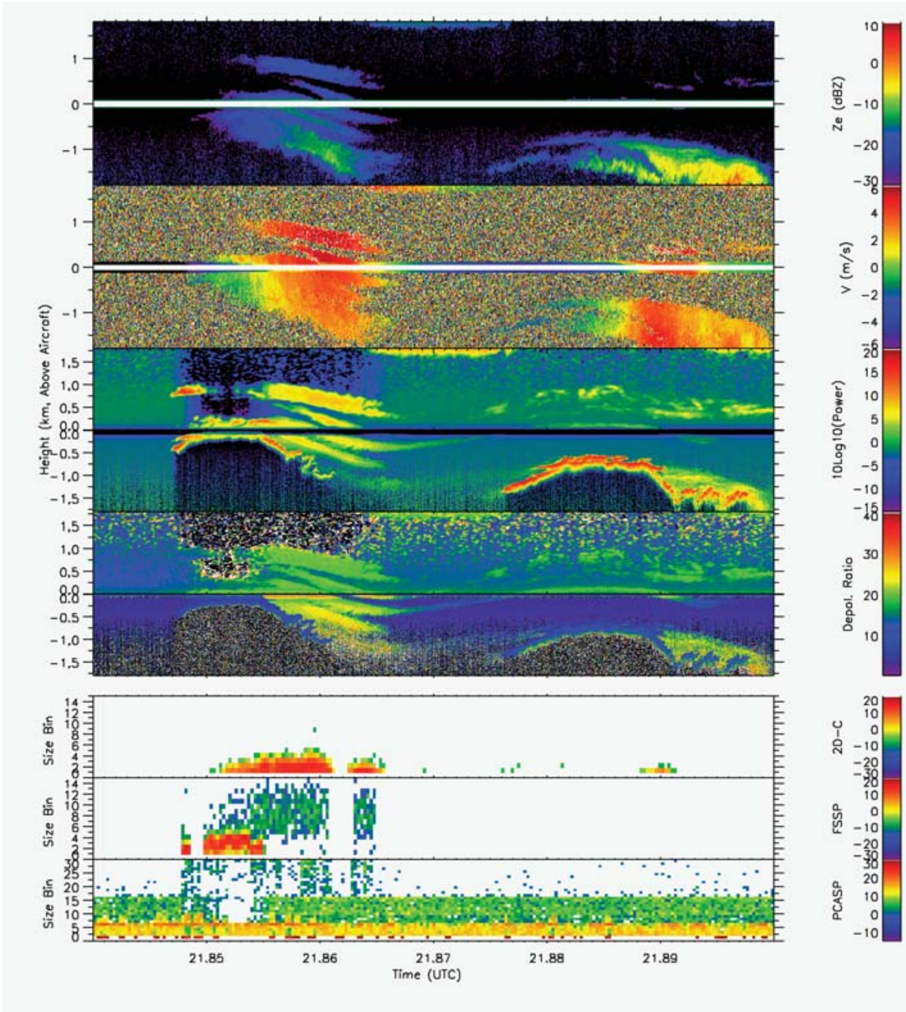

Fig. 10.17 (provided by Zhien Wang): RADAR (WCR), LIDAR (WCL) and in situ (Wyoming King Air) data collected in wave clouds. RADAR and LIDAR images are vertical sections combining data from upward and downward pointing beams. Wind is from left to right in the figure. The horizontal scale is ∼3.6 km per major time tick of 0.01 h. The wave cloud on the left produced RADAR echoes only from its downwide side where ice crystals grew larger. The LIDAR return depicts the upwind part of this wave too. The polarization data from the lowest layer of this cloud indicates the presence of liquid water drops (low depol ratio). Similarly, almost all of the wave on the right hand side of the figure consisted of supercooled droplets.
Available from
ftp://cat.uwyo.edu/pub/permanent/vali/suppl/10.22_WCR.WAICO09.tif

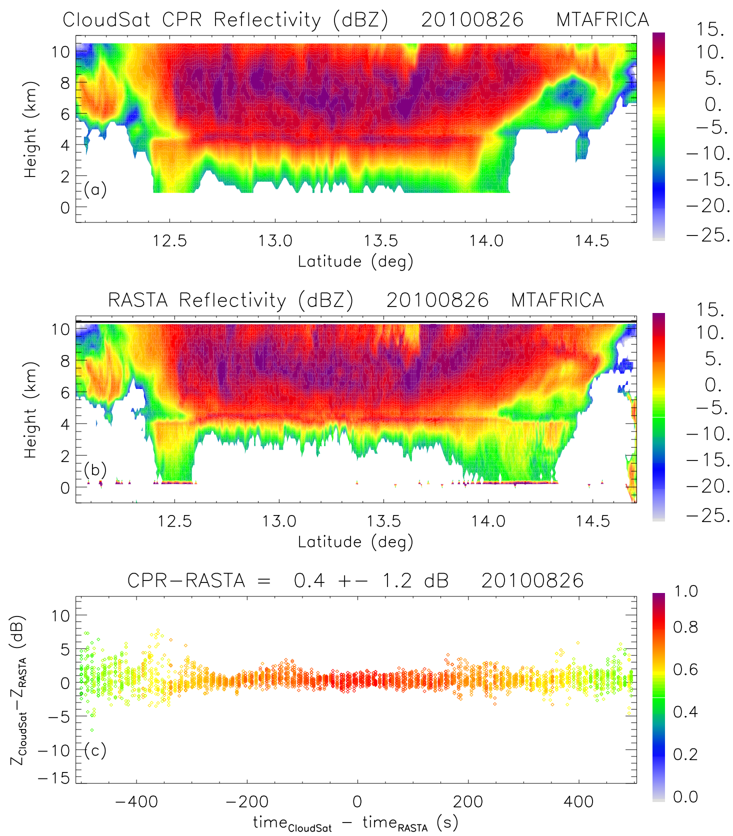

Fig. 10.18 (provided by A. Protat and J. Delanoe): Calibration check of the CloudSat CPR using the airborne cloud RADAR RASTA (Protat et al., 2009). Flights below the track of CloudSat with airborne cloud RADARs are a unique and direct way of evaluating the instrument and cloud microphysics products from the CloudSat mission. Direct comparisons of the ocean backscatter (σ_0) in Protat et al. (2009) indicate that on average CloudSat measures ocean backscatter 0.4 dB $\pm$1 dB higher than the airborne cloud RADAR. Panels a and b show collocated RASTA and CloudSat vertical cross-sections through the stratiform part of a West–African squall line. Panel c shows the difference as a function of time lag between observations and of distance (color code in panel c). These data show that ice cloud reflectivities measured by CloudSat are 0.4 dB $\pm$1.2 dB higher than the airborne cloud RADAR. Both numbers are within the uncertainties in calibration of the airborne cloud RADARs, so the conclusion is that CloudSat is well calibrated. The results have been further confirmed using long time series of ground–based cloud RADAR observations and a statistical approach (Protat et al., 2009).
Available from
ftp://cat.uwyo.edu/pub/permanent/vali/suppl/10.23_cpr-rasta.eps

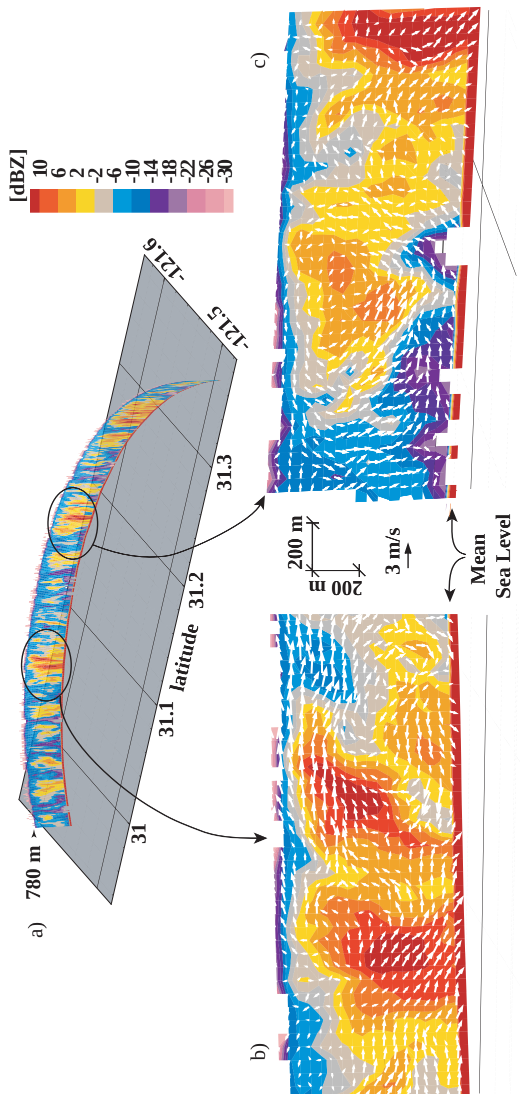

Fig. 10.19 (provided by R. Damiani, S. Haimov and G. Vali): Reflectivity and velocity measurements in marine stratus. Panel (a) depicts the reflectivity field between the aircraft flying above the cloud layer along a long arc at 780 m and the ocean surface; The presence of drizzle cells is evident. For two of those cells dual–Doppler analysis of the 2D flow field are shown in panels (b) and (c) which identify convergence at the bases of updraft regions and reveal that the drizzle cells coincide with those updrafts. From Stevens et al. (2003); Damiani and Haimov (2006).
Available from
ftp://cat.uwyo.edu/pub/permanent/vali/suppl/10.24_dycoms.eps

Figure 10.20 illustrates the dependence of LDR on beam elevation angle for different particle types and it also highlights the detection limitations of weak cross-polarization signals even at close range. Simultaneous LDR at low (side–view) and high (vertical–view) beam angles were collected using NAWX as the aircraft descended through ice clouds, the melting layer and rain. The maximum LDR is observed in the melting layer (–15 to –10 dB) with no noticeable dependence in elevation angle (side view at 20:02:00 vs. vertical at 20:02:30–20:04:00). In contrast, planar and columnar crystals show strong dependence on RADAR beam angle. The LDR of planar crystals are higher (∼–20 dB) at low (near horizontal) beam angles, while the opposite is the case in columnar crystals where the maximum LDR is observed at vertical incidence angle (∼19:56). These observations support the results shown in Figure 9.21.

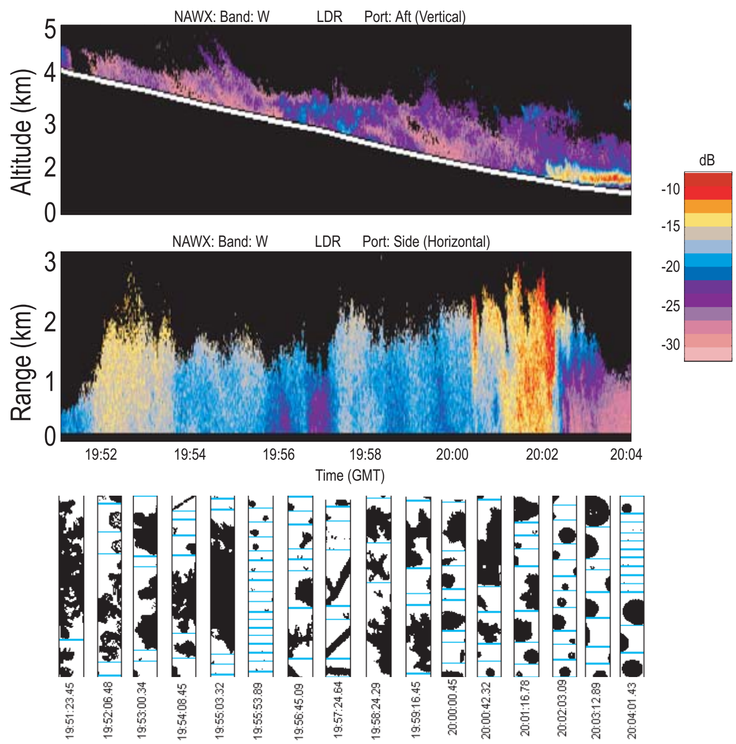

Fig. 10.20 LDR measured by NAWX on Mar 01, 2007 as the aircraft descended from an altitude of 4 km to 1.5 km. Top: Vertical cross-section from upward pointing RADAR beam. The white line shows the aircraft altitude. Middle: LDR from the side–looking dual–pol antenna. Bottom: Sample of PMS 2D–C images corresponding to the aircraft altitude.
Available from
ftp://cat.uwyo.edu/pub/permanent/vali/suppl/10.25_ldr.eps

10.6 Processing Toolbox

10.6.1 Introduction

Within the EUFAR framework, the Standards and Protocols (N6SP) group is tasked with developing recommendations for common solutions in data formats, metadata and data processing. Establishment of standards in these areas will reduce errors in data usage, and provide a common platform for comparison, exchange and dissemination of data. In addition, these developments can provide a useful resource for both new and experienced users of airborne science data. More information on these developments can be found on the N6SP wiki, hosted at http://www.eufar.net/N6SP

As a part of the N6SP common solutions, a software toolbox has been developed to provide a common platform for processing airborne measurements. This toolbox, known as the EUFAR General Airborne Data-Processing Software (EGADS), compiles processing algorithms provided by the EUFAR Expert Working Groups into a Python framework. These algorithms, many of which are based on concepts found in this book, are considered as best practice by the community, and thus, can be used as a reference for future work. Integration of the algorithms is an ongoing process - there are around 20 implemented algorithms at the time of this writing, and many more will be added in the near future.

Alongside the algorithms implemented in the EGADS framework are file input and output routines for common airborne data formats (NetCDF, NASA Ames, CSV, etc). Included in these file access routines are methods to automatically process any available metadata when reading file data. These allow EGADS to be used with most existing airborne data while following established data and metadata conventions. The EGADS package is completely free and open-source, thus, can be modified as needed if other file access methods are desired.

10.6.2 Installation and Use

EGADS is hosted for free download on Google Code at the following address: http://eufar-egads.googlecode.com, or through the Python Package Index (PyPI). EGADS is a Python-based library, thus to use it, Python version 2.5 or higher must be installed on your system. The toolbox depends on several commonly available libraries, which are all also freely available. A list of these libraries can be found in the included EGADS documentation. To install EGADS, simply download the code from Google Code and follow the included instructions, or install through Python's easy_install feature (see documentation included with EGADS for more detailed installation instructions for either method).

To use EGADS, import the package from the Python command line, and any of the included routines can then be used. The script below shows a short example of EGADS being used to process a series of data files.

```
#!/usr/bin/env python

# import egads package
import egads
# import thermodynamic module and rename to simplify usage
import egads.algorithms.thermodynamics as thermo

# get list of all NetCDF files in 'data' directory
filenames = egads.get_file_list('data/*.nc')

f = egads.input.EgadsNetCdf()
# create EgadsNetCdf instance

for name in filenames:
# loop through files

    f.open(name, 'a')
    # open NetCdf file with append permissions

    T_{\rm s} = f.read_variable('T_t')
    # read in static temperature
    P_{\rm s} = f.read_variable('P_{\rm s}')
    # read in static pressure from file

    rho = thermo.DensityDryAirCnrm().run(P_{\rm s}, T_{\rm s})
    # calculate density

    f.write_variable(rho, 'rho', ('Time',))
    # output variable

    f.close()
    # close file
```

For further usage information, refer to the documentation included in the EGADS package. There are two sets of documentation: the first - EGADS Documentation - describes the use of the toolbox itself, including examples on how to explore the package from Python, an overview and examples of the file access classes and a short sample processing script. Detailed descriptions of the EGADS API are also included in this document. The second set of documentation - the EGADS Algorithm Handbook - describes each included algorithm in detail. This includes expected algorithm inputs and outputs, as well as a theoretical description and background of the algorithm itself and references to any relevant literature.

For questions, bug reports or to get more information, please contact eufarsp@eufar.net.